Characterisation of Solar Electricity Import Corridors from MENA to Europe

Potential, Infrastructure and Cost

DLR

Characterisation of Solar Electricity Import Corridors from MENA to Europe

Potential, Infrastructure and Cost

July 2009

Report prepared in the frame of the EU project 'Risk of Energy Availability: Common Corridors for Europe Supply Security (REACCESS)' carried out under the 7th Framework Programme (FP7) of the European Commission (Theme - Energy-2007-9. 1-01: Knowledge tools for energy-related policy making, Grant agreement no.: 212011).

Franz Trieb, Marlene O'Sullivan, Thomas Pregger, Christoph Schillings, Wolfram Krewitt
German Aerospace Center (DLR), Stuttgart, Germany
Institute of Technical Thermodynamics
Department Systems Analysis & Technology Assessment
Pfaffenwaldring 38-40
D-70569 Stuttgart, Germany

Deutsches Zentrum
für Luft- und Raumfahrt e.V.
in der Helmholtz-Gemeinschaft

TABLE OF CONTENTS

1 INTRODUCTION

This report describes methodology, information sources and results of an analysis of solar electricity export potentials of MENA (Middle East and North Africa) countries and possible import corridors to EU27+. The analysis was done in the frame of the EU project 'Risk of Energy Availability: Common Corridors for Europe Supply Security (REACCESS)' carried out under the 7th Framework Programme (FP7) of the European Commission (Theme - Energy-2007-9. 1-01: Knowledge tools for energy-related policy making, Grant agreement no.: 212011). The study conducted as Task 2.3 in Work package 2 focuses on solar power as an additional and virtually limitless energy resource in contrast to fossil resources which were analysed in other Tasks of the REACCESS project. The interconnection of electric power transmission grids among the Mediterranean countries, including EU-countries as well as countries from the MENA region promises an increased level of energy security. The huge solar resources in the MENA countries, significant improvements in solar electricity generation and power transmission technologies, and the growing need for the decarbonisation of European electricity supply leads to increased interest in an EU-MENA electricity grid interconnection. The objective of this analysis was to specify the long term potential for solar electricity import from MENA countries into the EU, and to provide detailed technical and cost data for electricity generation and power transmission options. Concentrating solar power (CSP) plants including high temperature heat storage and high voltage direct current (HVDC) lines as transmission technology represent the key technologies for implementing this most promising option for import of renewable energy to EU27.

The report documents the data basis which was used for the identification and characterisation of potentials and corridors provided for REACCESS project as an input for risk assessment and scenario studies using multi-regional TIMES energy system models. Annex A lists identified solar resources and electricity generation potentials of possible supply regions and Annex B gives an overview of identified and characterised corridors for imports into EU27.

2 STATUS OF KNOWLEDGE - RESULTS FROM RECENT STUDIES

Methodologies and results of the study TRANS-CSP (Trieb et al., 2006) commissioned by the German Federal Ministry of the Environment, Nature Conservation and Nuclear Safety (BMU) were used as basis for work in WP2 Task "Electricity supply".

The TRANS-CSP study analysed the renewable electricity potentials in Europe and their capability to provide firm power capacity on demand. The concept includes an interconnection of the electricity grids of Europe, the Middle East and North Africa (EUMENA) and evaluates the potential and benefits of solar power imports from the South. The results of the TRANS-CSP study can be summarized in the following statements:

- A well balanced mix of renewable energy sources backed by fossil fuels can provide sustainable, competitive and secure electricity for Europe. For the total region, the scenario starts with a reported share of 20 % renewable electricity in the year 2000 and reaches 80 % in 2050. An efficient future backup is necessary to complement the renewable electricity mix, providing firm capacity on demand by quickly reacting, natural gas fired peaking plants, and an efficient grid infrastructure is required to distribute renewable electricity from the best centres of production to the main centres of demand.

- After initiation, a change to a sustainable energy mix leads to less expensive power generation than a business as usual strategy in a time span of about 15 years. Imported fuels with escalating cost will be increasingly substituted by renewable, mostly domestic energy sources. The negative socio-economic impacts of fossil fuel price escalation can be reversed by 2020 if an adequate political and legal framework is established at time. Feed-in tariffs like the German or Spanish Renewable Energy Acts are very effective instruments for the market introduction of renewables. If tariff additions are subsequently reduced to zero, they can be considered a public investment rather than a subsidy.

- Solar electricity generated by concentrating solar thermal power stations in MENA and transferred to Europe via high voltage direct current transmission can provide firm capacity for base load, intermediate and peaking power, effectively complementing European electricity sources. Starting between 2020 and 2025 with a transfer of 60 TWh/y, solar electricity imports could subsequently be extended to 700 TWh/y by 2050. High solar irradiance in MENA and low transmission losses of 10-15 % will yield competitive import solar electricity costs of around 0.05 $€_{2000}$/kWh.

- Carbon emissions can be reduced to 25 % compared to the year 2000. 1 % of the European land would be required for the renewable power sources, which is equivalent to the land used at present for transport and mobility.
- European support for MENA for the market introduction of renewables can attenuate the growing pressure on fossil fuel resources that would otherwise result from the economic growth of this region as described in the MED-CSP study (Trieb et al., 2005), thus helping to secure fossil fuel supply also in Europe. The necessary political process could be initiated by a renewable energy partnership and a common free trade area for renewable energies in EUMENA and culminate in a Community for Energy, Water and Climate Security.

The TRANS-CSP study describes the technical options of transferring solar electricity from MENA to Europe via hydrogen, through the conventional alternating current (AC) grid and by a possible future high voltage direct current (HVDC) infrastructure. Transport of solar energy via hydrogen over a distance of e.g. 3000 km would in principle be possible, but 75 % of the generated renewable electricity would be lost by the involved conversion, transport and storage processes. Consequently, this option was disregarded.

Transfer capacities of the conventional AC grid are rather limited, and even considering that the MENA countries would empower their regional electricity grid to Central European standards and would create additional interconnections all around the Mediterranean Sea, transfer would still be limited to about 3.5 % of the European electricity demand. Over a distance of 3000 km, about 45 % of the generated solar electricity would be lost by such a transfer.

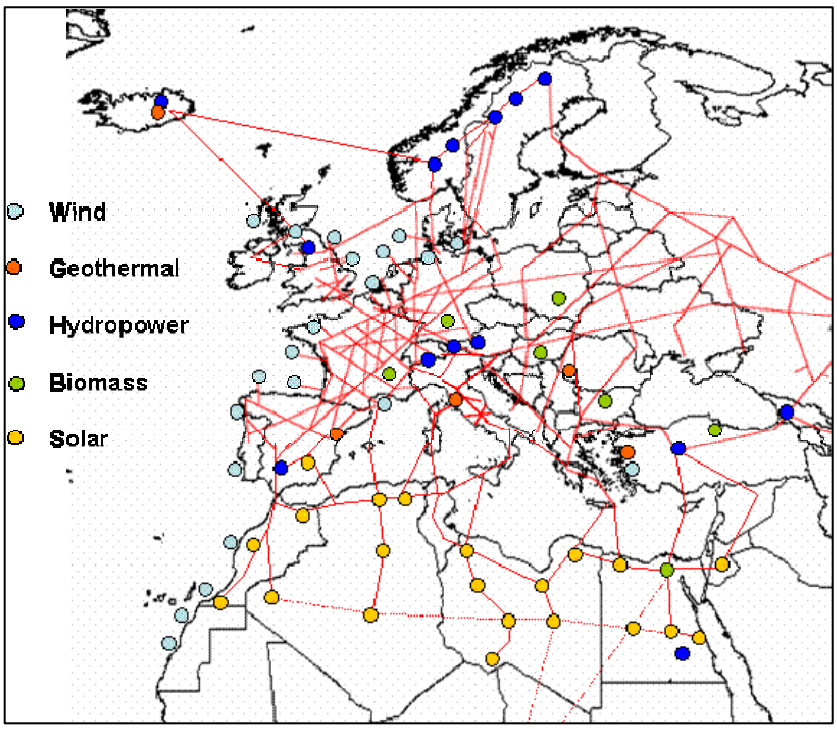

Figure 2-1: Vision of an EUMENA backbone grid using HVDC power transmission technology as “Electricity Highways” to complement the conventional AC electricity grid.

HVDC technology is becoming increasingly important for the stabilisation of large electricity grids, especially if more and more fluctuating resources are incorporated. HVDC over long distances contributes considerably to increase the compensational effects between distant and local energy sources and allows to compensate blackouts of large power stations through distant backup capacity. It can be expected that in the long term, a HVDC backbone will be established to support the conventional European electricity grid and increase the redundancy and stability of the future power supply system.

Table 2-1: Main indicators of the total EUMENA High Voltage Direct Current (HVDC) interconnection and Concentrating Solar Power (CSP) plants from 2020 to 2050 according to the TRANS-CSP scenario.

Year		2020	2030	2040	2050
Transfer Capacity GW		2 x 5	8 x 5	14 x 5	20 x 5
Electricity Transfer TWh/y		60	230	470	700
Capacity Factor		0.60	0.67	0.75	0.80
Turnover Billion €/y		3.8	12.5	24	35
Land Area	CSP	15 x 15	30 x 30	40 x 40	50 x 50
km x km	HVDC	3100 x 0.1	3600 x 0.4	3600 x 0.7	3600 x 1.0
Investment	CSP	42	143	245	350
Billion €	HVDC	5	20	31	45
Elec. Cost	CSP	0.050	0.045	0.040	0.040
€/kWh	HVDC	0.014	0.010	0.010	0.010

As a spin-off effect of this development, the import of solar electricity from MENA will become an attractive diversification of the European power generation portfolio. Solar and wind energy, hydropower, geothermal power and biomass will be generated in regions of best performance and abundance, distributed all over Europe and MENA through a highly efficient HVDC grid on the upper voltage level, and finally delivered to the consumers by the conventional interconnected AC grid on the lower voltage level. Analogue to the network of interstate highways, a future HVDC grid will have a low number of inlets and outlets to the conventional AC system as it will primarily serve long distance transfer, while the AC grid will have a function analogue to country roads and city streets.

Only 10 % of the generated electricity will be lost by HVDC transmission from MENA to Europe over 3000 km distance. In 2050, about twenty corridors with 5000 MW capacity each could provide about 15 % of the European electricity demand by solar imports, motivated by their low cost of around 0.05 $€_{2000}$/kWh and by their high flexibility for base-, intermediate- and peak load operation.

The study also demonstrates the capability of a well balanced mix of renewable and fossil energy sources to provide secure, inexpensive and sustainable electricity for the supply of each of the European countries. Renewable energy can provide the necessary amount of clean energy to achieve the targets for climate stabilisation and reduce the consumption of fossil fuels to the rare times when renewable energy supply and electricity demand do not coincide. The strategy of reducing fossil energy use to peaking power allows for firm capacity on demand and at the same time reduces the consumption of fossil fuels that are a very valuable, ideally stored form of energy that should be exclusively used for that purpose.

Europe has plenty renewable energy sources for power generation (see Figure 2-2). Their total economic potential amounts to about 145 % of the expected future electricity demand. This suggests that the coverage of the demand by 100 % should be achievable within a time span of 50 years. However, 60 % of this potential comes from wind and solar energy, both fluctuating resources that can provide electricity, but almost no firm power capacity on demand (Table 2-2). Moreover, the potentials are not distributed uniformly, but are concentrated in typical regions, e.g. hydropower in Scandinavia and the south central mountains, solar energy in the south, wind energy at the northern coasts and geothermal energy in South and Eastern Europe. Therefore, only 80 % of the power mix of the year 2050 will be derived from renewable sources.

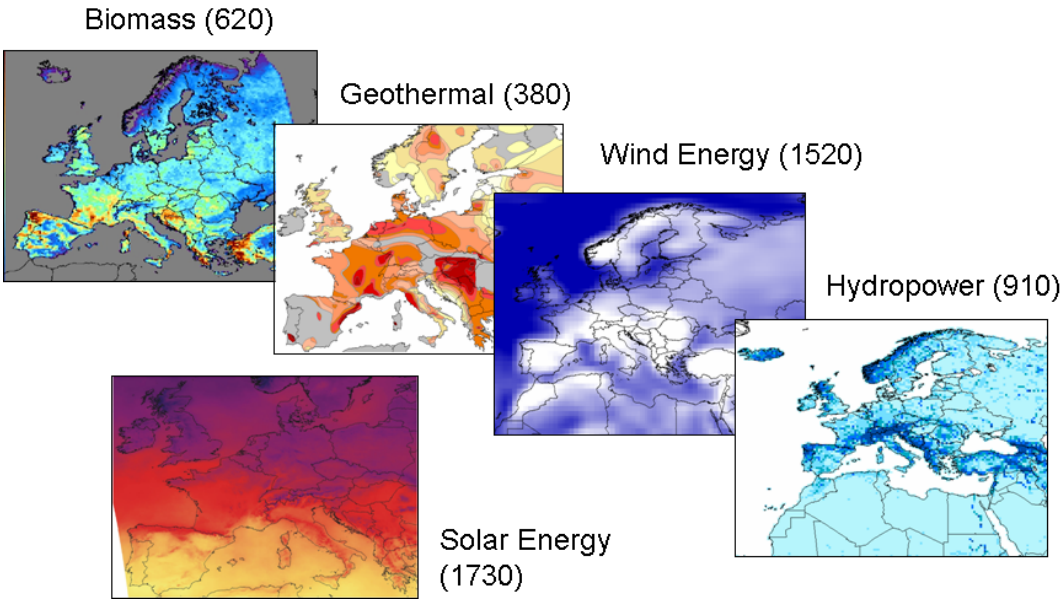

Figure 2-2: Renewable energy resource maps for the European region. Please refer to (Trieb et al., 2006) for the colour code and references. The numbers give the economic electricity potential in TWh/y. Solar energy includes both CSP and PV potentials. All renewables sum up to 5160 TWh/y. The total future electricity demand of the analysed countries amounts to about 4000 TWh per year.

An efficient backup infrastructure will be necessary to complement the renewable electricity mix, on one side to provide firm capacity on demand by quickly reacting, natural gas fired peaking plants, and on the other side by an efficient grid infrastructure that allows to distribute renewable electricity from the best centres of production to the main centres of demand. The best solution is a combination of HVDC electricity highways and the conventional AC grid. On the lower voltage level, decentralised structures will also gain importance, combining e.g. PV, wind and micro-turbines operating together just like one, virtual power plant. Such a grid

infrastructure will not be motivated by the use of renewables alone. In fact, its construction will probably take place anyway, with the purpose to stabilize the growing Pan-European grid, to provide higher security of supply, and to foster competition. Using fossil energies exclusively for backup purposes will reduce their consumption to a sustainable level and will reduce the quickly escalating cost of power generation. Fossil fuels will be used to provide firm capacity, while renewables will serve to reduce fossil fuel consumption.

Several renewable power technologies can also operate as base load and peaking plants: geothermal (hot dry rock) systems that are today still in a phase of research and development, hydropower plants with large storage dams available in Norway, Iceland and the Alps, most biomass plants and concentrating solar power plants in MENA, using the high annual solar irradiance of that region, the possibility of solar thermal energy storage for overnight operation and the option of backup firing with fuels. CSP in Europe is bound to significant seasonal fluctuations, and firm peaking power can only be provided with a considerable fossil fuel share. Due to a higher solar irradiance, the cost of CSP is usually lower in MENA than in Europe. Therefore, there will be a significant market for CSP imports to complement the European sources and provide firm power capacity at competitive cost (Figure 2-3).

A requisite of the electricity mix is to provide firm capacity and a reserve of about 25 % in addition to the expected peaking load (Figure 2-4). Before significant CSP imports start in the year 2020, this can only be provided extending the capacity and fuel consumption of natural gas fired peaking plants. In our scenario, the consumption of natural gas doubles with respect to the starting year 2000, but is then brought back to the initial level, after introducing in 2020 increasing shares of import CSP, geothermal power and hydropower from Scandinavia by HVDC interconnections. As shown in Figure 2-2, the European renewable energy sources that could provide firm capacity are rather limited from the point of view of their potentials. Therefore, CSP imports will be useful to reduce both the installed capacity and the fuel consumption of gas fired peaking plants and to provide firm renewable power capacity.

Table 2-2: Some characteristics of contemporary power technologies.

	Unit Capacity	Capacity Credit *	Capacity Factor **	Resource	Applications	Comment
Wind Power	1 kW – 5 MW	0 – 30 %	15 – 50 %	kinetic energy of the wind	electricity	fluctuating, supply defined by resource
Photovoltaic	1 W – 5 MW	0 %	5 – 25 %	direct and diffuse irradiance on a tilted surface	electricity	fluctuating, supply defined by resource
Biomass	1 kW – 25 MW	50 - 90 %	40 – 60 %	biogas from the decomposition of organic residues, solid residues and wood	electricity and heat	seasonal fluctuations but good storability, power on demand
Geothermal (Hot Dry Rock)	25 – 50 MW	90 %	40 – 90 %	heat of hot dry rocks in several 1000 meters depth	electricity and heat	no fluctuations, power on demand
Hydropower	1 kW – 1000 MW	50 - 90 %	10 – 90 %	kinetic energy and pressure of water streams	electricity	seasonal fluctuation, good storability in dams, used also as pump storage for other sources
Solar Updraft	100 – 200 MW	10 to 70 % depending on storage	20 to 70 %	direct and diffuse irradiance on a horizontal surface	electricity	seasonal fluctuations, good storability, base load power
Concentrating Solar Thermal Power	10 kW – 200 MW	0 to 90 % depending on storage and hybridisation	20 to 90 %	direct irradiance on a surface tracking the sun	electricity and heat	fluctuations are compensated by thermal storage and (bio)fuel, power on demand
Gas Turbine	0.5 – 100 MW	90 %	10 – 90 %	natural gas, fuel oil	electricity and heat	power on demand
Steam Cycle	5 – 500 MW	90 %	40 – 90 %	coal, lignite, fuel oil, natural gas	electricity and heat	power on demand
Nuclear	> 500 MW	90 %	90 %	uranium	electricity and heat	base load power

* Contribution to firm power and reserve capacity. ** Average annual utilisation.

Except for wind power that is already booming today, and hydropower that is already introduced, renewable energy will hardly become visible in the electricity mix before 2020. At the same time, the fade out of nuclear power in many European countries and a stagnating use of coal and lignite due to climate protection will imply increasing pressure on natural gas resources, increasing their consumption as well as their installed capacity. As described above renewables will primarily reduce fuel consumption until 2020, but hardly substitute power capacities. Therefore, the total installed capacity will grow faster than the peaking load (Figure 2-4). Due to the growth of consumption and the substitution of nuclear power, fossil fuel consumption for power generation in Europe cannot be reduced before 2020. Fuel oil for electricity will fade out in 2030, nuclear power will follow after 2040. The consumption of gas and coal will be reduced by 2050 to a compatible and affordable level.

The electricity mix of the year 2000 depends mainly on five resources, most of them limited and imported, while the mix of 2050 will be based on ten energy sources, most of them domestic and renewable (Figure 2-3). Thus, the TRANS-CSP scenario responds to the European Strategy for Sustainable, Competitive and Secure Energy declared by the European Commission in the corresponding Green Paper and Background Document, aiming at higher diversification and security of the European energy supply.

The political and financial issues of a strategy following the TRANS-CSP scenario are also discussed. Industry and private investors need a reliable political and legal framework to introduce and expand renewables in the power market. It can be stated that many countries are already on that track, with a large portfolio of instruments to foster renewable energy market introduction in many countries. The present share of renewables on global power investment of 25 % and industrial production growth rates of up to 60 % per year speak a clear language. Most successful instruments seem to be the feed-in tariffs like the German and Spanish Renewable Energy Acts that provide a fixed premium or revenue for renewable electricity that is individually adapted to the requirements of each technology and granted for the total economic lifetime of the plants.

Renewable energy feed-in laws provide long term, guaranteed power purchase agreements with local utilities. Private investments under such a scheme are usually provided at interest rates that are 50 % lower than those in the conventional power sector, thus effectively reducing the cost of market introduction of renewables. Feed-in tariffs (for new plants) are subsequently reduced year by year, thus motivating intensive research and development for cost reduction. Although such instruments are already effective in some European countries, adequate policies have been adapted only by a few, and there is still a long although promising way to achieve a European standard.

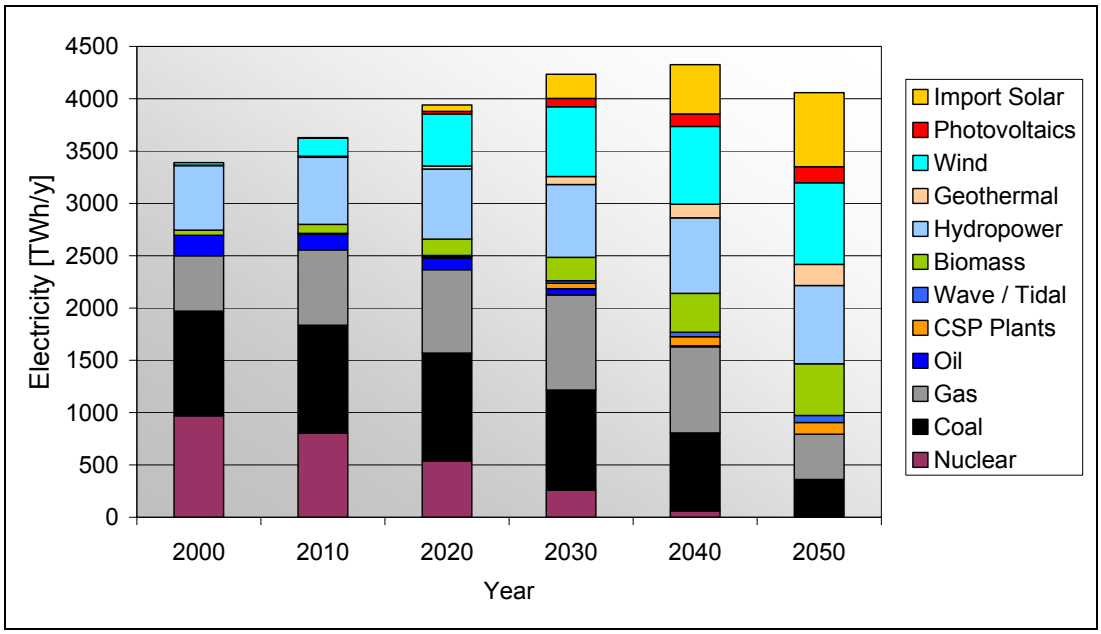

Figure 2-3: TRANS-CSP scenario of gross electricity production and import for the analysed European countries until 2050. The import of other than solar electricity to the region is negligible.

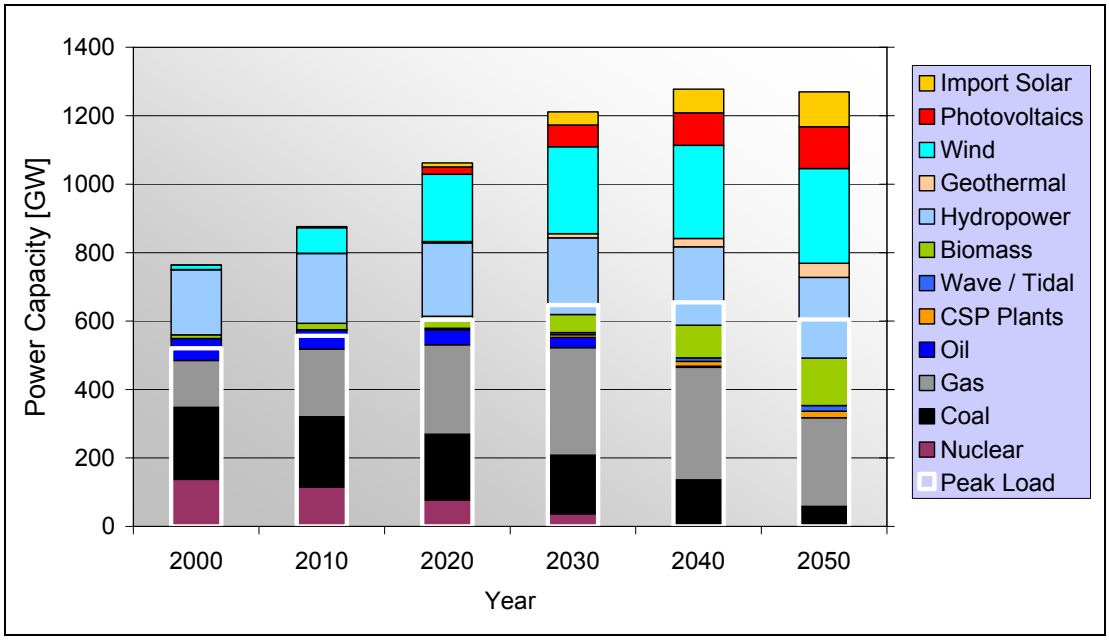

Figure 2-4: TRANS-CSP scenario for the total installed power capacities and peak load for the analysed European countries until 2050.

The TRANS-CSP concept also addresses socio-economic issues. The diversification of resources and empowering of the electricity grid will increase the European security of power supply. Import dependency will be reduced through the improved use of domestic renewable energy (Figure 2-5). A growing pressure on natural gas resources will be avoided.

In contrast to the common belief that for every wind park a backup power plant must be installed, the analysis shows that the need of peaking plants is relatively constant although the share of fluctuating sources (PV and wind) increases. Fact is that the necessary peaking capacity is already there, with the purpose to cover the fluctuations of demand. No extra capacities are needed as long as the fluctuating renewable energy share is smaller than the existing peaking capacity, which is the case in our scenario. Wind and PV plants cannot considerably reduce the required installed capacity of conventional power plants, but they will reduce their consumption of fossil fuels. Establishing a well balanced mix of technologies and sources, fossil peaking capacities will remain, while fossil and nuclear base load plants will be subsequently replaced.

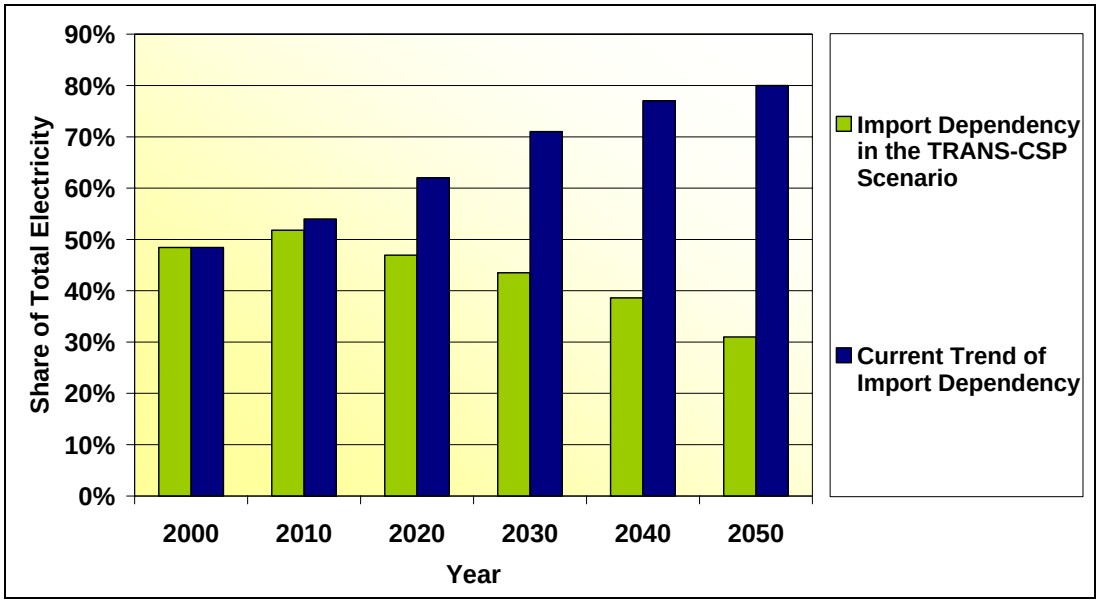

Figure 2-5: Import dependency inclusive CSP import in the TRANS-CSP scenario compared to the current trend of import dependency in the EU.

As shown in Figure 2-6 for the example of Spain, the introduction of renewables will also add to the average cost of power generation, and thus to the negative impacts of electricity cost escalation. However, during the first twenty years, this impact is relatively small, because the share of renewables is small, too. Most of the cost escalation is due to fuel prices and to new power plant capacity investments. By 2020 most renewables will be cheaper than conventional power, and from that point,

the renewable energy shares and their stabilising impact on the electricity cost will become much more noticeable. This demonstrates the danger of policy decisions based on short term scenarios that simply overlook the unique chance of abandoning the present trend of cost escalation, not in the short term – because the necessary investments must still be done – but in the medium and long term. Individual cost learning curves for the different power technologies are shown in Figure 2-7. To become effective in time, they will require an adequate political and legal framework that allows for the implementation of the necessary power capacities to achieve the related economies of scale.

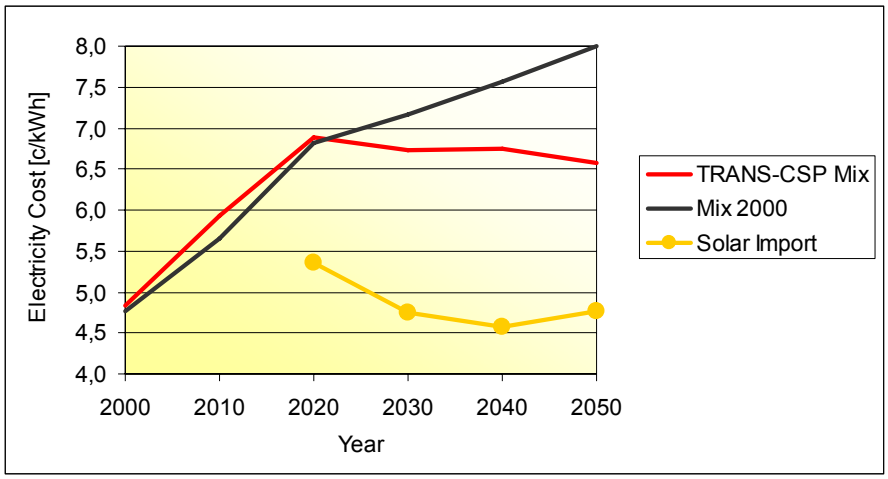

Figure 2-6: Average cost of electricity from new plants within the TRANS-CSP scenario and within a conservative scenario based on the electricity mix of the year 2000, in comparison to the cost of electricity imports from MENA for the example of Spain. For other countries please refer to the annex of (Trieb et al., 2006) (€-ct$_{2000}$/kWh).

Carbon emissions are effectively reduced to values that are considered as compatible with the goal of stabilising the CO2 content of the atmosphere at 450 parts per million, as stated by the International Panel on Climate Change. Starting with 1400 million tons of carbon dioxide per year in the year 2000, the emissions are reduced to 350 Mt/y in 2050, instead of growing to 2350 Mt/y in a business as usual case. The final annual per capita emissions of 0.59 tons/cap y are acceptable in terms of a maximum total emission of 1-1.5 tons/cap/y that has been recommended by the German Scientific Council on Global Environmental Change (WBGU).

The land used for the renewable energy infrastructure scheduled for 2050 amounts to roughly 1 % of the total land area, which is comparable to the land presently used for the transport and mobility infrastructure in Europe.

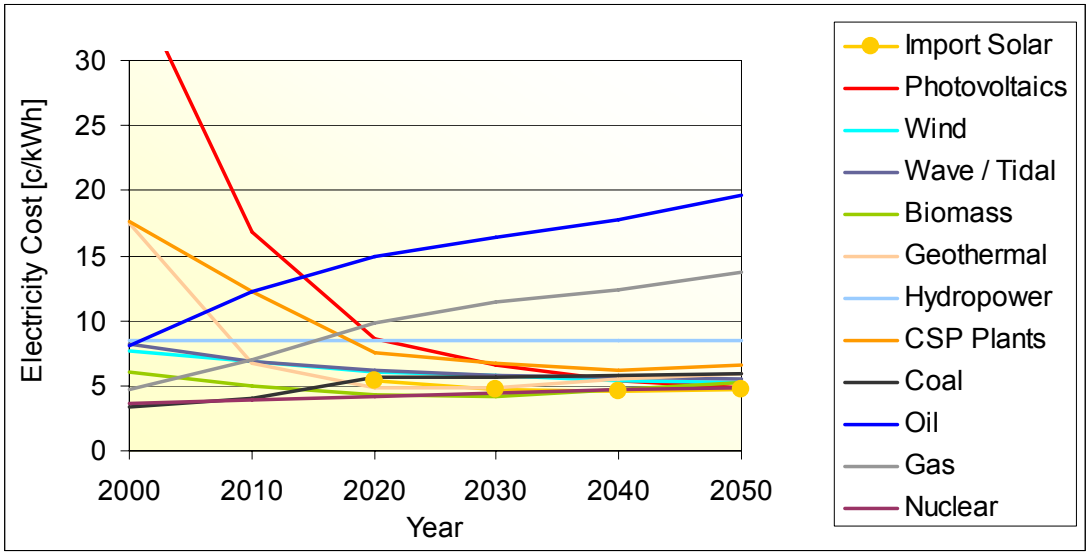

Figure 2-7: Electricity generation cost of new power plants. In the medium term, renewables are the least cost option for power. The curve "Import Solar" starts in 2020 (€-ct$_{2000}$/kWh).

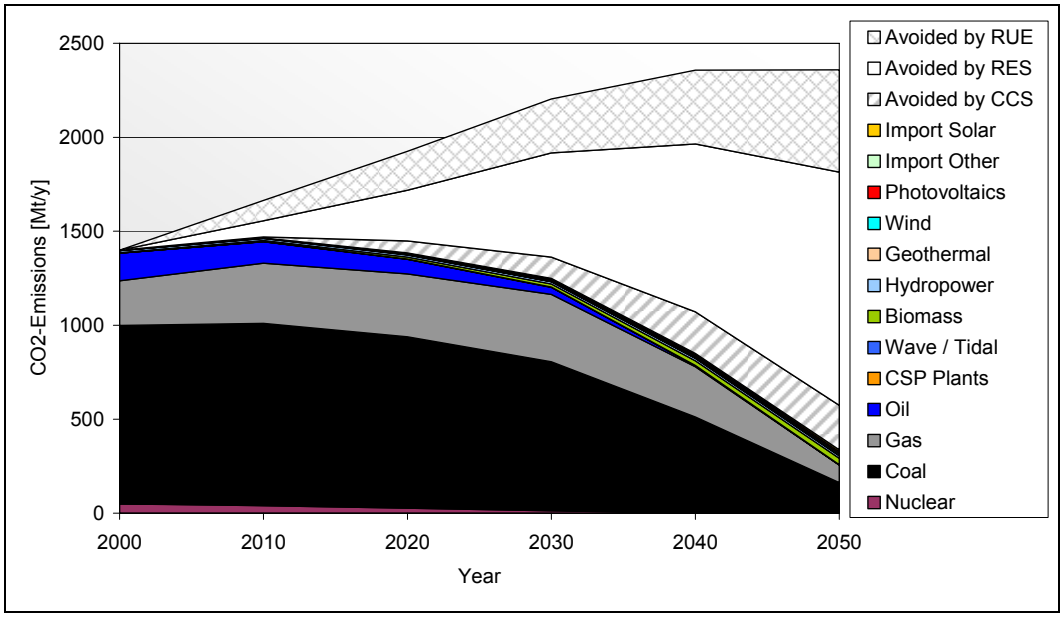

Figure 2-8: CO_2-emissions from power generation in million tons per year for all countries of the TRANS-CSP scenario and emissions avoided by Rational Use of Energy (RUE 22%), Renewable Energy Source (RES 66%) and by Carbon Capture and Sequestration (CCS 12 %) with respect to an electricity mix equivalent to that of the year 2000.

In addition to the TRANS-CSP and MED-CSP studies, results of the EC project ENCOURAGED recently published in (EC, 2007a) and (Vailati et al., 2006) were reviewed. In the frame of ENCOURAGED a comprehensive analysis of electricity corridors between the enlarged EU and the neighbouring countries was done. The study focused on optimised configurations of existing and future corridors and exchanges mainly based on the AC grid interconnections. Several workshops were organised in order to include stakeholders and regional experts which helped to compile information on existing and planned facilities, development strategies and technically and economically characterisations of electricity markets and interconnections.

Transnational interconnections such as the UCTE system (Union for the Coordination of Transmission of Electricity) were basically designed to increase security of supply. The risk of a regional/national supply shortage could be significantly reduced by the possibility of transnational exchange. The UCTE system was initially little used for electricity export/import and therefore resulted in relatively small electricity exchanges. The development of a transnational economic trade in the European electricity market led to an increase of cross border exchanges e.g. between 1998 and 2005 of about 90 %. Because limited cross border connections are becoming a limitation of the European electricity market a priority interconnection plan was established and several concrete projects for an increase of exchange capacities are currently planned or even under construction. An overview of these planned grid infrastructure developments can be found in (EC, 2007a) and in the UCTE Transmission Development Plan (UCTE, 2008). The strategy aims on the one hand for the removal of congestion and bottlenecks within the EU and on the other hand focuses the expansion of the EU power system eastwards and southwards. Therefore ENCOURAGED carried out a mid-term assessment up to the year 2015 focussing internal bottlenecks and also a long term analysis up to 2030 dealing with grid expansion based on a completely developed internal electricity market and cross-border interconnections without congestions.

Electricity corridors are defined in ENCOURAGED as “each point of the system where transmission/interconnection capacity is not adequate, in other words each point of the pan-European system where there could be an additional net socio-economic benefit from additional investments in interconnection capacity”. The optimisation analysis in ENCOURAGED includes cost data gathered from data reviews and a calculation of economic benefits due to the transmission reinforcements. An economic benefit was defined as the economic effect of substituting expensive generation with a cheaper one, including the effect of lower greenhouse gas emissions. Benefits due to increased system reliability and adequacy, increased market competition, improved security of supply, export diversification and internal value for the exporting countries were not explicitly considered in the study. It was assumed that in the long run perspective market

prices for electricity, being the main driver for electricity exchanges, will follow production costs due to liberalised and fully interconnected markets. Electricity production costs include generation costs, load shedding costs and transport fees.

Main results of the mid-term economic optimisation analysis in ENCOURAGED for the year 2015 are described in the following:

- The planned new interconnection (2000 MW) between Turkey and Central Europe is used for energy export to Central Europe of about 17 TWh in 2015.
- Due to low efficiency power plants in Russia and Ukraine, these countries increase their electricity import from Central Europe, NORDEL and Baltic region to about 50 TWh. If an additional generation capacity of 6 GW can be realised in Russia (nuclear power plants were assumed in ENCOURAGED), this region becomes a net exporter of electricity to Europe.
- If new transfer capacities from North Africa to Italy and Spain/Portugal of each 1000 MW and surplus generation capacities (gas power plants) of 2000 MW are assumed, an export to Europe of 25 TWh was calculated. This is partly induced by the absence of CO_2 extra-costs (emission trading) for gas-fired power generation in North Africa which results in cost advantages but does not support climate protection.
- Average reduced costs (marginal benefit/reduction of costs for transfer capacity in the entire system) are below 2 €/MW for additional interconnections within Europe, 6 to 7 €/MW for interconnections to Turkey and 9.5 €/MW (reference scenario) resp. 18 €/MW (scenario with high gas and oil prices) to North Africa.

The following main results of the long-term economic optimisation analysis for 2030 were discussed in ENCOURAGED (see also Table 2-3):

- Due to the increasing electricity demand – especially in the neighbouring regions – electricity exchanges in the analysed pan-European region are expected to be a small percentage (~ 2%, 170 TWh) of the total demand of about 8000 TWh in 2030 (4700 TWh demand in EU27 in 2030).
- However, a massive increase of transfer and generation capacities has to be assumed to calculate this relatively small contribution to European energy import.
- In the reference case, significant power flows are expected from North Africa to Southern Europe (25 TWh) and from Turkey to South-Eastern Europe (15 TWh) with a utilisation of more than 90 % of the transfer capacities assumed to be available until 2030. Electricity was assumed to be produced by new gas-fired power plants in these regions (low gas price, no CO_2 extra costs). Exchanges from North Africa can be increased up to 41 TWh, if an increase of transfer capacity up to 4700 MW is realised (new HVDC connections).

- There will be a bi-directional exchange between Russian Federation/Ukraine and Europe depending on seasonal effects and the European region considered. The bi-directional exchange was estimated to be about 40 TWh in the reference case. If a massive increase (factor two, 25 GW) of the Russian nuclear power plant capacity was assumed, a net export of 40 TWh resulted.
- Average reduced costs (reduction of costs for the entire system) shows the highest values for the interconnection North Africa – Europe of 6 €/MW up to 9 €/MW (corresponding to 50,000 – 80,000 €/year reduction of supply system costs due to power exchange with a 1 MW increase of net transfer capacity).

Table 2-3: Results of ENCOURAGED project: Modelled electricity import to EU in 2030.

Corridor	Maximal import to EU 2030	Share of consumption in EU 27 in 2030	Scenario assumptions
Reference case with moderate reinforcements			
North Africa – UCTE	25 TWh	0,5%	2700 MW HVAC/DC transfer capacity, massive increase of gas power generation
Turkey – UCTE	15 TWh	0,3%	2000 MW HVAC transfer capacity, massive increase of gas/hydro power generation
Russia – UCTE	-8 TWh	-	Existing 5100 MW HVAC transfer capacity, IPS/UPS connection to UCTE
Russia – Baltic	10 TWh	0,2%	Existing 2700 MW HVAC transfer capacity
Russia – NORDEL	4 TWh	0,1%	2200 MW HVAC transfer capacity
Maximum case of economic assessment			
North Africa – UCTE	41 TWh	0,9%	4700 MW HVAC/DC transfer capacity, massive increase of gas power generation
Turkey – UCTE	32 TWh	0,7%	5000 MW HVAC transfer capacity, massive increase of gas/hydro power generation
Russia – UCTE	40 TWh	0,9%	Existing 5100 MW HVAC transfer capacity, IPS/UPS connection to UCTE; massive increase of nuclear power generation of 25 GW

ENCOURAGED project provided important results regarding strategies for and benefits of improved energy interconnections between UCTE transmission grid (HVAC) and neighbouring regions. The main objectives of this study were an analysis of mid-term grid reinforcements for the removal of grid bottlenecks and cost reduced supply of future demand due to increased energy exchanges. However, model results show only relative small energy exchanges between the model regions until 2030. Net imports to EU27 of maximal 110 TWh per year (~2.5 % of expected EU27 electricity demand in 2030) occur if a strong increase of generation capacities were assumed for Turkey, North Africa and Russia.

Complementary to results of ENCOURAGED, this study analyses solar electricity import via HVDC lines as an additional and virtually unlimited energy resource which may provide a renewable electricity import of about 15% to 20% of EU27 demand

until 2050. Import corridors and potentials based on specific scenario assumptions made in the frame of ENCOURAGED - such as additional gas power capacities in regions outside the CO_2 emission trading system or a massive increase of nuclear power generation in Russia - were not considered, as import potentials for fossil/nuclear energy carriers are already covered in REACCESS by other WP2 and WP3 Tasks.

Beneficial for a sustainable European import strategy might be also other renewable import options than CSP, which were analysed based on (Skjølsvik, 2007), (Evrendilek & Ertekin, 2003), (Dmitriev, 2001), (WEC, 2007) and (Trieb et al., 2005). Table 2-4 summarises estimations for renewable capabilities which may represent export options of these countries compared to their 2005 exploitation/generation and electricity demand (derived from (Vailati et al., 2006), (Trieb et al., 2005) and (IEA, 2007)). Potential exports from Norway and Iceland are part of the internal European electricity trade which is already represented in the energy system models. Main renewable potential suitable for import in EU27 seems to be hydro power from Russia. However, as this potential would be mainly due to the construction of large dams its implementation may cause significant environmental impacts - a fact which reduces the probability of the option. The rising electricity demand in Russia and the need for an increased deployment of renewable sources will also lead to an increasing use of hydro power for domestic electricity supply. Renewable economic potentials of Turkey are rather small compared to its rising demand. Estimated economic exploitable capability for wind power from Russia also appears to be small although the overall technical potential is huge. Due to the highly fluctuating power generation using wind energy and the resulting low full load hours an import of wind electricity is in general far less attractive than the import of solar electricity from the MENA region. Due to the aforementioned constraints, capabilities of Turkey and Russia as well as wind power from the MENA region were not included in the REACCESS database. Nevertheless they might also contribute to some limited extent to the import of electricity in the long term future.

Table 2-4: Other renewable capabilities (without solar) for electricity export compared to current generation and electricity demand of the countries.

	Generation 2005 [TWh]	Demand 2005 [TWh]	Estim. demand 2030 [TWh]	Techn. exploit. capability [TWh/a]	Econ. exploit. capability [TWh/a]
Hydro power					
Turkey	35	129	530	216	130
Iceland	7	8	9	64	40
Norway	136	112	130	200	187
Russia	165	650	1150	1670	852*
Geothermal power					
Iceland	1.7	8	9		20
Wind power					
Turkey	0.06	129	530	~170	50
Jordan	0.003	8.4	27	109	2
Saudi-Arabia	0	135	268	300	20
Algeria	0	26.7	145	7278	35
Libya	0	16.9	27	5363	15
Egypt	0.55	87.5	312	7650	90
Tunisia	0.042	11.2	40	50	8
Morocco	0.206	17.6	116	1188	25
Norway offshore	0.5	112	130	14,000 (0-300m)	125 (0-30m)
Norway onshore				1165	76
Russia “Europe”	0.02	650	1150	2308	90**
Russia “East”				3910	?

* mainly large dams

** existing economical potential in Russia according to P. Bezrukikh, Energy Strategy Institute, Moscow

3 EXPORT POTENTIALS – RESOURCES AND PRODUCTION

3.1 SOLAR ENERGY RESOURCES IN POTENTIAL EXPORT COUNTRIES

3.1.1 Solar Energy Resource Assessment

Planning and control of concentrating solar systems like parabolic troughs, Fresnel technology, heliostats or dish-Stirling systems need information about the direct fraction of solar radiation. Contrary to the diffuse fraction this beam irradiance can be focused in order to yield higher energy flux densities at the receiver. The direct normal irradiance (DNI) serves as reference for those systems. DNI is defined as the radiant flux density in the solar spectrum (0.3 μm to 3 μm) incident at the earth's surface perpendicular to the direction to the sun integrated over a small cone tracing the sun.

The German Aerospace Center (DLR) has developed a method that models the optical transparency of the atmosphere to calculate the Direct Normal Irradiance (DNI) on the ground at any time and any site, by detecting and quantifying those atmospheric components that absorb or reflect the sunlight, like clouds, aerosols, water vapour, ozone, gases and other. Most of this information is derived from satellite remote sensing (Schillings et al., 2004). The DNI is the natural energy source for Concentrating Solar Power Stations (CSP).

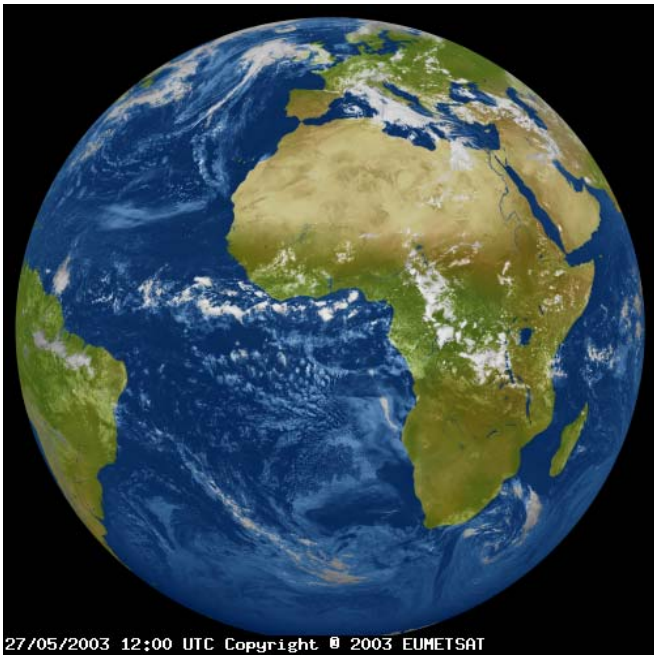

Figure 3-1: View of METEOSAT 7 weather satellite from geostationary orbit at 36,000 km, visible channel.

Weather satellites like Meteosat-7 from the European Organization for the Exploitation of Meteorological Satellites (EUMETSAT) are geo-stationary satellites at a distance of 36,000 km at a fix point over the globe that send half-hourly images for weather forecasting and other purposes (Figure 3-1). From those images, the optical thickness of clouds can be derived obtaining half-hourly cloud values for every site. Of all atmospheric components, clouds have the strongest impact on the direct irradiation intensity on the ground. Therefore, a very high spatial (5 x 5 km or better) and temporal (0.5 hour or better) resolution is required for this atmospheric component. A long-term archive established at DLR allows the extraction of specific time series and specific sectors of the total data set for specific regions and time slots to be analyzed (SOLEMI, 2008).

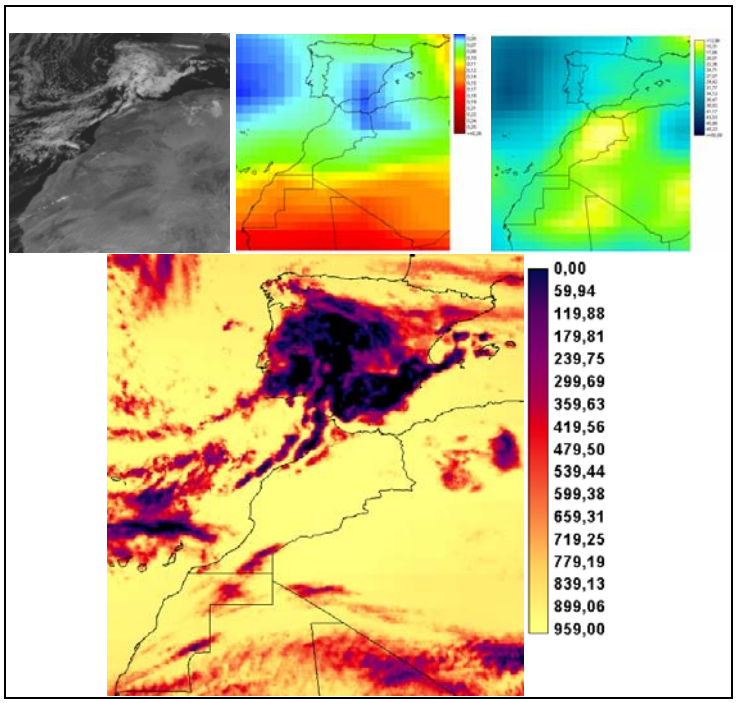

Figure 3-2: Original image from METEOSAT 7 (top left), aerosol content from GACP (top centre), water vapour content from NCAR-NCEP (top right) and resulting map of the hourly Direct Normal Irradiance (bottom) in Wh/m² for the Iberian Peninsula and the Maghreb Region on February 7, 2003, 12:00 (SOLEMI, 2008).

Aerosols, water vapour, ozone etc. have less impact on solar irradiation than clouds. Their atmospheric content can be derived from several orbiting satellite missions like NOAA and from re-analysis projects like GACP or NCEP/NCAR and transformed into corresponding maps/layers of their optical thickness. The spatial and temporal resolution of these data sets can be lower than that of clouds. The elevation above sea level also plays an important role as it defines the thickness of the atmosphere. It

is considered by a digital elevation model with 1 x 1 km spatial resolution. All layers are combined to yield the overall optical transparency of the atmosphere for every hour of the year. Knowing the extraterrestrial solar radiation intensity and the varying angle of incidence according to local time, the direct normal irradiation can be calculated for every site and for every hour of the year. Electronic maps and geographic information system (GIS) data of the annual sum of direct normal irradiation can now be generated as well as hourly time series for every single site. The mean bias error of the annual sum of direct normal irradiation is typically in the order of ± 8 %.

The analysis was made for the countries of the Middle East and North Africa (MENA) as shown in Figure 3-4 for the year 2002. For concrete project development, performance analysis and site assessment of solar power stations, at least 5-15 years of data should be processed, as the inter-annual climatic fluctuations can be in the range of ± 15 %. However, for the assessment of the total solar electricity potential and its geographic distribution within large regions, a one-year basis is good enough, especially because in most MENA countries, the total solar energy potential is some orders of magnitude higher than the demand.

Figure 3-3 shows schematically a solar ray on its way through the atmosphere and the main atmospheric components which attenuate the ray. The diminishment is originated by the absorption by ozone, the Rayleigh-scattering and absorption by air molecules, the scattering and absorption by aerosols, the reflection, scattering and absorption by clouds and the absorption by water vapour. All shown atmospheric components are taken into account by the used model.

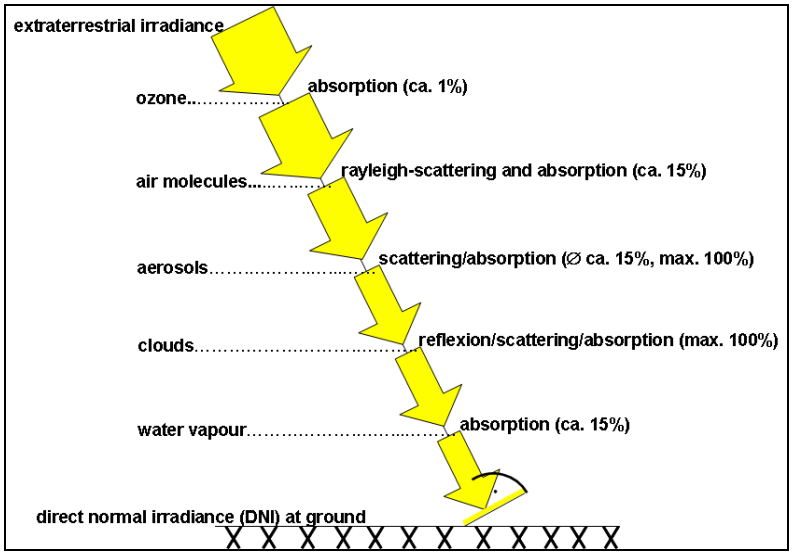

Figure 3-3: The attenuation of radiation by the atmospheric components.

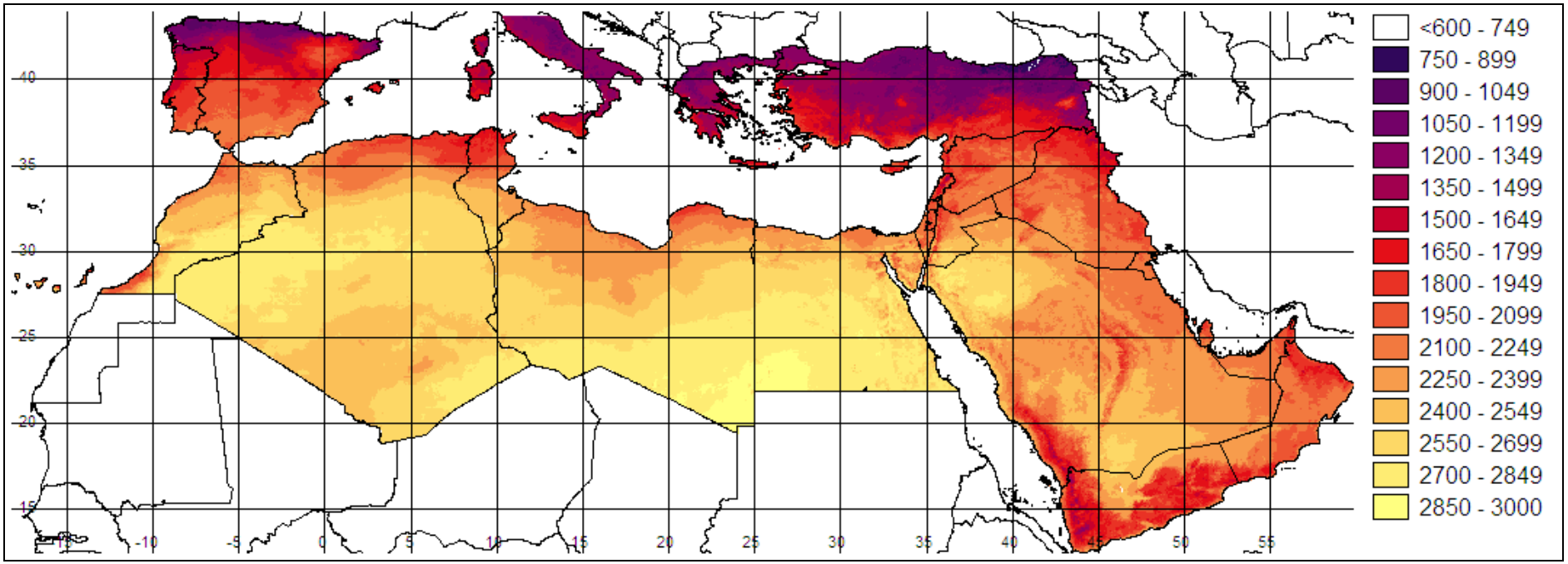

Figure 3-4: Direct Normal Irradiance of the year 2002 in kWh/m²/y (Source: DLR 2005).

The calculation of solar direct normal irradiance at the ground is based on a clear-sky parameterisation model developed by Bird (1981) and modified by Iqbal (1983). Accuracy assessments and detailed comparisons with other parameterisation models in several studies (Gueymard, 1993; Battles et al., 2000) have shown that this model performs as one of the best for clear-sky conditions. Bird's clear-sky-model needs atmospheric input data on Oxigen O_2, Carbon Dioxide CO_2, Ozone O_3, water vapour and aerosol optical thickness to calculate the broad-band DNI. To use this model also for cloudy-sky conditions a transmission coefficient for clouds is added based on a cloud detection algorithm developed by Mannstein et al. (1999) and (Schillings et al., 2004).

Using the eccentricity corrected solar constant

$$E_0 = \overline{E}_0 \left(\frac{\overline{r}}{r} \right)^2 = \overline{E}_0 \left(1 + 0.033 \cos \frac{2\pi \times doy}{365} \right) \qquad \text{Equation (1)}$$

with the mean earth-sun distance $\overline{r}$, the actual earth-sun distance r, the day of year doy and the solar constant ($\overline{E}_0$ =1376 W/m²), the broadband DNI can be calculated with

$$DNI = E_0 \cdot \tau_R \cdot \tau_{Gas} \cdot \tau_{Ozone} \cdot \tau_{WV} \cdot \tau_{Ae} \cdot \tau_{Cl} \qquad \text{Equation (2)}$$

with the transmission coefficients for the attenuation by Rayleigh-scattering τ_R, for the attenuation by absorption of equally distributed gases (mainly CO_2 and O_2) τ_{Gas}, for the attenuation by absorption of atmospheric O_3 τ_{Ozone}, for the attenuation by absorption of water vapour τ_{WV}, for the attenuation by extinction of aerosols τ_{Ae} and for the attenuation by extinction of clouds τ_{Cl}.

The functions to derive the transmission coefficients shown in Equation 2 can be found in detail in (Iqbal, 1983) and (Schillings, 2004). The DNI can be calculated for each point of time of the year if the actual air mass is known.

The atmospheric parameters attenuate the incoming direct solar irradiance to a different extent. As shown in Figure 3-5 the DNI is mostly influenced by clouds, followed by aerosol, water vapour, Rayleigh scattering, O_3, O_2 and CO_2. The figure gives an example for a daily curve of DNI at ground and the attenuation by the different atmospheric components calculated by the method presented here. Although the clear-sky input parameters are constant during the day, their influence on the attenuation is stronger for higher zenith angles (in the morning and evening hours) due to the increased airmass. Information on clouds is based on hourly values as it can be seen in the constant DNI values for the parameter clouds for each hour. The extraterrestrial irradiance is constant from dawn until dusk due to the irradiated surface that is kept perpendicular to the incoming solar rays. As clouds and aerosols

have the strongest influence on the direct irradiance and are highly variable in space and time, data of these parameters should be as accurate as possible.

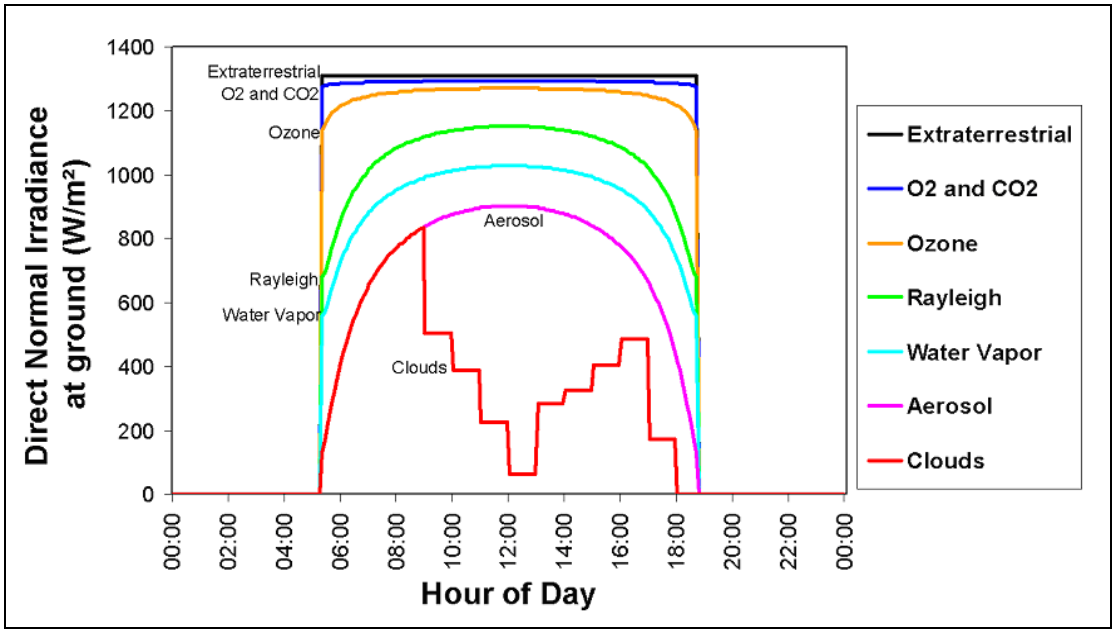

Figure 3-5: Example of daily irradiance variation for true solar time showing the influence of the different atmospheric constituents on the direct normal irradiance. Values are calculated by the method presented here.

The temporal and spatial variability of the accuracy for these parameters can not easily be described for a global scale. It strongly depends on the investigated region. The data are partly or completely derived from satellite remote sensing methods. The accuracy depends on the regional land properties like surface structure, homo- or heterogeneity of the surface, land-sea distribution etc. The used atmospheric data can easily be substituted if data with higher spatial and temporal resolution and higher accuracy become available.

All parameters described below are calculated having regard to the air mass that is influenced by the solar zenith angle and the geographical elevation over sea level for the investigated site. Following global atmospheric data sets, which are easily accessible through the internet, are used to derive the clear-sky attenuation:

Airmass

The attenuation of the radiation by the atmospheric components depends on the solar zenith angle Θ_Z, the air density and the site elevation. The relative optical airmass is defined as the ratio of the optical path along the oblique trajectory to the

vertical path in the zenith direction (Iqbal, 1983). Ignoring the earth's curvature and assuming that the atmosphere is non-refractive and completely homogenous (see Figure 3-6a), it can be seen that the relative optical airmass is

$$am = \frac{1}{\cos \Theta_Z} \qquad \text{Equation (3)}$$

with am = relative optical airmass []

θ_z = solar zenith angle [°]

However, density is actually variable with the height. Furthermore, because of the curvature of the earth and refraction of the atmosphere, the slant path of the beam radiation will follow of the path OP as shown in Figure 3-6b.

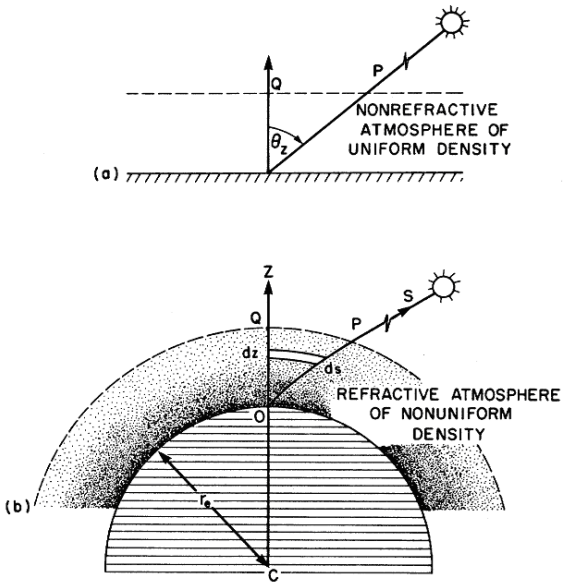

Figure 3-6: The trajectory of a solar ray through the earth's atmosphere. (a) Nonrefractive plane parallel atmosphere of uniform density. (b) Refractive spherical atmosphere of variable density. (Iqbal, 1983).

Kasten (1966) developed a function that takes into account the air density.

$$am = \frac{1}{\left[\cos\Theta_Z + 0.15(93.885 - \Theta_Z)\right]^{-1.253}} \qquad \text{Equation (4)}$$

with: am = relative optical airmass []

θ_z = solar zenith angle [°]

This equation is applicable to a standard pressure of 1012.25 mbars at sea level. For other pressures it should be modified with (Iqbal, 1983):

$$p = p_0 \cdot exp\left(-0.0001184 \cdot \frac{z}{m}\right) \qquad \text{Equation (5)}$$

$$am_p = am \cdot \frac{p}{1013.25hPa} \qquad \text{Equation (6)}$$

with: am_p = pressure corrected airmass []

am = relative optical airmass []

p = pressure at station [*hPa*]

or using the elevation in [m] with (Iqbal, 1983):

$$p = p_0 \cdot exp\left(-0.0001184 \cdot \frac{z}{m}\right) \qquad \text{Equation (7)}$$

with: p = pressure at station [*hPa*]

p_0 = pressure at sea level [*hPa*]

z = elevation above sea level [*m*]

Elevation

As described above, the elevation for each site is needed for the correct airmass determination. This parameter can be derived from Digital Elevation Models (DEM) which can provide global elevation information. For this study the Global Land One-km Base Elevation Digital Elevation Model (GLOBE) as shown in Figure 3-7 is used. This DEM has a spatial resolution of 30''. (Hastings & Dunbar, 1999)

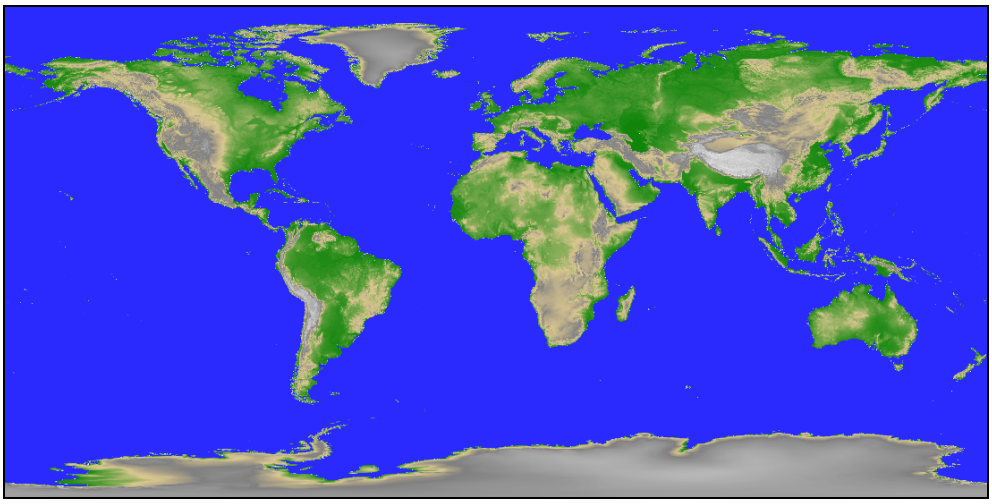

Figure 3-7: Elevation in [m] based on GLOBE. (Hastings & Dunbar, 1999).

Rayleigh Scattering and Equally Distributed Gases

The Rayleigh scattering of the clear atmosphere and the absorption of equally distributed gas, mainly CO_2 and O_2 are taken into account using fixed values for the atmospheric components based on the U.S. Standard Atmosphere 1976 (U.S. Department of commerce, 1976).

Ozone

Ozone absorbs radiation mainly at wavelengths smaller than 0.3 µm. Thus, the broadband attenuation of DNI influenced by ozone is relatively small. The variability of ozone depends on the geographical latitude and the season. In the sunbelt ozone varies in the range from about 0.2 to about 0.4 cm [NTP] with moderate seasonal variability and a slightly decrease through the years. This affects the DNI on ground in the magnitude of lower 1%. Therefore the use of monthly mean values with a spatial resolution of 1° x 1.25° derived by the Total Ozone Mapping Spectrometer (TOMS onboard NASA's Earth Probe satellite) as input parameter is sufficient. The uncertainty of TOMS long-term mean values is indicated with 1% (McPeters et al., 1998).

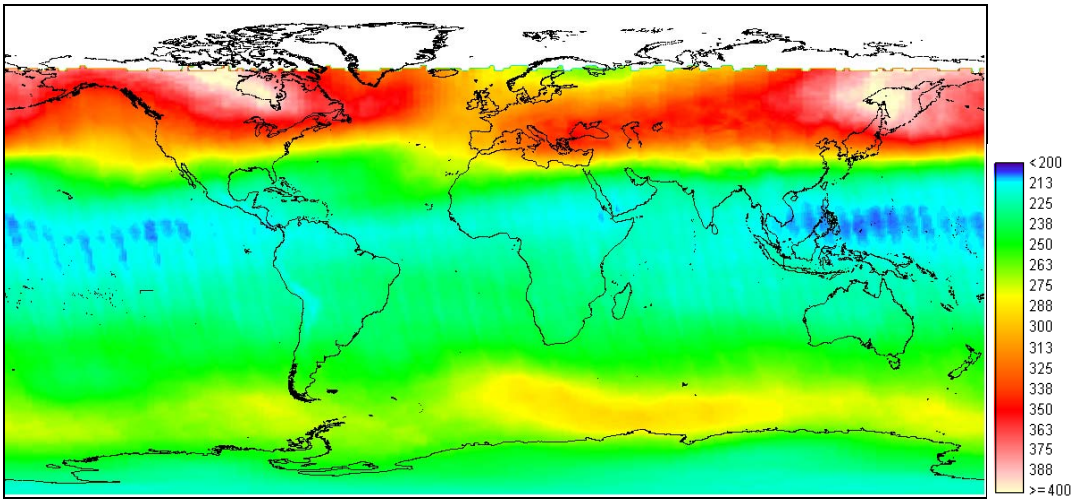

Figure 3-8: Monthly mean ozone for February 2002 in [DU] based on TOMS. (McPeters et al., 1998).

Water-Vapour

Water Vapour absorbs radiation mainly at thermal wavelengths. Its influence on the broadband attenuation is larger than that of ozone. Analysing data of a 4-year monthly means for the sunbelt (10°-40° N/S) the mean spatial variability for the investigated latitudes ranges from about 0.5 to about 6.5 cm[NTP] which results in a DNI-variability of up to 15%. Due to this high variability we use daily values of precipitable water from NCEP-Reanalysis of the Climate Diagnostic Center (CDC-NOAA) with a spatial resolution of 2.5° x 2.5°. These values are computed using daily mean values of the NCEP Reanalysis, based on 6-hour values. The calculated fields are divided into four quality classes (A,B,C,D) depending on the relative influence of the used input data which can be measured or modelled. The precipitable water data set is declared as a 'B'-class value. This means that there is a strong modelling component although measured data is also used. More information about the NCEP-Reanalysis can be found in (Kalnay et al., 1996). The used data are interpolated to a 1° x 1° grid, consistent to the other atmospheric input data.

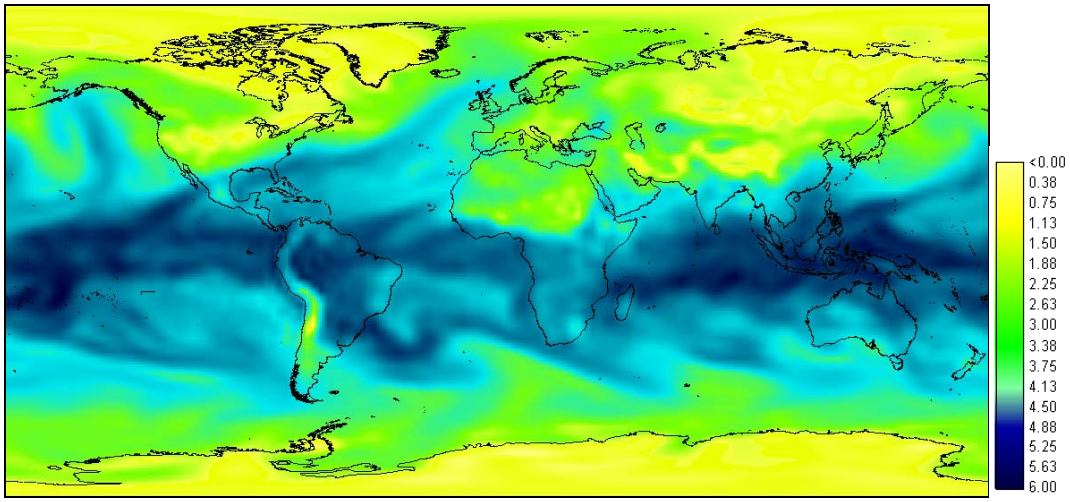

Figure 3-9: Daily mean of water vapour for the day 07.02.2002 in cm[NTP] based on NCEP/ NCAR-Reanalysis.

Aerosols

Aerosols are small solid or liquid particles that remains suspended in the air follows the motion of the air within certain broad limits. In contrast to molecules of the permanent atmospheric gases, suspended particles within the atmosphere display considerable diversity in volume, size, distribution, form and material composition. Such particles are for example dust, pollen, sea salt, black carbon etc. Aerosols have a strong influence on the solar beam irradiance at clear-sky conditions. Detailed information on aerosol optical thickness (AOT) in a high temporal and spatial resolution is not yet available in a global scale. Such information would be useful because of the high spatial and temporal variability of aerosols. Depending on the region, AOT can be in the range from 0.05 for clear coastal regions to greater than 2 for regions affected by desert dust or soot. This can affect the DNI on ground by a decreasing of down close to 0 W/m² (e.g. in a desert storm). A compromise between global availability and an appropriate spatial and temporal resolution was found in the climatological values of AOT derived by a transport model from the Global Aerosol Climatology Project (NASA-GACP). This project was started 1998 within the NASA Radiation Sciences Program and the Global Energy and Water Cycle Experiment (GEWEX). GACP bases on the combination of global distributions of aerosol loading resulting from transport models for soil dust, sea salt, sulphate aerosols and carbonaceous aerosols. The used GACP model and the accuracy of the modelled aerosol optical thickness is described in (Tegen et al., 1997), (Chin et al., 2002) and (Penner et al., 2002). More information on GACP can be found in (Mishchenko et al., 2002). The used data are interpolated to a 1° x 1° grid, consistent to the other atmospheric input data.

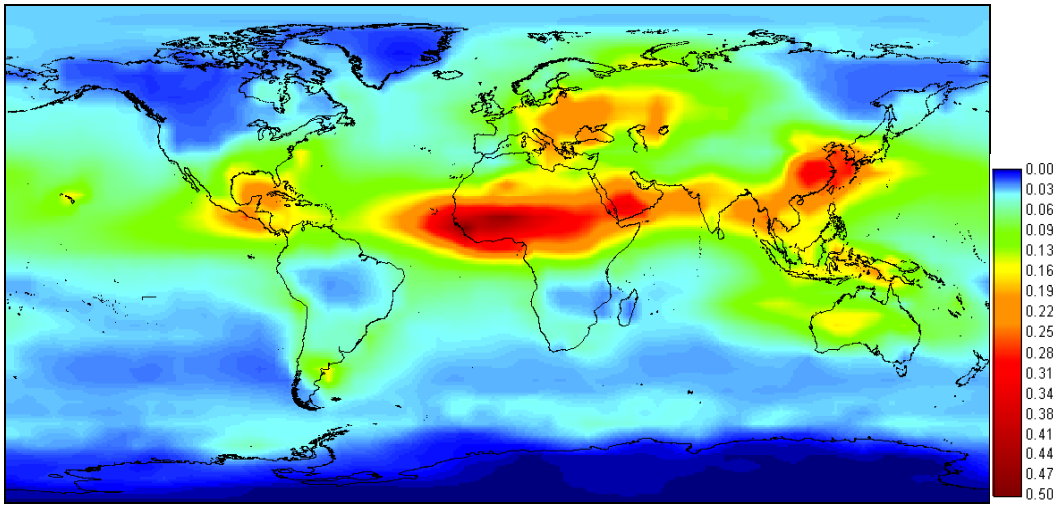

Figure 3-10: Aerosol optical thickness (AOT) for the wavelength of 550 nm for February based on GACP-climatology. (Mishchenko et al., 2002).

Using this data despite the high influence of aerosols is only a rough assumption, but global transport models that are validated against ground-based measurements can provide a first estimate of global aerosol distribution in space and time. We plan to use more detailed aerosol data derived by new satellites (e.g. ENVISAT) in the near future.

Cloud Parameterisation

Solar irradiance at ground is mostly affected by clouds. In fact, beam irradiance can decrease close down to 0 W/m² due to clouds even during daylight, in contrast to global irradiance that is always substantially greater than 0 W/m² due to its diffuse fraction. Additionally, clouds have a high variability in space and time. Strong influence and high variability lead to a need of information on clouds in a high temporal and spatial resolution to meet the demand of accurate solar irradiance data at ground.

The clouds detection algorithm developed by Mannstein (1999) uses data of the geostationary satellite Meteosat (Meteorological Satellite) to calculate hourly information on the clouds in a spatial resolution of up to 5 x 5 km². The bispectral cloud detection scheme uses infrared (IR) and visible (VIS) channels from the Meteosat-7 satellite. It is based on self adjusting, local thresholds which represent the surface conditions undisturbed by clouds. The calculated cloud-index (CI) is in the range of 0 for no clouds to 100 for completely cloudy pixels with high optical depth. CI represents the effective cloud transmission which is an integral value influenced by the cloud amount and by the average cloud optical depth within the analysed pixel. For each region within the Meteosat full disk shown in Figure 3-11 the

detection algorithm can be performed. Due to the spatial range and the possible marginal position of the selected area of investigation within the Meteosat full-disk, the spatial resolution of the cloud cover can range from 5 x 5 km² at the sub-satellite point to about 10 x 10 km² at marginal positions of the image.

Figure 3-11: Example image of the Meteosat data used to derive the cloud index (Meteosat-7, coloured IR-Channel). © EUMETSAT, 2005.

In both spectral channels the basic principle of the algorithm is the same:

- Construct a reference image without clouds from previous images
- Compare the actual image to the reference image to detect clouds
- Update the information for the construction of the reference image using the cloud-free pixels.

Nevertheless there are differences in processing of both channels:

IR-Scheme

The crucial task for getting a good estimate of cloud cover from an IR channel is the definition of a local temperature threshold as reference temperature which is close to the temperature of the cloud-free surface. As surface observations are difficult to access and not available in a sufficient temporal and spatial resolution, we have to

derive the reference temperature from the Meteosat data itself. To achieve this, we sort the available images as a 3-dimensional array for each day with the spatial coordinates X and Y and the temporal coordinates T (time, every half hour, from 1 to 48). Single missing images do not affect this routine. The reference temperature of land surface as shown in Figure 3-12 is described by the following parametric function for every pixel:

$$T = a_0 + a_1\left(\cos\left(x - a_3 + \sin\left(a_2\right)\cdot\sin\left(x - a_3\right)\right) + 0.1\cdot\sin\left(x - a_3\right)\right) \qquad \text{Equation (8)}$$

with x = t/24 * 2π and t = decimal hours of the satellite scan (UTC). a_0 gives the daily mean temperature, a_1 the temperature amplitude, a_2 influences the width and steepness of the daily temperature wave and a_3 gives the phase shift which is dominated by the local solar time. These four parameters are fitted daily for each land-pixel using the cloud-free pixels.

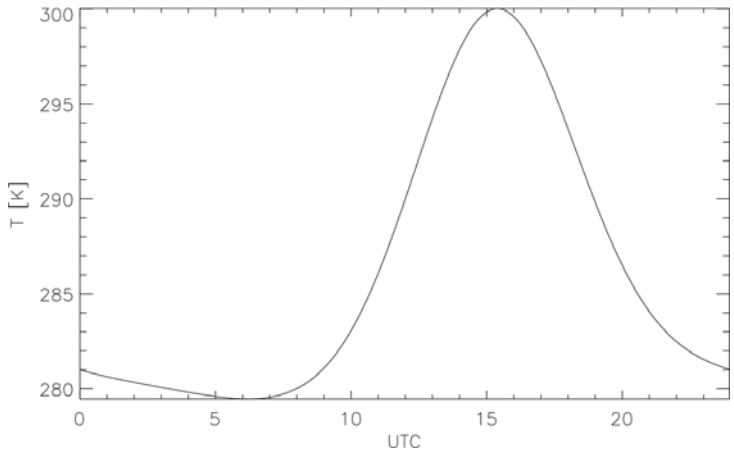

Figure 3-12: Daily background temperature curve for a pixel over land surface derived from the fitting parameters a0=290, a1=10, a2=1 and a3=4 which are calculated by the IR-scheme.

Over sea only a_0 is variable, the other coefficients are set to zero (the temperature over sea is kept constant during one day).

The parameters are fitted from those pixels, which are with a high probability not contaminated by clouds and therefore representing the temperature of the land surface as it is measured by the satellite without any atmospheric correction. After the processing of 48 half-hourly images, we make an update on the coefficients a_0 to

a_3. Both, new cloud-free temperature values and the old coefficients enter into the new fit of the coefficients, which enables us to remember the surface properties even during longer cloudy periods. The influence of the new surface temperature is weighted depending on the elapsed time to the last cloud-free scene and the quality of the new data.

We use the following properties of surface versus clouds for a first cloud detection:

- Clouds are cold. Every pixel with a temperature colder than the estimated reference temperature is valued as cloud. There is also an absolute limit which depends on the region under consideration.
- Clouds move. We compare the data to the previous image and the image of the day before. Clouds are colder and show up as local differences.
- Surface temperature has a regular daily variation and depends on the landscape. We compare the data to the predicted image. Clouds again show up as local differences.
- Weather patterns have a larger scale than pixel size. We allow for deviations from the predicted temperatures if they are of the same magnitude within regions of pixels with similar surface properties. This information is used to make an additive update of the predicted surface temperature.

As the quality of the predicted data is variable, the decision process depends on weights similar to a fuzzy-logic decision. Figure 3-13 shows the IR-cloud detection scheme for the defined window for the date of July 9, 2001, 12:00 UTC. The actual IR-image is shown in (a) with the measured temperature in °C. The mean temperature a_0 is given in (b); (c) shows the temperature amplitude a_1 which is constant zero for the sea and therefore consistent black. Over land a_1 varies depending on the surface properties: the brighter the pixel the higher the difference between day and night temperatures. The cloud-free reference temperature for 12:00 UTC is shown in (d). The result is presented in (e) where the surface features vanished nearly completely.

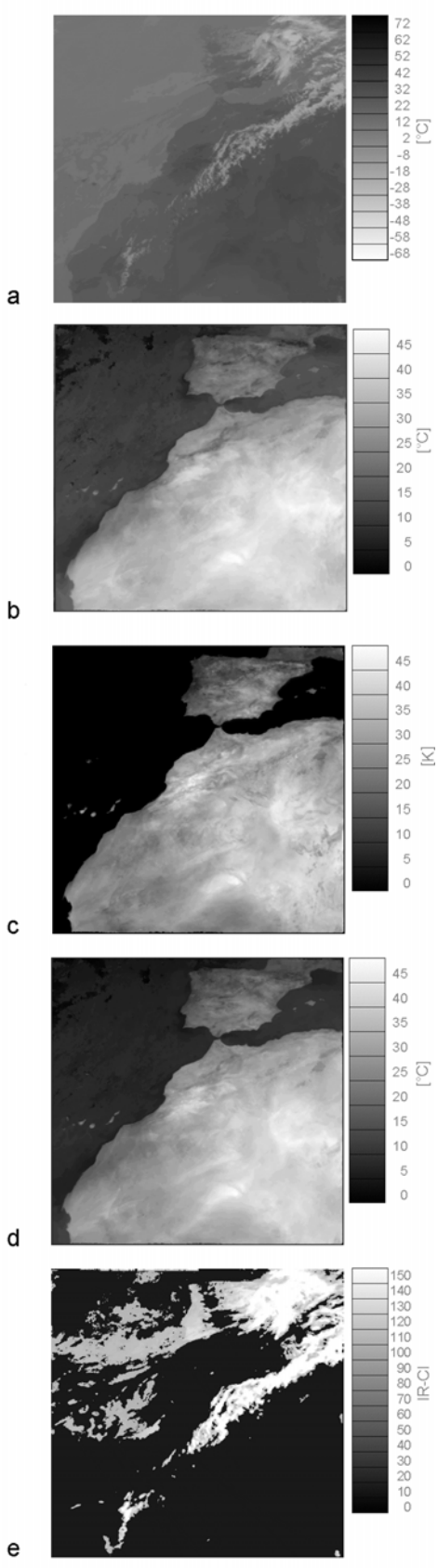

Figure 3-13:
Scheme of the IR-cloud-detection for the defined window: (a): actual IR-image; (b) coefficient a0 (mean daily temperature); (c) coefficient a1 (temperature amplitude); (d) calculated cloud free reference-image (reference-temperature); (e) difference between (d) and (a). All images refer to the date July 9, 2001, 12:00 UTC.

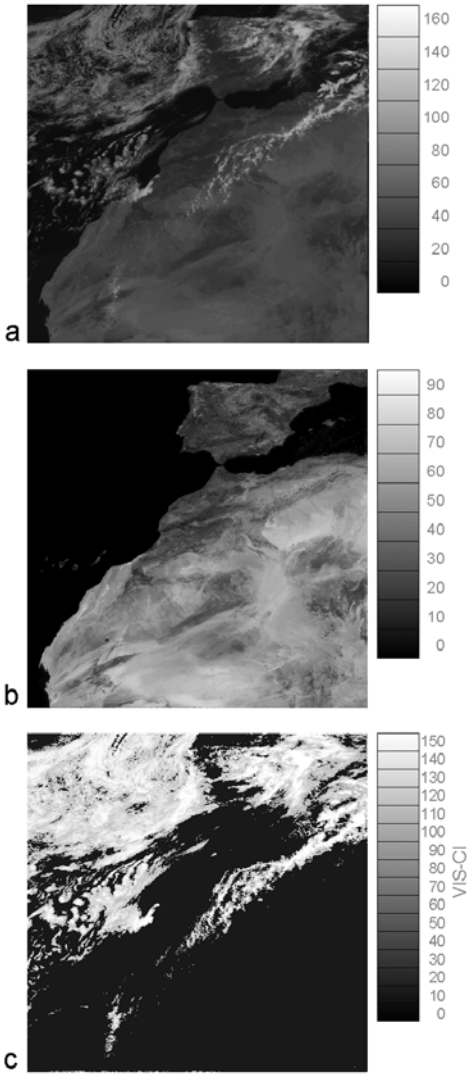

Figure 3-14:
(a) Actual Meteosat VIS data; (b) calculated reference image (c) difference between calculated cloud-free reference image (b) and actual Meteosat data (a). All images refer to the date July 9, 2001, 12:00 UTC.

VIS-Scheme

Different from the infrared data, the daily variation of the reflected sunlight data is mainly influenced by geometrical factors. The Meteosat counts are first corrected against the local solar zenith angle. For further corrections we analysed one year of VIS data to extract the distribution of counts with respect to solar zenith angle and the angular distance to specular reflection.

We selected the 1% percentile to represent the mini-mum count which is subtracted from the data to ac-count for atmospheric influences like forward and backward scattering within the atmosphere. VIS data is included into the decision process at locations, where the cosine of the solar zenith angle is greater than 0.1 (the sun is more than 5.7° over the horizon).

The VIS information is weighted proportional to the cosine of the solar zenith angle. Similar to the IR, we derive from the data a reference image, which is in this case not variable throughout the day. The actual VIS images are compared against the

predicted reference image and the previous image. The corrected count has to be higher than a threshold derived from the predicted 'cloud-free' scene. Figure 3-14 shows the actual VIS-image (a), the reference image (b) and the resulting image (c).

Cloud Index

From the IR and VIS channels, a cloud index is derived by linear interpolation between the expected 'cloud-free value' and a threshold for a 'fully cloudy' pixel (-40°C in the IR and a corrected count of 150 in the VIS channel). Both, IR and VIS information are combined to select those values that are used for the update of the clear-sky properties and also for the final calculation for the cloud-index CI. The self-learning cloud-algorithm needs several days lead time to calculate the reference fit. To simulate hourly mean values we have chosen a simple filter which weights the scenes before and after the nominal time with 25%, while the scene at nominal time is weighted with 50%. E.g., the cloud index value for 12 UTC is the weighted mean value from the indices derived from the nominal times at 11:00, 11:30 and 12:00, where the half hour gets a double weight.

Accuracy of Derived DNI

The validation takes into account two measurements sites in Brazil, four in Spain and one in Morocco. From the inter-comparisons at these 7 different sites we conclude that the derivation of the long-term average from satellite data without further proof by measurements has reached a high level of confidence. The maximum underestimation against measurements is observed with a relative root mean bias deviation (rMBD) of -6.0% for the site Caico in Northeastern Brazil. The maximum overestimation of the satellite-derived values is noticed for Tabernas in Southern Spain at the Plataforma Solar de Almeria with an rMBD of +2.0%. It must be noted, that in principal the given accuracy of the satellite-derived values depends on the quality of the measurements used for validation. Therefore additionally the average measurement error of 3% has to be taken into account. Applying Gaussian error propagation finally a 1 sigma accuracy of 5% for the long-term satellite-derived DNI-values is derived. (Meyer et al., 2004)

Figure 3-15 shows the hourly monthly mean values for DNI for a site in Spain. The solar regime of the measured ground data (top) is very well represented by the satellite-based radiation data (bottom).

Figure 3-16 gives example hourly values for DNI for a validation site. Ground data are marked black-dotted, remote (satellite) data are marked red-solid. The curves

give an idea on how accurate the satellite-based DNI represents the measured values.

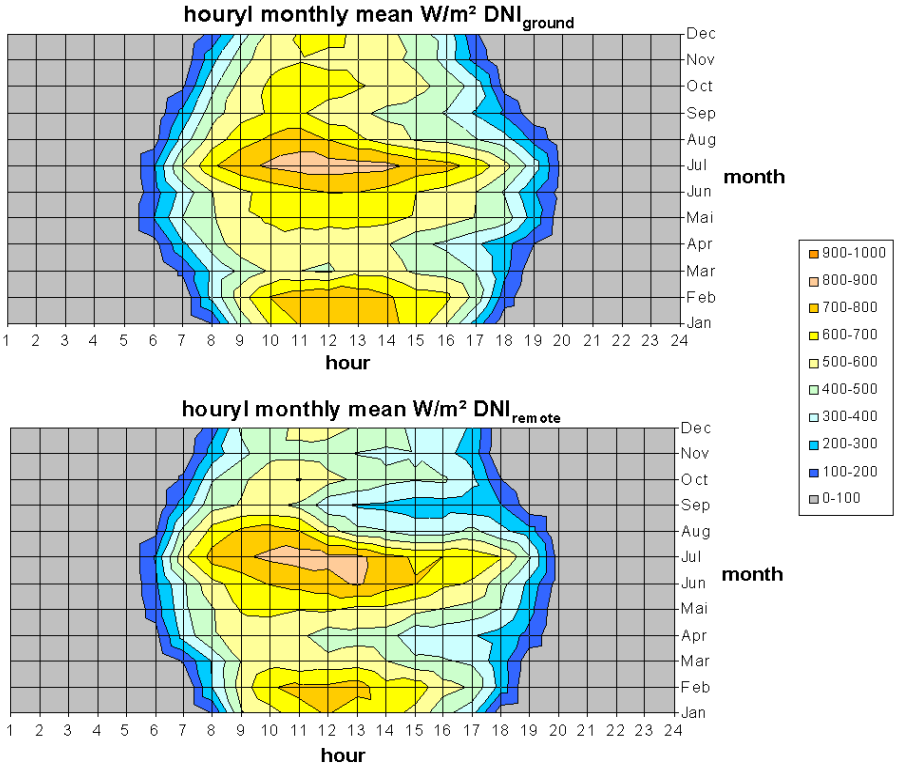

Figure 3-15: Hourly monthly mean of DNI derived from ground data (top) and from satellite data and the describe method (bottom) for an example site in Spain.

Besides absolute accuracy an important factor for the valuable simulation of solar thermal power plants is also the realistic representation of short-term fluctuations of the solar resource from hour to hour. This can be described by the temporal standard deviation of the two time-series: for the measurements on average this is 346 W/m², while it is 352 W/m² for the Meteosat-derived DNI. This means the satellite derived DNI shows little higher variability than the measurements (Meyer et al., 2004).

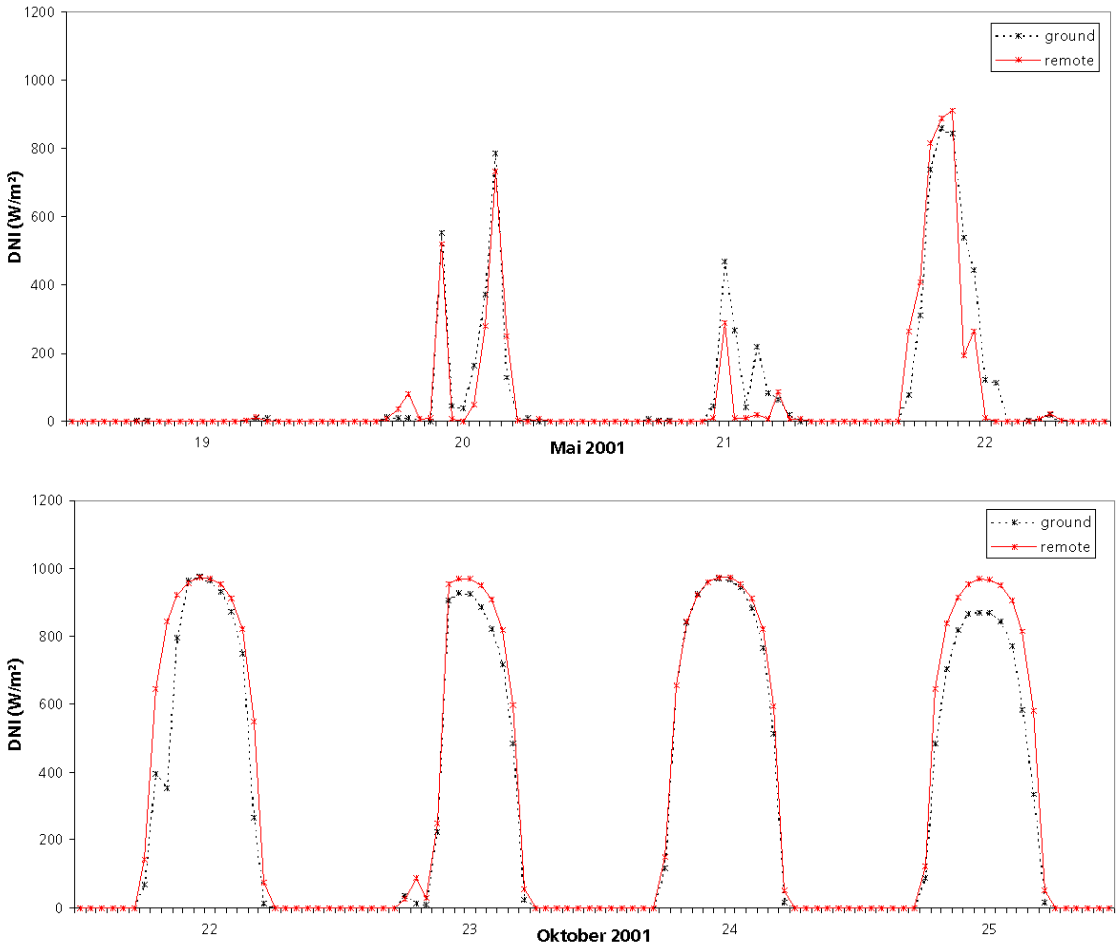

Figure 3-16: Example for a time-series and measurements for a few days in May and October 2001 for a validation site. Ground data are marked black-dotted; remote (satellite) data are marked red-solid. The upper graph shows cloudy days, the lower one cloud-free days.

The methodology described here shows the algorithm used to produce the MENA solar irradiation atlas for the year 2002 shown in Figure 3-4. The quality of this atlas can be considered sufficient to estimate the overall potential of the solar energy resource in the respective countries, but not for concrete project development on specific sites or for economic performance analysis of concrete solar power projects. This would require a more detailed analysis of solar irradiation based on at least ten years of data. Such data can in principle be produced but was not used here, as it requires large personnel efforts and funding (SOLEMI, 2008).

3.1.2 Land Resource Assessment

The next step of our analysis was the detection of land resources which allow for the placement of the concentrating solar collector fields. This is achieved by excluding all land areas that are unsuitable for the erection of solar fields due to ground structure, water bodies, slope, shifting sand, protected or restricted areas, forests, agriculture etc. Geographic features are derived from remote sensing data and stored in a geographic information system (GIS). Finally, those data sets are combined to yield a mask of exclusion criteria for a complete region or country (Figure 3-17). The remaining sites are in principle potential CSP project sites with respect to the exclusion criteria applied (Table 3-1).

There are compulsive criteria and optional criteria for site exclusion. For example, water bodies, protected areas and shifting sands are considered as compulsive criteria for excluding a side, while agricultural use or forests may optionally be used for the placement of the CSP collector fields, although there will be a competition on land use. In our analysis we have applied both compulsive and optional criteria for site exclusion, which yields a conservative estimate of the available land resources.

Each dataset has to be transferred to a GIS-tool and C-routines that were used to perform this work. The following figures show some example criteria that are applied for the land resource assessment.

For each exclusive criterion the following databases were used for this analysis:

- Globe – The “Global Land One-kilometer Base Elevation” for elevation and slope information
- USGS – U.S. Geological Survey” for land cover and land use information
- WDPA – World Commission on Protected Areas” for protected areas information
- DCW – Digital Chart of the World” for land use information
- FAO - Food and Agriculture Organization of the United Nations” for land use information

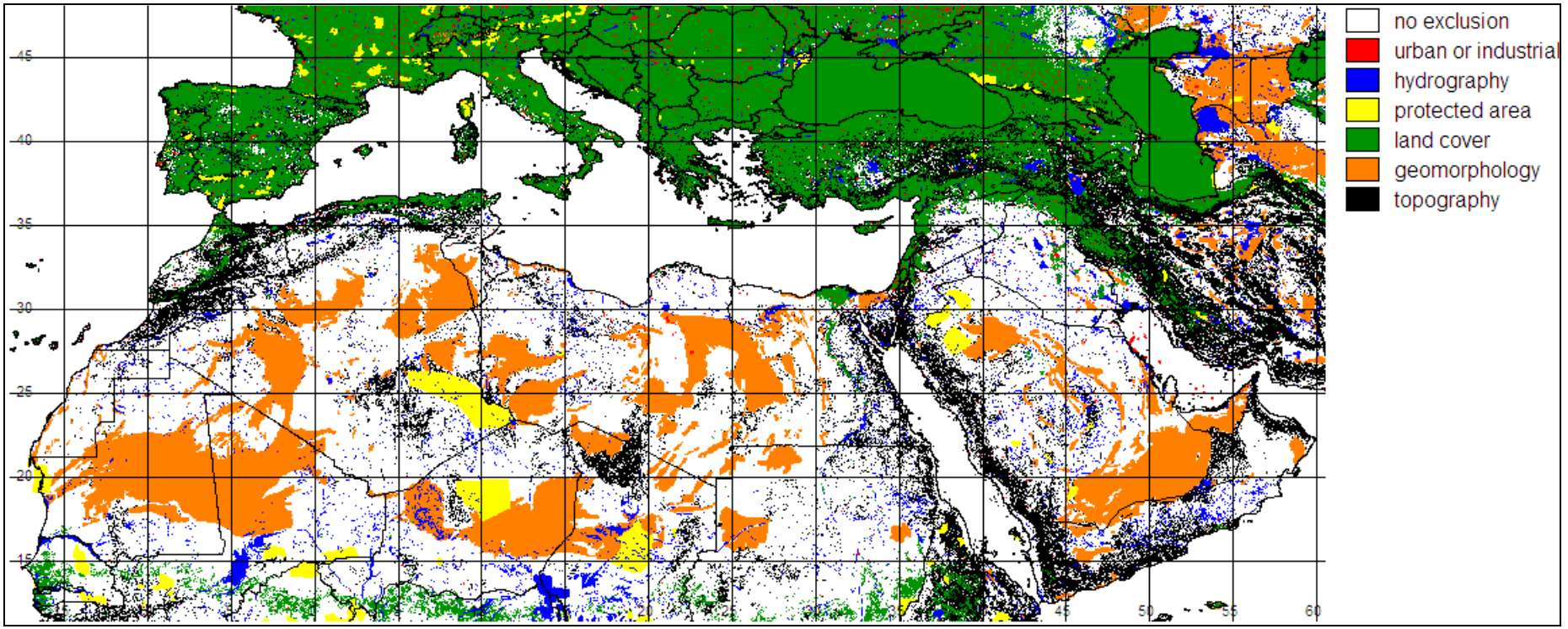

Figure 3-17: Exclusion areas for concentrating solar thermal power plants in MENA

Table 3-1: Compulsive and optional criteria for the exclusion of terrain for CSP plants. All criteria were applied for the site exclusion of CSP.

Exclusion Criteria for CSP Plants	compulsive	optional
Slope of Terrain		
> 2,1 %	x	
Land Cover		
Sea	x	
Inland Water	x	
Forest		x
Swamp	x	
Agriculture		x
Rice Culture		x
Hydrology		
Permanent Inland Water	x	
Non-Permanent Inland Water		x
Regularly Flooded Area		x
Geomorphology		
Shifting Sand, Dunes	x	
Security Zone for Shifting Sands 10 km		x
Salt Pans		x
Glaciers	x	
Security Zone for Glaciers		x
Land Use		
Settlement		x
Airport		x
Oil or Gas Fields		x
Mine, Quarry		x
Desalination Plant		x
Protected Area, Restricted Area		x

Slope

The land slope can be derived from a digital elevation model shown in Figure 3-18. Figure 3-19 shows the slope derived from that data set. For this figure, a slope greater than 2.1% is coloured with red. Global Land One-km Base Elevation Digital Elevation Model (GLOBE) is used for the determination of the slope (Hastings & Dunbar, 1999). A slope higher than 2.1% is excluded for the building of solar thermal power stations. The value of 2.1% is determined by the slope-function based on the elevation, the error of the GLOBE-data and the error propagation (Kronshage, 2001).

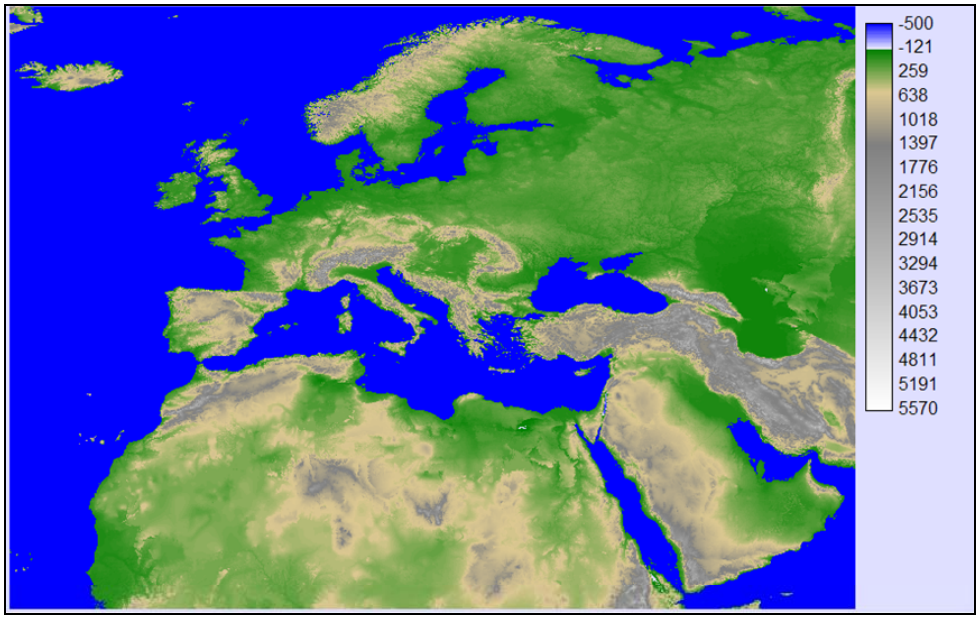

Figure 3-18: Global Land One-km Base Elevation Digital Elevation Model in meters above sea level (GLOBE) from (Hastings & Dunbar, 1999).

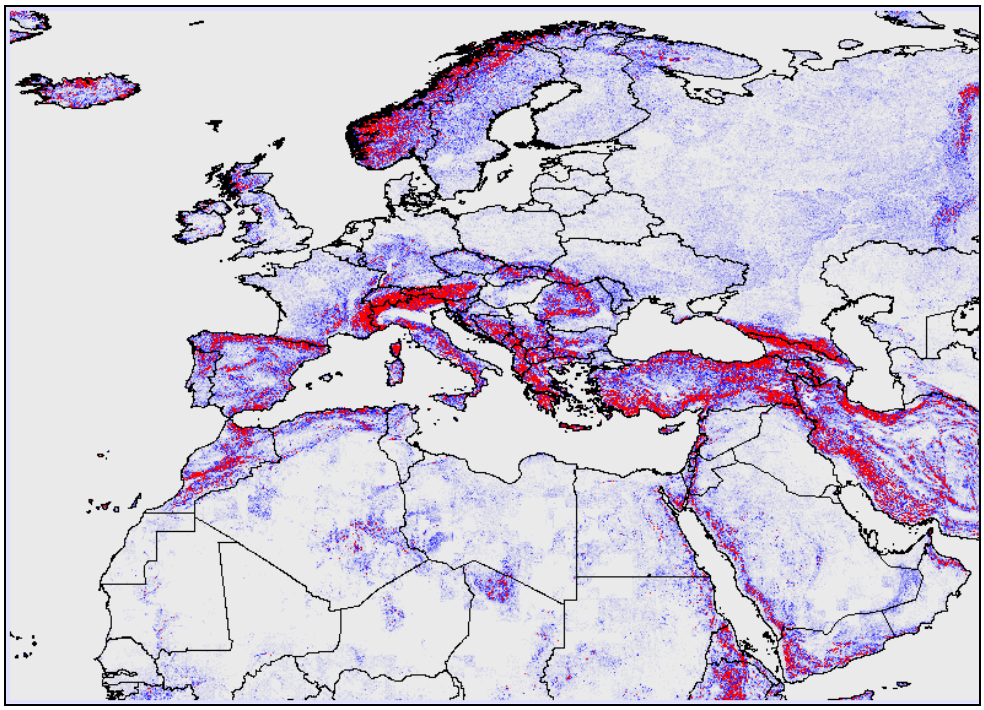

Figure 3-19: Areas with a slope higher than 2.1% that are excluded for CSP. This information is derived from the Digital Elevation Model (DEM) GLOBE (Hastings & Dunbar, 1999). In this figure slope higher than 2.1% is marked as red, while smaller slopes are given in different tones from white (flat) to dark blue (2.1%).

Land Cover

Information on land cover is taken from the Global Land Cover Characterization (GLCC) Database (USGS, 2000) which is based on classified NDVI (Normalized Difference Vegetation Index) data. The used 10 land cover classes are a comprehensive compilation of the Global Ecosystems Classification by Olson (1994) and Brösamle (2000). Figure 3-20 gives the 10 classes of land cover used here.

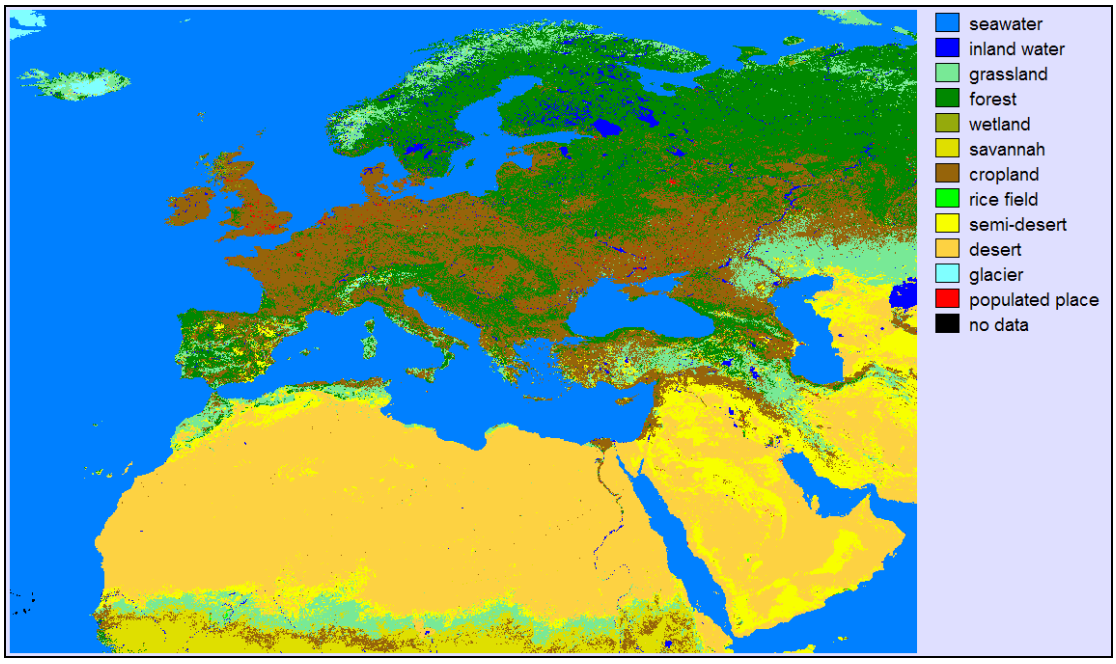

Figure 3-20: Landcover in the Euro-Mediterranean Region (USGS, 2000).

Hydrology

Hydrological data on rivers, lakes etc. are based on the Global Land Cover Characterization (GLCC) Database, Version 2.0 (USGS, 2000) and on the Digital Chart of the World in ASCII (DCW), Version 3.0 (Ph.D., 1998). Figure 3-21 shows the main hydrological features of the analysed region. Small rivers are not taken into account because a shift up to 500 meters for the possible site is acceptable. Large rivers, mostly near the sea-confluence, are considered.

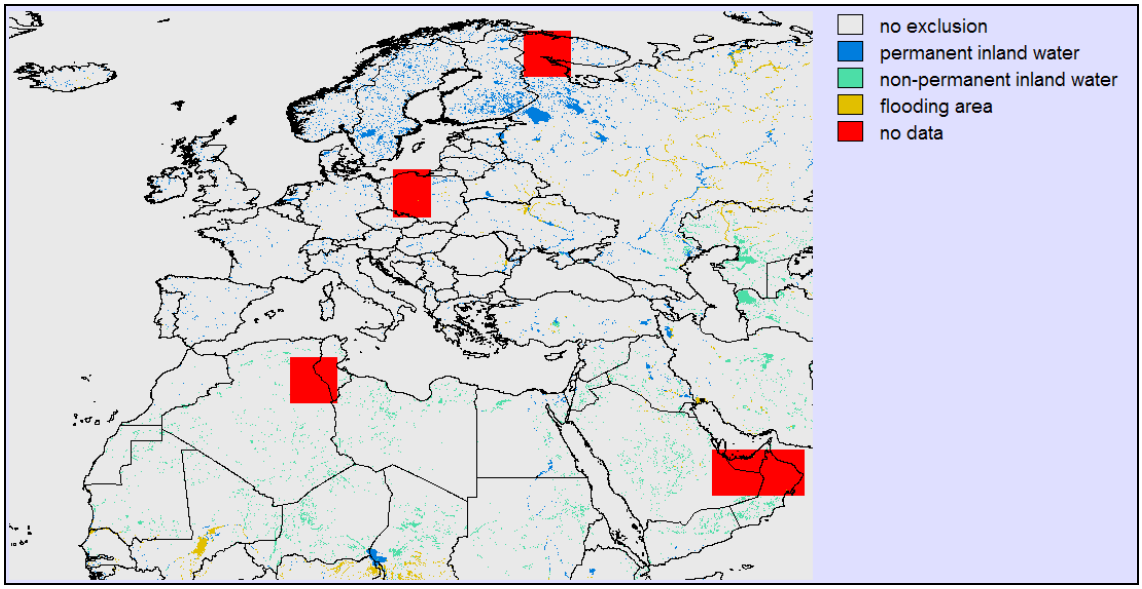

Figure 3-21: Hydrology of the Euro-Mediterranean Region (USGS, 2000; Ph.D., 1998).

Geomorphologic Features

Certain areas and soils are not suitable to be used as foundation for concentrating solar collector fields due to their geomorphologic features. Salt areas because of their heavy corrosive features belong to it. But also dynamic structures like shifting sands form an exclusion area, which additionally is extended by a safety zone for the duration of operating (here 50 years). As the flow velocities can amount to 200 m/y this safety zone has to be at least 10 km width (Kronshage & Trieb, 2002).

Sand dunes are unsuitable for the erection of pylons as the sand corns do not form a strong compound. Here the exclusion area also contains a safety zone which considers the mobility of certain dune types. Such shifting sands can cover around 30 m/y at a height of 10 m, therefore the safety zone is precautionary specified with a width of 10 km that eliminates the endangering of the facility for the duration of operation (here 50 years) (Cooke et al., 1993).

Spatial information about sand dunes and salt areas are taken from the ‘Digital Soil Map of the World’ (DSMW) of the FAO (FAO, 1995). The DSMW is based on the ‘Soil Map of the World’ (1:5 Mio.) of the FAO/UNESCO from the year 1978. The spatial resolution of the digital map amounts to approximately 10 km x 10 km.

Altogether the DSMW identifies in 26 groups of soil types 106 soil types and additional non-soil features, which include the dunes and salt areas of interest. Glaciers are taken from the digital land cover dataset (GLCC) and the DSMW.

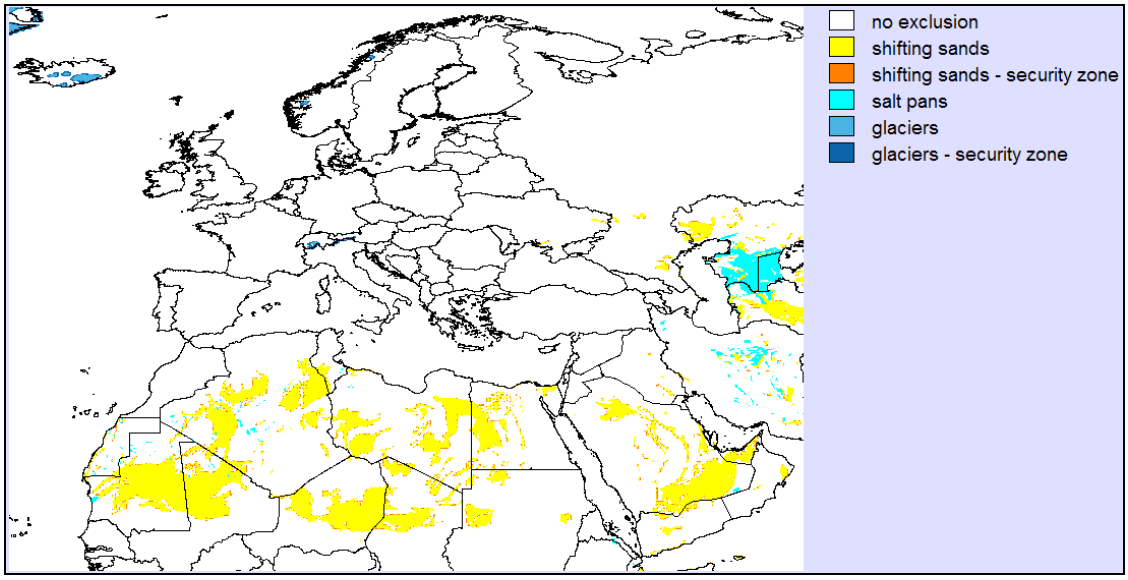

Figure 3-22: Geomorphologic exclusion criteria in the Euro-Mediterranean region.

Protected Areas

The information on the protected areas is based on data provided by The World Conservation Union (IUCN) and the World Commission on Protected Areas (WCPA). The definition of a protected area adopted by IUCN is: “An area of land and/or sea especially dedicated to the protection and maintenance of biological diversity, and of natural and associated cultural resources, and managed through legal or other effective means”. Although all protected areas meet the general purposes contained in this definition, in practice the precise purposes for which protected areas are managed differ greatly. IUCN has defined a series of six protected area management categories, based on primary management objective. In summary, these are:

CATEGORY Ia: Strict Nature Reserve: protected area managed mainly for science defined as an area of land and/or sea possessing some outstanding or representative ecosystems, geological or physiological features and/or species, available primarily for scientific research and/or environmental monitoring.

CATEGORY Ib: Wilderness Area: protected area managed mainly for wilderness protection defined as a large area of unmodified or slightly modified land, and/or sea, retaining its natural character and influence, without permanent or significant habitation, which is protected and managed so as to preserve its natural condition.

CATEGORY II: National Park: protected area managed mainly for ecosystem protection and recreation, defined as a natural area of land and/or sea, designated to (a) protect the ecological integrity of one or more ecosystems for present and future generations, (b) exclude exploitation or occupation inimical to the purposes of designation of the area and (c) provide a foundation for spiritual, scientific,

educational, recreational and visitor opportunities, all of which must be environmentally and culturally compatible.

CATEGORY III: Natural Monument: protected area managed mainly for conservation of specific natural features, defined as an area containing one, or more, specific natural or natural/cultural feature which is of outstanding or unique value because of its inherent rarity, representative or aesthetic qualities or cultural significance.

CATEGORY IV: Habitat/Species Management Area: protected area managed mainly for conservation through management intervention, defined as an area of land and/or sea subject to active intervention for management purposes so as to ensure the maintenance of habitats and/or to meet the requirements of specific species.

CATEGORY V: Protected Landscape/Seascape: protected area managed mainly for landscape/seascape conservation and recreation, defined as an area of land, with coast and sea as appropriate, where the interaction of people and nature over time has produced an area of distinct character with significant aesthetic, ecological and/or cultural value, and often with high biological diversity. Safeguarding the integrity of this traditional interaction is vital to the protection, maintenance and evolution of such an area.

CATEGORY VI: Managed Resource Protected Area: protected area managed mainly for the sustainable use of natural ecosystems, defined as an area containing predominantly unmodified natural systems, managed to ensure long term protection and maintenance of biological diversity, while providing at the same time a sustainable flow of natural products and services to meet community needs. Figure 3-23 shows as an example the different IUCN-categories of the protected areas for Spain.

The resulting data are collected in the World Database on Protected Areas (WDPA, 2005).

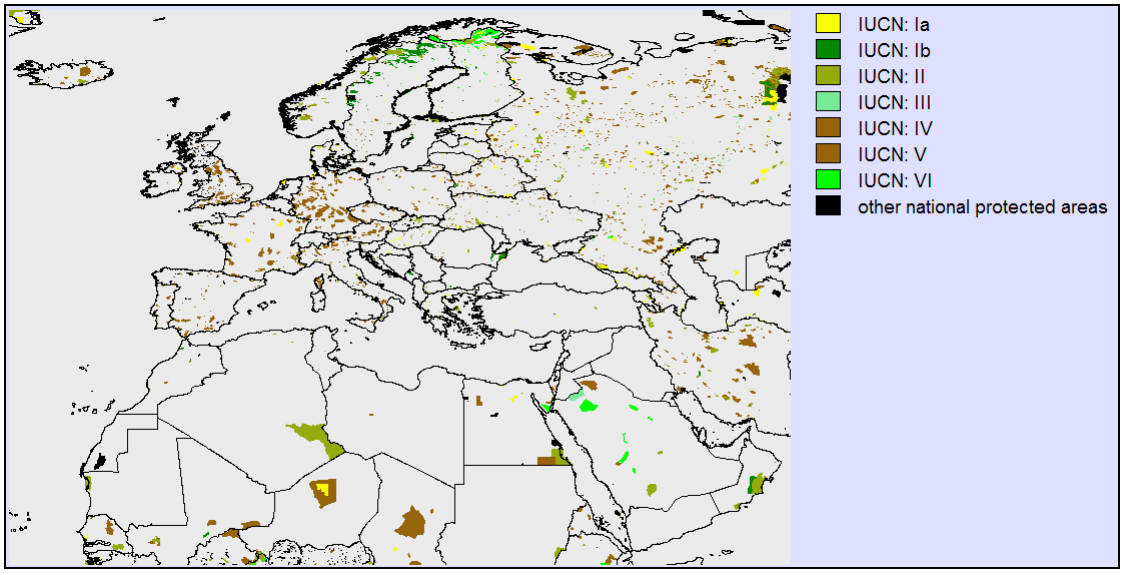

Figure 3-23: Protected areas of the Euro-Mediterranean Region (WDPA, 2005).

Industry and Population

Data on industry and highly populated places are based on the Digital Chart of the World in ASCII (DCW), Version 3.0 (Ph.D., 1998) as shown in Figure 3-24 for the total region.

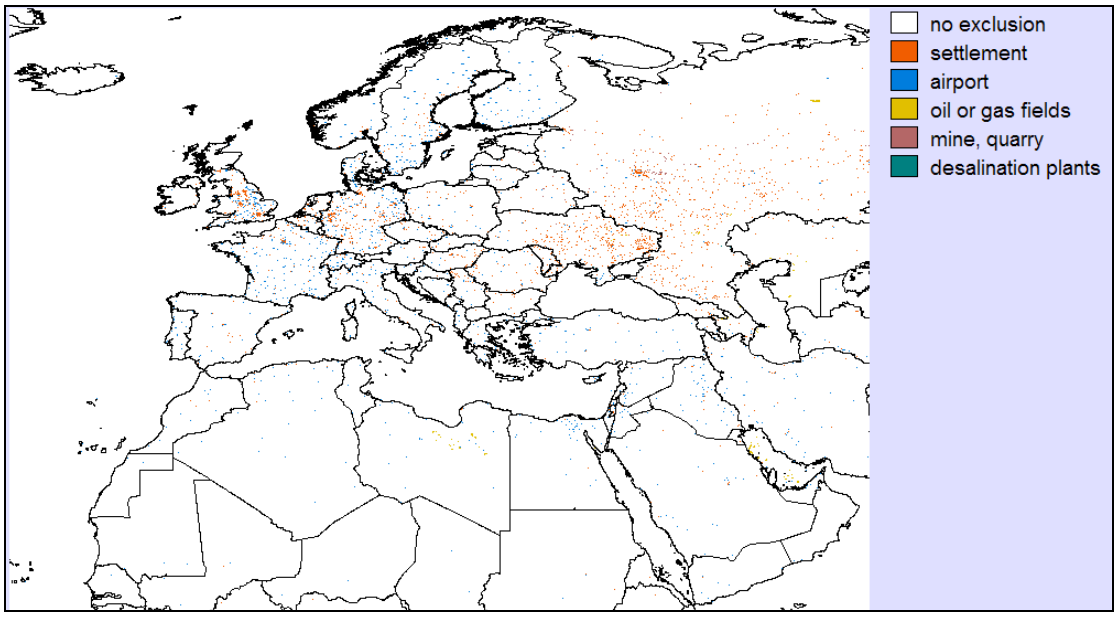

Figure 3-24: Industry and population of the Euro-Mediterranean region (Ph.D., 1998)

All information on the chosen criteria is finally combined in a single map as shown in Figure 3-17. This exclusion map shows all exclusion information available and gives something like a technical potential of land areas for the placement of CSP plants.

3.1.3 Potentials for Solar Electricity Generation in MENA

The data described before was used to generate maps showing the DNI at potentially suitable sites for CSP plants for each country (Figure 3-25). Those maps were statistically analysed yielding the land area available in each country with a certain direct normal irradiance (Table 3-2, Figure 3-26). From this information, the potential solar electricity yield for every class of solar irradiance can be calculated, defining the technical potential of areas suitable for CSP of each country. Although CSP generation is possible at lower values a threshold of 2000 kWh/m²/y of annual direct normal irradiance was used to define the overall technical potential of CSP.

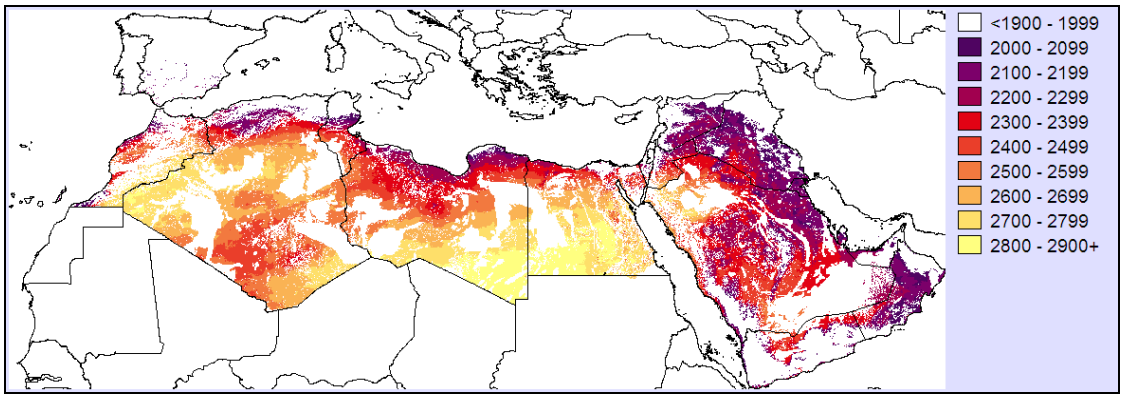

Figure 3-25: Annual direct normal irradiance in kWh/m²/y on non-excluded areas in MENA.

Table 3-2: Areas for CSP in km² available in the MENA countries for different DNI Classes

DNI Class	Morocco	Algeria	Tunisia	Libya	Egypt	Jordan	Saudi Arabia
2000-2099	6083	6237	9288	7773	206	2097	32,807
2100-2199	5650	34,142	6445	25,331	1481	5902	135,285
2200-2299	10,875	29,006	9864	109,712	16,846	19,197	336,109
2300-2399	17,194	39,462	19,464	176,659	40,969	10,985	334,997
2400-2499	34,348	222,860	22,823	152,875	41,347	10,742	187,726
2500-2599	30,569	384,570	11,637	183,342	44,613	7239	65,508
2600-2699	18,930	428,487	240	155,513	98,004	3152	42,773
2700-2800+	48,074	277,580		373,665	354,972		14,720
Total [km²]	171,724	1,422,344	79,761	1,184,870	598,439	59,315	1,149,927

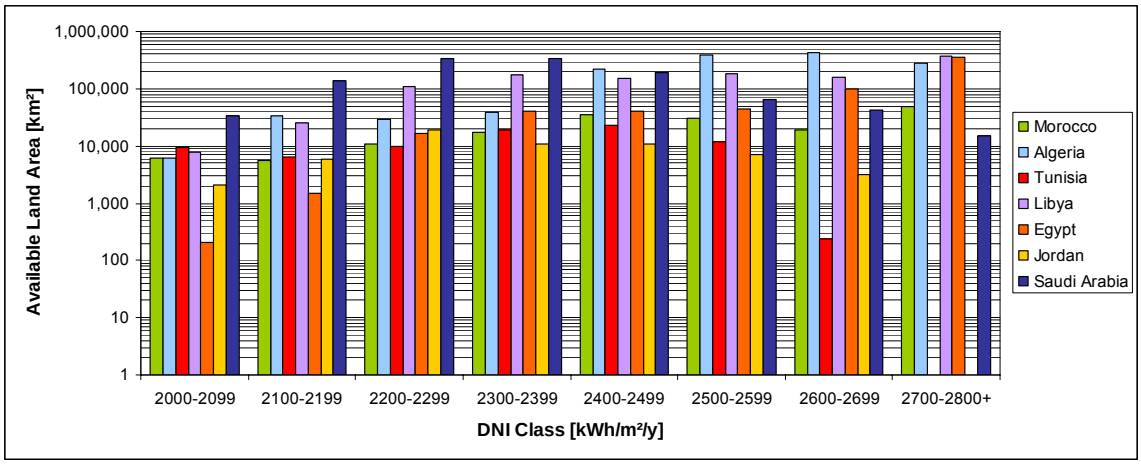

Figure 3-26: Potential areas for the placement of CSP plants in MENA, sorted by the annual direct normal irradiation classes in kWh/m²/y according to Table 3-2.

3.1.4 Potentials for Solar Electricity Generation World Wide

A world wide data set of direct normal irradiation is available from the NASA SSE 6.0. It is based on a climatology covering 22 years of data and has a spatial resolution of about 100 km, which is considered sufficient to assess the world wide potential of CSP plants in the world regions defined within the REACCESS project (Figure 3-27).

The site exclusion criteria for CSP plants were applied world wide (all data sets are available for the whole globe) yielding a global exclusion map as shown in Figure 3-28.

Again, both maps were combined to yield a global map of annual direct normal irradiance for potential CSP sites (Figure 3-29). This map was subdivided according to the world regions defined within the REACCESS project, and a statistical analysis of the distribution of DNI intensity classes was made for each region, yielding the land area available for CSP classified by DNI intensities (Table 3-3).

The analysis shows that most world regions except Canada, Japan, Russia and South Korea have significant potential areas for CSP at an annual solar irradiance higher than 2000 kWh/m²/y. Africa, Australia and the Middle East have the largest potential areas, followed by China and Central & South America.

The distribution of potential areas for CSP world wide confirms the possibility of applying the Euro-Mediterranean concept of solar electricity exports/imports to be applicable to many regions of the world. Most of the world population lives not further than 2000 km away from considerable CSP potentials. This indicates that solar electricity import corridors from arid desert regions to large centres of demand may help to reduce greenhouse gas emissions and stabilize electricity costs all over the world.

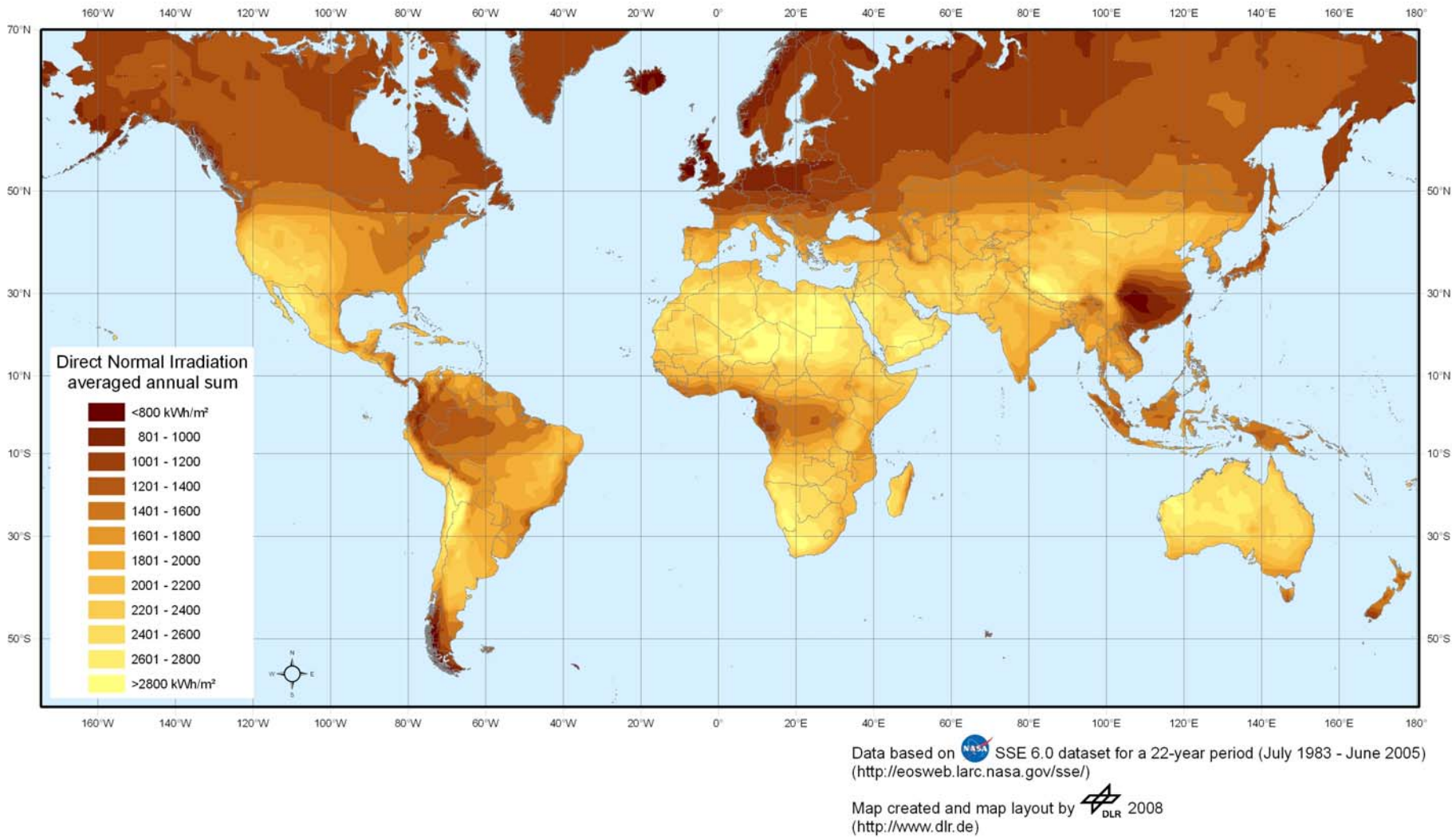

Figure 3-27: World wide annual direct normal irradiation in kWh/m²/y from NASA SSE 6.0 http://eosweb.larc.nasa.gov/sse/ (picture by DLR)

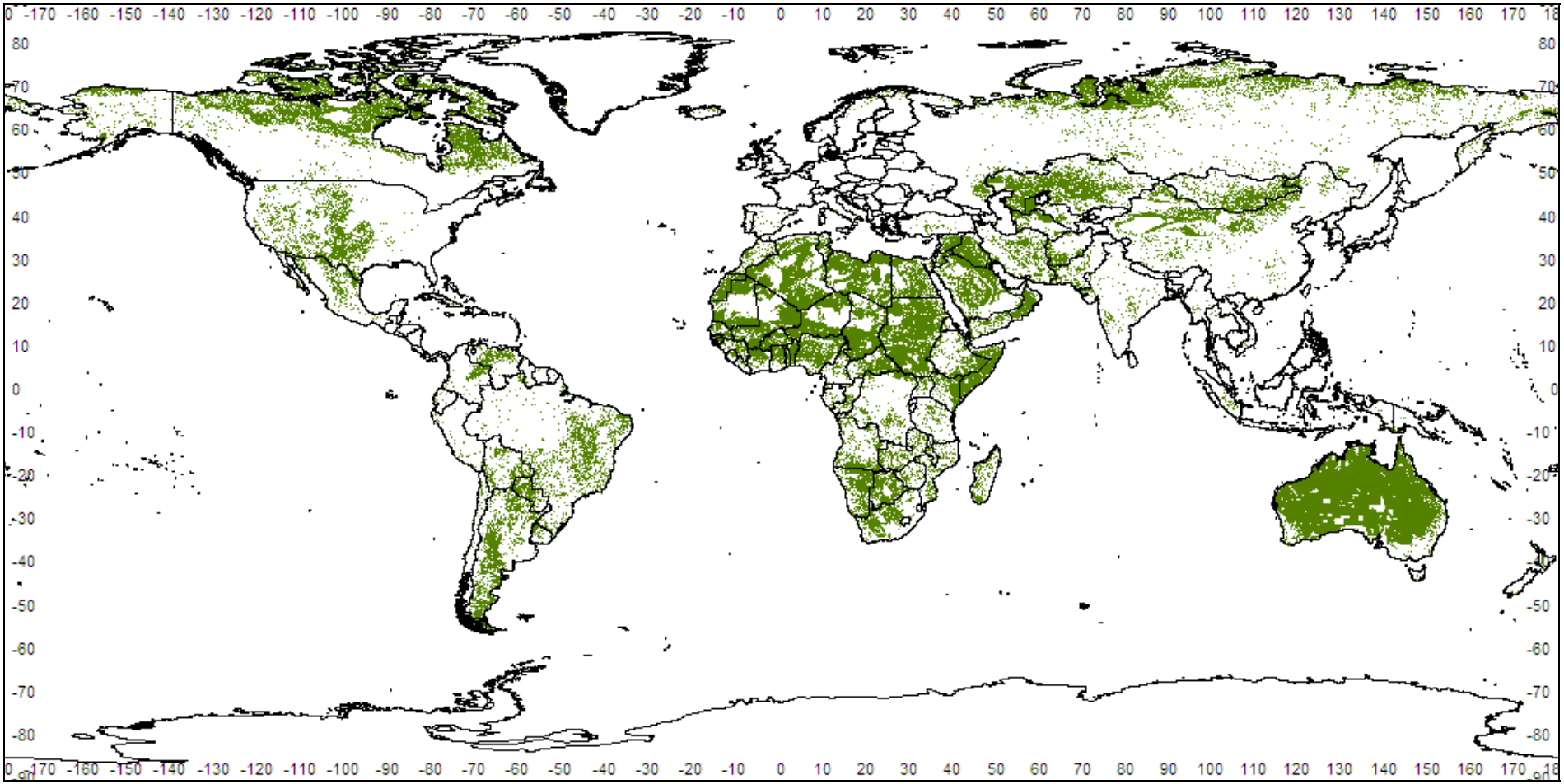

Figure 3-28: World wide exclusion of sites for CSP plant construction (green areas indicate suitable sites)

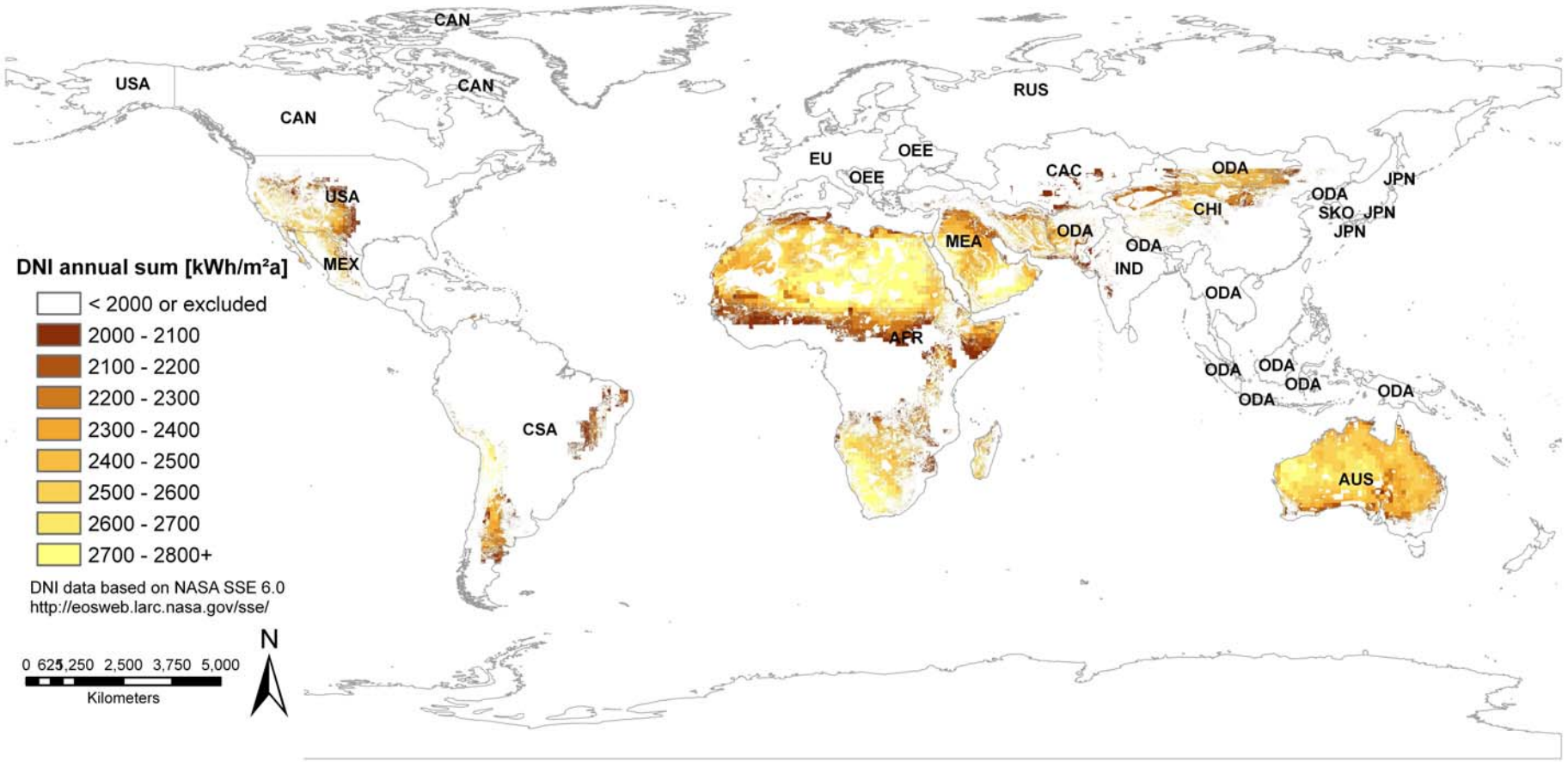

Data provided by DLR (2008) for EU-project REACCESS

Figure 3-29: Annual direct normal irradiation on non-excluded areas for all REACCESS world regions.

Table 3-3: Areas for CSP generation [km²] in the REACCESS world regions classified by DNI.

DNI Class	Africa	Australia	Central Asia, Caucase	Canada	China	Central South America	India	Japan
2000-2099	1,082,050	70,164	151,109		88,171	334,096	83,522	
2100-2199	1,395,900	187,746	3,025		184,605	207,927	11,510	
2200-2299	1,351,050	355,188	3,594		415,720	232,678	5,310	
2300-2399	1,306,170	812,512	1,642		263,104	191,767	7,169	
2400-2499	1,862,850	1,315,560	569		99,528	57,041	3,783	
2500-2599	1,743,270	1,775,670			96,836	31,434	107	
2600-2699	1,468,970	1,172,760			17,939	42,139	976	
2700-2800+	2,746,100	393,850			24,435	93,865	120	
Total	**12,956,360**	**6,083,450**	**159,939**	**0**	**1,190,338**	**1,190,948**	**112,497**	**0**

DNI Class	Middle East	Mexico	Other Developing Asia	Other East Europe	Russia	South Korea	EU27+	USA
2000-2099	36,315	16,999	47,520	59			9,163	149,166
2100-2199	125,682	34,123	52,262	129			5,016	172,865
2200-2299	378,654	35,263	105,768	23			6,381	210,128
2300-2399	557,299	53,765	284,963				1,498	151,870
2400-2499	633,994	139,455	172,043				800	212,467
2500-2599	298,755	60,972	37,855				591	69,364
2600-2699	265,541	12,628	2,084				257	19,144
2700-2800+	292,408	14,903	1,082				270	
Total	**2,588,648**	**368,108**	**703,577**	**211**	**0**	**0**	**23,975**	**985,005**

3.2 PRODUCTION TECHNOLOGIES, CAPACITIES AND COSTS

3.2.1 Solar Energy for Power Generation

“Renewable energy sources are dispersed, fluctuating and unpredictable, and therefore can never provide base load power”. With that argument, the introduction of renewable energy for power generation has been held back for a long time. However, in the meantime, this argument has been proven wrong:

1. Not all renewable energy sources are fluctuating. Electricity from hydropower dams, biomass or geothermal plants can be delivered continuously and predictably. Also concentrating solar power stations with thermal energy storage and fuel backup can deliver power at constant capacity or on demand, day and night. Only wind- and PV power generators produce electricity with fluctuating output that is not controlled by consumption, but by the natural resource. Even for those, predictability is steadily increasing due to increasing experiences in energy meteorology.

2. Base load is caused by an aggregate of millions of dispersed, fluctuating and unpredictable energy consumers. The aggregate of many dispersed, fluctuating and unpredictable renewable power generators can very well have a similar characteristic, if the mix of sources is balanced to fit demand, and if balancing power to outweigh demand and supply is provided by a sufficient share of storable sources.

3. Renewable energy sources are dispersed all over the world, which in fact is an advantage and not a disadvantage, as they may be harvested and used everywhere, reducing dependency on energy imports in form of fossil or nuclear energy carriers. However, the best sources of renewable energy are often concentrated in specific regions that are far away from human settlements, e.g. hydropower in the mountains, wind energy at the coasts and solar energy in the deserts. To activate those sources will require an infrastructure that connects them to the centres of demand, a necessity that would be similar for conventional, large scale power stations.

Within a balanced mix of renewable energy sources for power generation, concentrating solar power plants (CSP) have a very special role:

A major advantage of CSP for providing constant base load capacity can be appreciated in Figure 3-30, Figure 3-31 and Figure 3-32 for a time-series modelling of one week of operation of equivalent wind, PV and CSP systems with 10 MW installed power capacity each at Hurghada, Egypt: while wind and photovoltaic power systems deliver fluctuating power and either allow only for intermitting solar operation or require considerable conventional backup, a concentrating solar power plant can deliver stable and constant power capacity, due to its thermal energy storage capability and to the possibility of hybrid operation with fuel.

To cover a constant load or to follow a changing load by wind or PV electricity would additionally require the electricity grid and conventional plants for external backup. In both cases an additional backup capacity would have to be installed and operated for most of the time, generating a relatively small portion of electricity during daytime and wind periods, but full capacity during night and wind calms.

In our example the renewable share provided by CSP is about 90%, that of PV is 25% and that of wind power is about 35-40%. Depending on varying conditions at different locations, these numbers can be also considered as typical for the average annual renewable share of such systems.

As a consequence, CSP plants can save more fossil fuel and replace more conventional power capacity compared to other renewable energy sources like PV and wind power. Theoretically, instead of conventional backup power or fuel, electricity generated by all three systems could be stored in batteries, hydro-pump or hydrogen energy storage in order to provide continuous power capacity. In that case, the additional electrical storage capacities needed by CSP would be rather small, while significant storage would be required for PV and wind power, prohibitively increasing the overall system cost and energy losses.

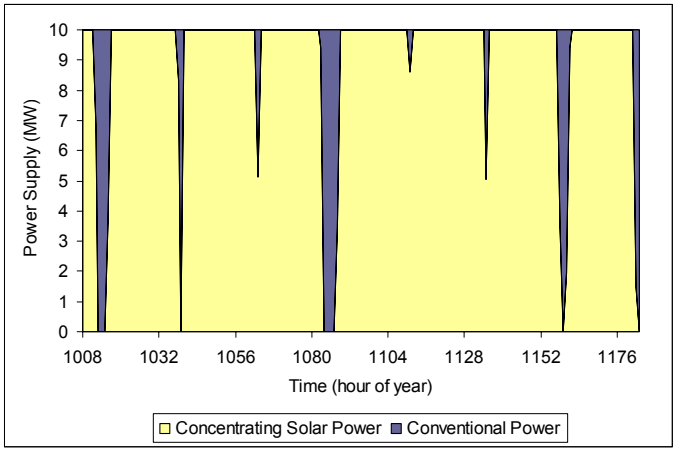

Figure 3-30: Solar power provided by a CSP-plant with 16 hour storage and conventional power from fuel from the same plant for constant 10 MW base load supply.

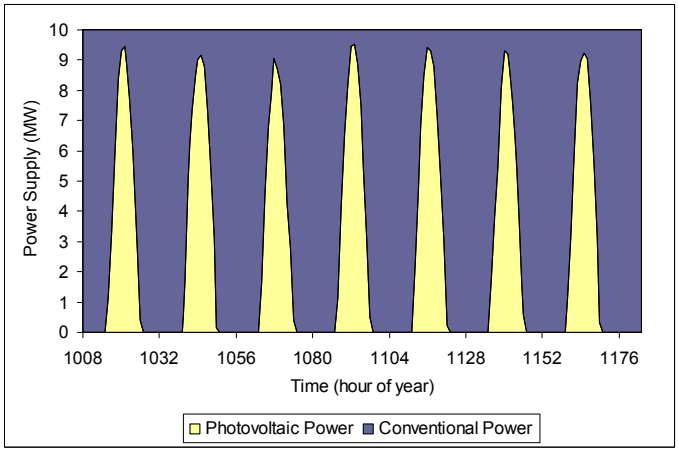

Figure 3-31: Power supplied by 10 MW PV capacity and conventional backup power from the grid needed to provide constant 10 MW base load supply.

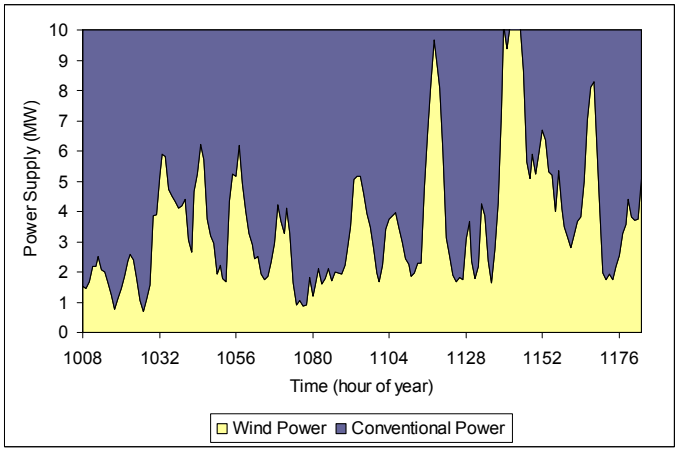

Figure 3-32: Power supplied by 10 MW wind capacity and conventional backup power from the grid needed to provide constant 10 MW base load supply.

Another major advantage of CSP power stations is the fact that the steam turbines used for power generation provide an excellent spinning reserve, which is very important for short time compensation of any failures or outages within the electricity grid. Spinning reserve can only be provided by rotating machines like steam or gas turbines. Moreover, the flexible design of CSP plants allows them to operate in all load segments from base load and intermediate load to peaking load services, just as required by grid operators.

Concentrating solar thermal power plants have the capability for thermal energy storage and hybrid operation with fossil or bio-fuels, allowing them to provide firm power capacity on demand. The principle of operation is drafted in Figure 3-33, also including the option for cogeneration of heat and power. The use of a simple cycle for electricity generation is of course also possible. In a future European mix of energy sources for power generation, CSP can serve to cover base load, intermediate load or peaking load and to compensate fluctuations of PV and wind power. From the point of view of a grid operator, CSP behaves just like any conventional steam cycle power station, thus being an important factor for grid stability and control. CSP plants can be designed from 5 MW to several 100 MW of capacity.

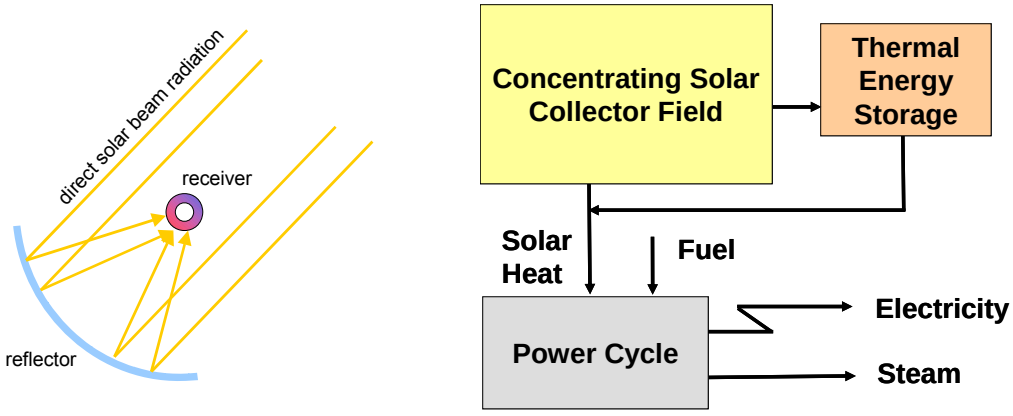

Figure 3-33: Principle of a concentrating solar collector (left) and of a concentrating solar thermal power station for co-generation of electricity and process steam (right).

A reasonable economic performance of concentrating solar power plants is given at an annual direct solar irradiance of more than 2000 kWh/m²/y. The economic potential of CSP in Europe has been assessed in (Trieb et al. 2005). It is limited to Spain, Portugal, Greece, Turkey and the Mediterranean Islands and amounts to 1580 TWh/y of which 1280 TWh/y are located in southern Spain. Although there is a relatively large CSP potential in Europe, more attractive sites are located south of the Mediterranean Sea with an annual direct solar irradiance of up to 2800 kWh/m²/y.

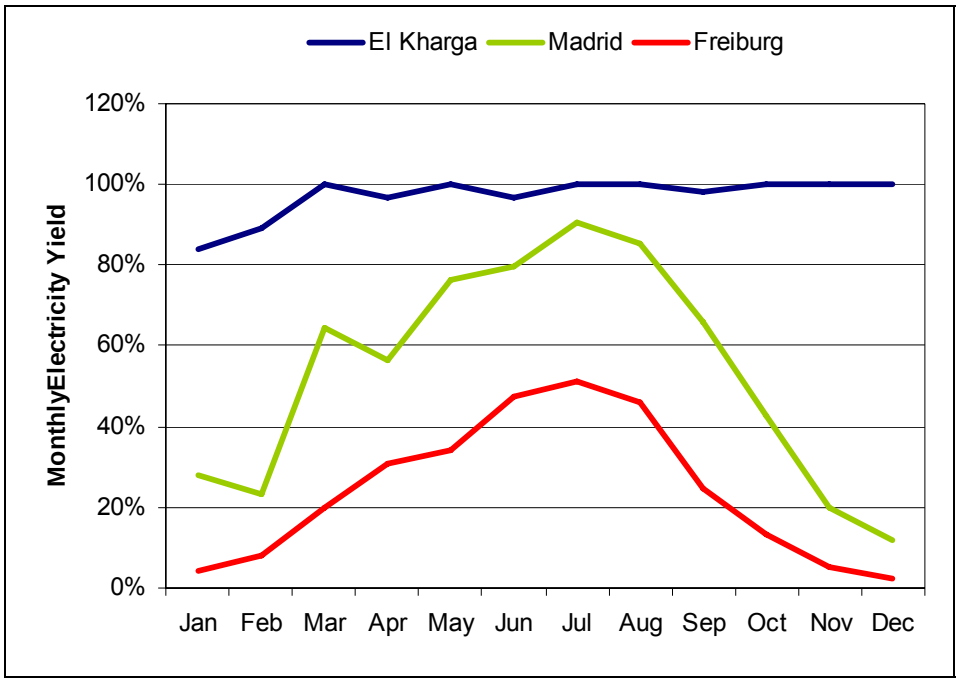

Figure 3-34: Simulation of the relative monthly electricity yield of a solar thermal power plant with 24 hour storage at sites with different annual solar irradiance and latitude assuming solar only operation without fuel input. Total equivalent annual full load hours achieved: Freiburg (Germany) 2260 h/y, Madrid (Spain) 5150 h/y, El Kharga (Egypt) 8500 h/y. Source: (May 2005).

Figure 3-34 shows the monthly electricity yield of a solar thermal power plant with a one-day thermal energy storage capacity at different locations in Europe and North Africa. The site El Kharga in Egypt represents the best case in this comparison. Throughout the whole year the solar electricity yield stays at almost 100 %, just in January and February it declines to about 85 %, a behaviour that correlates very well with local power demand. The more the plant is located to the North the lower is its monthly electricity yield. In Madrid and Freiburg values of less than 20 % are achieved in wintertime, and neither achieves 100 % in summer, compared to the site in Egypt.

Due to the geographic distribution of solar energy that shows considerably more stable and reliable sunshine in the South, the option of importing solar electricity from the Middle East and North Africa to Europe within certain energy corridors is assessed within the REACCESS project as described here.

3.2.2 Overview of Concentrating Solar Power Technology

In general, solar thermal technologies are based on the concept of concentrating solar radiation to produce steam or hot air which can then be used for electricity generation using conventional thermodynamic power cycles. Efficiently collecting and concentrating solar energy which has relatively low spatial density is one of the main engineering tasks of solar thermal power plant development. For concentration most systems use curved or flat glass mirrors because of their very high reflectivity. Point focusing and line focusing collector systems are used, as shown in Figure 3-35. These systems can only use the direct portion of solar radiation, but not the diffuse part of the sunlight because that can not be concentrated. Line focusing systems are easier to handle, but have a lower concentration factor and hence achieve lower temperatures than point focusing systems. Therefore, line concentrating systems will typically be connected to steam cycle power stations, while point concentrating systems are also capable of driving gas turbines or combustion engines.

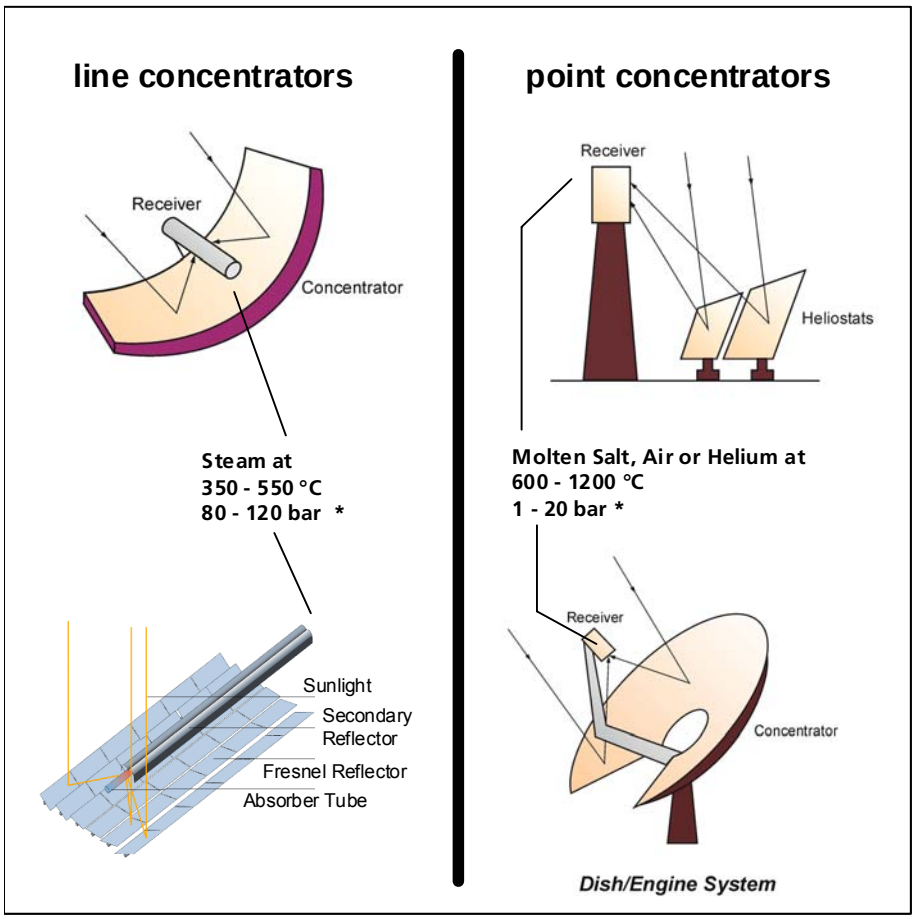

Figure 3-35: Concentrating solar collector technology mainstreams: Parabolic trough (top left), linear Fresnel (bottom left), central receiver solar tower (top right), dish-Stirling engine (bottom right).

Concentrating Solar Power for Steam Turbines

As shown in Figure 3-36 and Figure 3-37, some line focusing systems use ***parabolic trough*** mirrors and specially coated steel absorber tubes to convert sunlight into useful heat. The troughs are normally designed to track the sun along one axis, predominantly north-south. To generate electricity, a fluid flowing through the absorber tube – usually synthetic oil or water/steam – transfers the heat to a conventional steam turbine power cycle. Concentrating the sunlight by about 70 - 100 times, typical operating temperatures are in the range of 350 to 550 °C. Plants of 200 MW rated power and more can be built by this technology. Hybrid operation with all kinds of fossil or renewable fuels is possible (Müller-Steinhagen & Trieb, 2004). In order to increase the number of solar operating hours beyond the times when the sun shines, the collector field can be designed to provide, under standard conditions, more energy than the turbine can accept. This surplus energy is used to charge a heat storage, which can provide the required energy input to the turbine system during periods of insufficient solar radiation (Tamme et al., 2004).

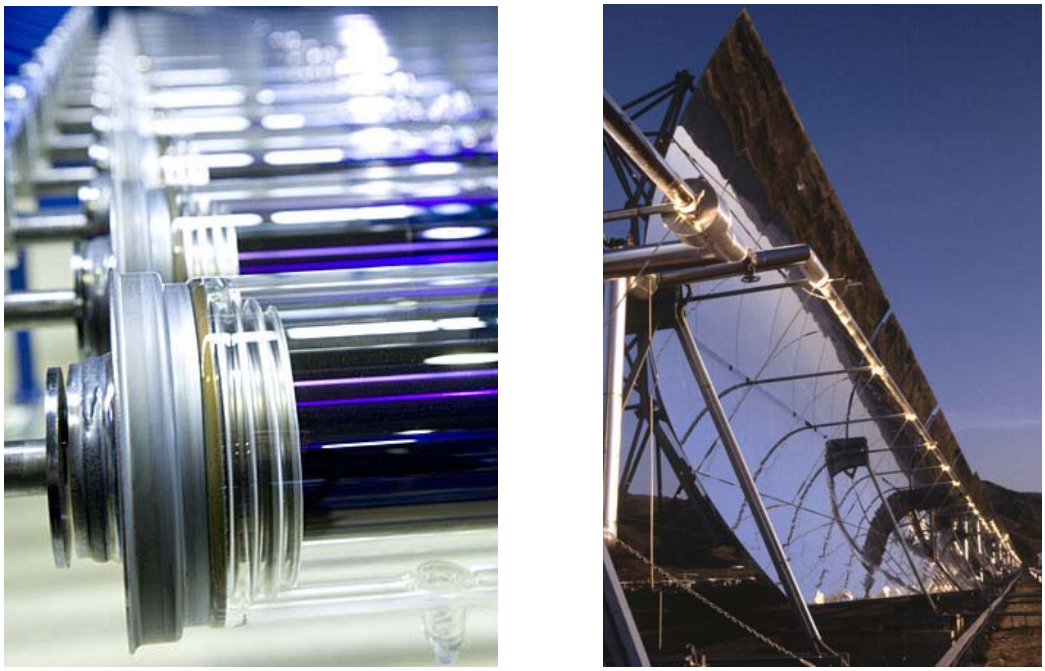

Figure 3-36: Absorber tube with selective coating and evacuated glass envelope by Schott Solar AG, Germany (left) and parabolic trough collector assembly at the Plataforma Solar de Almeria, Spain (right).

Heat storage consists of two large tanks, each containing a molten nitrate salt mixture as storage medium with the necessary heat capacity for several hours of full load operation of the turbine. Heat is transferred from or to the heat transfer fluid of the collector via a heat exchanger. The liquid molten salt is pumped through this heat

exchanger from the cold tank to the hot tank during charging and vice versa during discharging periods (Figure 3-37 and Figure 3-38).

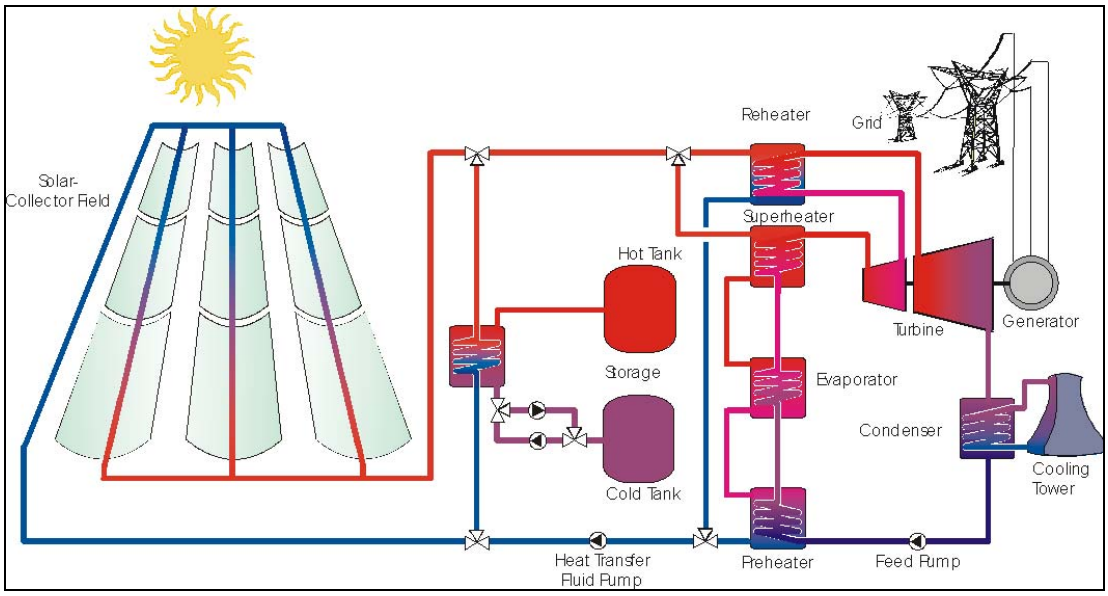

Figure 3-37: Oil-cooled parabolic trough collector coupled to a steam cycle power station.

Figure 3-38: Andasol-1 parabolic trough solar field, storage tanks and power station during construction in December 2007 (Source: ACS Cobra S.A., Spain).

A first plant of this type with 50 MW rated power using synthetic oil as heat transfer fluid and a molten salt tank system with 7 full load hours storage capacity is presently commissioned in the Spanish Sierra Nevada. On July 20th 2006, construction started near Almería/Spain for the 50 MW_{el} parabolic trough plant ANDASOL 1, which will be followed by identical plants ANDASOL 2 & 3 in the next couple of years. Its collector area of over 510,000 square meters makes Andasol 1 the world's largest solar power plant. It will generate approximately 179 GWh of electricity per year to supply some 200,000 people with solar electricity after a construction time of two years. Another 64 MW parabolic trough plant was commissioned in Nevada in summer 2007. All in all, there is a world-wide capacity of over 2000 MW to be commissioned within the coming 5 years period.

The present parabolic trough plant design uses a synthetic oil to transfer energy to the steam generator of the power plant cycle. ***Direct solar steam generation*** in the absorber tubes of parabolic trough collectors is a promising option for improving the economy of solar thermal power plants (Eck & Steinmann, 2005), since all oil-related components become obsolete and steam temperature (and hence efficiency) can be increased. Steam temperatures up to 400 °C at 100 bar pressure have been reached within the framework of a European projects DISS and INDITEP undertaken over 6000 operating hours at the Plataforma Solar de Almería, Spain. The test loop with 700 m length and an aperture of 5.70 m has been custom designed and constructed for the purpose of demonstrating safe operation and controllability under constant and transient operating conditions.

Figure 3-39: View of the two ET-100 collectors installed at the DISS test facility in 2003 (PSA)

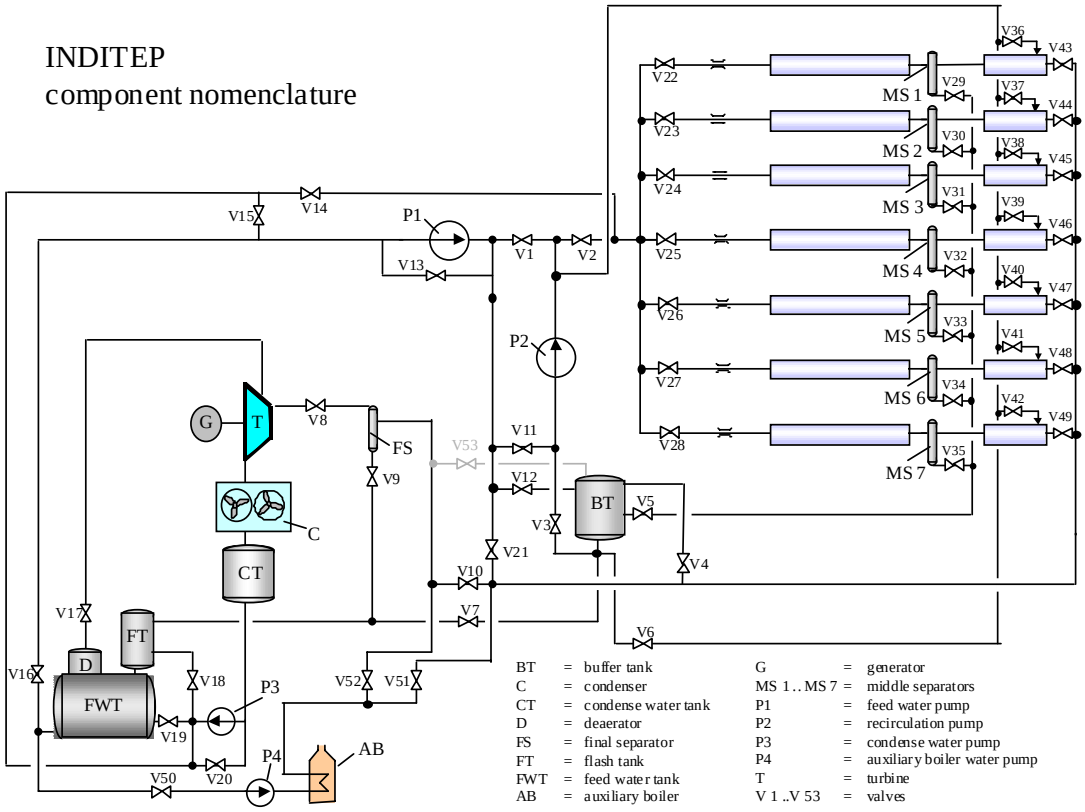

Figure 3-40: Schematic diagram of a direct steam generating solar collector field for a 5 MW pre-commercial solar thermal power plant designed by DLR (INDITEP, 2004).

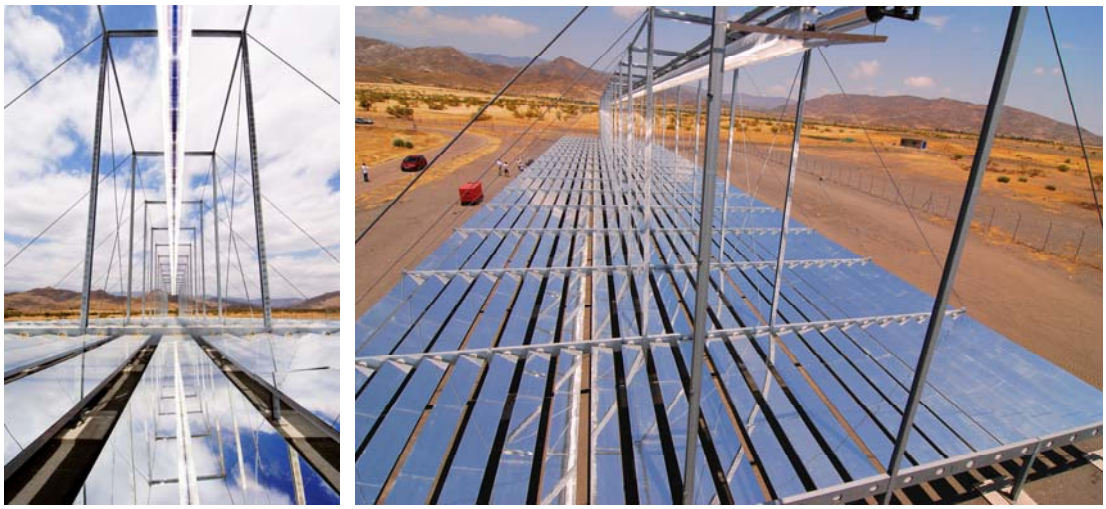

Figure 3-41: Absorber tube box (left) and linear Fresnel collector assembly (right) of the FRESDEMO project at Plataforma Solar de Almeria, Spain (Source: MAN/SPG).

Linear Fresnel systems have recently been developed by several companies with the goal to achieve a more simple design and lower cost than the parabolic trough.

The first prototypes realised up to now are promising, and first power plants are presently in the design phase. It is expected that this technology will be commercially available around the year 2010. In a Fresnel system, the parabolic shape of the trough is split into several smaller, relatively flat segments. These are put on a horizontal rag and connected at different angles to a rod-bar that moves them simultaneously to track the sun during the day. Due to this arrangement, the absorber tube can be fixed above the mirrors in the centre of the solar field, and does not have to be moved together with the mirror during sun-tracking.

While parabolic troughs are fixed on central pylons that must be very sturdy and heavy in order to cope with the resulting central forces, the Fresnel structure allows for a very light design, with the forces absorbed by the four corners of the total structure. Large screws instead of pylons are literarily screwed into the ground and hold the lateral bars of the Fresnel structure.

Compared to the existing parabolic trough, the linear Fresnel collector system designed for example by Novatec-Biosol, Germany shows a weight reduction per square metre of 80%. This structure reflects not only a lower cost, but also leads to lower life cycle emissions of pollutants. On the other hand, the simple optical design of the Fresnel system leads to a lower optical efficiency of the collector field, requiring about 33-38% more mirror aperture area for the same solar energy yield compared to the parabolic trough.

In terms of integration of the solar field to its environment, Fresnel systems have considerable advantages over parabolic troughs. Land use is much better, as the distances between mirrors are much smaller. The collector aperture area covers between 65% and 95% of the required land, while for a parabolic trough, only 30% of the land is covered by mirrors, because the distances between the single parabolic-trough-rows required to avoid mutual shading are considerable. Land use efficiency of a linear Fresnel can thus be about 3 times higher than that of a parabolic trough. Considering the lower optical efficiency of the Fresnel (2/3 of that of a parabolic trough), this leads to a roughly two times better solar energy yield per square meter of land of the Fresnel system when compared to a parabolic trough.

This fact may not be of much importance in remote desert areas were flat, otherwise unused land is not scarce, but it may be of importance when integrating CSP to industrial or tourist facilities, or placing CSP near the coast and close to urban centres of demand. The flat structure of the Fresnel segments can be easily integrated to industrial or agricultural uses. In the hot desert, the shade provided by the Fresnel segments may be a valuable extra service provided by the plant. It could cover all types of buildings, stores or parking lots protect certain crops from excessive sunshine and reduce water consumption for irrigation.

The PS10 central receiver solar tower plant was built by Abengoa Solar after several years of research and development and began operation on March 30th, 2007. It is located in the Spanish province of Sevilla, in Sanlúcar la Mayor, and sits on 150 acres (60 ha). It is the first solar tower in the world commercially delivering electricity. As seen in the operating schematic the plant generates saturated pressurized steam to run a conventional power cycle with 11 MW nominal power. The PS10 plant has 624 heliostats that are 120 m² each, which have an independent solar tracking mechanism that directs solar radiation toward the receiver. Heliostats have to be regularly cleaned and - when wind speed is higher than 36 km/h - they have to be set vertically to avoid structural damages. The receiver is located in the upper section of the tower. The receiver is a “cavity” receiver of four verticals panels that are 5.5 m wide and 12 m tall. The panels are arranged in a semi-cylindrical configuration and housed in a squared opening 11 m per side.

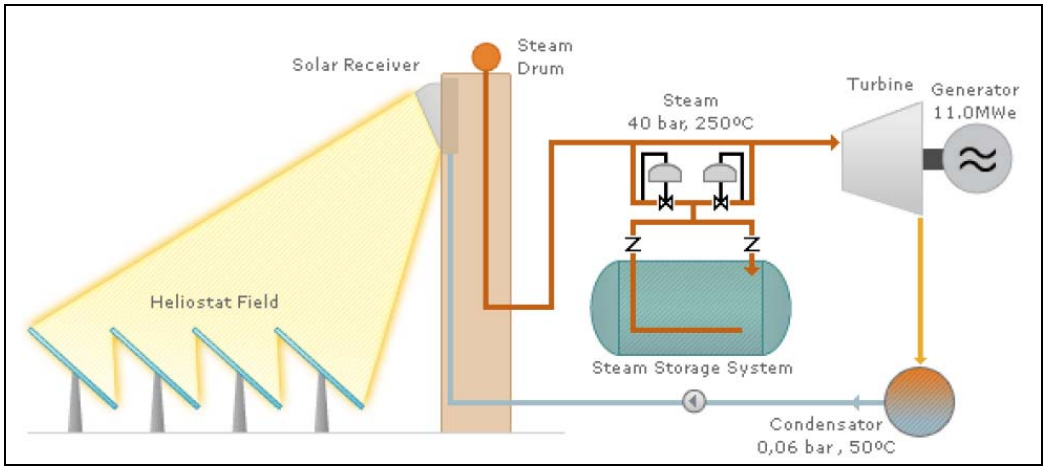

Figure 3-42: PS10 central receiver solar tower schematic (Abengoa Solar)

Figure 3-43: PS 10 central receiver solar tower facility near Sevilla, Spain (Abengoa Solar)

Concentrating Solar Power for Gas Turbines

Solar towers use a large field of two-axis tracking mirrors (heliostats) that reflect the sunlight to a central receiver on top of a tower, where the concentrated solar energy is converted to high temperature heat. The typical optical concentration factor ranges from 200 to 1000, and plant sizes of 5 to 150 MW are feasible. The high solar fluxes impinging on the receiver (average values between 300 and 1000 kW/m²) allow working at high temperatures over 1000 ºC and to integrate thermal energy into steam cycles as well as into gas turbines and combined cycles (Figure 3-44). These systems have the additional advantages that they can also be operated with natural gas during start-up and with a high fossil-to-electric efficiency when solar radiation is insufficient. Hence, no backup capacities of fossil fuel plants are required and high capacity factors are provided all year round. In addition, the consumption of cooling water is reduced significantly compared to steam cycle systems.

The high temperature for gas turbine operation and the heat transfer using air require a different receiver concept than the absorber tubes used in linear concentrating systems. Volumetric receivers do not absorb the concentrated solar radiation on an outer tube surface, but within the volume of a porous body. Air can be used as heat transfer medium which is flowing through that porous material, taking away the heat directly from the surface where it has been absorbed. Due to the excellent heat-transfer characteristics, only a small temperature gradient between the absorber material and the air exists, and thermal losses are reduced. Also, the heat flux density can be much higher than in gas cooled tube receivers (Buck et al., 2002).

The porous material can be a wire mesh for temperatures up to 800 °C or ceramic material for even higher temperatures (Fend et al., 2004). There are two principal designs of volumetric receivers: the open or atmospheric volumetric receiver uses ambient air sucked into the receiver from outside the tower. The heated air flows through the steam generator of a Rankine cycle. The second concept is the closed or pressurised volumetric receiver that uses pressurised air in a receiver closed by a quartz window (Figure 3-45).

This system can heat pressurised air coming from the compressor of a gas turbine power cycle. A first pilot system has been installed and tested on the Plataforma Solar de Almería in Spain and the following targets have been reached:

- receiver outlet temperature 1050 °C with pressures up to 15 bar,
- 90 % secondary concentrator efficiency,
- external cooling of window to maintain glass temperatures below 800 °C, with negligible thermal losses,
- demonstration of controlled system operation, 230 kW electric power output achieved.

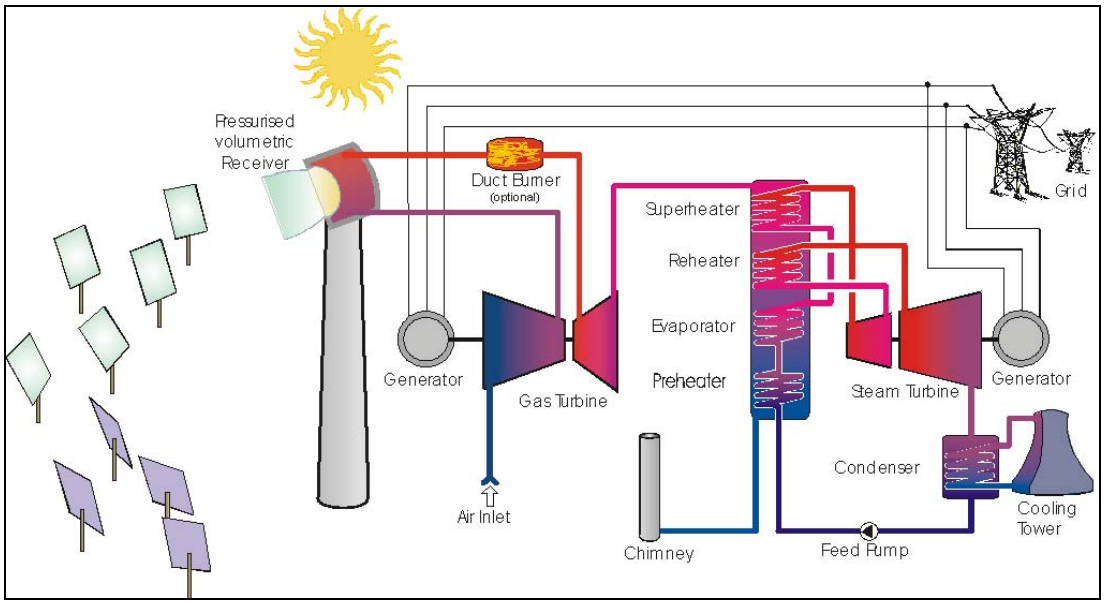

Figure 3-44: Solar tower used for gas turbine operation in a combined cycle power plant

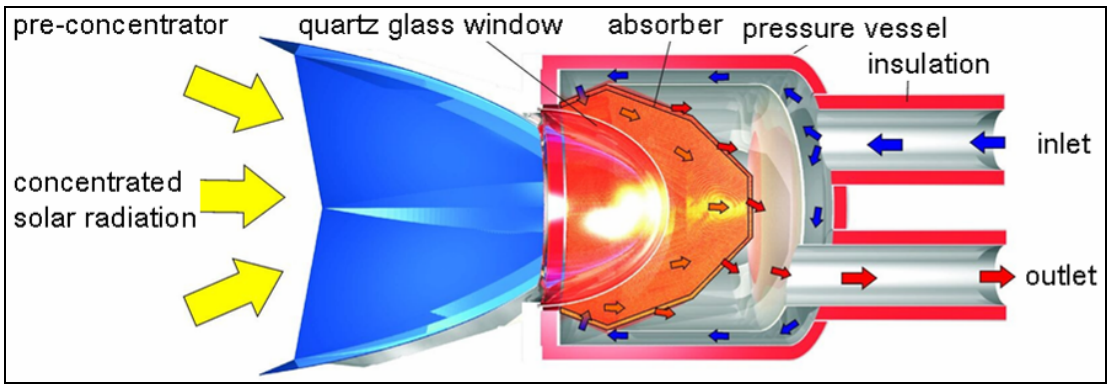

Figure 3-45: Pressurised air heated by solar energy using a volumetric receiver

Concentrating Solar Power for Combined Electricity and Heat

By the end of 2006, a feasibility study was finished by a Jordanian/German consortium to assess the technical and economical feasibility of an integrated production of 10 MW of power, 10,000 tons/day of desalted water and 40 MW cooling capacity for the Ayla Oasis Hotel Resort in Aqaba, Jordan. The system allows for a very efficient use of fossil fuel and uses concentrated solar energy as fuel saver.

A parking lot of 110,000 m² was designated for the integration of the solar field. A linear Fresnel concentrating collector field was selected as solar component (Kern et al., 2009). The flat Fresnel structure fitted better than parabolic trough to this

particular requirement of integration, and the solar energy yield of the Fresnel field on the limited space is roughly twice of that of an equivalent parabolic trough field.

A standard solution for the hotel resort would have been purchasing electricity and water from the public grid and cooling by conventional rooftop compression chillers. As electricity and water are already limited in Aqaba, additional power plant capacity for power and desalination would have been required. As shown in Figure 3-46, the conventional supply of the required commodities would require a natural gas consumption of 85 MW.

The insecurity of future prices for fossil fuels has led to the investigation of the feasibility of an alternative power plant concept for on-site production based on the combined generation of electricity and heat for absorption cooling and multi-effect desalination. The absorption chillers are used for base load operation during the holiday season, while the compression chillers are only used for peaking and intermittent demand. A cold water district cooling grid will be used to distribute the cooling power from the central plant to the different users in several hotels, residential areas and commercial centres and for the technical operation of the resort. The result of the analysis shows that the integrated process will require 35% less fuel input, due to the better efficiency of combined generation and the solar fuel saver (Figure 3-47 from Kern et al., 2009).

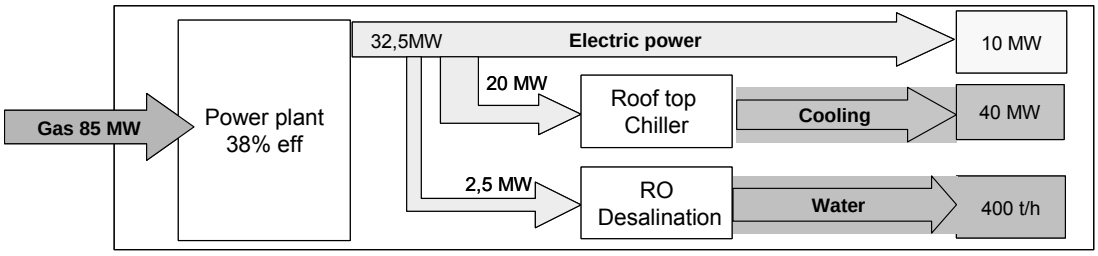

Figure 3-46: Conventional solution for power, cooling and water for a hotel resort in Aqaba

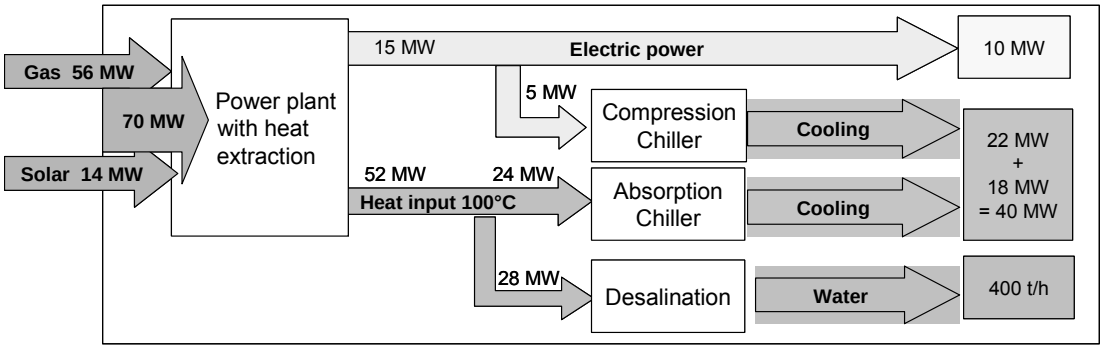

Figure 3-47: Integrated solution for power, cooling and water supported by CSP

An advantage of onsite production of commodities like power, water and cooling is that the production cost competes with purchase prices (that include distribution and public infrastructure) rather than with the production cost of large conventional power plants. With revenues of 0.10 $/kWh for electricity, 0.04 $/kWh for cooling and 1.50 $/m³ for water, the project can be realised with a good internal rate of return without depending on subsidies.

In general, there is a good coincidence of solar energy and cooling demand (50 % of the electricity load in the MENA-Region is caused by air-conditioning due to intensive solar radiation), which allows for a very efficient use of the solar energy and for fuel savings specifically during peak load times.

The only requisite for such a relatively large on-site system is a rather large on-site consumption. This innovative concept opens considerable market opportunities for the unsubsidised use of solar energy. The engineering for the power plant is expected to be initiated in early 2009, and commissioning is planned for early 2011.

3.2.3 Current CSP Project Development

The current development of CSP projects is very dynamic and therefore difficult to assess. At the end of 2008 approximately 482 MW capacity of commercial plants were in operation of which almost 419 MW were installed in the USA, 63 MW in Spain and another 0.36 MW in Australia. The concept mostly used is parabolic trough mirrors with an overall capacity of 468.8 MW. The remaining 16.36 MW are a tower project in Spain with 11 MW and a Fresnel reflector system with 2 MW in Spain and another one in Australia with 0.36 MW capacity (Table 3-4).

Most of the existing capacity was built in a period from the mid 80ies to the early 90ies. The development back then was ascribed to the oil shock in the late 70ies and the resulting rise of electricity prices. As the prices declined shortly afterwards no further CSP projects were initiated due to the decreased competitiveness and the missing political promotion.

Table 3-4: CSP plants in operation at the end of 2008.

Plant name	Net Power Capacity [MW_e]	Type	Constructor	Country	Year of initial operation
SEGS 1	13,8	Parabolic trough	Luz	USA	1985
SEGS 2	30	Parabolic trough	Luz	USA	1986
SEGS 3	30	Parabolic trough	Luz	USA	1987
SEGS 4	30	Parabolic trough	Luz	USA	1987
SEGS 5	30	Parabolic trough	Luz	USA	1988
SEGS 6	30	Parabolic trough	Luz	USA	1989
SEGS 7	30	Parabolic trough	Luz	USA	1989
SEGS 8	80	Parabolic trough	Luz	USA	1990
SEGS 9	80	Parabolic trough	Luz	USA	1991
Arizona Public Services Saguaro Project	1	Parabolic trough	Solargenix Energy	USA	2006
Nevada Solar One	64	Parabolic trough	Acciona/ Solargenix Energy	USA	2007
PS10	11	Tower	Abengoa Solar	Spain	2007
Liddell Power Station	0.36	Fresnel reflector		Australia	2007
Andasol 1	50	Parabolic trough	Solar Millenium and ACS/Cobra	Spain	2009
Puerto Errado 1	2	Fresnel reflector	Tubo Sol Murcia, S.A.	Spain	2009

As the use of renewable energies became more important in the recent years and several governments adopted promotion schemes, the use of CSP is experiencing a revival. In 2007 three installations with a total capacity of about 75 MW came into operation followed by another installation with 52 MW in 2008.

Another 16 project were under construction at the end of 2008 summing up to a capacity of 540 MW (Table 3-5). Again Spain with 389 MW and the USA with 86 MW are the largest contributors to this development. The remaining projects are constructed in Egypt (25 MW) as well as Algeria (20 MW) and Morocco (20 MW).

Table 3-5: CSP plants under construction at the end of 2008.

Plant name	Net Power Capacity [MW_e]	Type	Constructor	Country
Martin Next Generation Solar Energy Center	75	ISCC	FPL	USA
Andasol 2	50	Parabolic trough	Solar Millenium and ACS/Cobra	Spain
Andasol 3	50	Parabolic trough	MAN Solar Millenium (JV MAN Ferrostaal + SM), Duro Felguera S.A. Energía, Gijón	Spain
Extresol 1	50	Parabolic trough	ACS/Cobra	Spain
Solnova 1	50	Parabolic trough	Abengoa Solar	Spain
Solnova 3	50	Parabolic trough	Abengoa Solar	Spain
Puertollano	50	Parabolic trough	Iberdrola	Spain
La Risca 1 or Alvarado	50	Parabolic trough	Acciona	Spain
Kuraymat Plant	25	ISCC	Solar Millenium	Egypt
Hassi R'mel	20	ISCC	Abengoa Solar	Algeria
Ain Beni Mathar Plant	20	ISCC	Abengoa Solar	Morocco
PS 20	20	Tower	Abengoa Solar	Spain
Solar Tres	19	Tower	Sener/Torrosol	Spain
Esolar Demonstrator	5	Tower	Esolar	USA
Kimberlina	5	Fresnel	Ausra	USA
Keahole Solar Power	1	Parabolic trough	Sopogy	USA

The dominating technology is once again parabolic trough. Eight projects use this technology summing up to an overall installation of 351 MW. Another four projects are hybrid installations so called Integrated Solar Combined Cycle (ISCC) plants. This technology combines a solar field of parabolic trough collectors with a gas fire combined cycle plant. The capacities referred to in Table 3-5 are the solar share of the overall capacity. The tower technology is applied in three projects under construction at the moment aiming for 44 MW of installed capacity. The Fresnel technology is currently in the process of installation in one project in the USA. Figure 3-48 shows CSP capacities currently in operation or under construction per country.

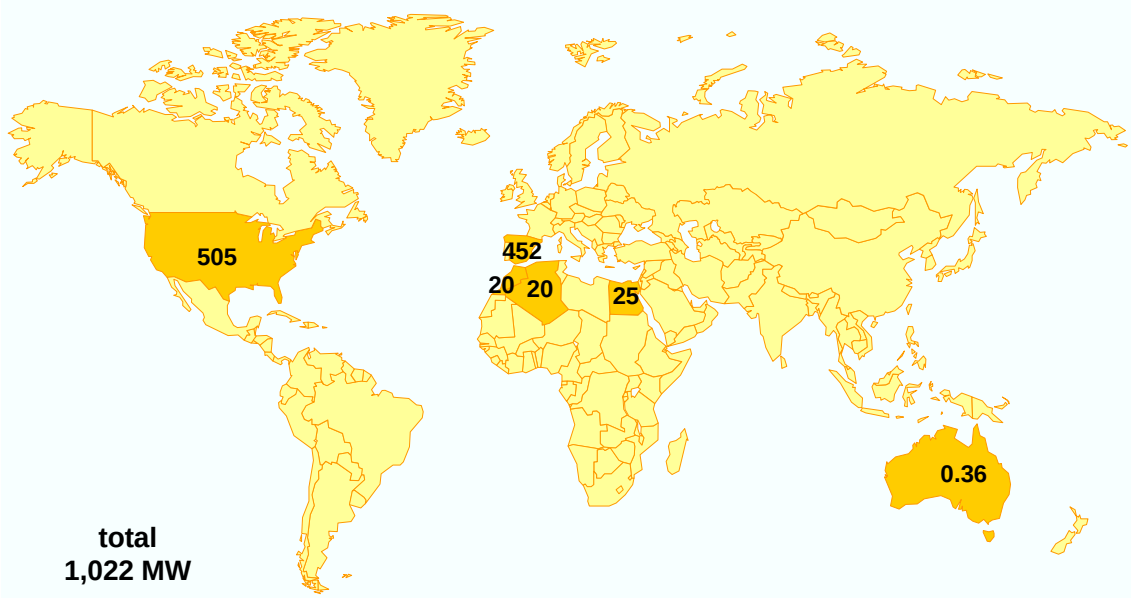

Figure 3-48: CSP capacities in operation or under construction at the end of 2008.

It is not clear how large the number of currently planned installations is. Declarations of intend can be found on many different levels regarding existing technology as well as demonstration projects of new technological developments. The status of many of these projects is constantly changing. Figure 3-49 and the following Tables give an overview of announced projects at the end of 2008 excluding political goals like Chinas target to install 1000 MW CSP capacity until 2020.

Overall 5975 to 7415 MW planned capacity of CSP plants could be identified on a project level that was announced until the end of 2008 (Figure 3-49). The countries that account for the majority of these projects are once again the USA and Spain. Table 3-6 shows a detailed list of the announced installations in the USA that amounted to 3407 to 4847 MW. Another 1980 MW are planned in Spain (Table 3-7). It can be observed that the list of projects in Spain is a lot larger than the one in the United States even though the overall announced capacity is smaller. The reason for this is the promotion scheme of Spain that provides a feed in tariff for installations up to 50 MW. The remaining announcements of another 588 MW planned capacity can be found in various other countries (Table 3-8).

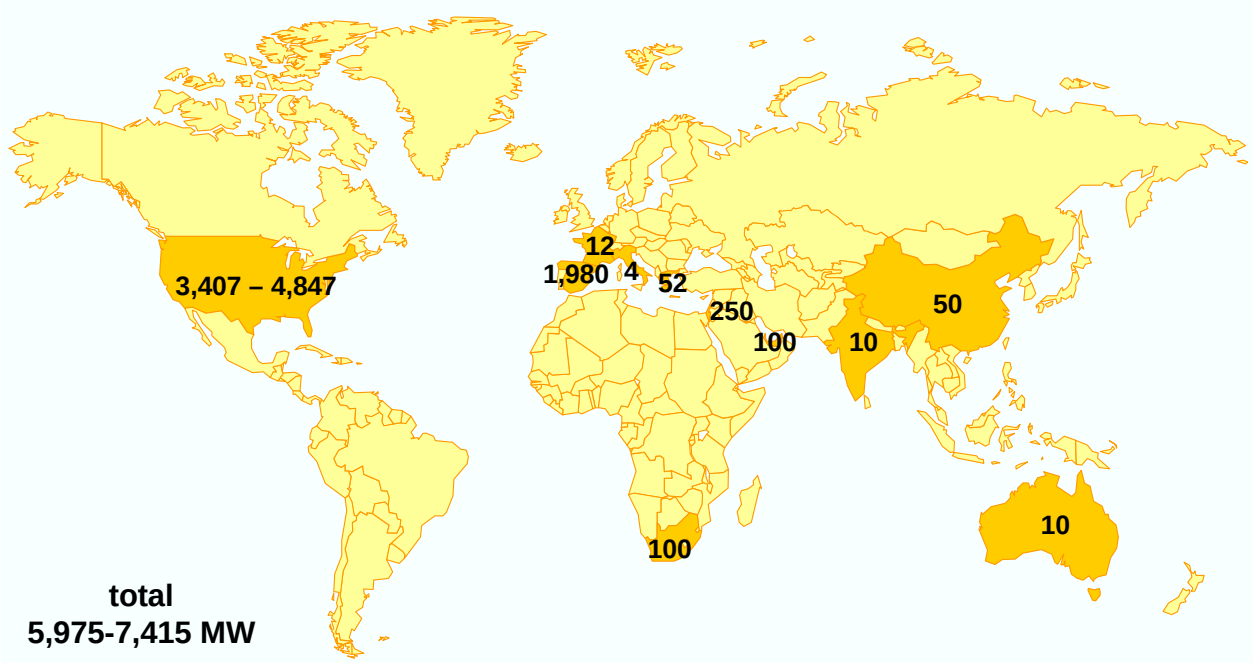

Figure 3-49: Announced CSP installations at the end of 2008.

Table 3-6: Announced CSP installations in the USA.

Plant name	Net Power Capacity [MW_e]	Type	Constructor	Country
Ivanpah 1	123	Tower	Brightsource	USA
Ivanpah 2	100	Tower	Brightsource	USA
Ivanpah 3	200	Tower	Brightsource	USA
(Brightsource other)	100 (+400)	Tower	Brightsource	USA
Mojave Solar Park	553	Parabolic trough	Solel	USA
SES Solar One	500 (+300)	Dish	Stirling Energy Systems	USA
SES Solar Two	300 (+600)	Dish	Stirling Energy Systems	USA
Solana	280	Parabolic trough	Abengoa	USA
Carrizo Solar Farm	177	Fresnel	Ausra	USA
Beacon Solar Energy Project	250	Parabolic trough	FPL	USA
Gaskell Sun Tower	105-245	Tower	Esolar	USA
San Joaquin Solar 1 & 2	107	Parabolic trough	Martifer Renewables	USA
City of Palmdale Hybrid Power Project	62	ISCC		USA
Harper Lake Energy Park	500	Parabolic trough		USA
Victorville 2 Hybrid Power Project	50	ISCC		USA

Table 3-7: Announced CSP installations in Spain.

Plant name	Net Power Capacity [MW_e]	Type	Constructor	Country
Lebrija 1	50	Parabolic trough	Solel	Spain
Andasol 4	50	Parabolic trough	ACS/Cobra	Spain
Extresol 2	50	Parabolic trough	ACS/Cobra	Spain
Extresol 3	50	Parabolic trough	ACS/Cobra	Spain
Manchasol 1	50	Parabolic trough	ACS/Cobra	Spain
Manchasol 2	50	Parabolic trough	ACS/Cobra	Spain
Andasol 5	50	Parabolic trough	Solar Millenium	Spain
Andasol 6	50	Parabolic trough	Solar Millenium	Spain
Andasol 7	50	Parabolic trough	Solar Millenium	Spain
Solnova 2	50	Parabolic trough	Abengoa	Spain
Solnova 4	50	Parabolic trough	Abengoa	Spain
Solnova 5	50	Parabolic trough	Abengoa	Spain
AZ 20	20	Tower	Abengoa	Spain
Aznalcollar TH	0.08	Dish	Abengoa	Spain
Ecija 1	50	Parabolic trough	Abengoa	Spain
Ecija 2	50	Parabolic trough	Abengoa	Spain
Helios 1	50	Parabolic trough	Abengoa	Spain
Helios 2	50	Parabolic trough	Abengoa	Spain
Almaden Plant	20	Tower	Abengoa	Spain
Termesol 50	50	Parabolic trough	Sener	Spain
Arcosol 50	50	Parabolic trough	Sener	Spain
Ibersol Badajoz	50	Parabolic trough	Iberdrola	Spain
Ibersol Valdecaballeros 1	50	Parabolic trough	Iberdrola	Spain
Ibersol Valdecaballeros 2	50	Parabolic trough	Iberdrola	Spain
Ibersol Sevilla	50	Parabolic trough	Iberdrola	Spain
Ibersol Almería	50	Parabolic trough	Iberdrola	Spain
Ibersol Albacete	50	Parabolic trough	Iberdrola	Spain
Ibersol Murcia	50	Parabolic trough	Iberdrola	Spain
Ibersol Zamora	50	Parabolic trough	Iberdrola	Spain
Enerstar Villena Power Plant	50	Parabolic trough	Enerstar	Spain
Gotasol	10	Fresnel	Solar Power Group	Spain
Aste 1 A	50	Parabolic trough	Aries	Spain
Aste 1 B	50	Parabolic trough	Aries	Spain
Aste 3	50	Parabolic trough	Aries	Spain
Aste 4	50	Parabolic trough	Aries	Spain
Astexol 1	50	Parabolic trough	Aries	Spain
Astexol 2	50	Parabolic trough	Aries	Spain
Puerto Errado 2	30	Fresnel	Tubo Sol Murcia, S.A.	Spain
La Risca 2	50	Parabolic trough	Acciona	Spain
Palma del Rio 1	50	Parabolic trough	Acciona	Spain
Palma del Rio 2	50	Parabolic trough	Acciona	Spain
Consol 1	50	Parabolic trough	Conergy	Spain
Consol 2	50	Parabolic trough	Conergy	Spain

Table 3-8: Announced CSP installations various countries.

Plant name	Net Power Capacity [MW_e]	Type	Constructor	Country
Ashalim	250	Parabolic trough		Israel
Uppington	100	Tower	Eskom	South Africa
Shams	100	Parabolic trough		ABU DHABI
Cloncurry solar power station	10	Tower	Ergon Energy	Australia
Archimede	3.75	ISCC	Enel etc.	Italy
Solenha	12	Parabolic trough	Solar Euromed	France
Theseus Project	52	Parabolic trough	Solar Millenium	Greece
	50	Parabolic trough	Solar Millenium	China
	10		ACME	India

As the development is rapid and many projects might have slipped through the collection displayed above a number of other publications will be referenced in the following.

Already in May 2008 New Energy Finance published an overview of planned CSP capacities that amounted to 6.7 GW (Figure 3-50). This figure is including projects that are past the “site banking” stage. Again the US is the most important market followed by Spain.

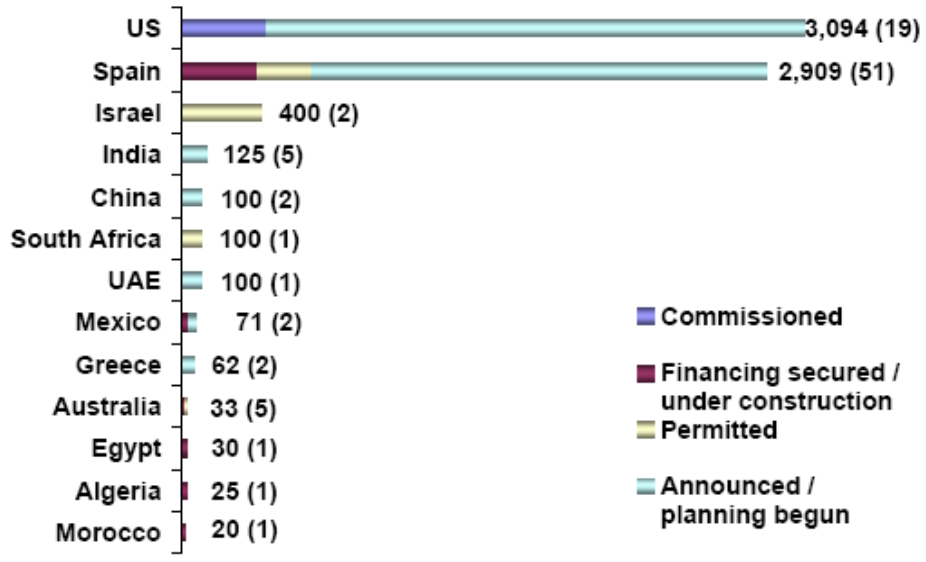

Figure 3-50: The global CSP pipeline, by geography in MW (New Energy Finance, 2008).

On the basis of the announcements made by the CSP industry the Prometheus Institute expects 11 GW of total installed CSP capacity in 2012 (Grama et al., 2008). As can be seen in Figure 3-51 not only solar thermal technology is included in this figure but also Concentrated Photovoltaic systems (CPV). Disregarding this figure together with the so called “other” technologies that are still at the development stage a total installed capacity of 8 GW CSP is expected until 2012.

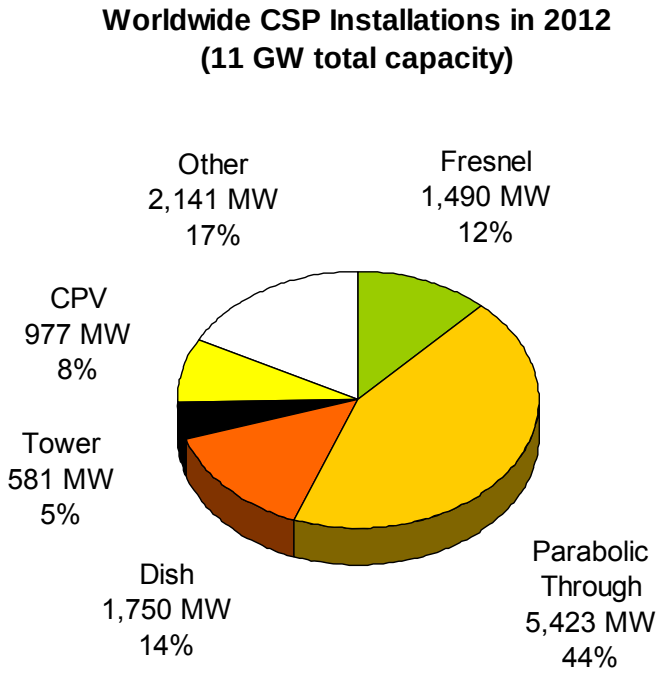

Figure 3-51: Worldwide CSP installations – distribution by technology in 2012 (Grama et al., 2008).

The actual development of CSP installations in the coming years however, will not only depend on the intention of project developers but also on permission procedures as well as the capacities of equipment manufacturers. Some data regarding the installation time and required workforce can already be obtained from experience with existing projects. Andasol 1 with a capacity of 50 MW for example had a construction time of 2 to 2.5 years. During this period up to 500 people where engaged in this activity. For the operation period about 40 people are expected to be employed at the site (Solar Millennium, 2008).

A realistic assumption regarding the dynamic development of projects as well as the expansion of equipment manufacturers is to have 5000 MW overall installed CSP capacity by 2015.

3.2.4 CSP Plant Performance Model

Table 3-9 gives an overview of some technical parameters of different concentrating solar power concepts. Parabolic troughs, linear Fresnel systems and power towers can be coupled to steam cycles of 10 to 200 MW of electric capacity, with thermal cycle efficiencies of 30 to 40%. The values for parabolic troughs, by far the most mature technology, have been demonstrated in the field. Today, these systems achieve annual solar-to-electricity-efficiencies of about 10 to 15%, with the perspective to reach about 18% in the medium and long term. The values for the other systems are, in general, projections based on component and prototype system test data and the assumption of mature development of current technology. The overall solar-electric efficiencies are lower than the conversion efficiencies of conventional steam or combined cycles, as they include the conversion of solar radiation to heat within the collector and the conversion of the heat to electricity in the power block. The conversion efficiency of the power block remains basically the same as in equivalent fuel fired steam cycle power plants.

Table 3-9: Performance data of various concentrating solar power (CSP) technologies.

	Capacity Unit MW	Concen-tration	Peak Solar Efficiency	Annual Solar Efficiency	Thermal Cycle Efficiency	Capacity Factor (solar)	Land Use m²/MWh/y
Trough	10 – 200	70 - 80	21% (d)	10 – 15% (d)	30 – 40 % ST	24% (d)	6 - 8
				17 – 18% (p)		25 – 70% (p)	
Fresnel	10 - 200	25 - 100	20% (p)	9 - 11% (p)	30 - 40 % ST	25 - 70% (p)	4 - 6
Power Tower	10 – 150	300 – 1000	20% (d)	8 – 10 % (d)	30 – 40 % ST	25 – 70% (p)	8 - 12
			35 % (p)	15 – 25% (p)	45 – 55 % CC		
Dish-Stirling	0.01 – 0.4	1000 – 3000	29% (d)	16 – 18 % (d)	30 – 40 % Stirl.	25% (p)	8 - 12
				18 – 23% (p)	20 – 30 % GT		

(d) = demonstrated, (p) = projected, ST steam turbine, GT Gas Turbine, CC Combined Cycle.

Solar efficiency = net power generation / incident beam radiation

Capacity factor = solar operating hours per year / 8760 hours per year

Because of their thermal nature, each of these technologies can be “hybridized”, or operated with fossil fuel as well as solar energy. Hybridization has the potential to dramatically increase the value of CSP technology by increasing its power availability, by decreasing its cost (making more effective use of the power block equipment), and reducing the technological risk by allowing conventional fuel use in case the collector may have to be repaired. Solar heat collected during the daytime can be stored in concrete, molten salt, ceramics or phase-change media. At night, it can be extracted from the storage to run the power block. Fossil and renewable fuels like oil, gas, coal and biomass can be used for co-firing the plant, thus providing power capacity whenever required.

Moreover, the solar energy can be used for the co-generation of electricity and heat. In this case, the high value solar energy input is used with best possible efficiencies of up to 85 %. Possible applications cover the combined production of electricity, industrial process heat, district cooling and sea water desalination.

It is generally assumed that solar concentrating systems are only economic for locations with direct solar irradiation above 2000 kWh/m²/y. Typical examples are Barstow/USA with 2700 kWh/m²/y and Almeria/Spain with 2100 kWh/m²/y). Today, all concepts would have capacity factors of 25%, equivalent to about 2000 full load operating hours per year, with the perspective to expand their time of solar operation to base load using thermal energy storage and larger collector fields. To generate one Megawatt-hour of solar electricity per year by CSP, a land area of 4 to 12 m² is required. This means, that one km² of arid land can continuously and indefinitely generate as much electricity as any conventional 50 MW coal or gas fired power station.

In our model, we have taken a typical parabolic trough steam cycle power station with thermal energy storage as reference for assessing the solar-to-electricity conversion efficiency. With respect to the aperture area, a parabolic trough system with wet cooling has an average annual efficiency of 15%. That means that 15% of the solar irradiation on the reflector aperture area of a parabolic trough collector can be transformed to net electricity delivered to the power grid. In our case, we assumed a dry cooling system for the steam cycle, which typically reduces efficiency to around 12%. Dry cooling is assumed as it can be applied everywhere without constraints of water availability. With respect to the total available land surface for CSP plant installation – which is the original resource potential described in Chapter 3.1 – a parabolic trough collector covers about 37%. Multiplying 37% times 12% yields an overall land use efficiency of 4.5% of a typical parabolic trough power station with dry cooling tower with respect to the solar energy irradiated per year on the total land surface covered by the plant (Table 3-10).

The following equations were used to calculate land-use efficiency of concentrating solar power stations with respect to the total land area available:

$$\textbf{Solar Electric Efficiency} = \frac{\text{Annual Net Power Generation}}{\text{Annual Direct Irradiance on Aperture}}$$

$$\textbf{Land Use Factor} = \frac{\text{Aperture Area of Reflectors}}{\text{Total Land Area Required}}$$

$$\textbf{Land Use Efficiency} = \textbf{Solar Electric Efficiency x Land Use Factor}$$

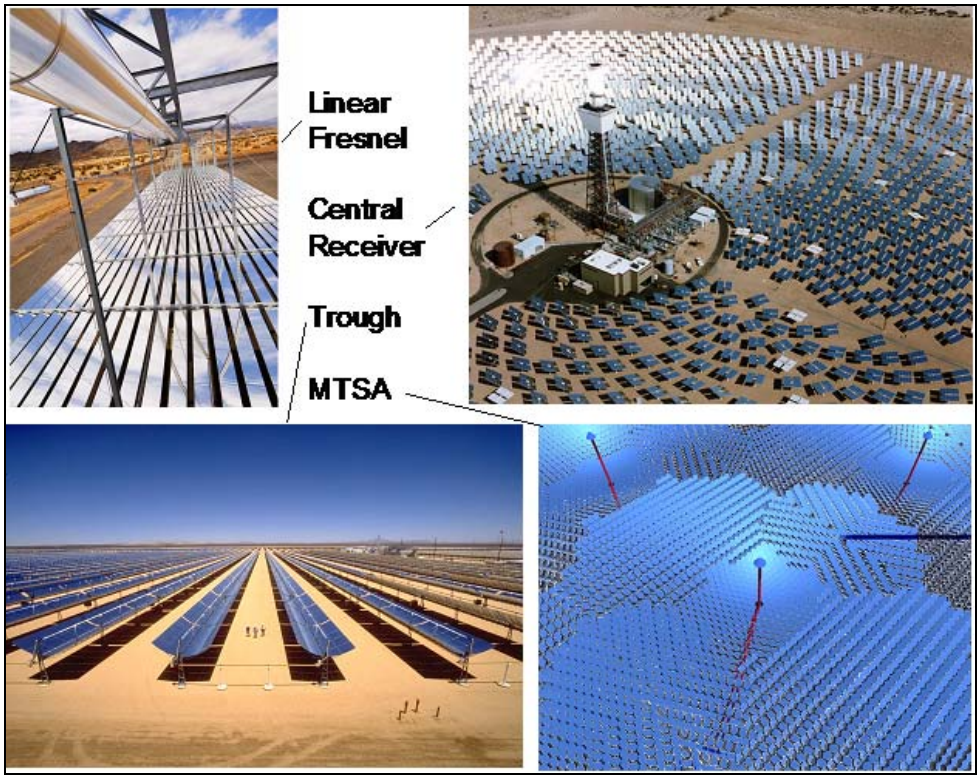

Figure 3-52: Land use of different concentrating solar collector concepts (Multi-Tower Solar Array MTSA shows an artist view of a potential future central receiver concept with very high land use efficiency presently under development).

Table 3-10: Solar-electric efficiency, land use factor and land use efficiency of different CSP technologies. A parabolic trough system with 12% solar-electric efficiency, 37% land use factor and 4.5% land use efficiency was taken as reference system for REACCESS.

Collector & Power Cycle Technology	**Solar-Electric Aperture Related Efficiency**	**Land Use Factor**	**Land Use Efficiency**
Parabolic Trough Steam Cycle	11 – 16%	25 – 40%	3.5 – 5.6%
Central Receiver Steam Cycle	12 – 16%	20 – 25%	2.5 – 4.0%
Linear Fresnel Steam Cycle	8 – 12%	60 – 80%	4.8 – 9.6%
Central Receiver Combined Cycle*	20 – 25%	20 – 25%	4.0 – 6.3%
Multi-Tower Solar Array Steam or Combined Cycle*	15 – 25%	60 – 80%	9.0 – 20.0%

* future concepts

3.2.5 CSP Production Potentials in MENA and the World Regions

In order to calculate the technical CSP electricity potentials in the MENA region and world wide, land areas available for CSP plant erection from Table 3-2 and Table 3-3 were multiplied with the land use efficiency of 4.5% described before. This simple approach yields a good estimate of the technical potentials of CSP represented by the well proven parabolic trough technology (Table 3-11 and Table 3-12). The analysis yields a total overall CSP potential of 537,680 TWh/y for the MENA region and 2,945,926 TWh/y world wide. Comparing those numbers to the present world electricity consumption of 17,000 TWh/y we see that the available technical CSP potentials could theoretically cover this demand many times. The best solar irradiation category in Algeria alone has a technical CSP potential that exceeds the world electricity demand by a factor of two. The methodology used here is summarized in Figure 3-55 and data is introduced to the REACCESS database.

Table 3-11: CSP electricity potentials in TWh/y available in the MENA countries for different DNI Classes based on resource assessment described in Chapter 3.1.

DNI Class	Morocco	Algeria	Tunisia	Libya	Egypt	Jordan	Saudi Arabia
2000-2099	575	589	878	735	20	198	3,100
2100-2199	559	3,380	638	2,508	147	584	13,393
2200-2299	1,126	3,002	1,021	11,355	1,744	1,987	34,787
2300-2399	1,857	4,262	2,102	19,079	4,425	1,186	36,180
2400-2499	3,864	25,072	2,568	17,198	4,652	1,209	21,119
2500-2599	3,577	44,995	1,362	21,451	5,220	847	7,664
2600-2699	2,300	52,061	29	18,895	11,907	383	5,197
2700-2800+	6,057	34,975	0	47,082	44,727	0	1,855
Total	19,915	168,336	8,597	138,303	72,840	6,394	123,296

Table 3-12: CSP electricity potentials in TWh/y available in the REACCESS world regions for different DNI Classes based on resource assessment described in Chapter 3.1.

DNI Class	Africa	Australia	Central Asia, Caucase	Canada	China	Central South America	India	Japan
2000-2099	102,254	6,631	14,280	0	8,332	31,572	7,893	0
2100-2199	138,194	18,587	300	0	18,276	20,585	1,140	0
2200-2299	139,834	36,762	372	0	43,027	24,082	550	0
2300-2399	141,066	87,751	177	0	28,415	20,711	774	0
2400-2499	209,571	148,001	64	0	11,197	6,417	426	0
2500-2599	203,963	207,753	0	0	11,330	3,678	13	0
2600-2699	178,480	142,490	0	0	2,180	5,120	119	0
2700-2800+	346,009	49,625	0	0	3,079	11,827	15	0
Total	**1,459,370**	**697,600**	**15,193**	**0**	**125,835**	**123,992**	**10,928**	**0**

DNI Class	Middle East	Mexico	Other Developing Asia	Other East Europe	Russia	South Korea	EU27+	USA
2000-2099	3,432	1,606	4,491	6	0	0	866	14,096
2100-2199	12,443	3,378	5,174	13	0	0	497	17,114
2200-2299	39,191	3,650	10,947	2	0	0	660	21,748
2300-2399	60,188	5,807	30,776	0	0	0	162	16,402
2400-2499	71,324	15,689	19,355	0	0	0	90	23,903
2500-2599	34,954	7,134	4,429	0	0	0	69	8,116
2600-2699	32,263	1,534	253	0	0	0	31	2,326
2700-2800+	36,843	1,878	136	0	0	0	34	0
Total	**290,639**	**40,675**	**75,561**	**21**	**0**	**0**	**2,409**	**103,704**

Besides of the total technical potential of harvesting solar electricity at different solar irradiation levels described before, the capability of CSP for providing base, intermediate or peaking power must be described. For this purpose, we have developed a simple model describing the achievable annual full load operating hours as function of plant configuration. The configuration of a CSP plant is best described by the so called Solar Multiple (SM). For example a steam cycle power station with a Solar Multiple of 1 has a solar field just large enough to provide nominal capacity under nominal irradiation conditions, e.g. at 800 W/m². A CSP plant with a solar multiple SM2 would have a solar field twice as large and a thermal energy storage system large enough to totally store the energy produced by the second solar field during the day (Figure 3-53). Thus, one solar field will directly drive the turbine, while the other solar field will serve to fill the storage for night time operation.

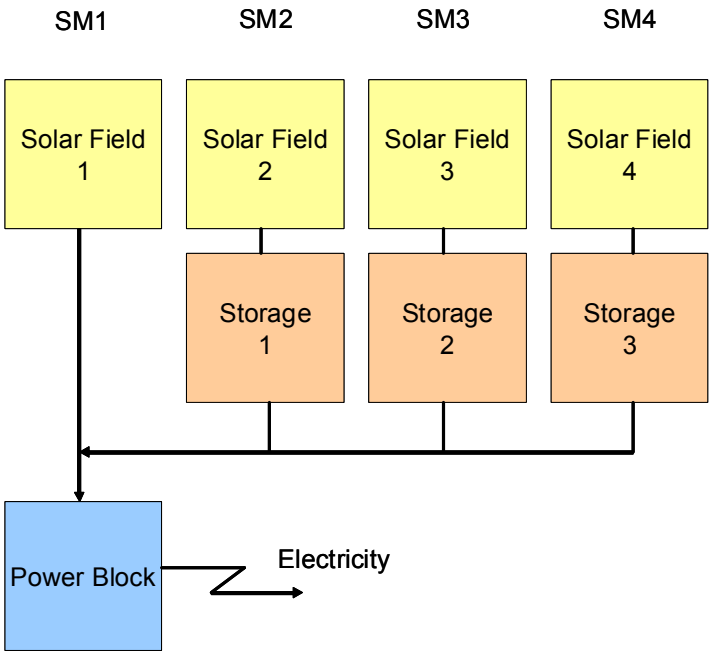

Figure 3-53: Definition of CSP plant configuration with different Solar Multiple (SM).

The following function was derived from hourly time series analysis of the performance of different CSP plant configurations under different irradiation conditions. It describes the achievable annual full load operating hours (Flh) of a CSP plant as function of the solar multiple (SM) and annual irradiation (DNI):

$$Flh = (2.5717 \cdot DNI - 694) \cdot (-0.0371 \cdot SM^2 + 0.4171 \cdot SM - 0.0744)$$

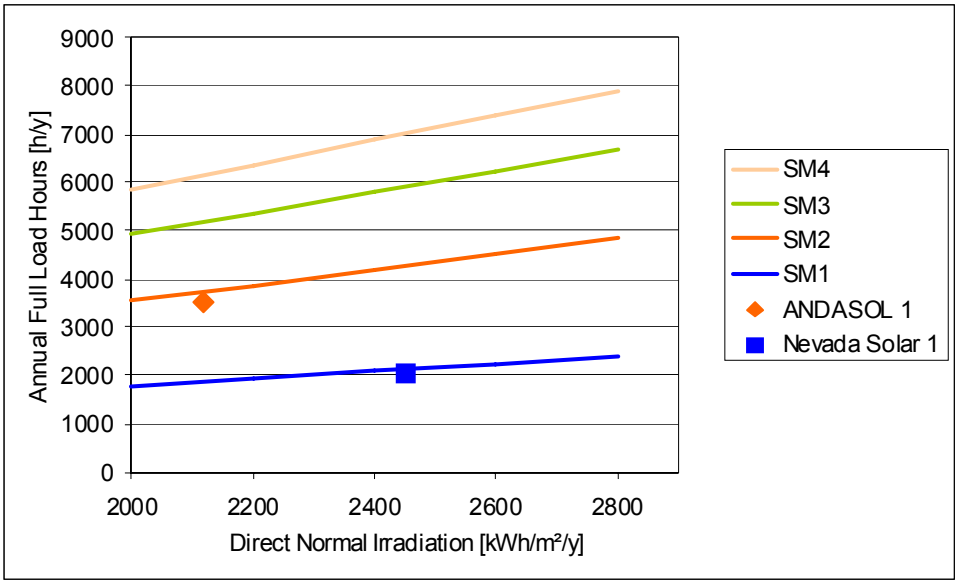

Figure 3-54: Annual full load hours of a CSP plant (h/y) as function of annual direct normal irradiation and solar multiple SM1 - SM4 compared to project data from ANDASOL 1 (Nebrera 2008) and NEVADA Solar 1 (Cohen 2007).

Table 3-13: Annual full load hours (h/y) of CSP plants for different Solar Multiple (SM) and different annual direct normal irradiation (DNI).

DNI [kWh/m²/y]	SM4	SM3	SM2	SM1
2000	5840	4921	3569	1784
2200	6354	5355	3883	1941
2400	6869	5788	4198	2098
2600	7383	6222	4512	2255
2800	7898	6655	4827	2413

A standard solar field with solar multiple SM1 defines a collector field with an aperture area of 6000 m² per installed MW of power capacity. Each storage unit has a capacity of 6 full load operating hours. This model considers current parabolic trough technology with molten salt storage, steam cycle power block and dry cooling tower as reference.

Modelling results for the annual full load hours are shown in Table 3-13 and Figure 3-54 for different configurations and different annual solar irradiation. As an example, a CSP plant with a solar multiple 4 has 4 x 6000 = 24,000 m²/MW solar field area plus 3 x 6 = 18 hour storage capacity. Such a plant will achieve 5840 full load operating hours at an annual solar irradiation of 2000 kWh/m²/y in Southern Spain and about 7900 full load hours in Egypt at a solar irradiation of 2800 kWh/m²/y. SM4 has been chosen as reference case for the REACCESS model.

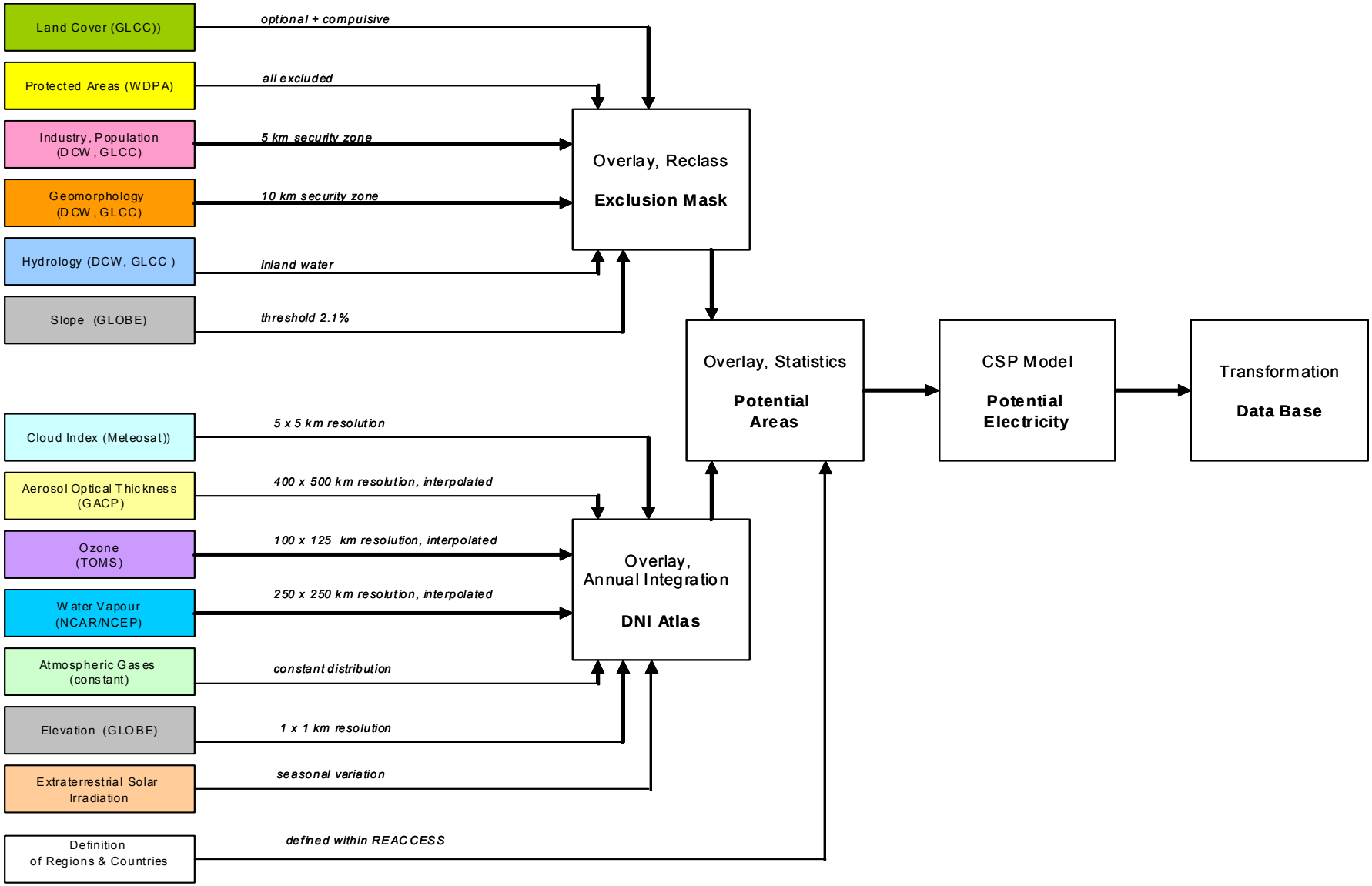

Figure 3-55: Methodology of concentrating solar power resource assessment and performance model used within REACCESS

3.3 CONCENTRATING SOLAR POWER PLANT COST MODEL

The cost of concentrating solar power plants was modelled in different ways with respect to the different components of such plants. For each component, a separate learning curve and progress ratio for future cost development was assumed

Table 3-14). The learning curve of each component (investment cost *c* as function of time *x*) was calculated from the total installed capacity *P* and from the progress ratio *PR* according to the following Equation 9, where P_0 was the installed capacity at the starting year 2005 and P_x was the installed capacity in the year *x*, and c_0 and c_x stand for the respective specific investment at that time:

$$c_x = c_0 \cdot \left(\frac{P_x}{P_0} \right)^{\frac{\log PR}{\log 2}}$$ Equation (9)

Table 3-14: Start values c_0 and PR for CSP plant components taking current parabolic trough technology and molten salt storage as reference.

	Progress Ratio	Start 2005
Solar Field	90%	360 €/m²
Power Block	98%	1200 €/kW
Storage	92%	60 €/kWh

A progress ratio of 90% means that the specific investment is reduced by 10% each time the world wide installed capacity doubles. The model was based on a scenario of world wide CSP expansion adopted by (Viebahn & Lechon, 2007) as optimistic/realistic scenario. It starts with 354 MW solar power capacity installed in 2005 and expands to 5000 MW by 2015, 150,000 MW by 2030 and 500,000 MW by 2050. According to this expansion and the learning rates assumed here, the total specific investment of CSP plants would develop as shown in Table 3-15 and Figure 3-56 for different plant configurations with varying solar multiple and solar operating hours (SM1 - SM4). Again here, a solar multiple of SM4 has been taken as reference for the performance and cost modelling for REACCESS (base load plants).

Table 3-15: Total specific investment of CSP plants in €/kW as function of the Solar Multiple SM and time taking into account CSP economies of scale and world wide expansion of CSP according to (Viebahn & Lechon, 2007) optimistic/realistic scenario. SM4 was taken as reference for REACCESS database and modelling.

Year	2005	2015	2030	2050
SM1	3360	2559	1869	1690
SM2	5880	4269	2907	2560
SM3	8400	5978	3944	3429
SM4	10920	7688	4982	4299

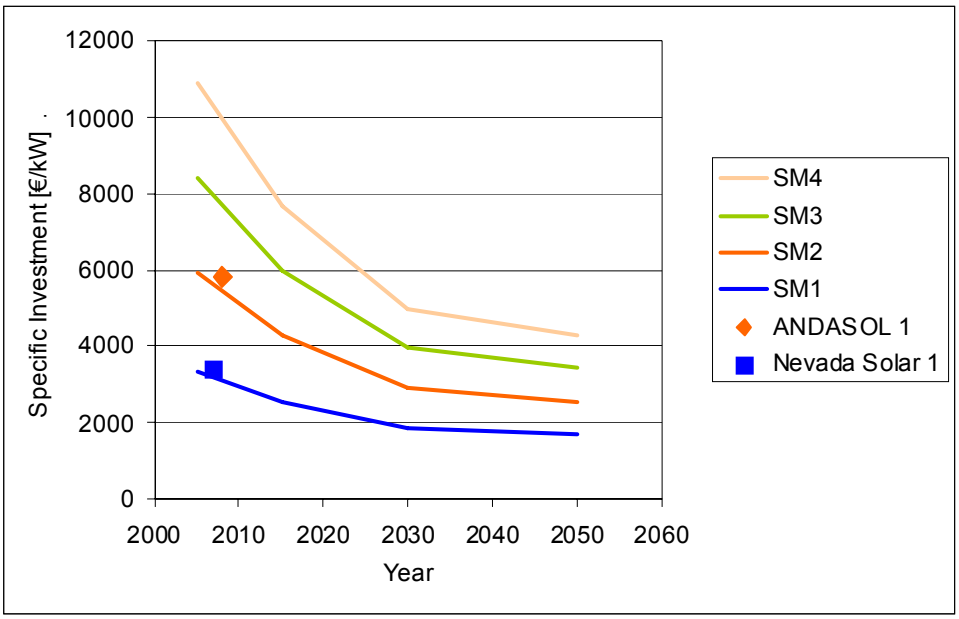

Figure 3-56: Learning curves for the specific investment of CSP plants as function of the solar multiple and time compared to project data from ANDASOL 1 (Nebrera 2008) and NEVADA Solar 1 (Cohen 2007)

Taking into account the annual full load operating hours from Table 3-13 and the related investment learning curve for a solar multiple of SM4 from Table 3-15, it is possible to calculate the total electricity cost as function of solar irradiation and time (Table 3-16 and Figure 3-57). The model assumes constant € value of 2005, a real discount rate of 6%, plant lifetime of 25 years, an annual operation and maintenance cost rate of 2% of the initial investment, an annual insurance rate of 0.5% of the initial investment, and the learning rates and achievable full load hours described before. An example calculation is shown in Table 3-17 for sites with direct normal irradiance of 2700 kWh/m²/y. At such sites, CSP plants with SM4 would start with an electricity cost of 0.140 €/kWh in 2005 and achieve a cost as low as 0.055 €/kWh by 2050.

Table 3-16: Electricity cost learning curves in €/kWh until 2050 as function of direct normal irradiation in kWh/m²/y for CSP reference plants with a solar multiple SM4.

DNI [kWh/m²/y]	2005	2015	2030	2050
2000	0.183	0.129	0.083	0.072
2200	0.168	0.118	0.077	0.066
2400	0.155	0.109	0.071	0.061
2600	0.144	0.102	0.066	0.057
2800	0.135	0.095	0.062	0.053

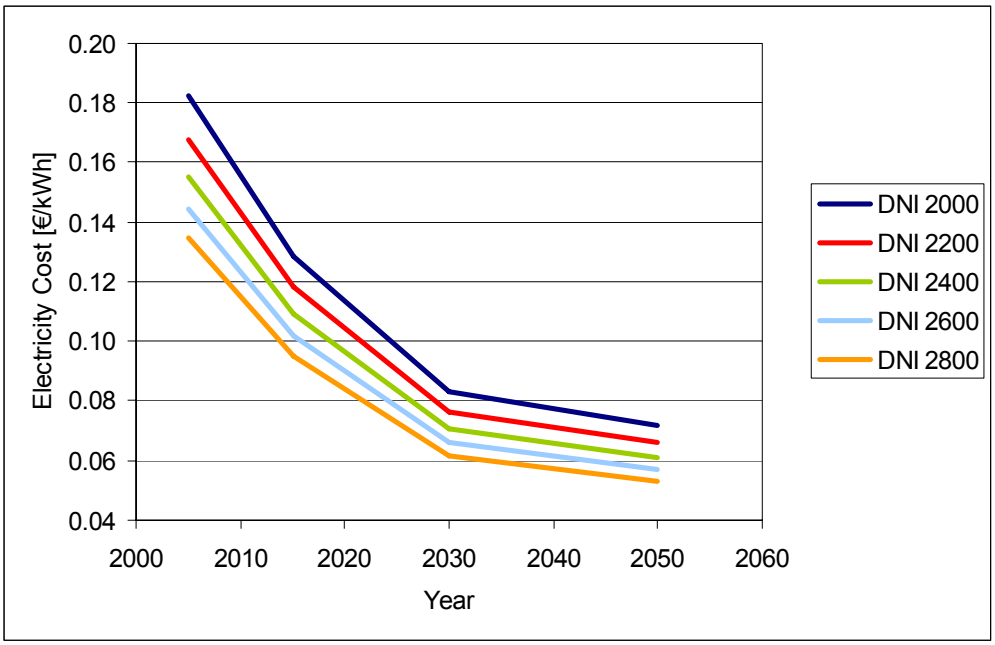

Figure 3-57: Electricity cost learning curves in €/kWh until 2050 as function of direct normal irradiation in kWh/m²/y for CSP reference plants with a solar multiple SM4.

The CSP cost model for REACCESS considers current parabolic trough technology with molten salt storage and steam cycle power block with dry cooling tower as reference. Table 3-17 shows a more detailed calculation of specific investment and annual full load hours for the reference technology.

Table 3-17: Calculation of specific investment and annual full load hours with the CSP performance and cost model developed for REACCESS.

Year	2005	2015	2030	2050	Unit	
World CSP Capacity	354	5000	150000	500000	MW	NEEDS, Optimistic-Realistic Scenario
Solar Field Cost	360	241	144	120	€/m²	90% Progress Ratio Solar Field
Power Block Cost	1200	1111	1006	971	€/kW	98% Progress Ratio System Integration
Solar Field Size (SM1)	6	6	6	6	m²/kW	
Total Solar Field Size	24	24	24	24	m²/kW	
Storage Cost	60	44	29	25	€/kWh	92% Progress Ratio Storage
Storage Capacity	18.0	18.0	18.0	18.0	kWh/kW	
Storage Cost	1080	785	522	451	€/kW	
Solar Field Cost	8640	5792	3454	2876	€/kW	
Discount Rate	6.0%	6.0%	6.0%	6.0%	%/y	
Plant Lifetime	30	30	30	30	y	
Solar Multiple	4	4	4	4		
Direct Normal Irradiance	2700	2700	2700	2700	kWh/m²/y	
Specific Investment	**10920**	**7688**	**4982**	**4299**	**€/kW**	
Full Load Hours per Year	**7641**	**7641**	**7641**	**7641**	**kWh/kW/y**	
Fixed Charge Rate	7.3%	7.3%	7.3%	7.3%	%/y	
O&M Cost	2.0%	2.0%	2.0%	2.0%	%Inv./y	
Insurance Cost	0.5%	0.5%	0.5%	0.5%	%Inv./y	
Annual Capital Cost	793.3	558.5	361.9	312.3	€/kW/y	
Annual O&M Cost	218.4	153.8	99.6	86.0	€/kW/y	
Annual Insurance Cost	54.6	38.4	24.9	21.5	€/kW/y	
Total Annual Cost	**1066.3**	**750.7**	**486.4**	**419.8**	**€/kW/y**	
Levelised Electricity Cost	**0.140**	**0.098**	**0.064**	**0.055**	**€/kWh**	

4 IMPORT INFRASTRUCTURES

4.1 TRANSMISSION TECHNOLOGIES, CAPACITIES AND COSTS

Two technical concepts for the transmission of electricity exist. It can be transmitted as either alternating current (AC) or direct current (DC). Even though the first electricity transmission systems were direct current systems, alternating current is the transmission system widely used today. Historically this can be explained with direct current transmission being not feasible for transport over long distances at low voltage due to high losses. With the invention of high voltage valves and the increasing need for electricity transport over distances above 500 km, the use of DC transmission became an attractive option again.

4.1.1 HVDC versus HVAC

Both technologies for the transmission of electricity high voltage direct current (HVDC) as well as high voltage alternating current (HVAC) do have their advantages. Therefore its use needs to be assessed for each project. There are however some good reasons to favour HVDC over HVAC when it comes to the import of electricity from CSP. First of all the investment costs of HVDC lines are considerably lower than for HVAC lines. However, as generation plants as well as consumer goods have grown to use the AC technology a conversion from AC to DC is needed on both sides of the line. The costs of these converter stations are considerably larger than those of transformer stations. Taking these costs into account the use of HVDC does become economically feasible at a distance between 600 and 800 km for overhead lines and about 50 km for sea cables (ABB, 2007).

Another positive aspect is the lower losses of electricity in HVDC lines over long distances compared to HVAC lines. As this argument was used once against the DC technology it has to be stressed that the reduction of those losses occurs over the increase of voltage which proved to have a stronger impact on the DC technology. As an example you can compare an 800 kV HVDC with an 800 kV HVAC overhead line. The HVDC line does have losses of 3% per 1000 km whereas the losses of the HVAC line are at around 7% per 1000 km. Taking a look at sea cables the differences are even more striking. As losses of HVDC sea cables are in the same range as overhead lines which does not put any limitation to the possible distance, a 750 kV HVAC sea cable does have losses of approximately 60% per 100 km. Again the different losses of either the converter or the transformer station have to be taken into consideration. As these account only for 0.6% vs. 0.2% of additional losses per station they don't have such a considerable influence on the comparison.

Environmental issues are not so much relevant for the economical comparison of the two systems. They do have however a strong impact on the viability of transmission

projects. The influences on the environment boil down to the use of land. To make the difference clear it has to be explained that a transmission line with the same voltage level of HVDC is capable to transport significantly more capacity than a HVAC line. Taking the example used above again. A ±800 kV HVDC line can transport a maximum capacity of 6400 MW whereas an 800 kV HVAC line is limited to 2000 MW. Also the number of lines differs between the technologies. HVDC lines typically consist of a dipole needing a positive and a negative line. A HVAC line however does consist of three phases and therefore needs to apply tree lines. The pylon construction for a HVAC line therefore needs to be larger than for a HVDC line. Figure 4-1 shows a comparison the space needed for the transmission of a 10 GW capacity in on AC and two DC technologies.

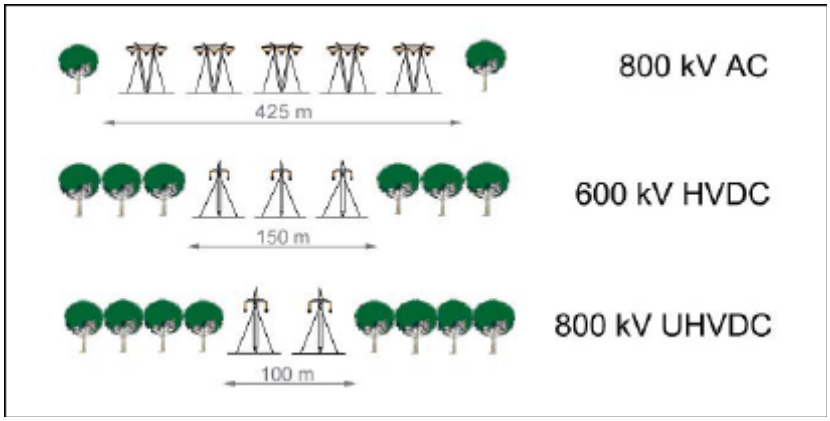

Figure 4-1: Comparison of the required number of parallel pylons and space to transfer 10 GW of electric capacity based on (Asplund, 2008).

Regarding technical security the HVDC technology can help to improve the AC system performance especially where stability is a limitation. On one hand the active power of the link into the AC grid can be easily controlled and never faces the risk to be overloaded. On the other hand additional automatic control facilities can be applied like constant frequency control, redistribution of the power flow in the AC network and damping of power swings in the AC networks (ABB, 2007).

Another reason to prefer HVDC over HVAC under certain circumstances is the possibility to connect asynchronous interconnections. One example is the UCTE grid of mainland Europe and the NORDEL grid in Scandinavia. Due to grid stability reasons it would be difficult to connect two asynchronous systems via an AC interconnection (ABB, 2007).

4.1.2 Characteristics of HVDC Technologies for Long Distance Transport

Conventional HVDC technology for recent long distance overhead line projects usually has a DC voltage of ±500 kV. In the future it will be possible to transmit bulk power exceeding 4000 MW covering a distance of about 2000 km with Ultra High Voltage Direct Current Systems (UHVDC). UHVDC refers to systems with a voltage level above ±600 kV. Currently ABB and Siemens are working on a ±800 kV UHVDC overhead line in China. The 2071 km long bipolar line from Xiangjiaba to Shanghai will have a power rating of 6400 MW and is scheduled to go into operation in 2011 (ABB, 2008). The voltage of the line is 33% higher than the voltage used for the Itaipu ±600 kV transmission in Brazil, until now the world's highest HVDC transmission voltage rating and the largest HVDC transmission with two bipolar lines having a total capacity of 6300 MW. The development to higher transmission voltages is also foreseeable in the ground and sea cable manufacture. Thus a bipolar ±600 kV mass-impregnated cable would be able to transfer 2000 MW. Oil-pressure cables would be able to transfer 2400 MW at the same voltage level (ABB, 2007). Indeed, they can only be used for middle distances. HVDC-light systems with extruded cables are a rather new and still developing transmission technology (introduced 1997) which meanwhile can be built in the range of up to ±320 kV and with a transfer capacity of up to 1200 MW (bipolar case) over long distances. HVDC light with overhead line can be implemented up to ±650 kV voltage and more than 2000 MW line capacity (Asplund, 2008). The number of the components needed for converting AC to DC and thus also costs are drastically reduced compared to the conventional HVDC technology.

The following applications for HVDC technologies are feasible:

- 2-point transmission over long distances
- Utilization as submarine cable
- Utilization as underground cable in congested areas
- Connection of asynchronous networks via back-to-back station
- Connection of power plants
- Multi-terminal system (> 2 stations)

Many of the submarine cable transmissions are monopolar with only one metallic conductor between the converter stations using the ground as the return path for the current. Most overhead line transmissions are bipolar, i.e. they use two conductors of opposite polarity. A bipolar transmission is a double circuit transmission which has a higher security of supply, since one pole can continue to transmit half of the total power when the other pole is out of service (see e.g. www.abb.com for more information).

Several aspects of lifetime expectancy and possible deteriorations caused by external conditions were discussed by (Skog, 2004) regarding submarine cables. They characterised the HVDC technology as well proven equipment. The cable and the main circuit apparatuses are all passive, robust and simple in their structure. The converters are supplemented with well-proven electronics for control and protection and equipped with standard type motors for cooling and venting. Skog stated that on a general basis HVDC submarine cables have a lifetime expectancy of minimum 50 to 60 years. The first cable to Gotland, Sweden was put into operation 50 years ago. Intrinsic deterioration (ageing) of a HVDC line is expected to be slower compared to HVAC because of lower operating temperature. Deterioration caused by external conditions might be due to sea current, wave action or corrosion. Abrasion due to strong sea current in connection with a cable free span and erosion/abrasion in the splash zone (landfall area) can be avoided by proper routing and protection of the cable. Corrosion of the armour can be prevented by outer serving, bitumen and zinc coating of the armour wires and proper burial reducing exposure to oxygen (Skog, 2004).

Main influence of overhead lines or underground cables on the environment is the use of land. A monopole cable with electrodes mounted on each side of the line is the cheapest possible submarine technology but may have some negative impacts upon the marine environment. In a monopole system the return current is conducted through the seawater and the seabed. This leads to significant quantities of chlorine being generated at the positive anode, but also electrolytic corrosion of metallic structures in the surrounding area and electro-magnetic fields that could potentially affect migratory species such as sharks. The most effective method of mitigation of the effects of stray currents on metallic infrastructure and chlorine concentrations is by replacing the sea/earth return with a metallic return. However, a metallic return monopole system still generates significant electro-magnetic fields. Possible impacts on the environment are not yet fully understood and discussed controversially as there is a substantial lack of quantifiable information. In contrast, a true bipolar system having the return cable incorporated in the same casing as the power cable and without electrodes is more expensive but has minimal impacts on the marine environment.

Regarding the costs of transmission lines a generalization appears to be quite difficult as information is not easily available. Table 4-1 shows specific data which provides a technical and economic characterisation of HVDC cables and overhead lines. The values are based on data reviews and expert interviews (see Trieb et al., 2006; Vailati et al., 2006; ABB, 2008; Siemens, 2008). As progress of HVDC technologies is fast-paced – especially for HVDC light and UHVDC – estimations of future costs and potentials regarding capacity and voltage are uncertain and may change within the next years.

Values used for the REACCESS database are rather conservative numbers based on ongoing projects and without speculative assumptions. Bipolar lines were assumed for both, overhead lines and submarine cables in order to increase security of supply, as half of the capacity is still available, if one line fails. For REACCESS, voltage of a corridor consisting of sea cable(s) and overhead line(s) was assumed to be ±600 kV for all corridor sectors technically possible until 2020. Maximal voltage of the complete line is limited by the sea cable (no DC-DC transformation possible) and also by the line capacity which is assumed to be in the range of 3000 MW per bipolar line for the reason of supply security in case of a line outage. It is not possible to include a DC-DC transformation in order to achieve a separate UHVDC voltage for overhead line sectors. On the other side higher investments in UHVDC are only recommended for bulk power transmission above 5000 MW which for safety reasons is not proposed for the electricity import to EU27+. Table 4-1 shows also the specifications of the ±600 kV HVDC classic including power losses of a transformer/converter station of 0.7%, of sea cables of 2.7%/1000 km and of overhead lines of 4.5%/1000 km. Investment costs assumed are for stations 120 €/kW, for sea cables 1.2 million €/km and for overhead lines 270,000 €/km. Operating costs are assumed to be 1% of investment costs per year. For the future, significant further developments of HVDC technology seem to be possible and also the outage capacity tolerated by the UCTE system may be higher than today. Data assumed for a ±600 kV HVDC corridor with 3,200 MW capacity, 3000 km land and 200 km sea distance having 6500 full load hours result in transmission costs of less than 2 ct/kWh transferred taking into account costs due to the loss of solar electricity with production costs of 6 ct/kWh. A discount rate of 6% was used for this estimation.

Table 4-1: Assumed technical parameters and costs of bipolar electricity lines

	Voltage [kV]	**Capacity max. [MW]**	**Station losses [%]**	**Line losses [%]**	**Lifetime [yr]**
HVDC OL	±800	6400	0.6	3	40
HVDC OL	±600	4000	0.7	4.5	40
HVDC OL	±500	3000	0.7	5	40
HVDC UC	±600	2200	0.7	3.5	40
HVDC SC	±500	1600	0.7	2.7	40
HVDC SC	±600	2000	0.7	2.7	40
In €$_{2005}$	**Station INV [€/MW]**	**Station O&M [€/MW]**	**Line INV [€/km]**	**Line O&M [€/km]**	**Data Source**
HVDC OL-800kV	120,000	1200	320,000	3200	Siemens
HVDC OL-600kV	120,000	1200	270,000	2700	ABB, Siemens
HVDC OL-500kV	120,000	1200	250,000	2500	ABB, Siemens
HVDC UC-600kV	120,000	1200	1,000,000	10,000	ABB, Siemens
HVDC SC-500kV	120,000	1200	1,200,000	12,000	Siemens
HVDC SC-600kV	120,000	1200	1,200,000	12,000	Siemens

* OL – overhead line SC – submarine cable UC – underground cable

4.2 PRESENT STATUS OF INFRASTRUCTURES

4.2.1 Transmission Systems in and around Europe

The European transmission grid is a complex system with transmission capacities at different voltage levels. The transmission networks mostly consist of HVAC lines on the 220 to 400 kV level. Higher voltage levels up to 750 kV can mainly be found in the eastern parts of Europe like Russia where it is necessary to transport electricity over very long distances. HVDC lines so far are only used to cross longer distances with sea cables (Figure 4-3).

The transmission systems of the countries in and around Europe are organised in blocks (Figure 4-2) that each follow a set of rules to run the national transmission systems synchronously. A major advantage of this approach is to enable national a national grid to interconnect with its neighbours in order to increase the reserve capacity within the system and thereby enhance the security of energy supply.

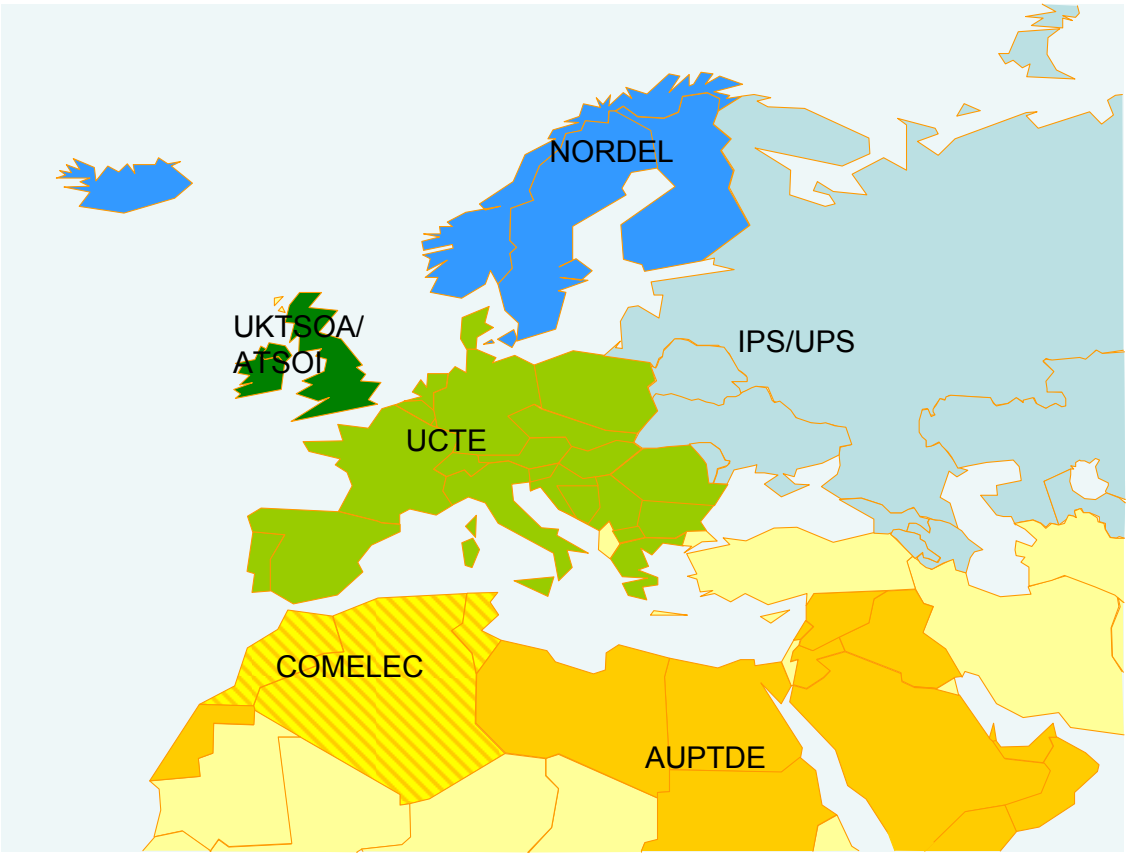

Figure 4-2: Integrated network in and around Europe.

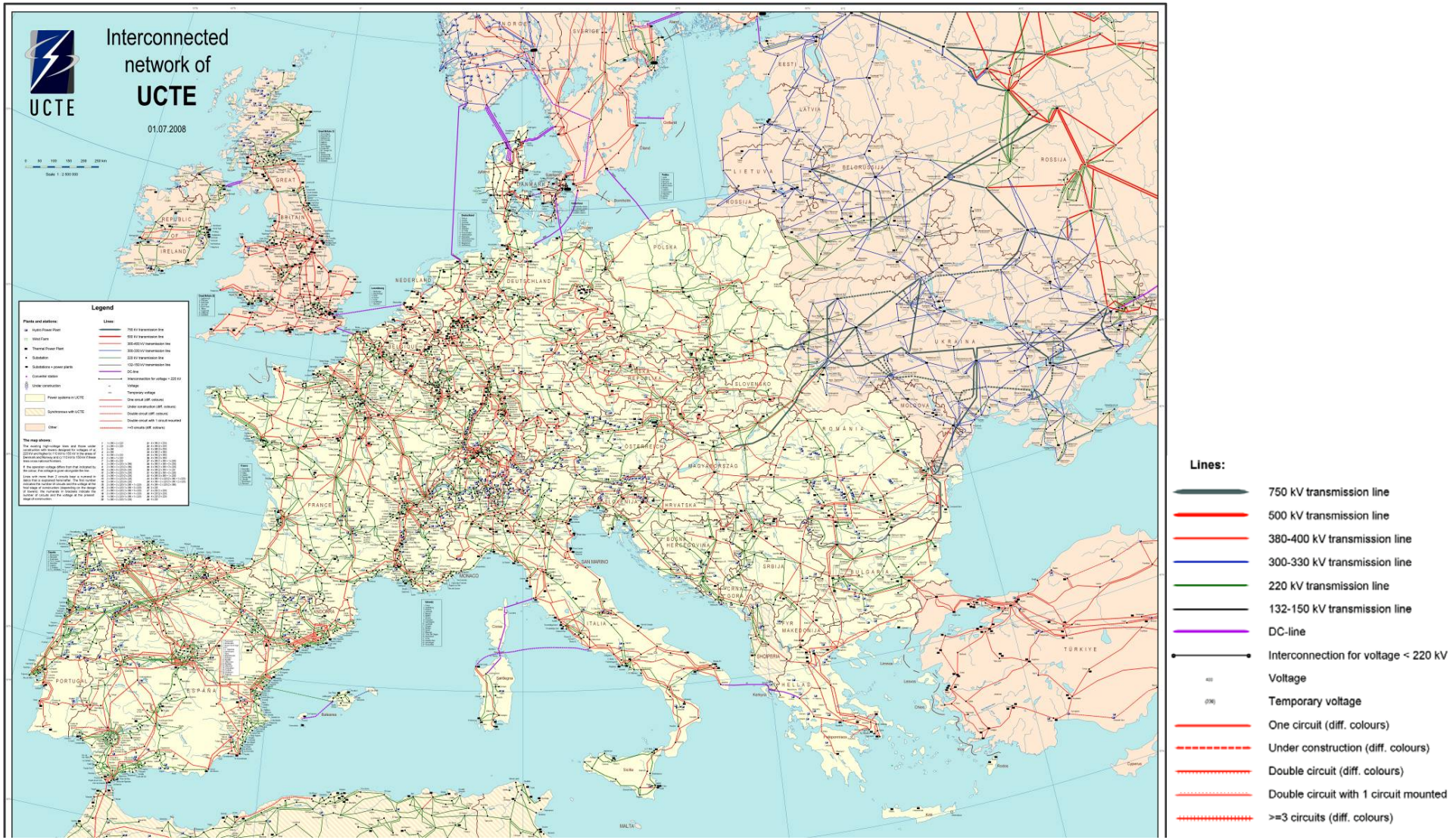

Figure 4-3: UCTE grid 2008 (Source: UCTE, 2008).

The UCTE (Organization of Transmission System Operators) is the largest system comprising 23 European countries [1] with an annual electricity consumption of approximately 2600 TWh. The System was build gradually with national systems being integrated under very strict UCTE standards. 1995 the CENTREL system (Czech Republic, Slovakia, Hungary and Poland) was integrated into the UCTE followed by Romania and Bulgaria in 2003. The part of the UCTE that was disconnected from the rest due to the war in former Yugoslavia was reconnected in October 2004.

The Organization for Nordic Power Co-Operation (NORDEL) is a network between Norway, Sweden, Finland, Iceland and parts of Denmark. It is interconnected with the UCTE network via HVDC sea cables as the systems are run asynchronously (Figure 4-4).

The United Kingdom Transmission System Operator Association (UKTSOA) and the Association of Transmission System Operators in Ireland (ATSOI) are connected via a HVDC cable in southern England with the USTE network in France.

To the east of UCTE the Interconnected / Unified Power Systems (IPS/UPS) comprises the power systems of the Baltic States (Latvia, Lithuania, and Estonia), Armenia, Azerbaijan, Belarus, Georgia, Moldova, Kazakhstan, Kyrgyzstan, Russia, Tajikistan, Ukraine and Uzbekistan. It is connected to the UCTE via several HVAC connections on different voltage levels. The connection to the NORDEL system exists via a sea cable between Finland and Estonia as well as a couple of land lines between Finland and Russia (Figure 4-4).

[1] Portugal, Spain, France, Belgium, Luxemburg, Netherlands, Switzerland, part of Denmark, Germany, Italy, Austria, Czech Republic, Slovenia, Poland, Slovakia, Hungary, Croatia, Bosnia and Herzegovina, Albania, Serbia and Montenegro, Former Yugoslav Republic of Macedonia, Greece, Romania, Bulgaria and western most part of Ukraine.

Figure 4-4: NORDEL grid 2008 (Source: NORDEL, 2008).

With the emerging internal electricity market in the European Union the need for an EU-wide harmonization of requirements for cross border trade arose. In 1999 ETSO (European Transmission System Operators) was created including all Members of the European Union as well as Norway and Switzerland (ETSO, 2008). The service of ETSO includes the supply of information of net transfer capacities in Europe that is published on their website twice a year (Figure 4-5).

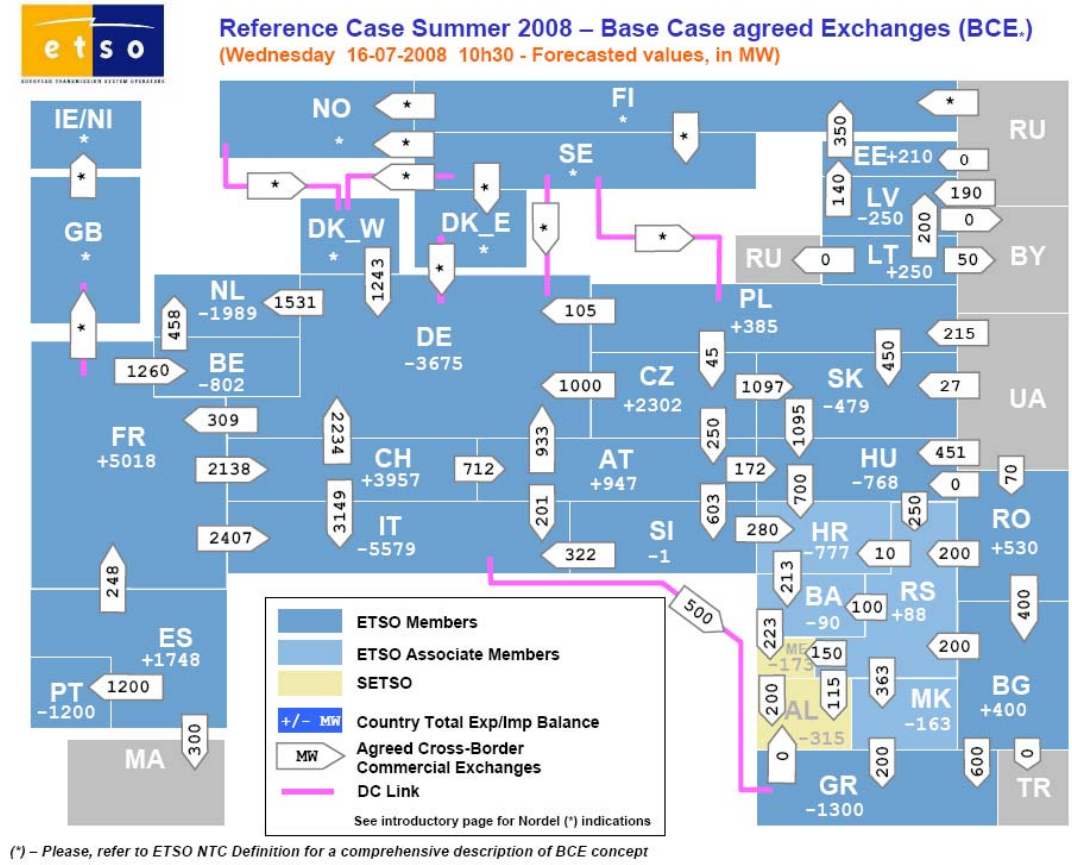

Figure 4-5: Map of net transfer capacities in summer 2008 (ETSO, 2008).

The electricity networks of the southern Mediterranean region are organized in a number of different unions. In the 1970ies the Comité Maghrébin de l'Electricité (COMELEC) was founded by the three Maghreb countries Algeria, Morocco and Tunisia to foster the interconnection of the national electricity networks (OME, 2008). Since 1997 COMELEC is connected synchronously via a 400 kV HVAC cable with the UCTE through the street of Gibraltar. Since 2006 a second cable came into operation increasing the possible capacity to 1400 MW.

In 1987 the Arab Union of Producers, Transporters and Distributors of Electricity (AUPTDE) was established. 18 countries[2] are organized in this union that amongst others aims to “pursue the interconnection of electrical networks in the Arab countries and accelerate the implementation of such interconnections” (AUPTDE, 2008).

Another organization is the Union of Producers, Transporters and Distributors of Electric power in Africa (UPTDEA) that established in 1970. It was created to foster the integration and development of African power systems through the interconnection of networks. All African countries are members in this organization (UPTDEA, 2008).

As the possibility of an interconnection network between the different Mediterranean countries the so called “Mediterranean Ring” evolved the necessity for an organizing body arose. At the beginning of the 1990ies MEDELEC (Mediterranean Committee for Electricity) was founded to foster the dialog between the Transmission system operators (TSO) of different regions. The organizations taking part in this MEDELEC are the UCTE, COMELEC, AUPTDE, UPDEA as well as the Union of the Electricity Industry (EURELECTRIC) and the Observatoire Méditerraneen de l'Énergie (OME). Its aim is to agree on a technical standard that will provide the necessary stability for an interconnected electricity network around the Mediterranean. Figure 4-6 shows the status of the electricity interconnection in the Mediterranean. As mentioned before an interconnection between Spain, Morocco, Algeria and Tunisia exists already. Also an interconnection between Libya, Egypt, Jordan, Lebanon and Syria is in operation. The existing interconnection between Tunisia and Libya could not be successfully synchronized so far. The same accounts for the connection between Turkey and the UCTE system. The interconnections from Turkey to its other neighbouring countries also depend on this synchronization.

[2] Jordan, UAE, Bahrain, Tunisia, Algeria, Saudi Arabia, Sudan, Syria, Iraq, Sultanate of Oman, Palestine, Qatar, Lebanon, Libya, Egypt, Morocco, Mauritania and Yemen

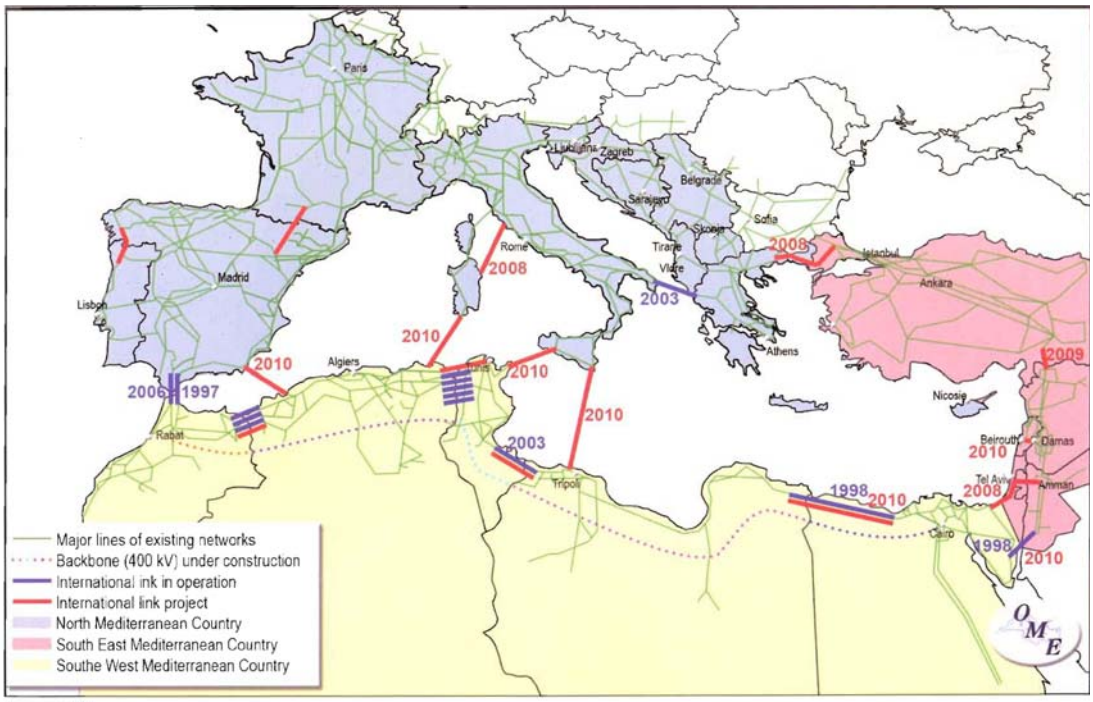

Source: OME.

Figure 4-6: Electricity Interconnections in the Mediterranean (OME, 2008).

4.2.2 Existing HVDC Transmission Lines

World wide HVDC transmission lines cumulate today to a total capacity of over 75 GW in more than 90 projects. Many of them connect renewable power sources from hydropower (e.g. Inga-Shaba, China, Brasil, New Zealand) or geothermal power (e.g. Phillipines) with distant centres of demand. Others are used to interconnect countries over sea (e.g. SwePol, Baltic Cable, Italy-Greece, Sardinia). Table 4-2 characterises selected existing HVDC lines and projects. A more complete list of projects is published e.g. by University of Idaho (ECE, 2008). Most important ongoing HVDC projects are:

- SAPEI HVDC link from Sardinia to the Italian mainland which will be a bipole of a total of 1000 MW, a DC voltage of ±500 kV. DC submarine cables will have a length of 2 x 420 km, the commissioning year will be 2010 (ABB).
- Upgrading of the Intermountain HVDC transmission between Utah and Los Angeles to 2400 MW at DC voltage of ±500 kV and a length of overhead line of 785 km (ABB).
- Hulunbeir-Liaoning HVDC link in the north-eastern part of China will transmit 3000 MW over 920 km with a DC voltage of ±500 kV. The link is scheduled for commercial operation in December 2009 (ABB).

- 800 kV Ultra High Voltage Direct Current (UHVDC) overhead line from Xinagjiaba to Shanghai in China. The 2071 km long bipolar line will have a power rating of 6400 MW and is scheduled to go into operation in 2011 (ABB and Siemens).
- 800 kV overhead line from Yunnan to Guangdong, China with a transmission capacity of 5000 MW and a length of 1418 km, start of operation 2010 (Siemens).
- 500 kV line under construction between Sumatera and Jawa (Indonesia) with a capacity of 3000 MW and a length of 700 km. Start of operation 2013.
- 500 kV line under construction between Ballia and Bhiwadi in India with 2500 MW capacity and 800 km length (Siemens).

Table 4-2: Selected existing HVDC transmissions (ABB, 2008; Siemens, 2008; ECE 2008).

Name/country	Design*)	Start of operation	Power [MW]	Voltage ±[kV]	Length [km]	System
SACOI/Sardinia-Corsica-Italy	SC, O	1967	300	200	423	bipolar, multiterminal
Cahora Bassa/Mozambique-South Africa	O	1977-79	1930	533	1420	bipolar, 2 lines
Inga-Shaba/Congo	O	1982	560	500	1700	2x monopolar
Itaipu/Brasilia	O	1984-87	6300	600	800	double-bipolar
Québec-New England/Canada-USA	O	1990-92	2000	450	1480	bipolar, multiterminal
BalticCable/Swe-Ger	SC	1994	600	450	250	monopolar
SwedPol/Sweden-Poland	SC	2000	600	450	260	monopolar, metallic return
GRITA, Italy-Greece	UC, SC, O	2001	500	400	310	monopolar
Tianshengqiao-Guangzhou, China	O	2001	1800	500	960	bipolar
Murraylink/Australia	UC	2002	220	150	177	bipolar, HVDC light
Estonia - Finland	SC, UC	2006	350	150	105	bipolar, HVDC light
East-South link, Orissa-Karnataka, India	O	2003	2000	500	1450	bipolar
Guizhou - Guangdong, China	O	2004	3000	500	980	bipolar
Basslink, Australia - Tasmania	SC	2006	500	400	290	monopolar, metallic return
Three Gorges-Shanghai, China	O	2006	3000	500	900	bipolar
Neptune, New Jersey-New York, USA	SC, UC	2007	660	500	105	monopolar, metallic return
Guizhou - Guangdong, China II	O	2007	3000	500	1225	bipolar
NorNed/Nor-NL	SC	2008	700	450	580	2x monopolar

*O – overhead line, SC – submarine cable, UC – underground cable

4.3 DEVELOPMENTS IN THE FUTURE

Up to now there is no production or export of solar electricity from CSP plants in the MENA region. First CSP plants for local needs are currently under construction in Egypt, Algeria and Morocco. However, in the frame of the Union for the Mediterranean, first political steps have recently been made to accelerate the expansion of CSP in the region and to start the preparation of CSP export schemes. Starting early 2009, a master plan study for the development of CSP and other renewable energy sources in the MENA region including export capacities to Europe is scheduled to be elaborated by European and Arabian research centres, utilities, industry, finance and policy stakeholders in the power sector. The results achieved within the REACCESS project can serve as a first guideline for the realisation of such efforts.

4.3.1 Definition of Sites for CSP Exports

Prior studies on CSP electricity exports from MENA to Europe did only specify a few exemplary sites where CSP plants could be erected for solar power exports. They did not yet look systematically for concrete sites for solar electricity generation taking into consideration all possible criteria for site selection like solar resource and land availability, local risks, available infrastructure and economic performance. This task was at the first time undertaken in the REACCESS project. The sites that were selected for analysis are a compromise between solar and land resource availability, availability of road infrastructure for access and closeness to the European centres of demand. The findings do not necessarily represent optimal sites – as we did not apply any optimisation function – but represent reasonably feasible sites for the production of solar electricity for export purposes.

Within REACCESS we have found eleven potential sites in the MENA region that are in principle suitable for the generation of solar electricity for export purposes. These sites are characterized by fairly good solar irradiance, large available land area, vicinity to road infrastructure for easy access and minimum distances to the centres of demand to be served in Europe.

Figure 4-7 and Figure 4-8 show the sites that have been identified in MENA for potential export of solar electricity using the GIS information available on DNI, site exclusion and infrastructure. In a real world, more criteria for site selection will play a role, like e.g. land properties, regional and national policies etc. that cannot be taken into consideration here, but will play a role as soon as it comes to the point of concrete decisions. The results presented here can serve decision makers as a first draft of such an export infrastructure of solar electricity and can provide first information on potential performance, economies and risks that can be expected from this approach.

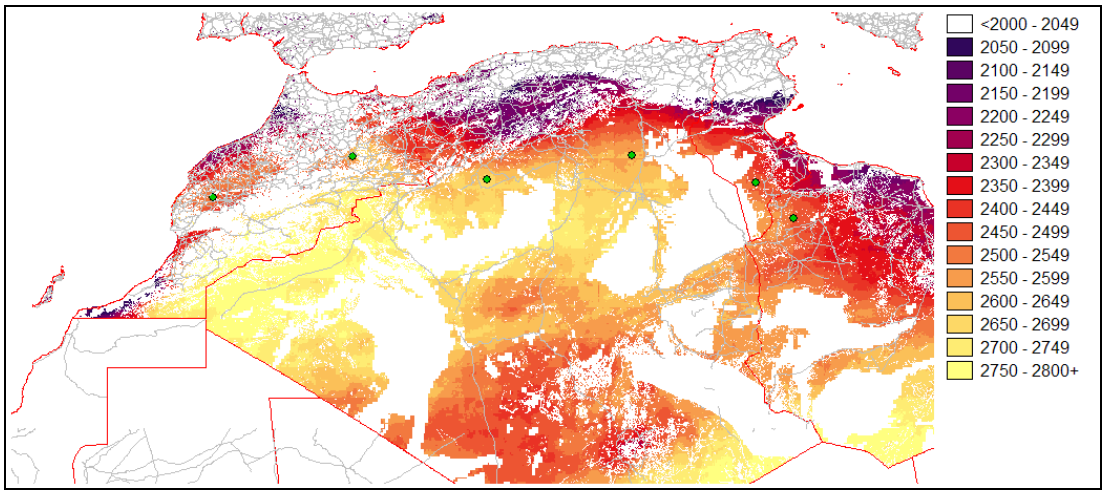

Figure 4-7: Sites (green dots) selected for CSP export in Morocco, Algeria and Tunisia. Background map shows solar direct normal irradiance in kWh/m²/y (see legend), road infrastructure (grey lines) and exclusion areas (white).

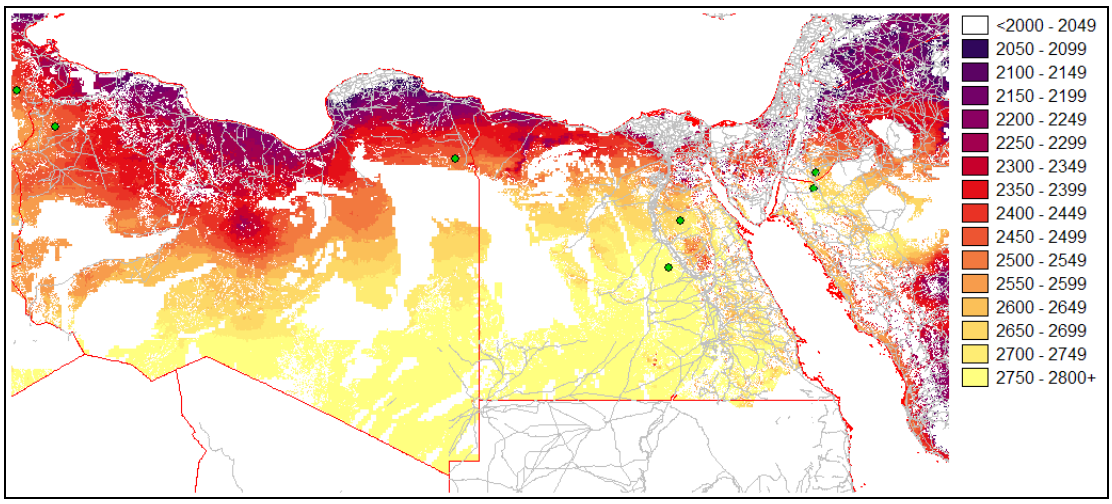

Figure 4-8: Sites (green dots) selected for CSP export in Libya, Egypt, Jordan and Saudi Arabia. Background map shows solar direct normal irradiance in kWh/m²/y (see legend), road infrastructure (grey lines) and exclusion areas (white).

The eleven sites that have been selected have a solar direct normal irradiance classified between 2500 and 2700 kWh/m²/y. They are not among the sites with highest possible DNI in MENA, but all show a DNI level higher than what is available in Europe. With that level of DNI a very good availability for solar power is possible, with 7200 to 7800 full load operating hours per year which is equivalent to the availability of conventional base load power stations. Taking into consideration better

sites with over 8000 full load operating hours per year, performance of the HVDC interconnections could still be enhanced further, if required.

Table 4-3: Coordinates of 11 selected sites for CSP export in MENA and of 27 centres of demand in Europe for CSP electricity import.

	End Points	Country	Longitude °	Latitude °	GIS File Name
1	Brussels	Belgium	4.158563	50.735346	END-BELGIUM-01-BRUSSELS.VCT
2	Sophia	Bulgaria	23.537323	42.648533	END-BULGARIA-01-SOPHIA.VCT
3	Prague	Czech Republic	14.86286	50.103632	END-CZECH-01-PRAGUE.VCT
4	Paris	France	2.193856	48.409654	END-FRANCE-01-PARIS.VCT
5	Lyon	France	4.605267	45.730073	END-FRANCE-02-LYON.VCT
6	Juelich	Germany	6.452441	50.969216	END-GERMANY-01-JUELICH.VCT
7	Berlin	Germany	12.70676	52.50016	END-GERMANY-02-BERLIN.VCT
8	Mainz	Germany	8.257679	49.934962	END-GERMANY-03-MAINZ.VCT
9	Karlsruhe	Germany	8.735788	48.987376	END-GERMANY-04-KARLSRUHE.VCT
10	Munich	Germany	11.460792	48.340043	END-GERMANY-05-MUNICH.VCT
11	Hamburg	Germany	10.087142	53.34594	END-GERMANY-06-HAMBURG.VCT
12	Hannover	Germany	9.364013	52.363724	END-GERMANY-07-HANNOVER.VCT
13	Thessaloniki	Greece	23.077678	40.78059	END-GREECE-01-THESSALONIKI.VCT
14	Athens	Greece	23.943897	37.977994	END-GREECE-02-ATHENS.VCT
15	Budapest	Hungary	18.788162	47.268113	END-HUNGARY-01-BUDAPEST.VCT
16	Milano	Italy	9.099475	45.277835	END-ITALY-01-MILANO.VCT
17	Firenze	Italy	10.772155	43.833473	END-ITALY-02-FIRENZE.VCT
18	Rome	Italy	12.57652	41.65507	END-ITALY-03-ROME.VCT
19	Naples	Italy	14.518791	40.905259	END-ITALY-04-NAPLES.VCT
20	Appledorn	Netherlands	6.080098	52.262701	END-NETHERLANDS-01-APELDORN.VCT
21	Warszaw	Poland	20.943717	52.057253	END-POLAND-01-WARSZAW.VCT
22	Lissabon	Portugal	-8.809323	38.820881	END-PORTUGAL-01-LISSABON.VCT
23	Bukarest	Romania	26.019906	44.333587	END-ROMANIA-01-BUKAREST.VCT
24	Madrid	Spain	-3.800142	40.245789	END-SPAIN-01-MADRID.VCT
25	Zaragoza	Spain	-0.642532	41.369829	END-SPAIN-02-ZARAGOZA.VCT
26	London	United Kingdom	-0.062819	51.16298	END-UNITEDKINGDOM-01-LONDON.VCT
27	Newcastle	United Kingdom	-2.093878	53.023119	END-UNITEDKINGDOM-02-NEWCASTLE.VCT

	Start Points	DNI (kWh/m²/y)	Longitude °	Latitude °	GIS File Name
1	Algeria_01	2700	0.743111	32.311637	START-ALGERIA-01.VCT
2	Algeria_02	2600	5.619601	33.133164	START-ALGERIA-02.VCT
3	Egypt_01	2700	31.667207	27.931443	START-EGYPT-01.VCT
4	Egypt_02	2500	31.278879	26.396768	START-EGYPT-02.VCT
5	Jordan_01	2600	36.112394	29.522145	START-JORDAN-01.VCT
6	Libya_01	2500	11.037962	31.027219	START-LIBYA-01.VCT
7	Libya_02	2500	24.220003	29.97231	START-LIBYA-02.VCT
8	Morocco_01	2500	-8.451073	31.718829	START-MOROCCO-01.VCT
9	Morocco_02	2700	-3.765717	33.091009	START-MOROCCO-02.VCT
10	Saudi_Arabia_01	2700	36.061776	28.99942	START-SAUDIARABIA-01.VCT
11	Tunisia_01	2500	9.772525	32.212836	START-TUNISIA-01.VCT

4.3.2 Definition of Sites for CSP Imports

In order to find potential sites for the import of CSP electricity, we have analysed the total electricity demand of the European countries, the population density and the land availability for placing the HVDC headers close to the selected centres of demand, using the internet tool Google Earth. The idea of accessing centres of demand is that large scale electricity imports via HVDC must be fed into the conventional electricity grid at sites with large demand were a powerful infrastructure is available that can cope with the large capacities to be imported. The end of a

HVDC power line needs a grid infrastructure capable of absorbing the electricity generated. These places are usually and preferably close to large centres of demand, which are usually the population centres in Europe. These can be depicted from Figure 4-9. Figure 4-10 shows all start and endpoints identified in the study.

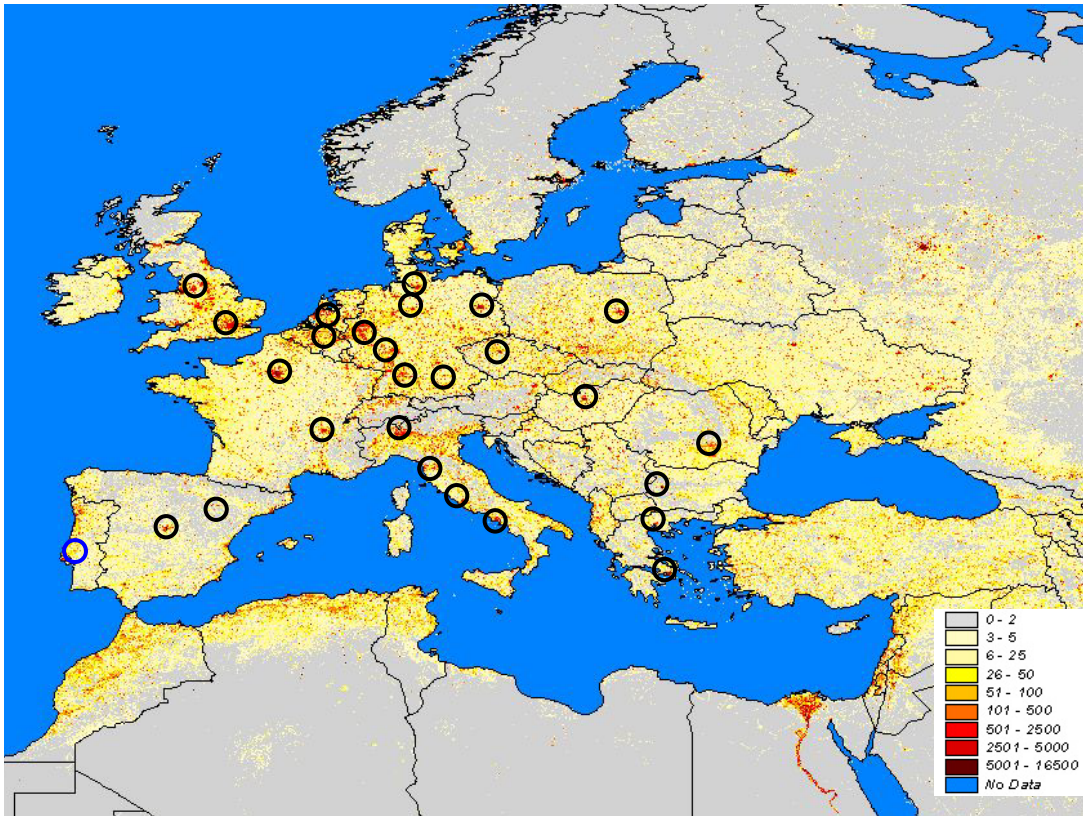

Figure 4-9: Population density in persons per km² from (ORNL, 2005) and end points of HVDC lines identified for CSP imports in Europe.

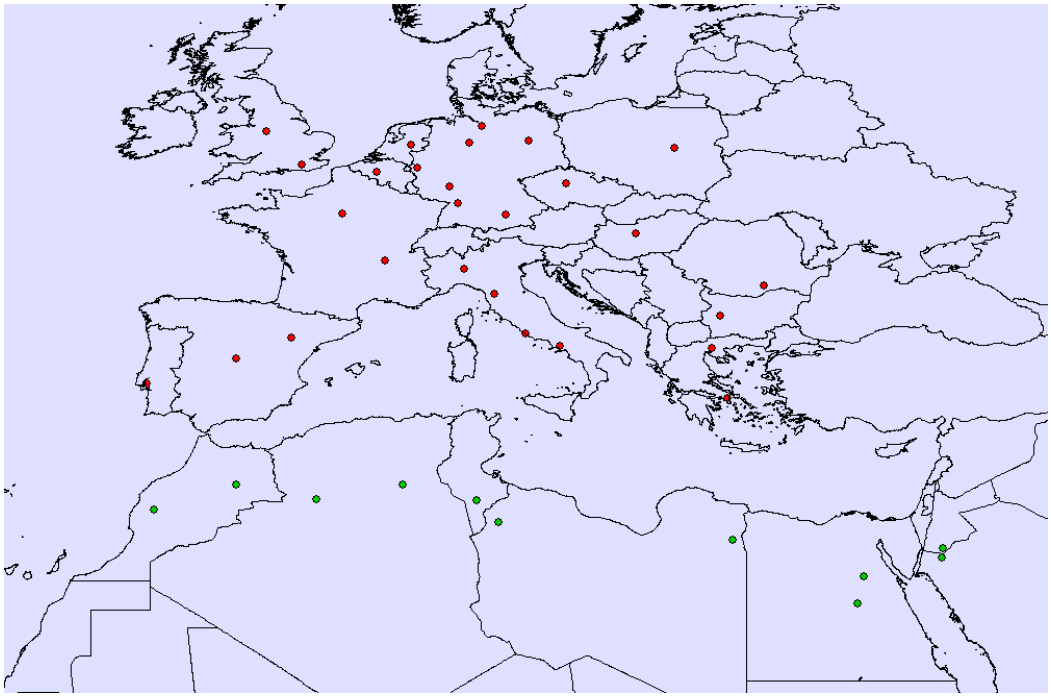

Figure 4-10: Start (green) and end (red) points of potential HVDC lines for CSP electricity imports identified in the REACCESS project according to Table 4-3.

4.3.3 Site Exclusion for HVDC Lines

The next step was to find the best corridors for HVDC lines interconnecting the points of solar power generation in MENA with the points of demand in Europe. The corridors should be as short as possible, not create significant environmental impact and not be submitted to significant natural risks.

The first task was to create a regional map excluding all sites that would not be suitable for the erection of HVDC lines. The methodology is very similar to that used for site exclusion of CSP plants, and applies similar criteria for site exclusion as described in the following:

Protected Areas

All protected areas have been excluded for HVDC lines as described in Chapter 3.1.

Industrial Locations

All industrial areas have been excluded for HVDC lines as described in Chapter 3.1.

Populated Places

High voltage lines must not pass through highly populated places. Therefore such areas have to be excluded from further analysis. Moreover, a minimum distance of

250 m between populated places and the line must be kept for reasons of electric and magnetic fields. All populated places have been excluded as described in Chapter 3.1.

Exclusion of Deep Sea Areas

Especially for the crossing of the Mediterranean Sea a maximum placing depth of 2000 m under sea level is assumed for a submarine cable. The NGDC provides the global, digital elevation model 'ETOPO2 Global 2' Elevations' (NGDC, 2005). The bathymetrical data was recorded from the 'ERS-1 Altimeter' of the European Space Agency (ESA) and from the 'Geosat Altimeter' of the US Navy (Smith & Sandwell, 2003). In order to cover the whole earth surface the different datasets shown in figure 85 (annex) were combined (Smith & Sandwell, 2003). The spatial resolution of the dataset amounts to nearly 4 km x 4 km 3 (NGDC, 2005). Statements about the accuracy of the data are not included in the documentation.

Areas that lie deeper than -2000 m are excluded and the remaining areas are weighted with a scaling factor described later. Up to now the maximum placing depth of a submarine cable amounts to -1000 m, therefore this is a prospective assumption.

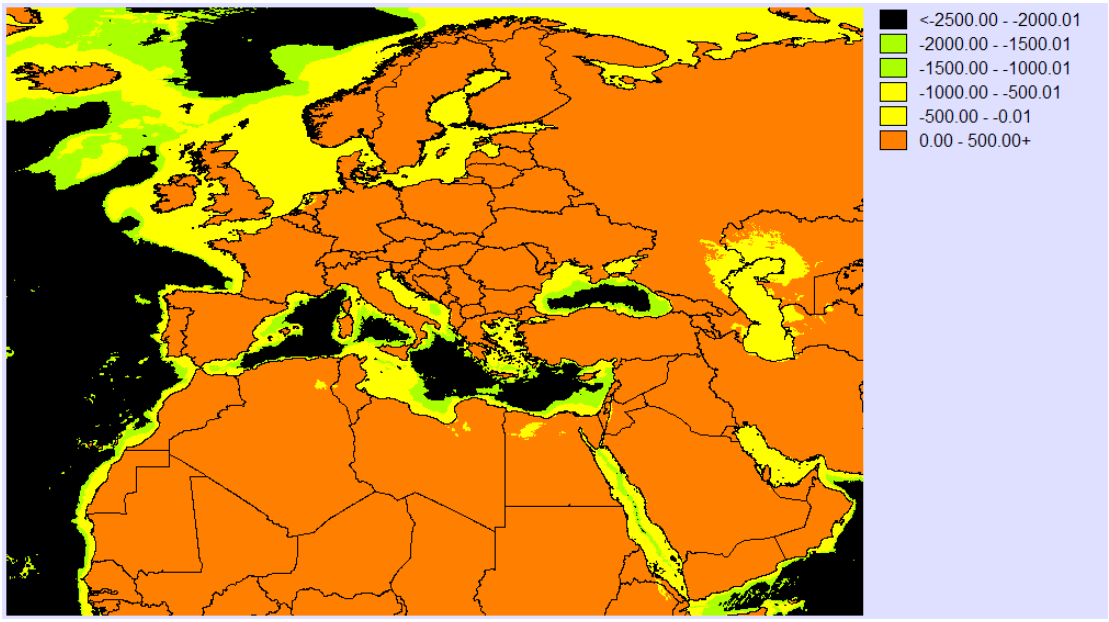

Figure 4-11: Sea depth in metres from ETOPO2.

[3] 3,7 km x 3,7 km at the equator corresponds to 2 arc minutes

Exclusion of Hydrological Features

In large areas of the Mediterranean region there are perennial and intermittent inland water bodies. Areas occupied by them are not suitable for the power lines and are therefore excluded. The required spatial information are included in the DCW and there classified according to the following features (Ph.D., 1998):

- Inland Water: Perennial/Permanent [4]
- Inland Water: Non-Perennial/Intermittent/Fluctuating [5]
- Land Subject to Inundation: Perennial/Permanent
- Land Subject to Inundation: Non-Perennial/Intermittent/Fluctuating

In the defined area there is no category 'Land Subject to Inundation: Perennial/Permanent' present. Not permanent areas of inundation are assumed as wetlands and get the same weighting factor. Dry valleys in arid areas - the so-called wadis -, which carry water just episodically, but then in large amounts, are included in the category 'Inland Water – Non-Perennial/Intermittent/Fluctuating' and can be taken into account.

As the GLCC land cover dataset also includes inland water, these are intersected with the DCW dataset. This way the DCW is extended by 40.6% more inland water. The Black and Caspian Sea are classified as seawater like the Mediterranean Sea and the Atlantic. In order to assign the criterion 'bridgeable' to extended inland water bodies and a width not more than 1', so e.g. for rivers, a filter is used that identifies pixels that have a connection to land at least at one side. All other pixels are excluded.

Exclusion of Geomorphologic Features

Certain areas and soils are not suitable to be used as foundation due to their geomorphologic features. Salt areas because of their heavy corrosive features belong to it. But also dynamic structures like glacier form an exclusion area, which additionally is extended by a safety zone for the duration of operating (here 50 years). As the flow velocities can amount to 200 m/y this safety zone has to be at least 10 km width (Kronshage & Trieb, 2002).

[4] Permanent lakes, currents, estuary, lagoons, not measured currents, reservoirs and navigable canals

[5] Episodically, seasonally fluctuating lakes, currents, wadis, sabkhas and not navigable canals

Sand dunes are also unsuitable for the erection of pylons as the sand corns do not form a strong compound. Here the exclusion area also contains a safety zone which considers the mobility of certain dune types. Such shifting sands can cover around 30 m/y at a height of 10 m, therefore the safety zone is precautionary specified with a width of 2 km that eliminates the endangering of the facility for the duration of operating (here 50 years) (Cooke et al., 1993).

Spatial information about sand dunes and salt areas are taken from the 'Digital Soil Map of the World' (DSMW) of the FAO (FAO, 1995). The DSMW is based on the 'Soil Map of the World' (1:5 Mio.) of the FAO/UNESCO from the year 1978. The spatial resolution of the digital map amounts to approximately 10 km x 10 km [6].

Altogether the DSMW identifies in 26 groups of soil types 106 soil types and additional non-soil features, which include the dunes and salt areas of interest. Glaciers are taken from the digital land cover dataset (GLCC) and the DSMW.

Adding all exclusion features mentioned before, the exclusion map for HVDC lines for the entire Euro-Mediterranean region shown in Figure 4-12 results from the analysis.

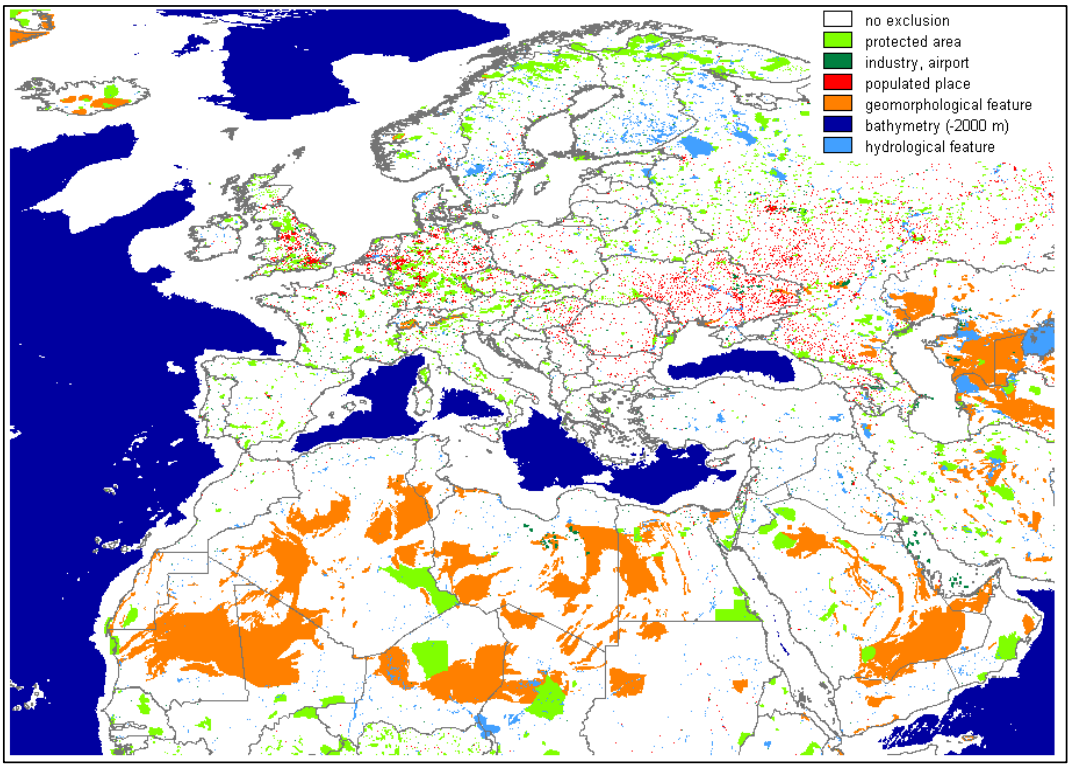

Figure 4-12: Site exclusion map for HVDC power lines (May, 2005).

[6] 9,3 km x 9,3 km at the equator corresponds to 5 arc minutes

4.3.4 Weighting of Non-Exclusive Land Characteristics

All remaining areas are weighted differently by means of further features in order to identify the least cost interconnection between supply and demand sites under ecological aspects. For this, relative costs – so called friction factors – are assigned to the land area for weighting concerning its suitability as line location.

Land Cover

The same land cover dataset as for the site assessment of CSP plants has been used. One weighting criterion is the land cover class of the area (usually one pixel), which is determined by the GLCC land cover dataset. Here, from seven classification methods provided, the 'Olson Global Ecosystems' classification with 96 designated classes was used (USGS, 2003). These classes are summarized to 11 main classes for further use (Figure 3-20).

A value of 1.0 is specified for the base cost value of the friction image. This corresponds to the cost that has to be raised to pass at least one pixel (Kronshage & Trieb, 2002). Areas which have been assigned a friction factor of 1.0 are areas with a high priority for a HVDC power line.

If a factor of 10,000 is assigned to certain land cover classes, theses classes can be excluded from further calculation steps and can therefore be considered as insurmountable barriers.

As the Mediterranean Sea, the Black See and the Caspian Sea do not represent absolute barriers for submarine cables, but their use causes considerable higher costs, the factor 10.0 is assigned to large surface water bodies. All other land cover features are rated as shown in Table 4-7.

Population Density

The LandScan database 2003 provides global information about the population density in a spatial resolution of 30" x 30" (ORNL, 2005). The dataset is less based on the precise place of residence of the people, but more on the spatial distribution of the population over a typical 24 hour day in order to carry out a better risk assessment. That means that also the way to work and the place of work of the population is taken into account (Figure 4-9).

Information about population, mostly on a sub national level, serves as input data, which is distributed among several cells of a 30" raster by means of country-specific likelihood coefficients. The coefficients are derived from remote sensing data about the nearness to roads, slope, land cover, light emissions by night and other datasets (ORNL, 2005).

By means of these databases it is possible to record agglomerations around cities. These areas should not be considered as exclusion feature as otherwise too many

areas fall out from a further analysis. The threshold is set on a population density of 500 inhabitants/km². By assignment of a higher factor this agglomerations can be weighted higher. For this, the areas are blended with the land cover dataset and afterwards classified together with the other features corresponding to the friction factors.

Visibility from Cultural and Religious Sites

An overhead line can lead to a visual impact on the landscape. Therefore the minimization of the visibility should be aspired already within the planning and permission phase. Different methods are used to assess the visibility of an overhead line in the terrain. It is distinguished between two fundamental types (Zewe, 1996):

- Quantitative methods for the assessment of the visual effect by calculation of evaluation parameters for the visibility of a projected overhead line (calculation with the help of simulation processes).
- Qualitative methods for the assessment of the impacts on the landscape by realistic representation of a projected overhead line in the landscape (photomontages, graphical data processing of air photographs and elevation models, interviews of test persons).

Such models are more and more used, but they are very complex and processing intensive. In case of qualitative methods this models are very realistic, but limited on certain points of views or, with the help of air photographs, with a too low resolution for the vicinity of a line. With a combined model it is aimed at a realistic representation of the line in the terrain and a quantitative visibility assessment (Zewe, 1996).

Due to the immense expenditure in assessing the visual effect of overhead lines and to the size of the section considered here the visibility is examined in the surroundings of cultural and religious sites to simplify matters. This carried out with the Idrisi tool ‘Viewshed’. All areas which are visible in a height of 2 m from the viewer’s point are charged with a factor of 7.0. The maximum visibility radius is set on 10 km. Areas lying in the sea are excluded from the visibility analysis as submarine cables are used. In forest areas the visibility of pylons can decrease up to 100 % because of the camouflage effect of trees (Zewe, 1996). Therefore forest areas which lie in the visual range are not rated higher.

The several site coordinates were taken from the ‘GEOnet Names Server’ (GNS) of the NGA (NGA, 2005). This database contains names and coordinates of different cultural and religious sites outside the United States, from which the sites listed in table 29 (annex) were selected for this analysis.

As the accuracy of the coordinates is limited on minutes, spatial deviations of the sites of 1' can result. The error amounts to ±1.7 km (23°) up to ±1.2 km (50°).

Existing Grid Infrastructure

On purpose of bundling lines a further weighting criterion must be developed which refers to the distance of existing high voltage lines (Figure 4-13). The weighting factor is selected in this way that it increases linearly with the increasing distance to the line up to a maximum value of 50.0.

The base data is the DCW, which includes all power lines which have been implemented until the year 1992 with a topographic accuracy of 500 m, however, without information about the voltage level of the lines. A schematic design (CAD) of existing and projected high voltage lines from 110 kV is available for North Africa and the easterly Mediterranean residential states. After geo-referencing the real course of the lines it is just represented as approximation. Nevertheless, due to a limited access to corresponding information this CAD was included in the analysis. Besides, there was no GIS dataset available for submarine cable transmissions.

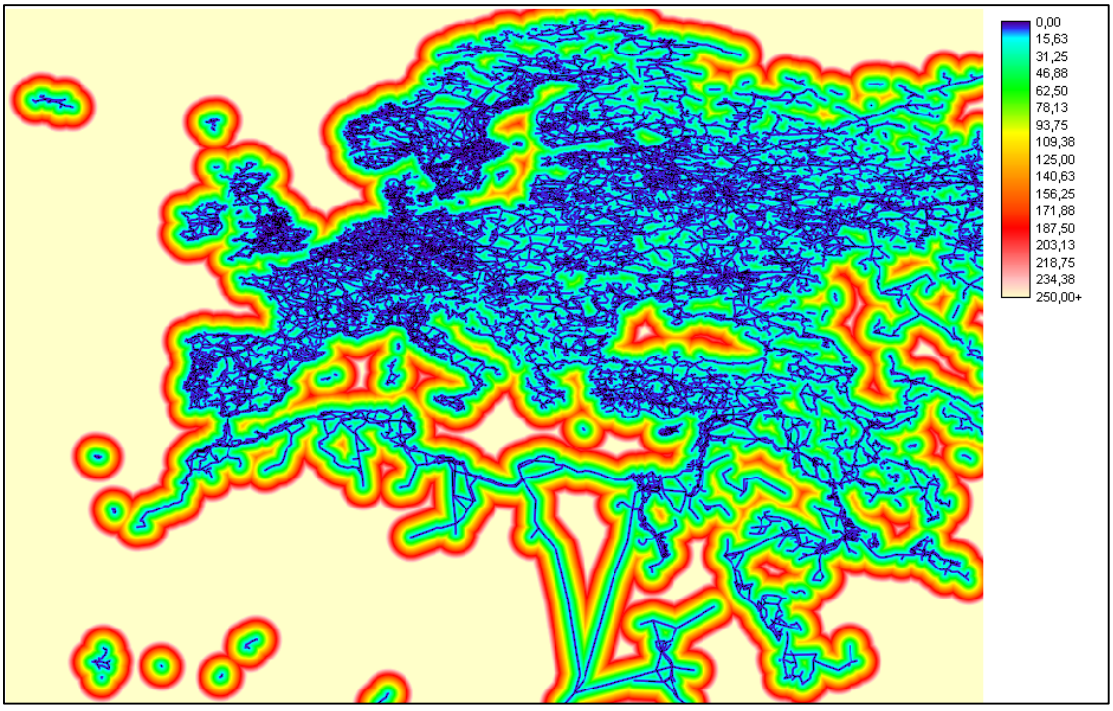

Figure 4-13: Distance image of the electricity network in the Mediterranean region in kilometres.

Natural Hazards

Up to now only areas of inundation have been taken into account in the model as areas concerned by natural hazards. Furthermore, earthquakes, storms (wind loads), and lightning among others can affect the operating safety of an overhead line. In order to resist such impacts the design of pylons and conductors must be adapted to the site conditions. Heavy wind loads often arising cause a more often use of guyed pylons and a higher demand in repairing within the duration of operation.

The dataset 'World Map of Natural Hazards' of the Munich Re Group contains the spatial distribution of different natural hazards, which are each subdivided in up to six risk classes (Table 4-4). But not all classes are represented in the Mediterranean region concerned. A risk potential by tropical storm is not present in these latitudes, for instance.

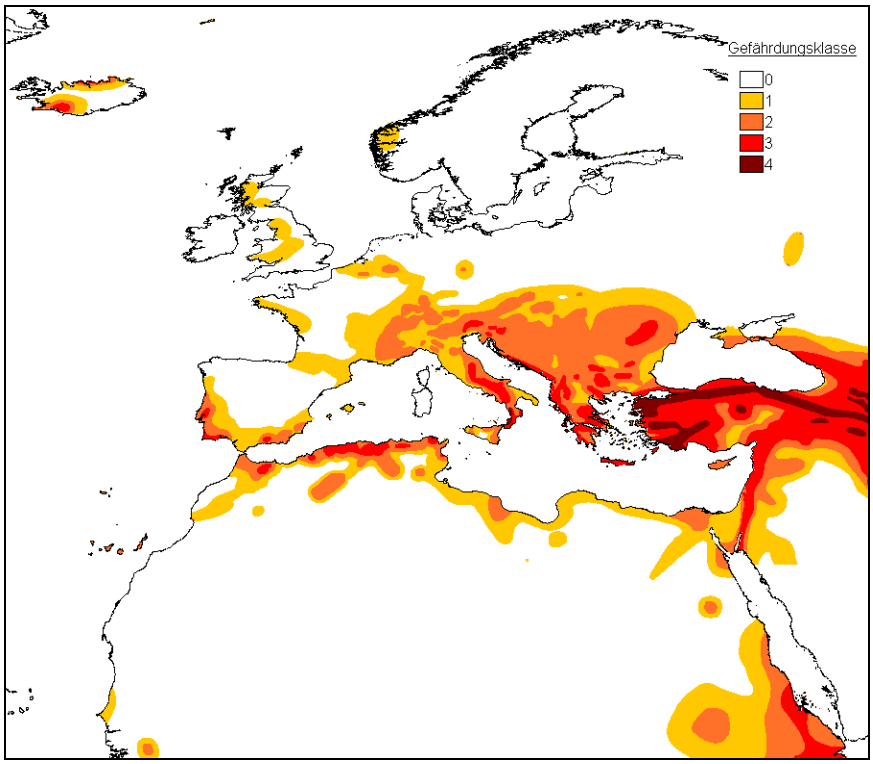

Figure 4-14: Risk of earthquakes (Source: OD, Münchener Rück, 2001).

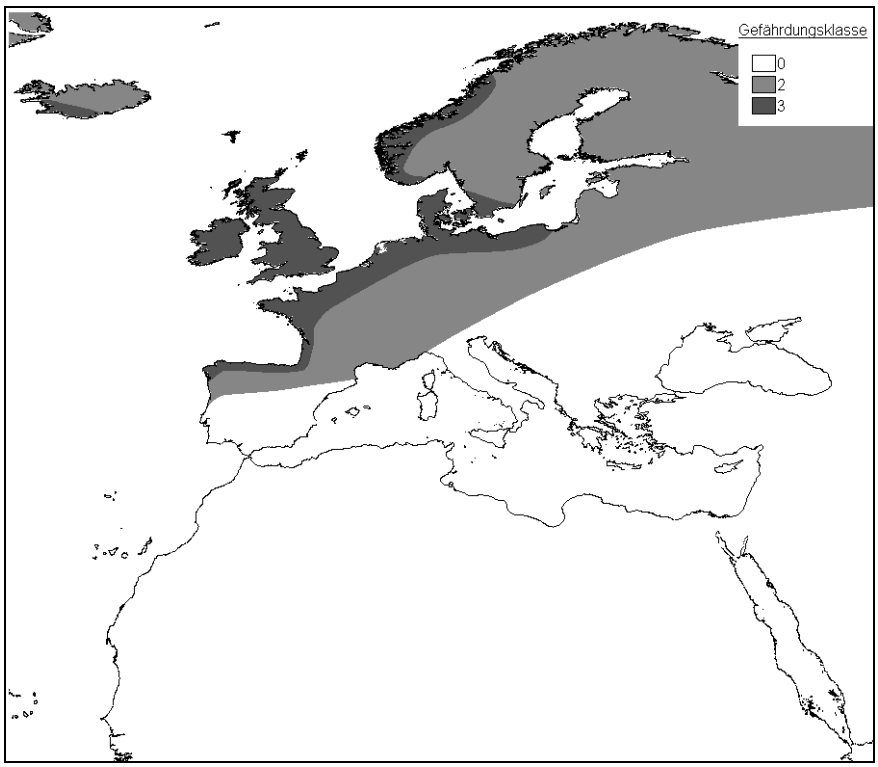

Figure 4-15: Risk of winter storms (Source: OD, Münchener Rück, 2001).

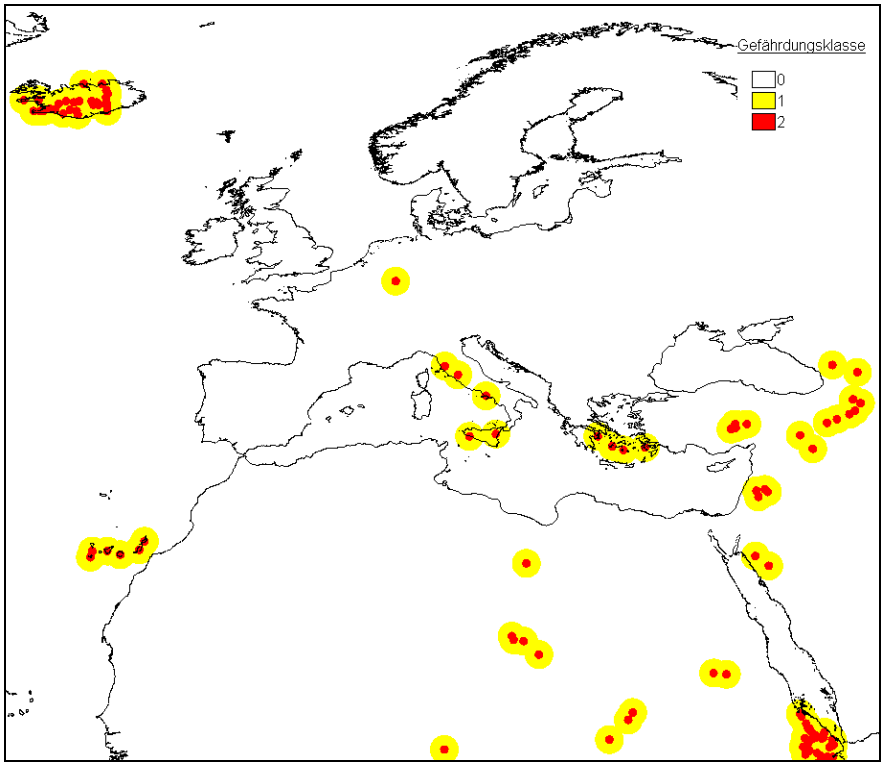

Figure 4-16: Risk of volcano eruptions (Source: OD, Münchener Rück, 2001).

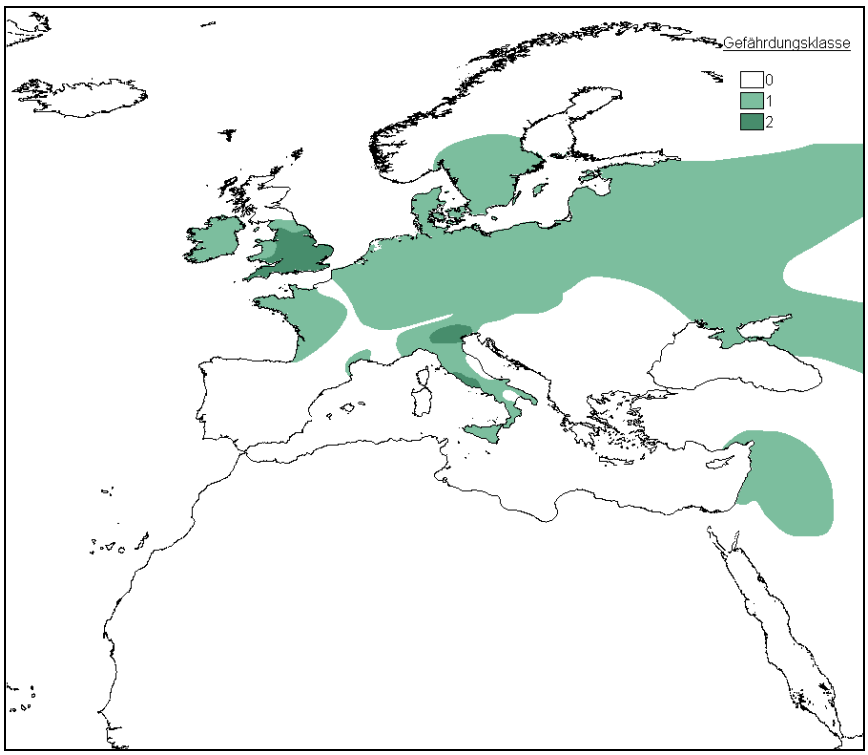

Figure 4-17: Risk of tornados (Source: OD, Münchener Rück, 2001).

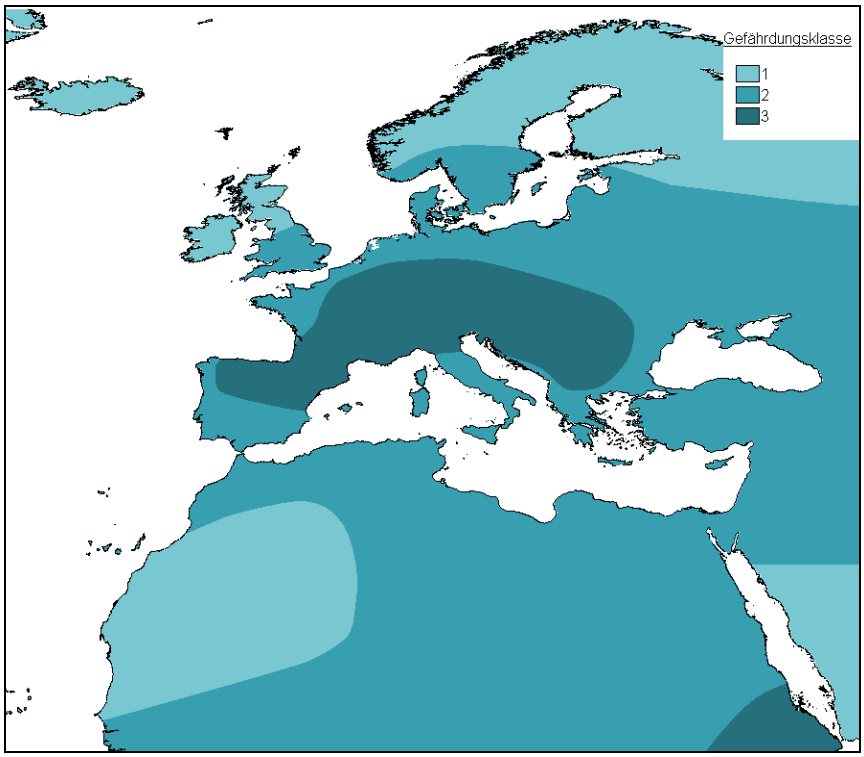

Figure 4-18: Risk of hailstorms (Source: OD, Münchener Rück, 2001).

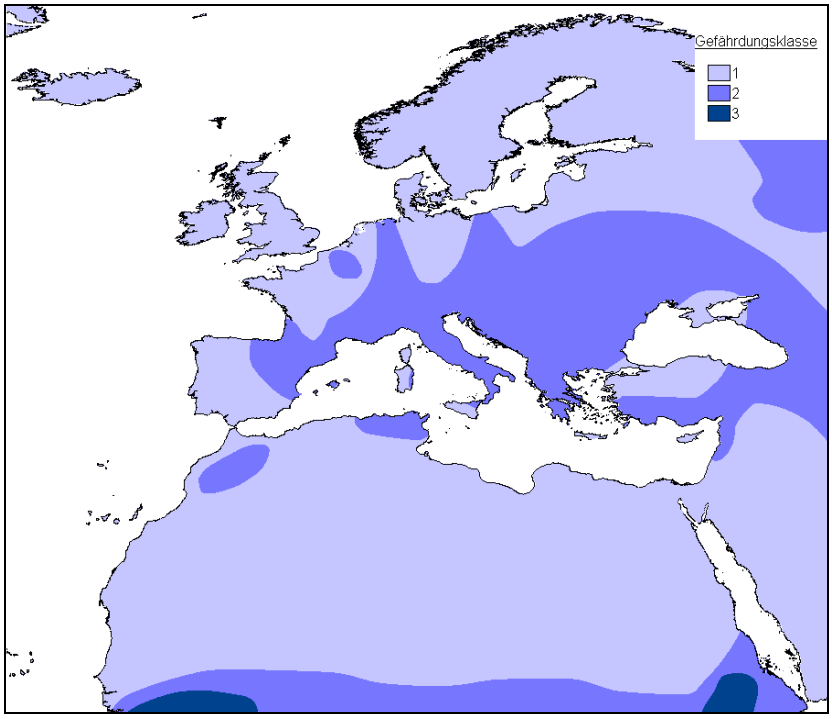

Figure 4-19: Risk of lightning (Source: OD, Münchener Rück, 2001).

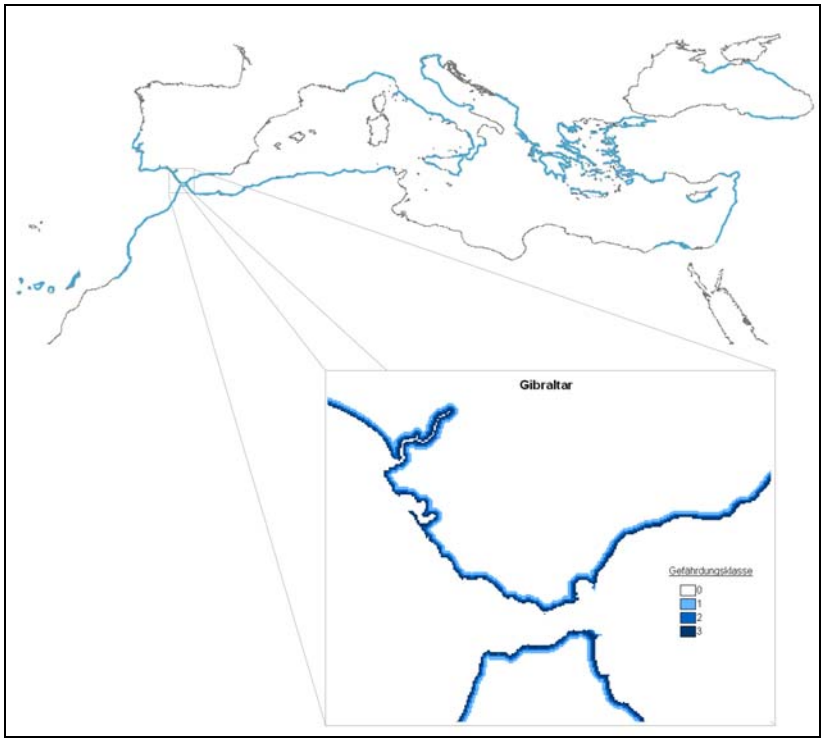

Figure 4-20: Risk of Tsunami formation (Source: OD, Münchener Rück, 2001).

Table 4-4: Risk classes of single natural hazards (Source: Münchener Rück, 2001).

Risk	Risk classes						Scale
	0	1	2	3	4	5	
Earthquake	< V	VI	VII	VIII	≥ IX	-	modified Mercalli, P = 10% (50 years)
Volcano Eruption*	no risk	100 km	30 km	-	-	-	distance to volcano
Tsunami*	no risk	low < 3 km	medium < 2 km	high < 1 km	-	-	distance to coast
Storm	no risk	-	-	high	-	-	distance to coast
Tropical Storm	no risk	118 - 153	154 - 177	178 - 209	210 - 249	≥ 250	Saffir-Simpson hurrican scale [km/h]
Winter Storm	no risk	-	medium	high	-	-	wind velocity
Tornado	no risk	< 0.1	0.1 - 2	> 2	-	-	events per 10,000 km² and year
Hail	-	< 1	1 - 3	> 3	-	-	hail days per year
Lightning	-	< 2	2 - 6	> 6	-	-	amount of strikes per km² and year

* blue marked classes are not present in the Mediterranean region

In this model areas with a higher risk by natural hazards are also assigned higher costs factors (Table 4-6). These factors are based on an insurance costs model for the site-specific calculation of the insurance premium for natural hazards as described in (Kronshage, 2001). According to this, the insurance rate $V_{h,F}$ for overhead lines in case of a positive risk is composed of the base insurance rate $V_{h,F\neq zero}$ and an exponential weighting factor $b_h^{r_h} - 1$. The exponential approach describes the spreading of the risk classes. For the exponent r_h it has to be inserted the risk class of the respective natural hazard h. Even if there is no risk, for some natural hazards a risk cannot be fully excluded so that the insurance rate is charged with the positive value $V_{h,zero}$ The values for the base of the insurance rate function b_h of the natural hazards h and the residual insurance charges have been determined on the basis of an expertise of the research group 'Earth Science' of the Munich Re Group (Kronshage, 2001).

Table 4-5: Insurance rates and base factors (Source: Kronshage, 2001).

h	Risk	$V_{h,zero}$ [‰]	$V_{h,F\neq zero}$ [‰]	b_h
1	Earthquake	0.2	0.08	4.1
2	Volcano eruption	0.0	0.03	4.6
3	Tsunami	0.0	0.21	2.5
4	Winter storm	0.1	3.64	1.1
5	Tornado	0.1	0.32	1.6
6	Hail	0.3	4.55	1.1
7	Lightning	0.3	4.55	1.1

Table 4-6: Total insurance rates.

h	Risk	Risk class r				
		0	1	2	3	4
1	Earthquake	0.2	0.3	1.3	5.4	22.5
2	Volcano eruption	0.0	0.1	0.6	-	-
3	Tsunami	0.0	0.3	1.1	3.1	-
4	Winter storm	0.1	-	0.8	1.2	-
5	Tornado	0.1	0.2	0.5	-	-
6	Hail	-	0.5	1.0	1.5	-
7	Lightning	-	0.5	1.0	1.5	-

$$V_{h,F} = \begin{cases} V_{h,zero} & r_h = 0 \\ (b_h^{\,r_h} - 1) * V_{h,F\neq zero} & r_h \neq 0 \end{cases} \qquad (h = 1, \ldots, 9)$$

Equation (10)

Generation of an Isotrophic Friction Image

The insurance costs factors of several risks are added up for every pixel and thus result in the friction feature natural hazard. All costs factors of the remaining features are first lowered by the base costs for the purpose of the formation of sums. After summing, the base costs are again added so that just one single isotropic friction image R_{iso} results:

$$R_{iso} = 1 + \sum F_k \qquad \text{Equation (11)}$$

with: F costs factor lowered by the base costs

k feature (land cover, infrastructure, natural hazard, visibility)

The greatest possible friction factor of 100.0 is not reached as this would always assume a maximum weighting of all friction images in one place. For example, the areas that are most far away from the network are located in the Atlantic Ocean. There neither a visibility analysis nor an assessment of natural hazards was carried out.

Finally, the exclusion mask is laid over the entire isotropic friction image so that the resulting image additionally includes the maximum value of 10,000 for exclusion areas (Figure 4-21).

From Figure 4-22 it can be appreciated how the lines finally found for interconnecting Point 1 in Egypt with the European centres of demand try to take the shortest way but avoid exclusion areas and areas with high isotrophic friction factors.

Table 4-7: Ratio of raised costs to base costs (= 1.0) from (May, 2005).

Feature k	Value F
Land Cover	
Grassland	1.0
Forest	5.0
Wetland	3.0
Savannah	1.0
Cropland	1.0
Rice field	3.0
Semi desert	1.0
Desert	1.0
Glacier*	10,000.0
Inland water*	10,000.0
Inland water (bridge)	3.0
Seawater	10.0
Populated place*	10,000.0
Agglomeration	10.0
Visibility	
Cultural/Religious sites	1.0; 7.0
Infrastructure	
Network	1.0 – 50.0
Natural hazards	
see Table 4-6	1.0 – 30.9
Exclusion mask	10,000.0
No Data	10,000.0

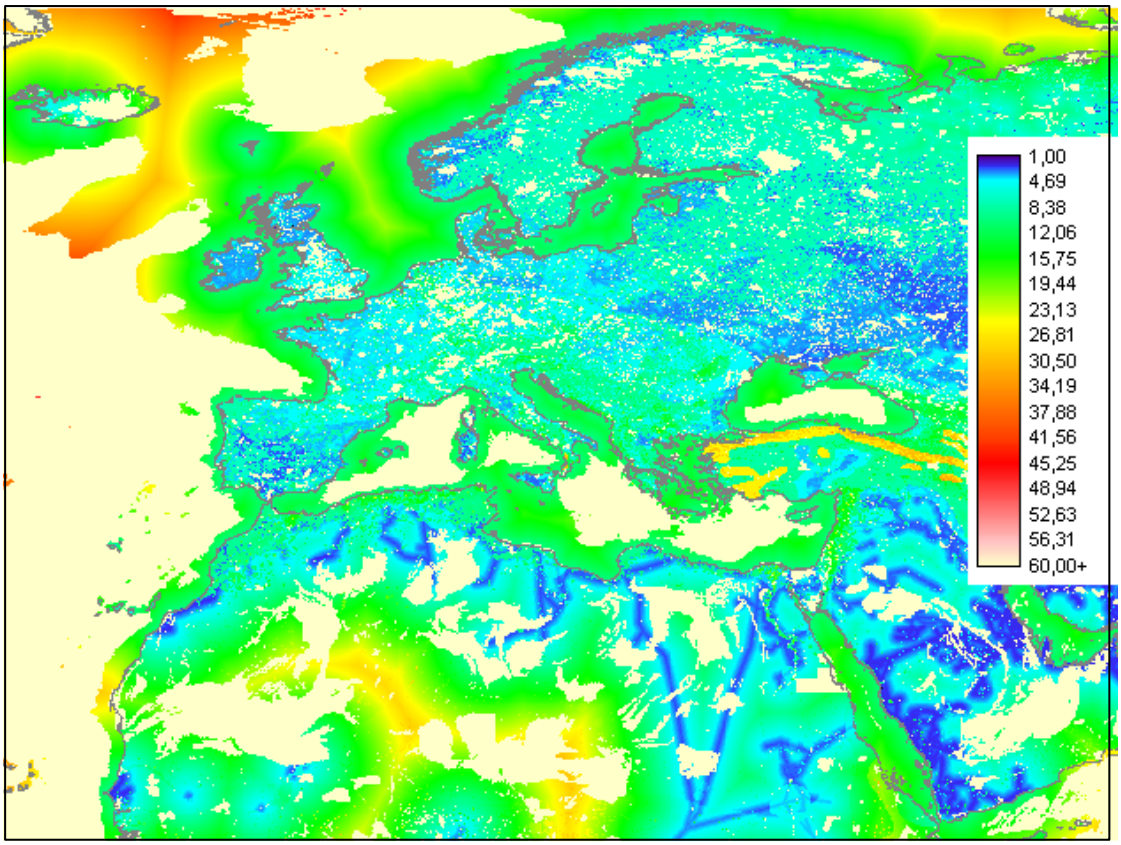

Figure 4-21: Isotropic total friction image. Values of 1 indicate best sites for HVDC lines.

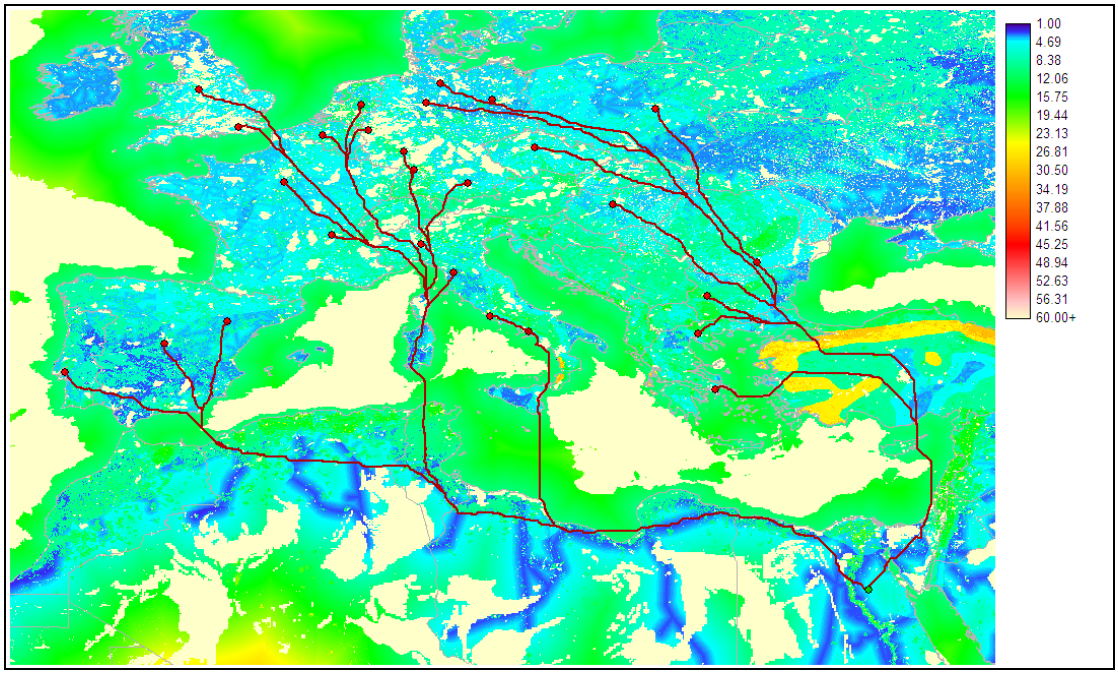

Figure 4-22: Lines found from Egypt Point #1 to all centres of demand in Europe as overlay to the isotrophic total friction image.

Generation of an Anisotrophic Friction Image

The former friction images contain isotropic features, which have the same value in all directions, whereas the slope of the terrain is an anisotropic feature.

Exemplarily, one can imagine a traveller who climbed up a slope, which is inclined to the south (180°), in a northerly direction (0°). In doing this he must overcome the maximum slope on the shortest way. If he would cross the slope from a south-easterly direction (135°), he could overcome the same slope on a longer way. At 90° the traveller would move along the contour line. As explained, the crossing of a non-flat raster cell is direction-dependent. The resulting prolongation of the way finally causes additional costs for the line.

Generally it is assumed that the line costs rise with the increasing slope. In order to spatially determine the continental elevation in the whole Mediterranean region, it is fallen back on the global digital elevation model ‘GLOBE’ of the NGDC, one of three national NOAA data centre (GLOBE Task Team et. al., 1999).

The raster dataset has horizontal resolution of approximately 1 km x 1 km and a vertical resolution of 1 m above sea level. Altogether six raster elevation models and five cartographic vector datasets have been either reprocessed or specially processed for the utilization in GLOBE (30” raster). Data from 18 different sources are included in GLOBE. The main part is provided by the raster dataset ‘Digital Terrain Elevation Data’ (DTED) of the NIMA and the GTOPO30 raster dataset of the USGS, which was originally produced out of the DCW by raster conversion (Hastings & Dunbar, 1999).

First of all a slope image is calculated with the IDRISI tool ‘Slope’ out of the digital elevation model and the corresponding aspect image which issues the inclination angle as azimuth for each pixel. A slope of 20% and higher is assumed as a stronger feature for the laying of the line. Above that, the additional expenditure in costs increases linearly so that classes are formed in steps of 45%. From 200% the magnitude of the slope is irrelevant for the additional costs and the maximum value is kept constant (Kronshage & Trieb, 2002). The maximum slope occurring in the Mediterranean region amounts to 151% at a 1-kilometre digital elevation model.

With the help of an anisotropic function the effective friction of the pixel is determined out of the aspect image. The full friction is just given for an angle difference of 0° and 180° between walking direction and slope by using a quadratic cosines function. All other angles lead to a decrease in the effective friction until the neutralisation of the slope at 90° and 270° (Eastman, 1999).

Slope [%]	Factor
0-20	1.0
20-65	1.2
65-110	1.4
110-155	1.6
155-200	1.8
>200	2.0

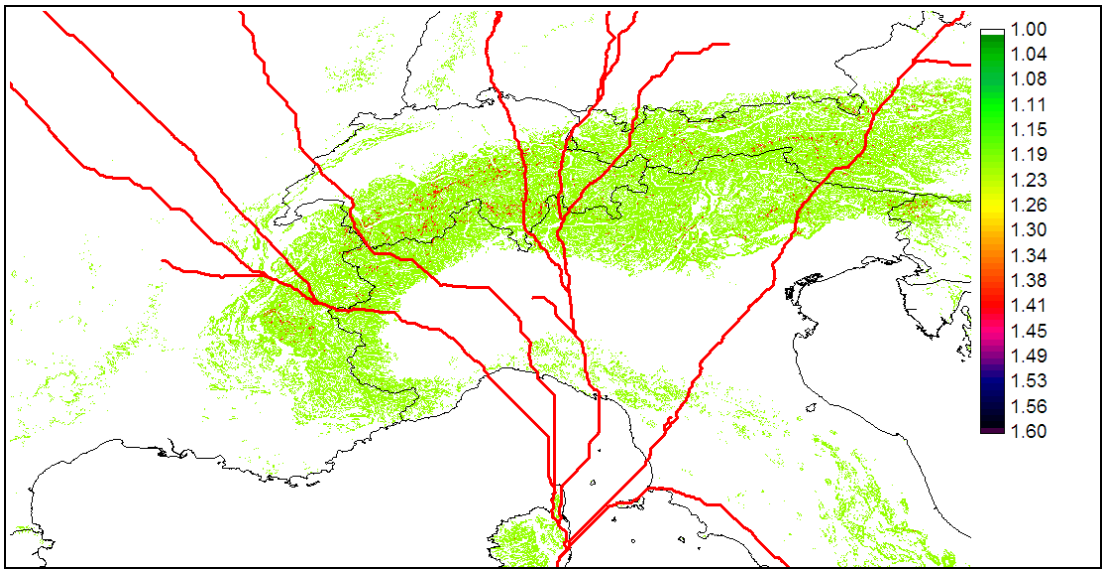

Figure 4-23: Anisotrophic friction map describing the weighting factor of slope of the terrain.

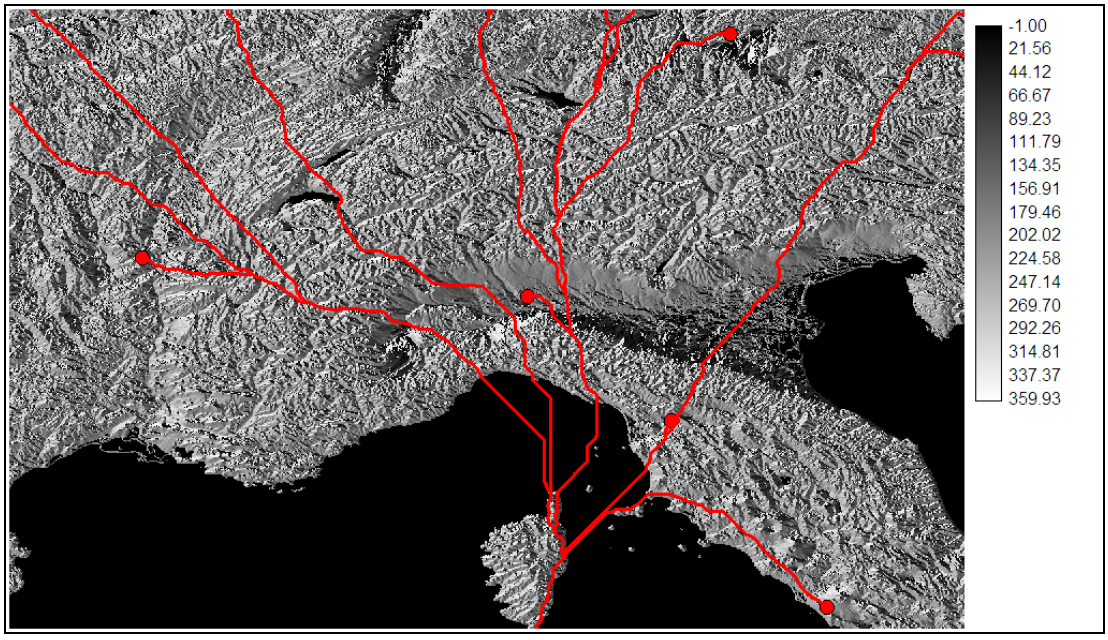

Figure 4-24: Aspect image (0° - 360°) derived from the digital elevation model.

Generation of a Cost-Distance Images and Identification of Least-Cost HVDC Lines

With the IDRISI-tool 'Varcost' a cost-distance image is calculated out of the isotropic friction image, the anisotropic friction image and its corresponding aspect image. For this the anisotropic friction image is multiplied by the isotropic friction image which represents the multiplication factor. The starting point is the site of the solar thermal power plant. Then 'Varcost' calculates the costs as distance raster equivalents for each raster image pixel which must be raised at least to get from the adjacent pixel to the plant. Exemplarily, a cell value of 100.00 means that the costs for bridging the distance between this pixel and the target pixel is equivalent to the movement over one-hundred cells with the base costs of 1.0 or over 50 pixel with a costs value of 2.0 or over one pixel with a costs value of 100.0 (Eastman, 1999).

After specifying the target, the tool 'Pathway' gives the favourable course of the line from the plant to the demand centre as line polygon.

Figure 4-25 shows exemplarily the cost-distance image calculated from the CSP plant location #2 in Morocco together with the final course of the lines to all European centres of demand. Due to the weighting of the underlying features, the values represented in the figure are not absolute, but relative costs. According to it, the favourable path with minimum cost has been selected.

Figure 4-26 and Figure 4-27 show the same procedure for the starting points in Tunisia and Saudi Arabia. Finally, Figure 4-28 shows the final result with all HVDC lines interconnecting 11 CSP production sites in MENA with 27 European centres of demand.

The total procedure for the identification of HVDC lines with minimum economic and environmental cost is summarized in Figure 4-29. The main steps are the following:

- Identify exclusion areas for HVDC lines,
- estimate non-directional cost factors for HVDC lines (isotrophic friction),
- estimate directional cost factors for HVDC lines (anisotrophic friction),
- identify start and end points of potential HVDC lines,
- produce cost-distance images for each start point,
- identify the interconnections from all start to all end points with the smallest relative environmental and economic impact.

Finally the results are transformed to the format of the REACCESS database and introduced as numerical data.

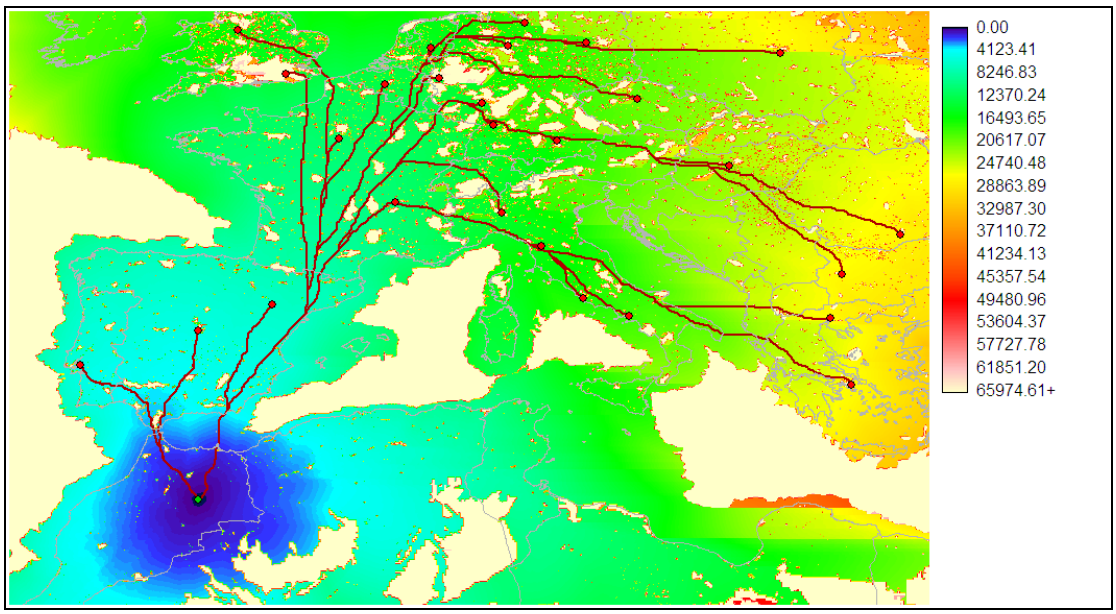

Figure 4-25: Cost-distance image for the HVDC line connecting production point Morocco #2 with all European centres of demand.

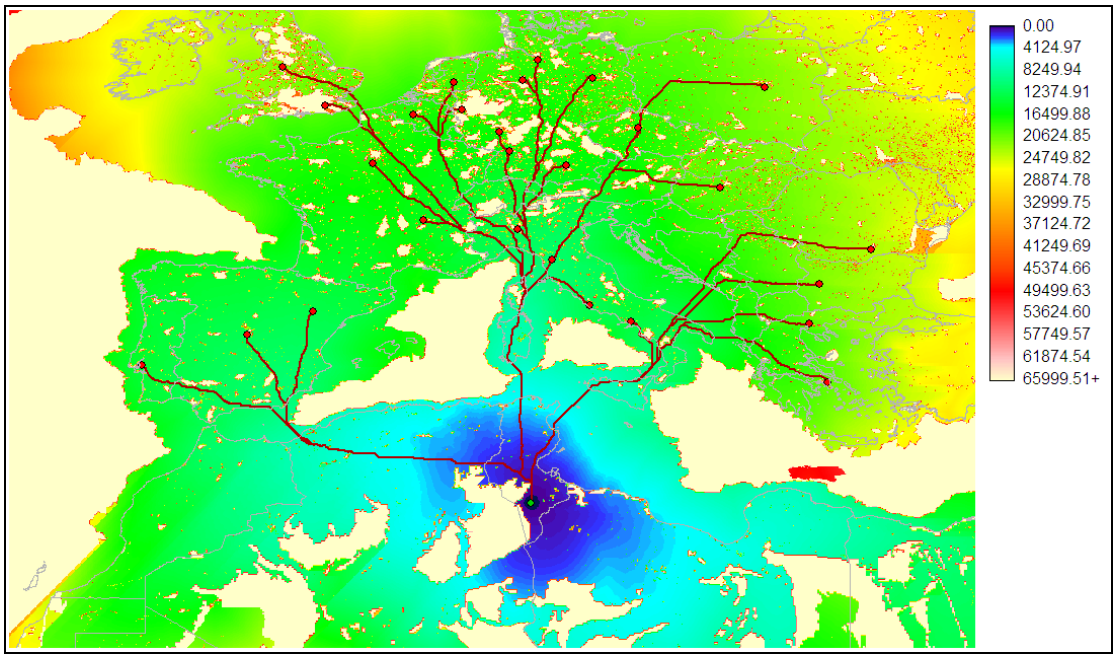

Figure 4-26: Cost-distance image for the HVDC line connecting production point Tunisia #1 with all European centres of demand.

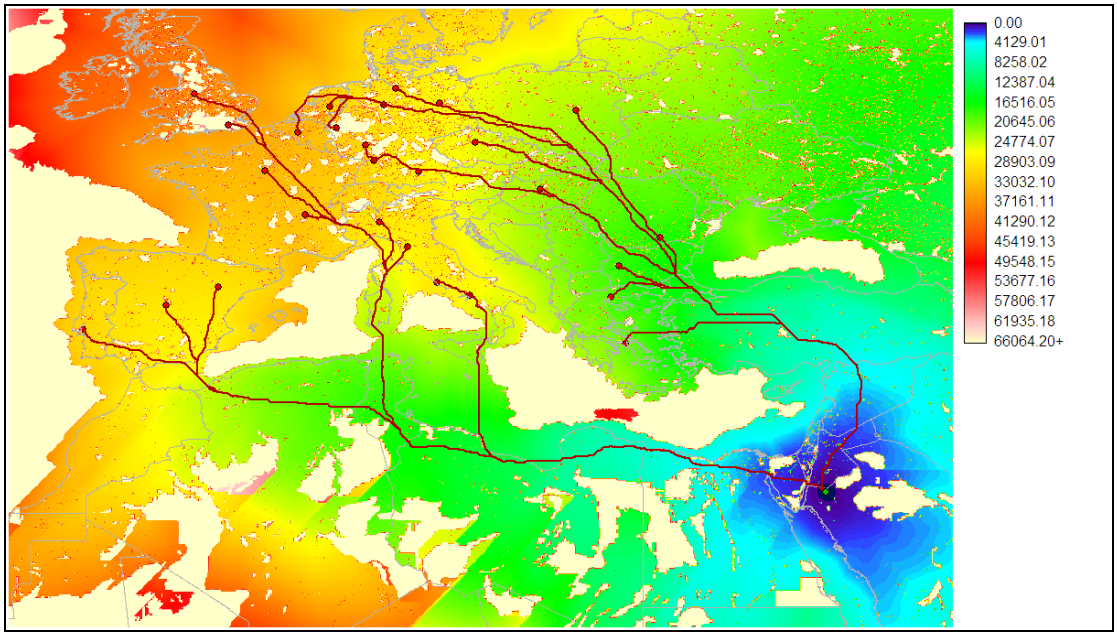

Figure 4-27: Cost-distance image for the HVDC line connecting production point Saudi Arabia #1 with all European centres of demand.

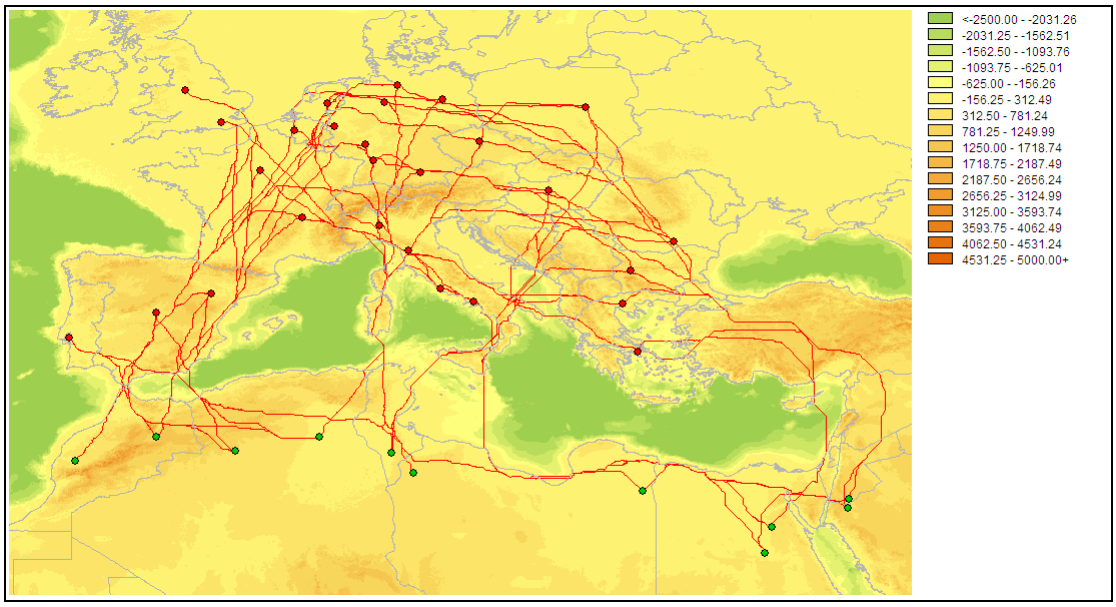

Figure 4-28: All HVDC lines interconnecting 11 CSP production sites in MENA with 27 European centres of demand as identified in the REACCESS study. The background map shows the elevation in metres above/below sea level.

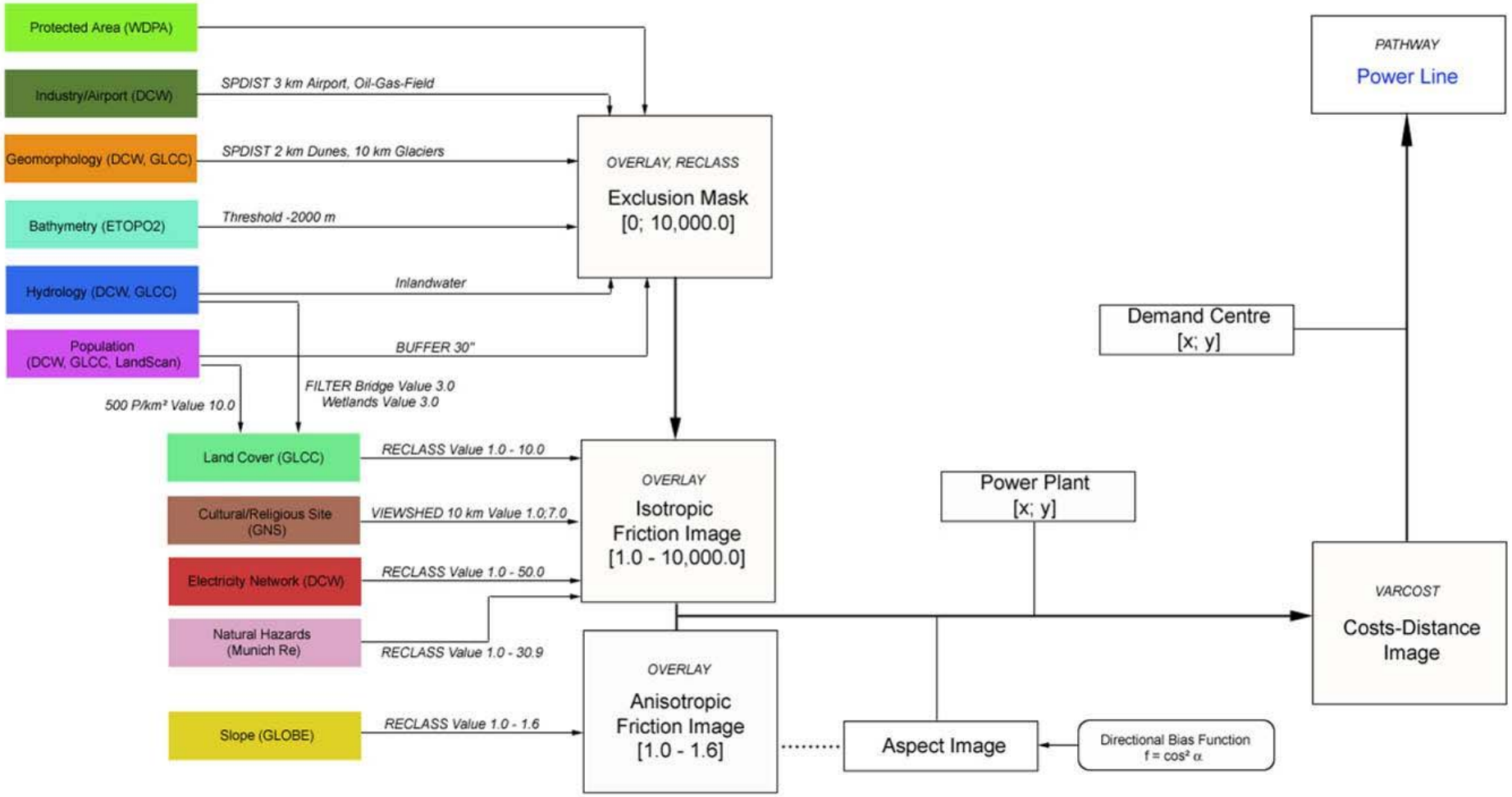

Figure 4-29: Model applied for the identification of least cost HVDC power lines in terms of economic and environmental impact (May 2005).

5 ASSESSMENT OF FRAMEWORK CONDITIONS

5.1 POLITICAL FRAMEWORK CONDITIONS

5.1.1 General European Directives

Discussions on climate change have been around for quite some time. However it needed the Stern report on economics of climate change to reach the necessary political awareness of the severeness of this subject (Stern, 2006). The report has led to the realisation that the inaction to tackle climate change will be much more cost intensive than a steady transition to a sustainable low-carbon, energy-efficient economy.

As a consequence the EU Commission has decided to tackle climate change as one of the biggest challenges that have to be faced. The way to reach an agreement took some time. In March 2007 the European Council agreed to set legally binding targets to show Europe's determination. Those targets were confirmed at a summit of the head of states and governments on the 11th and 12th of December 2008. Until 2020 the EU wants to reach a:

1. 20% reduction in greenhouse gas (GHG) emissions compared to 1990 (30 % if an international agreement is reached) (COM(2008) 30)
2. 20% share of renewables in overall EU energy consumption including a 10 % renewable energy component in transport fuel (COM(2008) 30)
3. 20% energy saving of the EU primary energy consumption compared to a business as usual development (EC, 2007b)

Regarding the expansion of the use of renewable energy the EU wide goal has been broken down to country level (Table 5-1).

Several methods on how to define the national targets were assessed during the consultation process including a flat rate increase, an increase related to the potentials of each country and an increase depending on the GDP. In the end three factors have been taken into consideration to reach the binding goals.

Starting from a share of 9% renewable energies in the overall EU final energy consumption in 2005 an increase of 11% is needed until 2020. Half of this increase (5.5%) is added as a flat rate to the 2005 RES share of each member state. The other half is assigned to each country weighted by GDP per capita. This approach was chosen as it includes the wealth of each member state. To consider the effort by member states to promote the use of RES in the past, an early starter bonus was additionally taken into account (Figure 5-1).

Table 5-1: National targets for the share of RES in 2020 (COM(2008) 19).

	Share of RES in final energy consumption 2005	Share of RES in final energy consumption 2020
Austria	23.3%	34%
Belgium	2.2%	13%
Bulgaria	9.4%	16%
Cyprus	2.9%	13%
Czech Republic	6.1%	13%
Denmark	17.0%	30%
Estonia	18.0%	25%
France	10.3%	23%
Finland	28.5%	38%
Germany	5.8%	18%
Greece	6.9%	18%
Hungary	4.3%	13%
Ireland	3.1%	16%
Italy	5.2%	17%
Latvia	15.0%	23%
Lithuania	34.9%	42%
Luxemburg	0.9%	11%
Malta	0.0%	10%
Netherlands	2.4%	14%
Poland	7.2%	15%
Portugal	20.5%	31%
Romania	17.8%	24%
Slovak Republic	6.7%	14%
Slovenia	16.0%	25%
Spain	8.7%	20%
Sweden	39.8%	49%
United Kingdom	1.3%	15%

The EC directive 2009/28/EG from April 23, 2009 explicitly foresees the import of renewable electricity from MENA to Europe in its Article 9 on Joint Projects of Member States and Third Countries. This directive defines the conditions that have to be fulfilled in order to account for electricity produced in third countries to reduce European carbon emissions until 2020 (EC 2009). It states that electricity must be produced from new renewable energy systems, construction for HVDC transport schemes must start before December 31, 2016 and the interconnection must be operative before December 31, 2022. The directive gives the frame for possible solar electricity imports from MENA to Europe as described here.

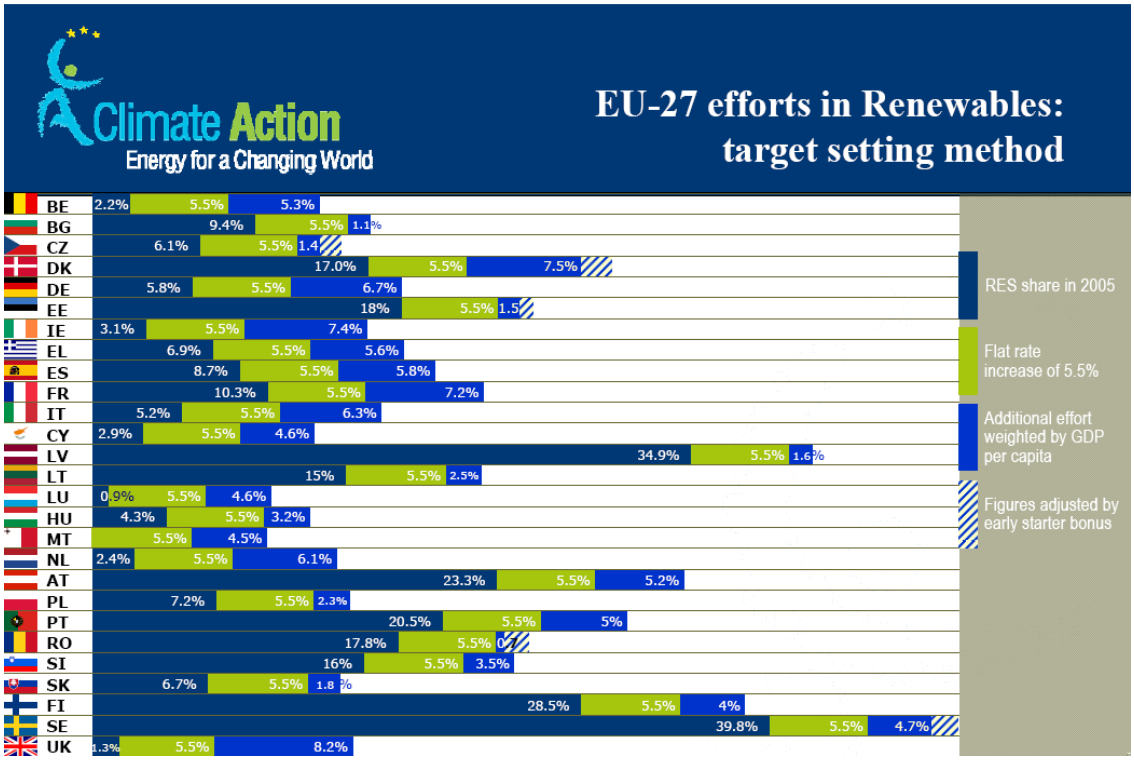

Figure 5-1: EU approach to set national goals for the expansion of RES until 2020 (van Steen, 2008).

To reach these set goals the countries of the European Union are free to decide on the promotion schemes they want to adopt. Various ways to promote the use of renewable energy are therefore existent in different specifications. The promotion of renewable electricity however is the most advanced and discussed way in most member states. Figure 5-2 shows the current promotion schemes in the EU-27.

There are mainly three approaches chosen. Feed in tariff systems provide investors with low risks due to fixed remunerations over a given length of time and have proven to be not only most effective but also most efficient. Therefore the majority of states have adopted this tool so far. The second approach that is chosen by a number of states is the quota system. This system is often referred to as the more market based promotion scheme and therefore favoured by some countries. The third approach is a promotion due to tax incentives and/or investment grants. These tools are used as the major promotion instrument in two countries but are additionally provided by some other countries with feed-in tariff or quota systems (Klein et al., 2008). The discussion on the various ways to promote renewable electricity is extensive and would go beyond the scope of this chapter. Further information however can be found at http://ec.europa.eu/energy/renewables/electricity/electricity_en.htm, http://www.feed-in-cooperation.org/, and http://www.res-legal.eu/en.

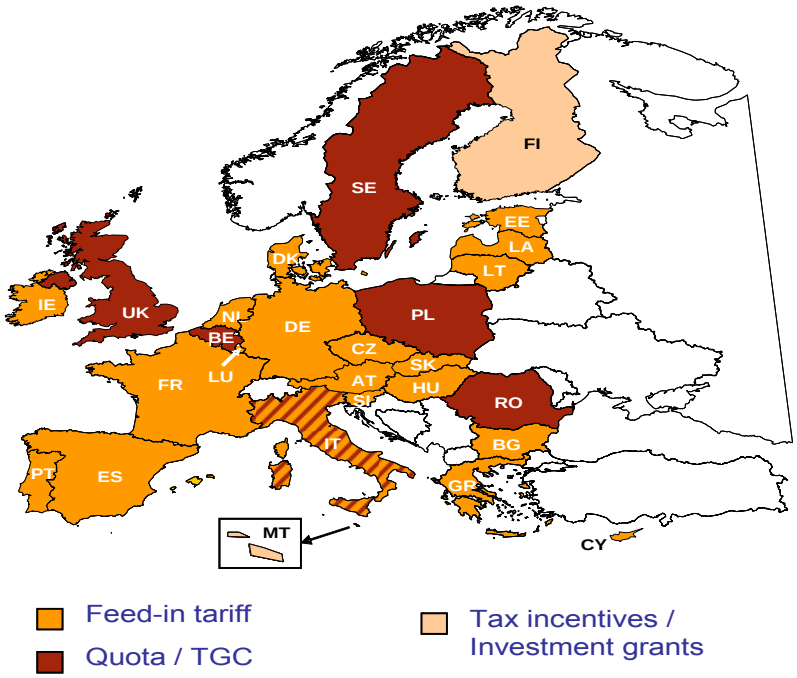

Figure 5-2: National promotion schemes for electricity from renewable energy in the EU-27 (Klein et al., 2008).

Most national promotion schemes only cover the expansion of capacities inside their own borders. However, the European Commission allows the countries to import electricity from RES outside the European Community (COM(2008) 19). In order to retain the purpose to limit greenhouse gas emissions by increasing the use of renewable energy sources, only installations that came into operation after the Directive came into force can account for the national binding targets.

5.1.2 Union for the Mediterranean and Mediterranean Solar Plan

The idea of the Mediterranean Union was originally a French initiative welcomed by the Mediterranean Countries and reframed to the “Union for the Mediterranean” (UfM) based on the Barcelona Process in order to include northern EU states and the European Commission. The Union was formally founded by a decision of the European Council in March 2008. The first summit of the heads of states was held in Paris on July 13th 2008. UfM Member states are EU plus EC plus countries bordering the Mediterranean (see Figure 5-3). The Arab League acts as an observer. Rotating Co-Presidency (one EU, one south Mediterranean, first France and Egypt) and biennial summits are planned to assure an open and vital process. UfM institutions are replacing existing EUROMED institutions with a Joint Permanent Committee in Brussels and a secretariat located in Barcelona.

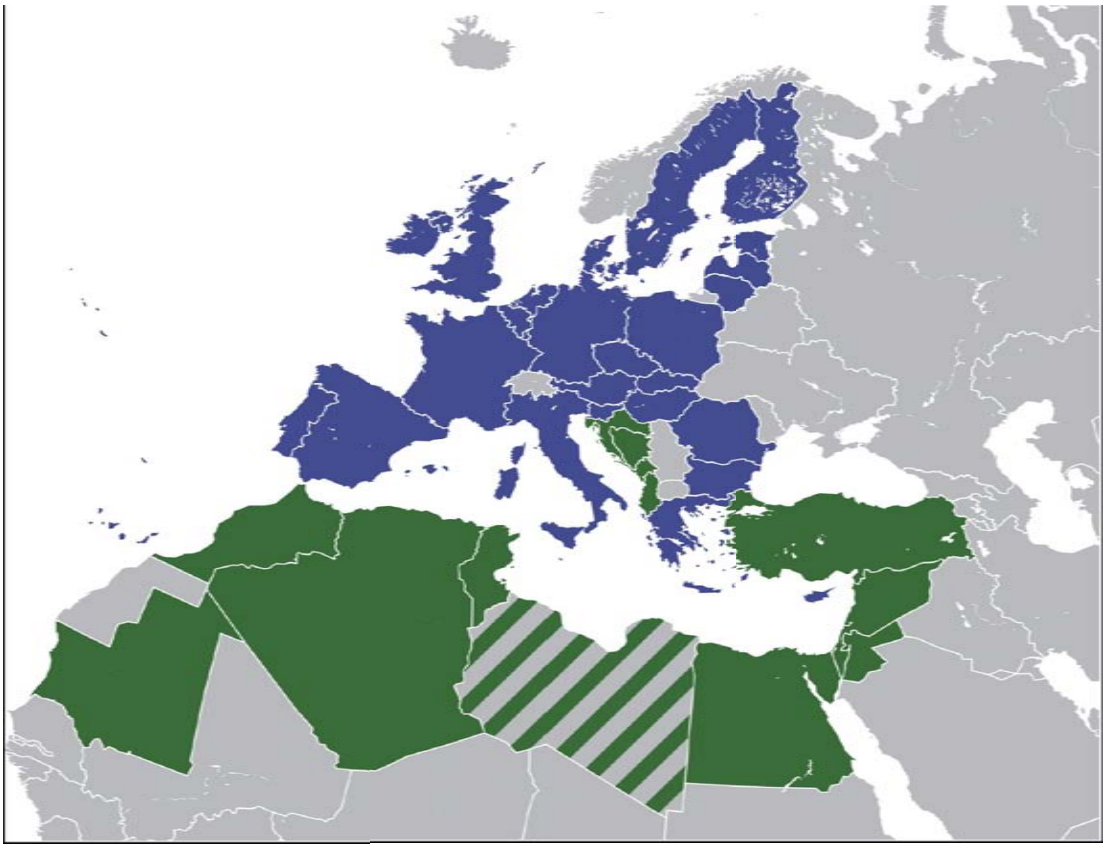

Figure 5-3: Member states of the Union for the Mediterranean (MEEDDAT 2008).

Key initiatives of the UfM are de-pollution of the Mediterranean, maritime and land highways, civil protection and alternative energies. The core of the latter is the Mediterranean Solar Plan (MSP) confirming the need to focus on alternative energy sources. The plan will integrate existing EUROMED policies, notably in the field of renewable energies Market development as well as research and development of all alternative sources of energy are seen therefore a major priority in efforts towards assuring sustainable development. The UfM secretariat was tasked to explore the feasibility, development and creation of a Mediterranean Solar Plan as one of the six UfM projects launched in July 2008 by the 43 participating head of states. This activity created a big political momentum in the region. The MSP has the following main objectives:

- New balanced North-South relationship based on concrete projects implementation.
- Greenhouse gases reduction.
- Creation of a new industry and a new market in the south.
- Development of new sustainable energy production plants in the South to meet local demand of electricity.

- Contribution to the implementation of the new European Energy-Climate package, using the possibility to export to Europe Green electricity.

The Mediterranean Solar Plan has been divided into three organisational phases, starting in 2008 with the definition of goals and an organisational frame. From 2009 to 2011 a pilot phase will take place including the compilation of an Immediate Action Plan (IAM) with the goal to start a series of pilot projects for the deployment of renewable electricity generation and efficiency enhancement in the Mediterranean Region. In the same time, a Master Plan Study (MPS) is to be elaborated detailing the strategy and measures necessary until 2020 to implement a total of 20 GW of renewable power capacity, save 20% of energy compared to business as usual and to start with first projects for the export of solar electricity from MENA to Europe. At the same time, long-term sustainable frame conditions shall be established in the region for the effective expansion of the use of renewable energy and energy efficiency beyond 2020.

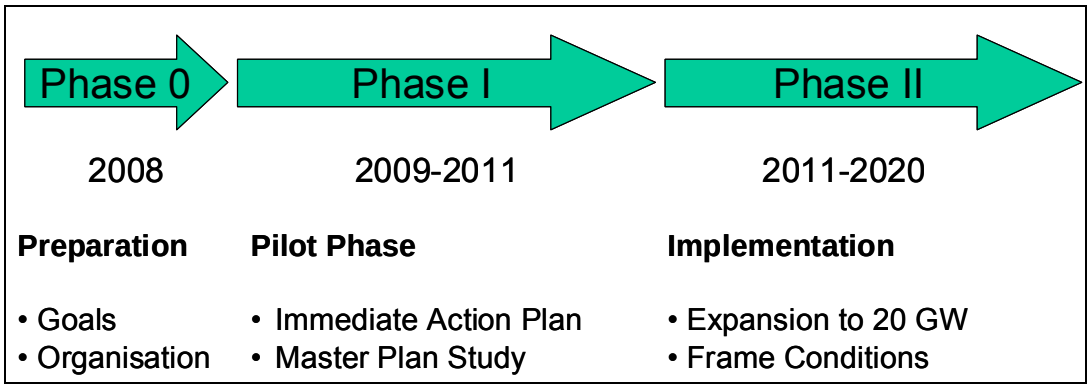

Figure 5-4: Main phases of the Mediterranean Solar Plan (MSP) scheduled within the Union for the Mediterranean (UfM)

The Master Plan Study (MPS) scheduled to be elaborated between 2009 and 2011 aims to provide the following benefits and results for the region until 2020:

- Developing concrete and profitable projects for both south and north countries
- Promoting Public/private and private/private projects in order to boost industrial developments
- Boosting energy market integration and regional harmonization
- Mainstreaming financial and administrative schemes to facilitate project implementation

- Changing habits by a better understanding of challenges at stake at both public and private levels (global warming, industrial opportunities)
- Planned or ongoing Studies: qualification of solar and wind resources, regulation and normalization, incentives (financial and public tools), control and evaluation methodologies, (European Commission, World Bank, EIB)

The Immediate Action Plan (IAP) aims to install in the short term a series of projects in the Mediterranean region, asking partner countries for a selection of priority projects to ensure broad political support, and specifying the main criteria for project selection as follows:

- capacity to launch the project in 2009/2010
- existence of an industrial project sponsor
- commitment of host country to ensure commercial viability of the projects

By February 2009 already 130 projects had been proposed that will be evaluated and selected for integration and realisation within the UfM before June 2009.

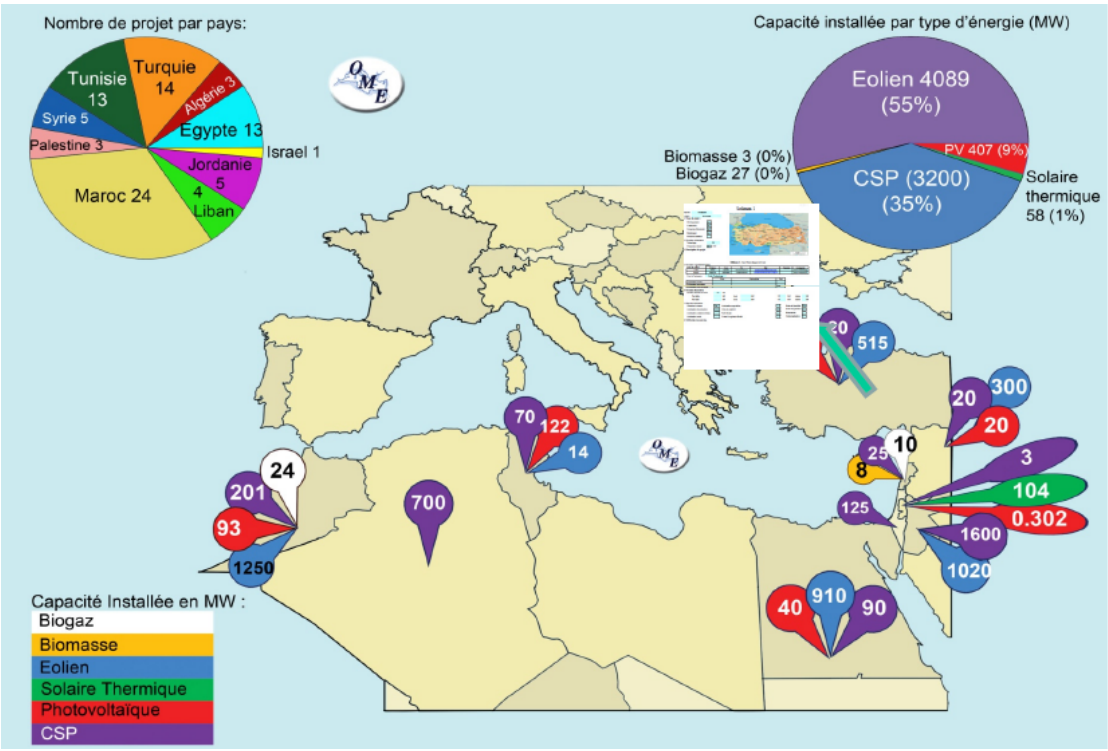

Figure 5-5: Projects proposed to the Immediate Action Plan by February 2009 (Lorec, 2009).

5.2 FINANCIAL FRAMEWORK CONDITIONS, OWNERSHIP STRUCTURE

The ownership structure of CSP plants as well as of the electricity lines used for the import to the EU is relevant for the risks assessment. Energy transfers have been used in the past as political instrument by some countries therefore the description of the ownership structure will focus on the involvement of the respective states.

5.2.1 Ownership Structure of Transmission Lines

HVDC lines have been built for the export / import of electricity between two countries, the most recent one being a sea cable of 580 km between Norway and the Netherlands. The ownership of these interconnections is mostly organised as cooperation between the Transmission System Operators (TSO) of both connecting countries. However, so far there has been no experience with ownership structures for transmission grids that bypass other countries as would be applicable for imports of solar electricity from Northern Africa to Europe.

To get an idea how the ownership of such a transmission line could be organised experiences from other sectors like gas pipelines can be gained. One of the most prominent examples is the Nabucco pipeline. Its ownership structure will be shortly outlined as an example.

The Nabucco pipeline runs from Turkey via Bulgaria, Romania and Hungary to Austria. It is owned by the Nabucco Gas Pipeline International GmbH, a company that belongs to the companies active for the transport of gas in each country affected by the pipeline. The Nabucco Gas Pipeline International GmbH is responsible for the planning, financing, construction, marketing as well as the maintenance of the pipeline. It operates independently from its parent companies as an autonomous economic entity (NABUCCO, 2008).

The corporate organisation for the Nabucco pipeline is a good role model for the construction of transnational electricity transmission lines. This becomes evident by looking at the obstacles regarding national or even regional permit procedures. Another synergetic effect that can be used is the existing maintenance network in each respective country.

The TSO in the EU 27+ are for the largest part state owned companies or companies where the state holds a large proportion of shares (Table 5-2). Some companies however are corporations that are today mostly subject to regulation by a state authority as transmission systems are a subject of indivisibility and therefore natural monopolies.

In many countries few companies are used to not only hold the transmission grid but also most of the electricity generation of the same area. With the liberalisation of the

energy sector in Europe and the formation of international European markets non-discriminatory access to the grid became a requirement. In order to ensure the independence of TSO and real competition between electricity producers it became important to prevent situations with a conflict of interest. Therefore strategic unbundling becomes the requirement for companies within the European Union, Norway and Switzerland. Since then there have been discussions whether this change was enough to open the market to new protagonists or if ownership unbundling would be the necessary step. Instead most countries have decided to improve the situation by setting up regulators.

Table 5-2: Ownership structure of Transmission System Operators within the EU27+.

Country name	Company	Ownership	Union member
Austria	TIWAG, Verbund and VKW	for the largest part state owned	UCTE
Belgium	Elia	corporation	UCTE
Bulgaria	ESO EAD	state owned	UCTE
Cyprus	TSO-Cyprus	state owned	none
Czech Republic	CEPS	state owned	UCTE/CENTREL
Denmark	Energinet.dk	state owned	UCTE/NORDEL
Estonia	Põhivõrk	state owned	BALTSO
Finland	Fingrid	corporation 12 % state owned	NORDEL
France	RTE (owned by EDF)	state owned	UCTE
Germany	EnBW, E.ON, RWE and Vattenfall Europe	corporations	UCTE
Greece	HTSO	corporation 51 % state owned	UCTE
Hungary	MAVIR	state owned	UCTE/CENTREL
Ireland	EirGrid	state owned	UKTSOA, ATSOI
Italy	Terna	corporation	UCTE
Latvia	Augstsprieguma	state owned	BALTSO
Lithuania	Lietuvos Energija	corporation 61.7 % state owned	BALTSO
Luxembourg	CEGEDEL	corporation 32.8 % state owned	UCTE
Malta	none	none	none
Netherlands	TenneT	state owned	UCTE
Norway	Statnett	state owned	NORDEL
Poland	PSE-Operator	state owned	UCTE/CENTREL
Portugal	REN	corporation 46 % state owned	UCTE
Romania	Transelectrica	state owned	UCTE
Slovak Republic	SEPS	state owned	UCTE/CENTREL
Slovenia	ELES	state owned	UCTE
Spain	REE	corporation	UCTE
Sweden	Svenska Kraftnät	state owned	NORDEL
Switzerland	ATEL, BKW, EGL and NOK	corporations	UCTE
United Kingdom	National Grid, SONI and SSE	corporations	UKTSOA, ATSOI

Table 5-3 gives an overview of the ownership structure of TSO in countries identified as relevant for potential import corridors to the EU 27+. State ownership is the

standard in most south Mediterranean countries. Only Saudi Arabia has a private TSO. In 2000, all Saudi electricity companies were merged to a single stock company. As Saudi Arabia is a kingdom ruled by the al Saud family and its provinces are governed by its members it can be expected that the Saudi electricity company is mostly in the hands of the royal family.

Table 5-3: Ownership structure of Transmission System Operators relevant for the import of solar thermal electricity outside the EU 27+.

Country name	Company	Ownership	Union member
Algeria	Sonelgaz Spa (Algerian Company for Electricity and Gas)	state owned	COMELEC, AUPTDE
Egypt	EETC (Egyptian Electricity Transmission Company)	state owned	AUPTDE
Israel	Israel Electric Corporation	state owned	
Jordan	NEPCO (National Electric Power Company)	state owned	AUPTDE
Libya	GECOL (General Electricity Company of Libya)	state owned	AUPTDE
Syria	PEEGT (Public Establishment of Electricity for Generation & Transmission)	state owned	AUPTDE
Morocco	ONE (Office Nationale de l'Electricité)	state owned	COMELEC, AUPTDE
Saudi Arabia	Saudi Electricity Company	corporation	AUPTDE
Tunisia	STEG (Société Tunisienne de l'Electricité et du Gaz)	state owned	COMELEC, AUPTDE
Turkey	TEIAŞ (Türkiye Elektrik Iletim A.S.)	state owned	

5.2.2 Ownership Structure of Production Plants

At the end of 2008 almost 500 MW of installed CSP capacity are globally in operation (Chapter 3.2.3). Regarding the ownership structure of these plants the three largest projects will be described.

The oldest and largest CSP facility in the world is the Solar Energy Generation Systems (SEGS) in California's Mojave Desert. It consists of nine solar power plants that went into operation between 1985 and 1991 and has an overall capacity of 354 MW. Originally it was owned and built by independent project companies of the Israel based company Luz. Luz as a provider of the technology went bankrupt and the ownership of the project companies went to its creditors. Today it is operated and partially owned by the Florida Power & Light Company (FPL energy).

The second largest CSP plant that came into operation in 2007 is the 64 MW installation called Nevada Solar One in Boulder City, Nevada. It is owned by the Spanish company ACCIONA SA that has specialized in providing renewable energy.

The third largest installation Andasol 1 in Granada, Spain, has an installed capacity of 50 MW and came into operation at the end of 2008. Two more plants (Andasol 2

and 3) are currently under construction and expected to start production in 2008 and 2011. Project companies are set up to own and operate the plants. The first company with the name Andasol 1 S.A. is owned by Grupo Cobra, the Spanish construction company responsible for the building of the plant, and the German Flagsol GmbH a subcompany of the German Solar Millennium AG that is specialized in the project development of CSP plants.

Generally new as well as established power producing companies can commission CSP plants. However, this depends on the market access as well as the cost-benefit-ratio this renewable technology can provide for each entity.

Regarding market access the situation in the South Mediterranean region needs to be described. Historically the electricity markets in this region are state owned monopolies. Due to the expected increase of electricity consumption in this region large investments are necessary to occur. In order to facilitate the needed investment in the power generation sector Morocco, Turkey, Tunisia and Egypt started to allow private participation in the production of electricity in the mid 1990ies. As a result 16 % of the current installed capacity in these countries is in the hand of independent power producers (IPP). As the access to the power generation was given to independent entities but suppliers still remained to be monopolies, Power Purchase Agreements (PPAs) were set up.

Experience has shown that the measures taken were not enough to attract the amount of investment needed as it can not fully be provided by national entities. Foreign investors however still regard the South Mediterranean region as risk intense and therefore relative unattractive for investment. Therefore many countries in the region have started to adopt further steps towards liberalized electricity markets providing private foreign investors with more guarantees (OME 2008).

Turkey for example has taken all the necessary steps towards the liberalisation of its electricity system. A Loan and Guarantee Agreement with the World Bank as well as the alignment to the European market have given way to this restructuring. In 2001, the state company TEIAŞ responsible for production, transmission and distribution was broken down in individual private companies with only the TSO TEIAŞ remaining in state ownership (TEIAŞ, 2008).

Also other countries in the South Mediterranean region have decided to establish new legislations or reforms of their electricity sector. One of these developments was to bring in regulatory bodies which were so far adopted in Turkey, Egypt, Algeria and Jordan.

Additionally, a new electricity law was promulgated in Algeria in 2002 allowing independent production and preparing for a progressive opening of the electricity sector to private investors. The sectors production, transmission and supply are subject to unbundling with only the transmission remaining in state ownership.

Another state that did unbundle its state owned electricity company is Jordan. The underlying legislation was already established in 1999.

Egypt already implemented an access for independent power producers as mentioned before but is heading towards a liberalization of the electricity market. This will most likely not occur before 2010.

In Morocco a new law for an opening of the electricity market alongside a regulatory entity is at the moment drafted.

Tunisia that was among those countries that allowed for the entrance of independent power producers does not see the necessity at the moment to bring in any further measures (OME, 2008).

All this shows that the South Mediterranean electricity market as a whole is in the process of restructuring. This development generally provides the possibility for new power producers to be involved in the development of CSP installations in this region.

The cost-benefit-ratio however also needs to be included in the considerations of future ownership structures. So far conventional energy sources in the South Mediterranean region are subject to high subsidies. As a result solar electricity production by CSP plants can not yet compete against conventional sources even though it can be produced much cheaper in this area compared to the European Union due to the higher solar potential. Therefore a promotion system like Power Purchase Agreements might be in order for the integration of renewable energy sources in the Southern Mediterranean electricity system. Regarding potential exports to the EU27+ electricity from CSP installations have to compete with the European market where prices for conventional energy carriers follow the world market. One option discussed is to enhance national regulations for feed-in tariffs in order to allow tariffs for imported solar and other renewable electricity from Non-EU-countries as possibility to significantly promote the built up of commercial CSP capacities in the MENA region. A harmonised European regulation and promotion might also set incentives for solar power import.

5.3 TRENDS OF COMPETING REGIONS

Solar energy resources and suitable land areas for CSP installations are large in the MENA region so that resource competition among EU27 and other regions is not plausible. However, domestic electricity consumption is expected to rise significantly in the supply countries considered and CSP potentials are an attractive future option also for supplying the domestic demand. This issue will be considered in the following.

The major driving forces for electricity demand are growth of population, growth of economy and efficiency measures. These issues can be addressed by a simple model developed by DLR for the MED-CSP and TRANS-CSP studies that will be presented in the following.

5.3.1 Electricity Demand Trends in MENA

The number and growth rate of population is one of the major driving forces for a national electricity demand. The scenario is based on the intermediate World Population Prospect of the United Nations that was revised in the year 2006. According to that analysis, the population in the total MENA region will steadily grow from about 300 million people today to over 600 million people in 2050 (UN, 2006). The population in North Africa will grow from today's 140 million to 240 million in 2050. In terms of population, Egypt is the dominating country, accounting for 50% of the population of the total region. The population in the Western Asian countries will grow from 120 to over 220 million people by 2050, Iran being the dominating country in this region. The population on the Arabian Peninsula will increase from today 50 million to over 150 million people in 2050. The dominating countries are Saudi Arabia and Yemen. The Saudi Arabian population will stabilize by the middle of the century, but Yemen's population will still be growing quickly by that time, becoming the most populated country in this region. While the European region shows a clearly stabilizing population just below 600 million by 2050, the population in MENA will grow from 300 to also 600 million within the same time span.

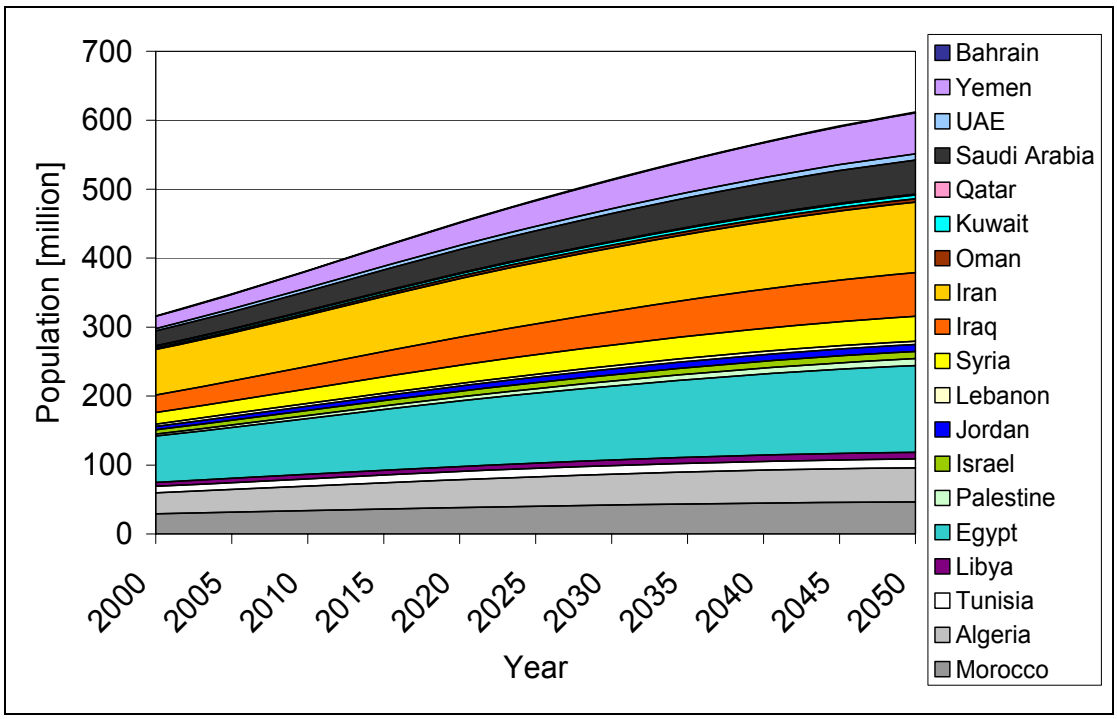

Figure 5-6: Growth of population in MENA countries according to UN medium growth scenario (UN, 2006).

Table 5-4: Growth of population in MENA countries according to UN medium growth scenario (UN, 2006).

Country	2000	2005	2010	2015	2020	2025	2030	2035	2040	2045	2050
Morocco	29.2	31.5	33.8	36.2	38.3	40.3	42.0	43.5	44.8	45.7	46.4
Algeria	30.5	32.9	35.4	38.1	40.6	42.9	44.7	46.2	47.5	48.6	49.5
Tunisia	9.6	10.1	10.6	11.1	11.6	12.0	12.4	12.6	12.8	12.9	12.9
Libya	5.3	5.9	6.4	7.0	7.5	8.0	8.3	8.7	9.0	9.3	9.6
Egypt	67.3	74.0	81.1	88.2	94.8	101.1	107.1	112.7	117.8	122.2	125.9
Israel	6.1	6.7	7.3	7.8	8.3	8.7	9.2	9.5	9.9	10.2	10.4
Palestine	3.2	3.7	4.3	5.0	5.7	6.4	7.2	7.9	8.7	9.4	10.1
Jordan	5.0	5.7	6.3	7.0	7.6	8.1	8.7	9.1	9.6	9.9	10.2
Lebanon	3.4	3.6	3.8	4.0	4.1	4.3	4.4	4.5	4.6	4.7	4.7
Syria	16.8	19.0	21.4	23.8	26.0	28.1	30.0	31.7	33.3	34.7	35.9
Iraq	25.1	28.8	32.5	36.5	40.5	44.7	48.8	52.8	56.7	60.3	63.7
Iran	66.4	69.5	74.3	79.9	85.0	89.0	92.3	95.2	98.0	100.4	101.9
Oman	2.4	2.6	2.9	3.2	3.5	3.8	4.1	4.3	4.6	4.8	5.0
Kuwait	2.2	2.7	3.0	3.4	3.7	4.0	4.3	4.6	4.8	5.1	5.3
Qatar	0.6	0.8	0.9	1.0	1.0	1.1	1.2	1.2	1.3	1.3	1.3
Saudi Arabia	21.5	24.6	27.7	30.8	34.0	37.2	40.1	42.9	45.3	47.5	49.5
UAE	3.2	4.5	5.0	5.6	6.1	6.7	7.2	7.7	8.2	8.7	9.1
Yemen	17.9	21.0	24.5	28.5	32.7	37.1	41.5	46.0	50.5	55.0	59.5
Bahrain	0.7	0.7	0.8	0.9	0.9	1.0	1.0	1.1	1.1	1.1	1.2

The second driving force for electricity demand is the economic growth, here represented by the change of the gross domestic product (GDP). The GDP is expressed in $US\$_{2001}$ purchasing power parity (PPP), defined by the basket of

commodities of the Penn World Tables (Heston et al., 2002). Long-term average growth rates for the different countries are selected in a range of reasonable values, most countries closing the gap of GDP per capita to a certain reference country with very high GDP per capita – we have selected USA for this purpose – by 50% in the year 2050. As the USA is a large country with very high GDP per capita, it represents something like an upper margin of productivity. Thus, the growth rate for the USA can be seen as reference case for a highly developed technical and organisational progress. The countries analyzed here reach higher GDP per capita growth rates as they are able to accelerate productivity growth by imitation, subsequently closing their gap to the USA.

Table 5-5: Average long-term per capita GDP growth rates in %/year selected for the scenario calculation.

Western Asia		**North Africa**		**Arabian Peninsula**	
Jordan	2.1	Morocco	4.6	Oman	3.2
Lebanon	1.9	Algeria	4.0	Kuwait	2.1
Syria	1.7	Tunisia	3.6	Qatar	1.9
Iraq	1.6	Libya	3.8	Saudi Arabia	2.7
Iran	1.6	Egypt	4.1	UAE	1.8
Israel	1.6			Yemen	6.5
		USA	**1.2**	Bahrain	2.3

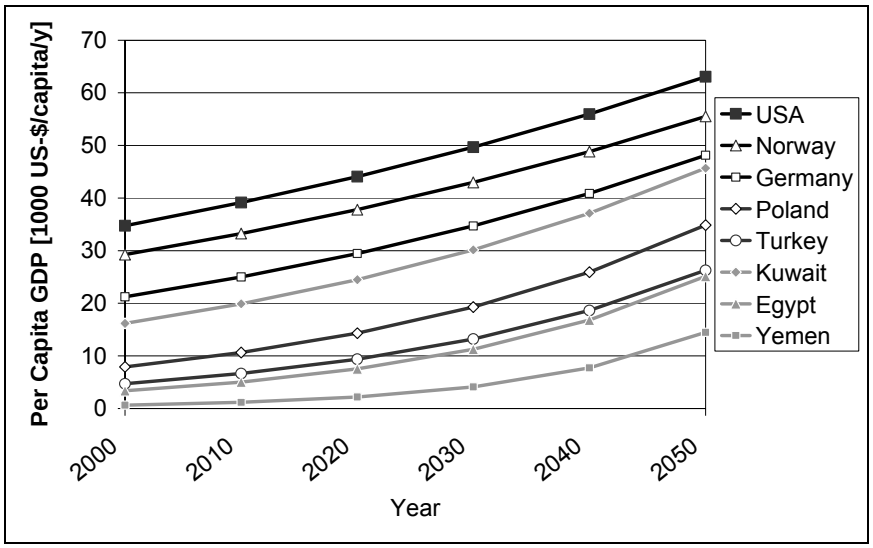

Figure 5-7: Outlook of per capita GDP in 1000 US-$/cap/year for selected countries in MENA compared to other countries.

The effect of such a model is a relative convergence of the economies of the different countries. The literature on economic growth rejects that a convergence in this sense has been taken place in the past. However, for sub-samples of countries a

convergence can not be rejected generally. If convergence exists, halving the difference in 50 years will be at the upper boundary (Barro & Sala-i-Martin, 1995). Following (IEA, 2002) the growth rate for the USA is assumed to be 1.2 %/year. Other sources assume a substantially higher growth rate.

The long-term average GDP growth rates used for calculating our scenario are given in Table 5-5. The resulting long-term development of the per capita GDP is given in Figure 5-7 for a selection of countries. The GDP per capita $x_{i,t}$ and the total final per capita electricity consumption $\hat{y}_{i,t}$ were correlated using a simple regression for a data sample of 25 selected countries (IEA, 2003a), (Heston et al., 2002)[7]. For this purpose we have used a simple power function with two fit parameters a_i and b_i. This regression has been repeated for each year from 1960 to 2001, with the time index t = 1960, 1961, ..., 2001 and the country index i = 1, 2, ..., 25 (Equation 12):

$$\hat{y}_{i,t} = a_t \cdot x_{i,t}{}^{b_t} \qquad \text{Equation (12)}$$

This approach leads to a set of parameter estimates {a_{1960}, b_{1960}}, { a_{1961}, b_{1961}}, ..., { a_{2001}, b_{2001}} across all countries for each year. Comparing the data from the years 1960 and 2000 in Figure 5-8 it becomes clear that in a time span of 40 years the per capita GDP in the analysed countries has grown considerably, but the per capita power consumption has grown at a slower rate. Also the relative difference of per capita power consumption between low and high income countries has decreased with time, varying by 2 orders of magnitude in 1960 and only by 1 order of magnitude in 2000.

The parameters *a* and *b* can be used for an extrapolation of the future per capita power consumption based on the experience of the past 40 years, if their transition in time is modelled, too. We now explicitly consider *a(t)* and *b(t)* as a function of time. Time trends of those two parameters were estimated using power functions and alternatively linear functions. Power functions gave a significantly better fit for the first term *a(t)* (Figure 5-9). For the second term *b(t)* it was hard to distinguish a linear trend from a power trend. The linear trend used here gives a scenario with high efficiency gains, while an exponential trend would result in low efficiency gains[8]. The

[7] Australia, Austria, Belgium, Canada, Czech Republic, Denmark, Finland, France, Germany, Greece, Hungary , Iceland , Ireland, Italy, Japan, Korea, Luxembourg, Mexico, Netherlands, New Zealand, Norway, Poland, Portugal, Slovak Republic, Spain, Sweden, Switzerland, Turkey, United Kingdom, United States. For some of these countries the time series start later than 1960. In the regression shown here, these were included as soon as data were available. Additionally for subsets of countries and/or shorter time series similar regressions were calculated. The results are similar.

[8] Fast economic growth can increase the adoption and development of new machinery which is likely to be associated with high efficiency gains. Experience shows that it is not imperative that this kind of efficiency gains will be achieved without determined policy measures. Their realisation requires technical, financial, social and political effort.

result is an empirical time dependent model for the total final consumption of electricity as function of the per capita gross domestic product with the parameters

$$a(t) = 13.65 \cdot \exp(0{,}0531 \cdot (t - t_o)) \qquad \text{Equation (13)}$$

$$b(t) = 2.2131 - 0.0212 \cdot (t - t_o) \qquad \text{Equation (14)}$$

being t the time variable and t_o = 1960 the first reference year[9]. Applying the model, a future extrapolation for the original sample of 25 countries can be made (Figure 5-10). As a countercheck, the model was additionally applied to a sample of 150 countries for the year 2001, showing an acceptable correlation, too. Therefore, it was assumed to be acceptable for general modelling (Trieb et al., 2005).

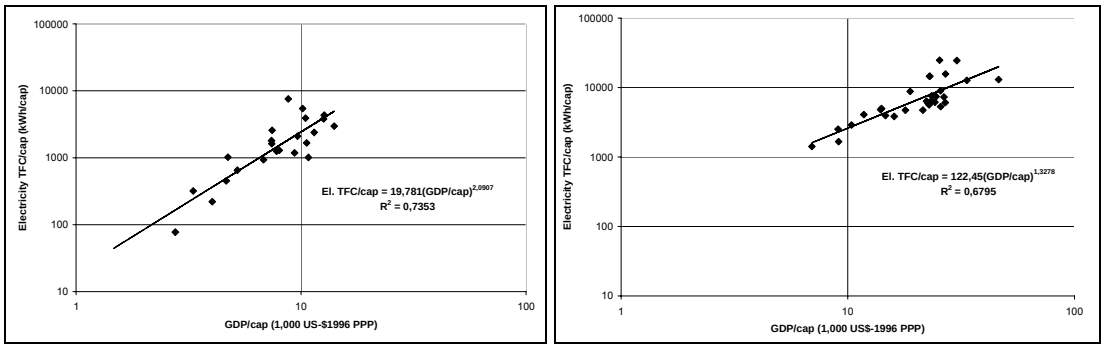

a) In the year 1960 **b) In the year 2000**

Figure 5-8: Examples for correlation between total final consumption per capita and GDP per capita. Data sources: (Heston et al. 2002), (IEA, 2003a, 2003b), (STBA, 2003).

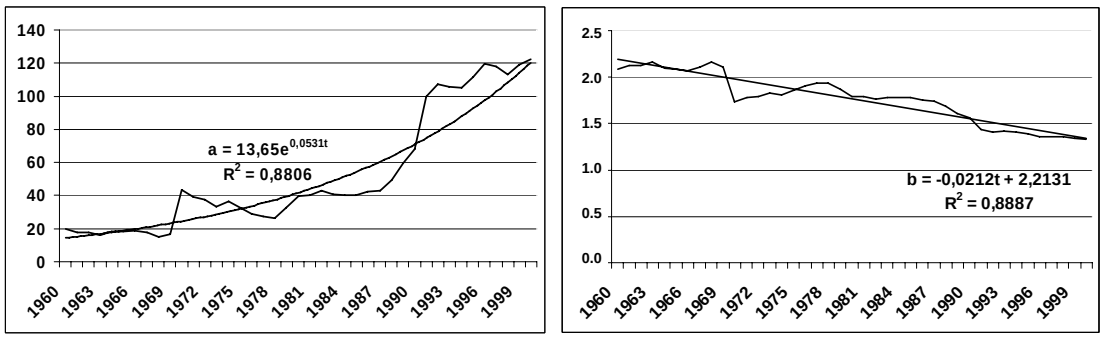

a) Exponential regression for absolute term *a* **b) Linear Regression for exponent *b***

Figure 5-9: Regressions for the time dependency of the parameters *a* and *b* (Trieb et al., 2005).

[9] Note that in line with the past experience the income will be less and less an explaining factor for differences of electricity consumption in cross country comparisons.

Knowing the time dependence of *a* and *b*, Equation 12 can now be formulated as a function of time. From the resulting total final electricity consumption $\hat{y}(t)$, the gross electricity demand $\tilde{y}(t)$ is modelled in Equation (15) using data from (IEA, 2003a) on distribution losses, consumption in the energy sector and the so called "own use". These parameters were aggregated into a proportional and a fixed term. The fixed term (fixed additional consumption $\varphi(t)$) is meant to accommodate energy use for oil and gas production and for a possible future transition to new electricity applications, as e.g. space heating, hydrogen production, electric cars, etc. The proportional term representing the electricity distribution losses $\delta(t)$ was reduced from the present state of the art in each country to a level which is now common in most industrial countries (i.e. 8 %), using the linear weighting function $\varepsilon(t)$, with the starting year t_S = 2001 and the final year t_E = 2050 of the scenario (Equations 16-18).

$$\tilde{y}(t) = \hat{y}(t) \cdot (1 + \delta(t)) + \varphi(t) \qquad \text{Equation (15)}$$

$$\delta(t) = \delta(t_E) \cdot \varepsilon(t) + \delta(t_S) \cdot (1 - \varepsilon(t)) \qquad \text{Equation (16)}$$

$$\varphi(t) = \varphi(t_E) \cdot \varepsilon(t) + \varphi(t_S) \cdot (1 - \varepsilon(t)) \qquad \text{Equation (17)}$$

$$\varepsilon = \frac{t - t_S}{t_E - t_S} \qquad 2001 \le t \le 2050 \qquad \text{Equation (18)}$$

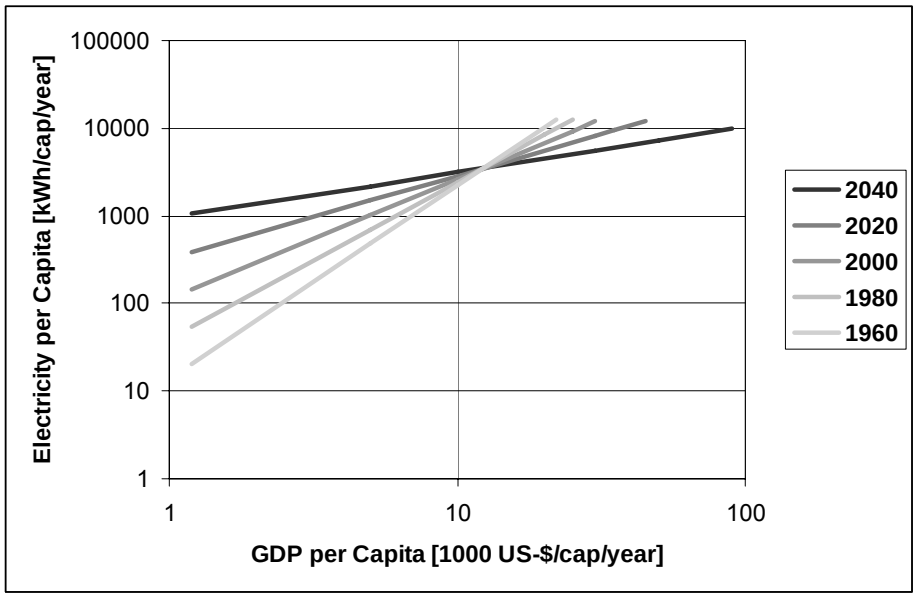

Figure 5-10: Simplified relation between per capita electricity consumption and per capita GDP. Each line follows a function of the type $\hat{y}(t) = a(t) \cdot x(t)^{b(t)}$ that was fitted to data of 25 selected countries for the years 1960 through 2001, where $\hat{y}$ is the net per capita electricity demand and x is the per capita GDP. The lines for 2020 and 2040 were extrapolated using an empirical time function of the parameters $a(t)$ and $b(t)$ as explained in the text.

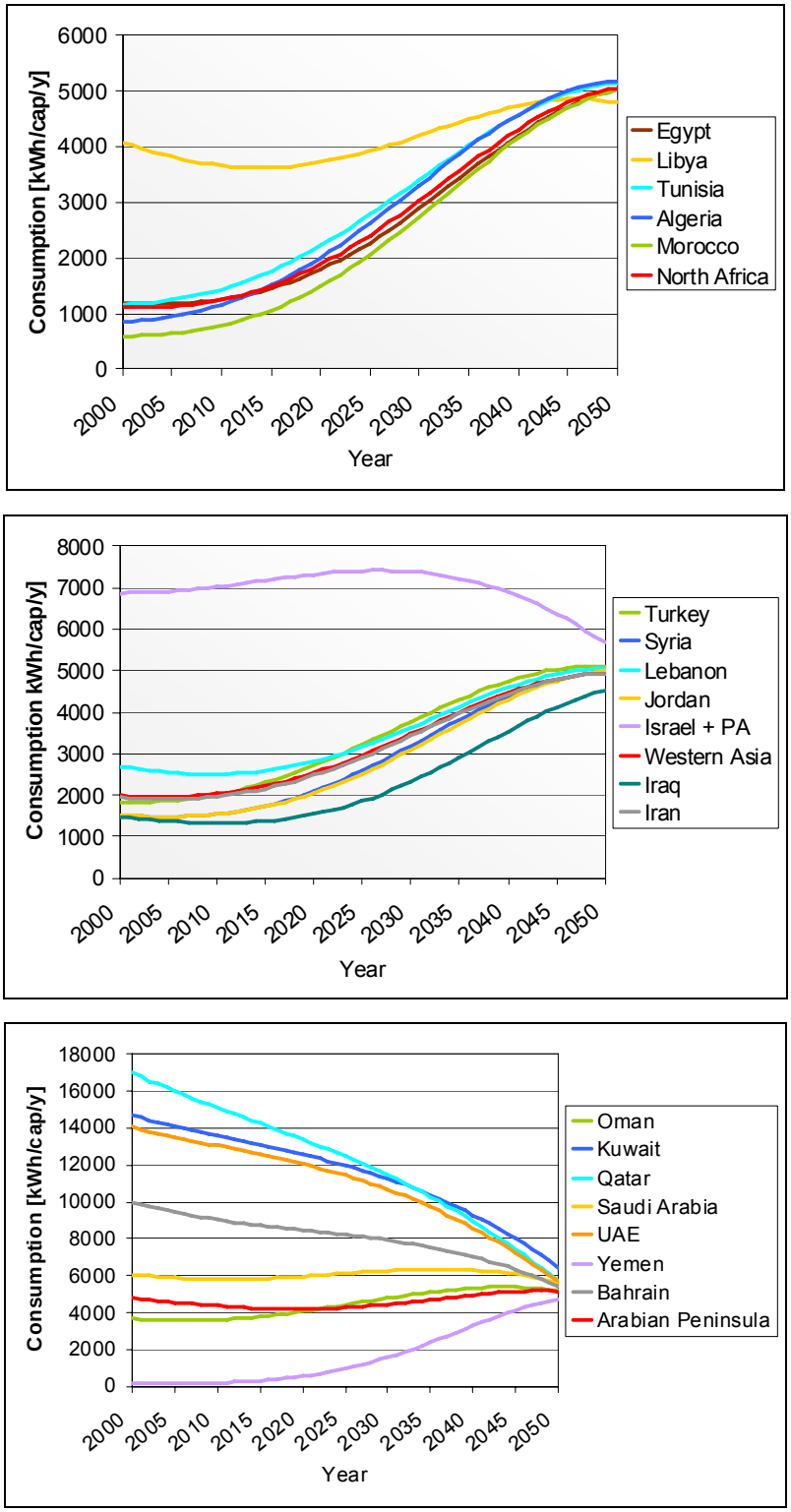

Figure 5-11: Per capita gross electricity consumption *ỹ(t)* aggregated by regions. The Arabian Peninsula is very heterogeneous with values ranging today from around 15,000 kWh/cap/y in the smaller emirates to values as low as 200 kWh/cap/y in Yemen.

The resulting general function of per capita gross electricity consumption *y(t)* is finally calibrated to the present situation in each country assuming a linear mix of the

current value $y(t_S)$ derived from national statistics (IEA, 2003a), and the model value $\tilde{y}(t)$. The weight of the model value is assumed to increase linearly from 0 in 2001 to 1 in 2050. For this purpose, again the weighting function ε was used:

$$y(t) = y(t_S) \cdot (1 - \varepsilon(t)) + \tilde{y}(t) \cdot \varepsilon(t) \qquad \text{Equation (19)}$$

This function was calculated for each country of the region. The aggregated results for the different analysed regions are displayed in Figure 5-11. It is interesting to note a certain evidence of convergence of the different, initially very heterogeneous regions at values around 5000 – 6000 kWh/cap/year. In contrast to the other regions, the per capita consumption slightly decreases in the Arabian Peninsula. This is due to the possibility of huge efficiency gains in the usage of electricity. A second reason applies for the Arabian Peninsula: Due to its fast growing population the low income country Yemen with its low electricity consumption substantially gains weight in the aggregate. As a final step, the per capita electricity consumption is multiplied with population for every year of the scenario analysis, yielding the absolute gross electricity consumption in each of the analyzed countries (Figure 5-12 and Table 5-6). By the middle of the century, with 3000 TWh/y, MENA will have a power demand similar to Europe today.

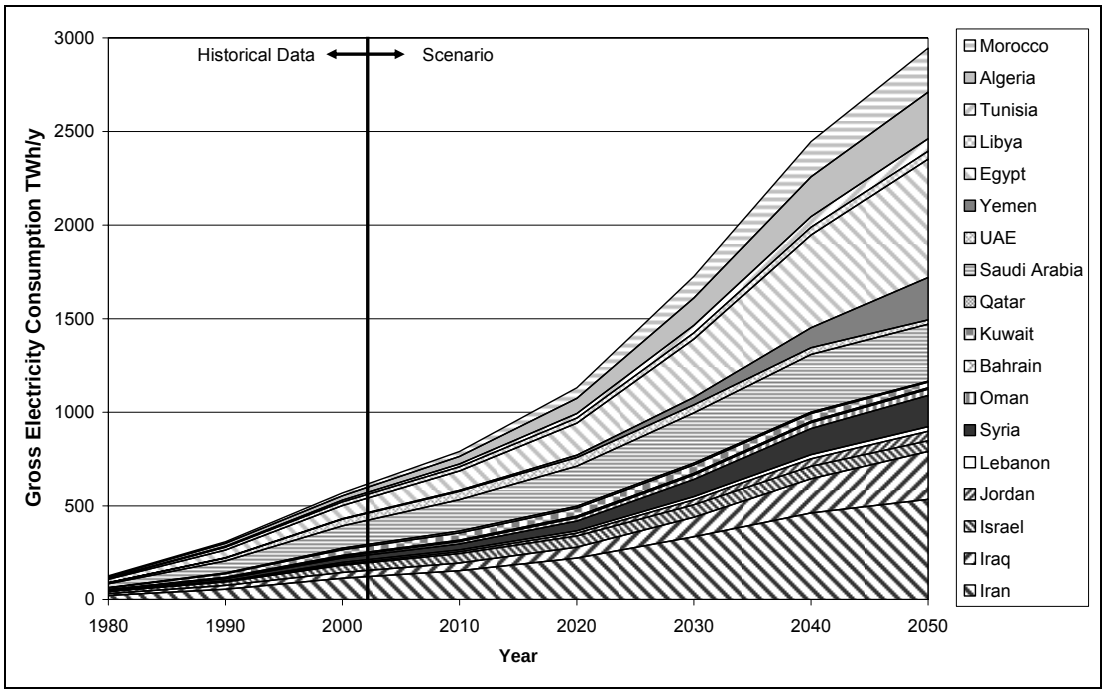

Figure 5-12: Scenario of electricity demand for the Middle East and North African countries.

Table 5-6: Electricity demand perspectives of the MENA countries until 2050 in TWh/y.

TWh/y	1980	1990	2000	2010	2020	2030	2040	2050
Bahrain	1.53	3.23	5.82	7.5	8.2	8.6	8.4	6.9
Iran	20.91	54.94	113.77	154.6	221.9	335.4	462.3	534.4
Iraq	10.56	20.38	31.22	40.0	57.9	104.4	182.6	257.0
Israel	11.36	18.91	38.18	50.8	59.9	66.2	65.9	56.6
Jordan	0.99	3.37	6.86	9.8	15.5	26.7	40.9	50.5
Kuwait	8.67	19.05	30.07	38.8	43.4	44.8	40.8	30.1
Lebanon	2.82	1.81	8.75	10.0	12.3	17.0	22.2	24.6
Oman	0.88	4.94	8.42	12.4	17.5	24.7	31.8	34.6
Qatar	2.24	4.45	8.68	10.1	10.1	9.4	7.7	5.0
Saudi Arabia	20.11	63.83	118.70	168.4	214.0	268.1	308.0	304.5
Syria	3.60	11.01	22.60	31.9	52.0	91.0	138.5	166.3
UAE	5.80	15.79	35.70	43.9	45.6	43.2	35.6	23.6
Yemen	0.46	1.54	2.74	4.8	12.5	39.5	106.3	225.8
Algeria	6.58	14.79	23.04	41.0	80.6	145.2	213.3	249.0
Egypt	17.95	40.72	70.71	102.8	171.5	311.7	495.7	631.3
Libya	4.45	15.53	19.18	23.1	27.2	34.0	41.4	43.9
Morocco	4.84	9.05	15.18	26.8	57.2	115.8	187.4	235.1
Tunisia	2.58	5.11	9.78	14.5	24.3	40.2	56.9	65.9

5.3.2 Chances and Limitations of Electricity Exports from MENA to Europe

Comparing the CSP potentials in the MENA region from Table 3-11 with the electricity demand perspectives from Table 5-6 it becomes clear that solar electricity is not a scarce commodity in the region, and that competition between local use and export of solar electricity to Europe is not an issue that would limit export potentials in the long-term.

Limitations can mostly be expected on the political level, as the relations between some MENA countries and Europe have always been problematic. However, a political change of paradigm is over-due: increasing conflicts on limited resources must be prevented by joint international efforts to tap renewable, unlimited resources.

In the short term until 2020, it will be decisive to create investment opportunities for CSP in MENA both for local consumption and for export. Such a scheme is presently developed within the Mediterranean Solar Plan (MSP) for the Union of the Mediterranean (UfM). The political process of the UfM has been stopped in early 2009 due to conflicts between Israel and Palestine. However, the initiative for the MSP has been continuously pursued and brought ahead by several international consortia, like the Observatoire Mediterraneen de l'Energie (OME) Initiative for the Mediterranean Solar Plan (IMSP) and the Renewable Grid Initiative of several NGO in July 2009.

The DESERTEC Industrial Initiative (DII) is an initiative of about twenty large scale private technology and investment companies, the Desertec Foundation of Club of Rome (DF) and Munich-Re-Insurance Company (Mu-Re) founded in July 2009. It has the scope to foster concentrating solar power generation in the MENA region and to pave the way for solar electricity transfer from MENA to Europe.

6 REFERENCES

ABB 2007: Why HVDC? Website download: 18.11.2008 (http://www.abb.com/cawp/gad02181/c1256d71001e0037c125683100390eb0.aspx).

ABB 2008: ABB HVDC Reference Projects. Website download: 18.11.2008 (http://www.abb.com/cawp/gad02181/c1256d71001e0037c1256c330030750d.aspx).

Asplund G. 2008: High-Voltage Direct Current (HVDC) power transmission. Presentation at DESERTEC Hannover, Germany, 2008-04-23. ABB Power Systems HVDC, Ludvika, Sweden.

AUPTDE 2008: Arab Union of Producers, Transporters and Distributors of Electricity. (http://www.auptde.org).

Barro R.J., Sala-i-Martin X. 1995: Economic Growth. Massachusetts Institute of Technology, Cambridge. New York, 1995.

Battles J.F., Olmo F.J., Tovar J. and Alados-Arboledas L. 2000: Comparison of cloudless sky parameterisation of solar irradiance at various Spanish midlatitude locations. Theoretical and Applied Climatology 66, 81-93.

Bird R.E. & Hulstrom R.L. 1981: Review, evaluation and improvement of direct irradiance models. J. of Sol. Energy Engineering 103, 182-192.

Broesamle H., Mannstein H., Schillings C., Trieb F. 2001: Assessment of Solar Electricity Potentials in North Africa based on Satellite Data and a Geographic Information System, Solar Energy, Vol. 70, Nr.1 (2001), S. 1-12.

Buck R., Bräuning T., Denk T., Pfänder M., Schwarzbözl P., Pitz-Paal R. 2002: Solar-hybrid gas turbine-based power tower systems (REFOS). J. Solar Energy Eng. ASME, 124(1) (2002) 2–9.

Chin M., Ginoux P., Kinne S., Holben B.N., Duncan B.N., Martin R.V., Logan J.A., Higurashi A., Nakajima T. 2002: Tropospheric aerosol optical thickness from the GOCART model and comparisons with satellite and sunphotometer measurements. J. Atmos. Sci. 59, 461-483.

COM (2008) 19: Directive of the European Parliament and of the Council on the use of energy from renewable sources, European Commission, Brussels, 23.1.2008.

COM (2008) 30: Communication from the commission to the European Parliament, the Council, the European Economic and Social Committee and the Committee of the Regions - 20 20 by 2020 Europe's climate change opportunity, European Commission, Brussels, 23.1.2008.

Cohen, G.E., Solar Steam at Nevada Solar One, SolarPaces Conference, Las Vegas, USA, 2008.

Cooke, R. U., Warren, A., Goudie, A. S. (1993): Desert Geomorphology. UCLPress Limited, University College, London.

Dimitriev G. 2001: Wind Energy in Russia. Report VetrEnergo for Gaia Apatity and INFORSE-Europe, First Part - June 2001 (http://www.inforse.dk/europe/word_docs/ruswind2.doc).

Eastman, R. J. (1999): Guide to GIS and Image Processing, Volume 2. IDRISI32, Clark Labs, Worcester, Massachusetts.

DLR 2005: Direktnormalstrahlung für das Jahr 2002. German Aerospace Center DLR, Institute of Technical Thermodynamics, Dep. Systems Analysis and Technology Assessment, Stuttgart.

Eck M. & Steinmann W.D. 2005: Modelling and design of direct solar steam generating collector fields. J. Solar Energy Eng., 127 (2005) 371–380.

ecoinvent Zentrum 2003: ecoinvent Daten v1.01. CD-ROM, Schweizer Zentrum für Ökoinventare, Dübendorf.

ESRI 1996: ArcAtlas™: Our Earth. CD-ROM, Environmental Systems Research Institute Inc., California, USA.

ETSO 2008: European Transmission System Operators (http://www.etso-net.org).

EC 2007a: European Commission, Directorate-General for Research: Energy corridors - European Union and neighbouring countries. Project Report EUR 22581, Luxembourg: Office for Official Publications of the European Communities, 2007.

EC 2007b: European Commission: 2020 Vision: Saving our energy, published by: European Commission, Directorate General for Energy and Transport, Brussels, 2007.

EC 2009: Directive of the European Commission 2009/28/EG, Brussels, April 23, 2009.

ECE 2008: HVDC Projects Listing. University of Idaho, College of Engineering Department of Electrical and Computer Engineering (http://www.ece.uidaho.edu/hvdcfacts/Projects/HVDCProjectsListingMay2008-existing.pdf).

Evrendilek F. & Ertekin C. 2003. Assessing the potentials of renewable energy sources in Turkey. Renewable Energy 28(15): 2303-2315.

FAO 1995: Digital Soil Map of the World and Derived Soil Properties (DSMW). CD-ROM, Version 3.5, Land and Water Digital Media Series 1, Food and Agriculture Organization of the United Nations, Rome, Italy.

Fend T., Pitz-Paal R., Reutter O., Bauer J., Hoffschmidt B. 2004: Two novel high-porosity materials as volumetric receivers for concentrated solar radiation. Solar Energy Mater. Solar Cells, 84 (2004) 291–304.

GLOBE Task Team and others (Hastings D.A., Dunbar P.K., Elphingstone G.M., Bootz M., Murakami H., Maruyama H., Masaharu H., Holland P., Payne J., Bryant N.A., Logan T.L., Muller J.P., Schreier G., MacDonald J.S.), eds. 1999: The Global Land One-kilometer Base Elevation (GLOBE) Digital Elevation Model, Version 1.0. National Oceanic and Atmospheric Administration, National Geophysical Data Center, 325 Broadway, Boulder, Colorado. (http://www.ngdc.noaa.gov/ mgg/topo/globe.html) 25.04.2005.

Grama S.; Wayman E.; Bradford T. 2008: Concentrating Solar Power – Technology, costs and markets, 2008 Industry Report, Prometheus Institute and Greentech Media, 2008.

Gueymard C. 1993: Critical analysis and performance assessment of clear-sky solar irradiance models using theoretical and measured data. Solar Energy 51 (2), 121-138.

Hastings D.A. & Dunbar P.K. 1999. Global Land One-kilometer Base Elevation (GLOBE) Digital Elevation Model. Documentation, Volume 1.0, Key to Geophysical Records Documentation (KGRD) 34. National Oceanic and Atmospheric Administration, National Geophysical Data Center, 325 Broadway, Boulder, Colorado. (http://www.ngdc.noaa.gov/mgg/topo/report/ index.html).

Heston A., Summers R., Aten B. 2002: Penn World Tables Version 6.1, Center of International Comparisons at the University of Pennsylvania (CICUP), 2002.

HM Treasury, Stern Review on the economics of climate change, 2006 (http://www.hm-treasury.gov.uk/stern_review_report.htm).

IEA 2002: International Energy Agency (IEA). World Energy Outlook 2002, Paris 2002.

IEA 2003a: International Energy Agency (IEA). Electricity Information, Paris 2003.

IEA 2003b: International Energy Agency (IEA). Energy Statistics of OECD Countries 1960 – 2001, Paris 2003.

IEA 2007: International Energy Agency (IEA). Energy balance of non-OECD countries (2007 edition) and Energy balance of OECD countries (2007 edition). IEA energy statistics (Beyond 2020), Paris 2007.

IFEU/IFU 2005: Umberto - Software für das innerbetriebliche Stoffstrommanagement. Version Umberto 5, Institut für Umweltinformatik Hamburg GmbH (ifu), Institut für Energie- und Umweltforschung Heidelberg GmbH (ifeu).

Iqbal M. 1983: An introduction to solar radiation. Academic Press, Toronto.

INDITEP 2004: European Commission, Contract ENK5-CT-2001-00540, Integration of DSG technology for electricity production.

Kalnay E., Kanamitsu M., Kistler R., Collins W., Deaven D., Gandin L., Iredell M., Saha S., White G., Woollen J., Zhu Y., Leetmaa A., Reynolds R., Chelliah M., Ebisuzaki W., Higgins W., Janowiak J., Mo K.C., Ropelewski C., Wang J., Jenne R., Joseph D. 1996: The NMC/NCAR 40-Year Reanalysis Project. Bulletin of the American Meteorological Society 77 (3), 437–472.

Kasten F. 1966: A new table and approximate formular for relative optical air mass. Arch. Meteorol. Geophys. Bioklim. Ser. B, Vol. 14, 206-223.

Kern J., Trieb F., Müller-Steinhagen H., Scharfe J., Kabariti M., Al Taher A. 2009: Technologies for large scale seawater desalination using concentrated solar radiation, Desalination 235 (2009) 33–43.

Klein A., Pfluger B., Held A., Ragwitz M. (ISI), Resch G., Faber T. 2008: (EEG): Evaluation of different feed-in tariff design options – Best practice paper for the International Feed-In Cooperation, October 2008.

Kronshage 2001: Kronsgae, S., Standortanalyse für solarthermische Kraftwerke am Beispiel des Königreichs Marokko, Diploma Thesis, DLR Stuttgart and University of Osnabrück, Germany, 2001

Kronshage, S., Trieb, F. (2002): Berechnung von Weltpotenzialkarten. Erstellung einer Expertise für den Wissenschaftlichen Beirat der Bundesregierung Globale Umweltveränderung (WBGU). Internal Documentation, DLR, Stuttgart.

Lorec P. 2009: Solar Plan for the Mediterranean, Ministere de l'Energie, du Development Durable et de l'Amenagement du Territoire (MEEDDAT), Mediterranean Solar Plan – a win-win opportunity! EREC Congress, 13.02.2009, Brussels, EUSEW 2009 (European Union Sustainable Energy Week). (http://www.erec.org/fileadmin/erec_docs/Events_Documents/ EUSEW_MSP_13_Feb_2009/ MSP_Philippe_Lorec_panel1.pdf).

Mannstein H., Broesamle H., Schillings C., Trieb T. 1999: Using a Meteosat cloud index to model the performance of solar-thermal power stations. Proceedings of Eumetsat Conference, Copenhagen. 239-246.

May N. 2005: Eco-Balance of a Solar Electricity Transmission from North Africa to Europe, Diploma Thesis, University of Braunschweig, 2005.

McPeters R.D., Bhartia P.K., Krueger A.J., Herman J.R., Wellemeyer C.G., Seftor C.J., Jaross G., Torres O., Moy L., Labow G., Byerly W., Taylor S.L., Swissler T., Cebula R.P. 1998: Earth Probe Total Ozone Mapping Spectrometer (TOMS) Data Products User's Guide. NASA Technical Publication 1998-206895, National Aeronautics and Space Administration, Washington, DC.

Meteonorm 2005: Global Meteorological Database for Solar Energy and Applied Meteorology. Version 5.0, Meteotest, GmbH, Nördlingen (http://www.meteotest.de/) 16.08.2005.

Meyer R., Hoyer C., Diedrich E., Schillings C., Lohmann S., Schroedter-Homscheidt M., Buell R., Trieb F. 2004: Solar Energy Mining: A High-Quality Satellite-based Service to Provide Direct Solar Radiation for Europe, Brazil, Africa and Asia, SolarPaces Conference in Oaxaca, Mexico.

Mishchenko M., Penner J.E., Anderson D. (Ed.) 2002: Global Aerosol Climatology Project. Special Issue of Global Aerosol Climate, J. of Atmospheric Science, 59 (3).

Müller-Steinhagen H. & Trieb F. 2004: Concentrating solar power plants. Royal Academy of Engineering, INGENIA, issues 18, 20 (2004).

Münchener Rück 2001: Weltkarte der Naturgefahren. Münchener Rückversicherungs-Gesellschaft AG, München.

NABUCCO 2008: Homepage of the Nabucco Gas Pipeline International GmbH, (http://www.nabucco-pipeline.com/).

Nebrera, J. A., Solar Thermal Power Generation - A Spanish Success Story, Feria Internacional de Energia y Medio Ambiente (genera08), Madrid, February 2008.

New Energy Finance 2008: The STEG revolution revisited, New Energy Finance Ltd., 20. May 2008.

NGA 2005: GEOnet Names Server (GNS). National Geospatial-Intelligence Agency, Bethesda, Maryland. (http://www.nga.mil) 20.04.2005.

NGDC 2005: 2-minute Gridded Global Relief (ETOPO2). National Geophysical Data Center (NGDC), National Oceanic Atmospheric Administration (NOAA), Boulder, Colorado, USA. (http://www.ngdc.noaa.gov/mgg/gdas/ gd_designagrid.html) 24.05.2005.

NORDEL 2008: NORDEL - Transmission grid. NORDEL Helsinki, Finland (http://www.nordel.org/content/Default.asp?PageID=208).

Olson J.S. 1994: Global ecosystem framework-definitions, USGS EROS Data Centre Internal Report, Sioux Falls, SD, 37 S, 1994.

OME 2008: Mediterranean Energy Perspectives 2008, Observatoire Méditerranéen de l'Energie, 2008.

ORNL 2005: LandScan Global Population 200x Database Release. Documentation, Oak Ridge National Laboratory, Oak Ridge, Tennessee (http://www.ornl.gov/sci/gist/) 01.05.2005.

Penner J.E., Zhang S.Y., Chin M., Chuang C.C., Feichter J., Feng Y., Geogdzhayev I.V., Ginoux P., Herzog M., Higurashi A., Koch D., Land C., Lohmann U., Mishchenko M., Nakajima T., Pitari G., Soden B., Tegen I., Stowe L. 2002: A Comparison of Model- and Satellite-derived Aerosol Optical Depth and Reflectivity. Special Issue of Global Aerosol Climate, J. of Atmospheric Science 59 (3), 441-460.

Ph.D. 1998: Digital Chart of the World in ASCII (DCW). CD-ROM, Version 3.0, Ph.D. Associates Inc., Toronto, Ontario, Canada.

Schillings C. 2004: Bestimmung langjähriger stündlicher Zeitreihen und räumlich hochaufgelöster Karten der Direkt-Normal-Strahlung auf der Basis von Meteosat-Daten und Atmosphärenparametern für die Nutzung in konzentrierenden Solarkraftwerken. Dissertation, Uni-Marburg. (in german).

Schillings C., Mannstein H., Meyer R. 2004: Operational method for deriving high resolution direct normal irradiance from satellite data. Solar Energy, 76 (4), S. 475 – 484.

Siemens, 2008: High-voltage DC Transmission Systems. Website Siemens AG 2008 (https://www.energy-portal.siemens.com/static/de/de/products_solutions/ 1650_kn03011202.html).

Skog J.E. 2004: HVDC Transmission and Lifetime Expectancy. Statnett SF, Oslo Memo 24-06-22.

Skjølsvik K.O. 2007: En Utredning av SWECO Grøner/Econ for Enova. ENOVA, Kristiansund, 1. November 2007 (www.fylkesmannen.no/ Enova_potensialstudie_havenergi_Kristiansund_BQ0ZK.pdf.file).

Smith, W. H. F., Sandwell, D. T. (2003): Exploring the Ocean Basins with Satellite Altimeter Data. Scripps Institution of Oceanography San Diego, California & Geosciences Laboratory, NOAA, Washington, District of Columbia. URL: http://www.ngdc.noaa.gov/mgg/bathymetry/predicted/explore.html, 28.04.2005.

Solar Millennium 2008: Andasol – The World's Largest Solar Thermal Power Plant Project Development in Andalucia (Spain), http://www.solarmillennium.de/upload/Download/ Technologie/eng/Andasol1-3engl.pdf, downloaded, 22.12.2008.

SOLEMI 2008: Solar Energy Mining Projekt, German Aerospace Center, www.solemi.de

STBA 2003: Statistisches Bundesamt. Statistisches Jahrbuch für das Ausland, Wiesbaden, 2003.

Stern N. (2006): Stern Review on the economics of climate change, UK Cabinet Office - HM Treasury, ISBN-13: 9780521700801, http://www.cambridge.org/9780521700801

Tamme R., Steinmann W.D., Laing D. 2004: High temperature thermal energy storage technologies for parabolic trough. J. Solar Energy Eng., 126 (2) (2004) 794–800.

TEIAŞ 2008: Homepage of the Turkish Electricity Transmission Company. (http://www.teias.gov.tr/eng/).

Tegen I., Hollrig P., Chin M., Fung I., Jacob D., Penner J.E. 1997: Contribution of different aerosol species to the global aerosol extinction optical thickness: Estimates from model results. J. of Geophys. Research, 102, 23895-23915.

Trieb F., Schillings C., Kronshage S., Viebahn P., May N., Paul C., Klann U., Kabariti M., Bennouna A., Nokraschy H., Hassan S., Georgy Yussef L., Hasni T., Bassam N., Satoguina H., 2005: Concentrating Solar Power for the Mediterranean Region (MED-CSP). Final Report DLR-ITT Stuttgart, commissioned by Federal Ministry for the

Environment, Nature Conservation and Nuclear Safety (BMU), Germany (www.dlr.de/tt/med-csp).

Trieb F., Schillings C., Kronshage S., Viebahn P., May N., Paul C., Kabariti M., Bennouna A., Nokraschy H., Hassan S., Georgy Yussef L., Hasni T., Bassam N., Satoguina H. 2006: Trans-Mediterranean Interconnection for Concentrating Solar Power (TRANS CSP). Final Report DLR-ITT Stuttgart, commissioned by Federal Ministry for the Environment, Nature Conservation and Nuclear Safety (BMU), Germany (www.dlr.de/tt/trans-csp).

UCTE 2008: Union for the Co-ordination of Transmission of Electricity (UCTE): UCTE Transmission Development Plan. Edition 2008, Brussels (www.ucte.org/_library/otherreports/tdp08_report_ucte.pdf).

UCTE 2008: Union for the Co-ordination of Transmission of Electricity (UCTE). UCTE Grid Map. (http://www.ucte.org/resources/uctemap/).

UPTDEA 2008: Union of Producers, Transporters and Distributors of Electric power in Africa (http://www.updea-africa.org).

U.S. Department of commerce 1976: U.S. Standard Atmosphere, 1976, U.S. Government Printing Office, Washington, D.C., 1976.

USGS 2000: Global Land Cover Characterization (GLCC) Database. Version 2.0, U.S. Geological Survey, Earth Resources Observation System (EROS) Data Center, Sioux Falls, South Dakota. (http://edcdaac.usgs.gov/glcc/glcc.asp) 21.04.2005.

USGS 2003: Global Land Cover Characteristics Database. U.S. Geological Survey, Earth Resources Observation System (EROS) Data Center, Sioux Falls, South Dakota. (http://edcdaac.usgs.gov/glcc/globdoc2_0.asp).

UN 2006: United Nations (UN). World Population Prospects. Population Division, Department of Economic and Social Affairs (UNDP), 2006.

Vailati R. et al. 2006: Final WP1 report on optimised electricity corridors between the enlarged EU and the neighbouring areas. EC FP 6 project ENCOURAGED (Energy Corridor Optimisation for European Markets of Gas, Electricity and Hydrogen), Work Package I, Deliverable III, July 2006.

van Steen H. (DG TREN) 2008: The European Commission's renewable energy proposal, Presentation, Norway, October 2008 (http://www.nve.no/admin/FileArchive/573/Norway%20Oct%2008%20final%20Hans%20van%20Steen.pdf).

Viebahn P., Lechon Y. 2007: Technology report (including road mapping, technology specification of current and future systems, development of costs) for solar thermal power plant technologies. Technical Paper No. 12.4 – RS Ia. EU-IP NEEDS (New Energy Externalities Developments for Sustainability), Stuttgart 2007.

WDPA Consortium 2005: World Database on Protected Areas 2005. CD-ROM, World Conservation Union (IUCN) and UNEP-World Conservation Monitoring Centre (UNEP-WCMC). (http://sea.unep-wcmc.org/wdbpa) 20.04.2005.

WEC 2007: 2007 Survey of Energy Resources. World Energy Council, London.

Zewe, R. (1996): Einfluß von Freileitungen auf das Landschaftsbild. Neue und verbesserte Verfahren zur Beurteilung der Sichtbarkeit. Dissertation, Technische Fakultät, Universität des Saarlandes, Saarbrücken

ANNEXES

ANNEX A – RESOURCES AND PRODUCTION

Table A: List of identified resources (technical potential) and production capacities in energy supply regions as input for the REACCESS database.

		Resources		Production	
COM_CODE	Country	Suitable land for CSP [km²]	Solar radiation [kWh/m² yr]	Full load hours [h/yr]	Potential CSP production capacity [MW]
CSP_001_01	Morocco	6083	2100	5813	98,903
CSP_001_02	Morocco	5650	2200	6125	91,323
CSP_001_03	Morocco	10,875	2300	6438	174,842
CSP_001_04	Morocco	17,194	2400	6750	275,105
CSP_001_05	Morocco	34,348	2500	7063	547,134
CSP_001_06	Morocco	30,569	2600	7375	484,967
CSP_001_07	Morocco	18,930	2700	7688	299,187
CSP_001_08	Morocco	48,074	2800	8000	757,171
CSP_002_01	Algeria	6237	2100	5813	101,401
CSP_002_02	Algeria	34,142	2200	6125	551,839
CSP_002_03	Algeria	29,006	2300	6438	466,351
CSP_002_04	Algeria	39,462	2400	6750	631,392
CSP_002_05	Algeria	222,860	2500	7063	3,549,979
CSP_002_06	Algeria	384,570	2600	7375	6,100,970
CSP_002_07	Algeria	428,487	2700	7688	6,772,190
CSP_002_08	Algeria	277,580	2800	8000	4,371,890
CSP_003_01	Tunisia	9288	2100	5813	151,006
CSP_003_02	Tunisia	6445	2200	6125	104,176
CSP_003_03	Tunisia	9864	2300	6438	158,584
CSP_003_04	Tunisia	19,464	2400	6750	311,428
CSP_003_05	Tunisia	22,823	2500	7063	363,550
CSP_003_06	Tunisia	11,637	2600	7375	184,614
CSP_003_07	Tunisia	240	2700	7688	3794
CSP_004_01	Libya	7773	2100	5813	126,382
CSP_004_02	Libya	25,331	2200	6125	409,425
CSP_004_03	Libya	109,712	2300	6438	1,763,915
CSP_004_04	Libya	176,659	2400	6750	2,826,546
CSP_004_05	Libya	152,875	2500	7063	2,435,172
CSP_004_06	Libya	183,342	2600	7375	2,908,605
CSP_004_07	Libya	155,513	2700	7688	2,457,870
CSP_004_08	Libya	373,665	2800	8000	5,885,218
CSP_005_01	Saudi Arabia	32,807	2100	5813	533,386
CSP_005_02	Saudi Arabia	135,285	2200	6125	2,186,654
CSP_005_03	Saudi Arabia	336,109	2300	6438	5,403,857
CSP_005_04	Saudi Arabia	334,997	2400	6750	5,359,947
CSP_005_05	Saudi Arabia	187,726	2500	7063	2,990,333
CSP_005_06	Saudi Arabia	65,508	2600	7375	1,039,246
CSP_005_07	Saudi Arabia	42,773	2700	7688	676,026
CSP_005_08	Saudi Arabia	14,720	2800	8000	231,836

		Resources		Production	
COM_CODE	Country	Suitable land for CSP [km²]	Solar radiation [kWh/m² yr]	Load factor [h/yr]	Potential CSP production capacity [MW]
CSP_006_01	Jordan	2097	2100	5813	34,097
CSP_006_02	Jordan	5902	2200	6125	95,391
CSP_006_03	Jordan	19,197	2300	6438	308,651
CSP_006_04	Jordan	10,985	2400	6750	175,753
CSP_006_05	Jordan	10,742	2500	7063	171,116
CSP_006_06	Jordan	7239	2600	7375	114,845
CSP_006_07	Jordan	3152	2700	7688	49,819
CSP_007_01	Egypt	206	2100	5813	3355
CSP_007_02	Egypt	1481	2200	6125	23,939
CSP_007_03	Egypt	16,846	2300	6438	270,840
CSP_007_04	Egypt	40,969	2400	6750	655,503
CSP_007_05	Egypt	41,347	2500	7063	658,627
CSP_007_06	Egypt	44,613	2600	7375	707,766
CSP_007_07	Egypt	98,004	2700	7688	1,548,941
CSP_007_08	Egypt	354,972	2800	8000	5,590,815

ANNEX B – CORRIDOR DESCRIPTION

The following Annex provides a brief description of the individual electricity import corridors defined and characterised in detail in the REACCESS database developed in Work Packages 2 and 3.

1 Electricity Corridors *(General info on the methodology and data sources used)*

The methodology for identifying and characterising solar power import corridors is based on the results of recent studies MED-CSP and TRANS-CSP (Trieb et al. 2005, 2006) analysing the technical and economic potentials of an import of solar thermal power from the MENA region via HVDC lines (High Voltage Direct Current). In a first step, all sites that would not be suitable for the built up of HVDC lines were excluded in GIS exclusion maps (protected, industrial, urban areas, deep sea, areas with special hydrological and geomorphologic features). Non-exclusive land characteristics were then weighted (ratio of raised costs to base costs) according to land cover, population density, visibility from cultural and religious sites, existing grid infrastructure and impacts of natural hazards (risk of earthquakes, winter storms, volcano eruptions, tornados, hailstorms, lightning and tsunami formation). Information on slope was added as an-isotrophic friction image. This information were used to generate cost-distance images and to identify least-cost HVDC lines using a GIS tool o the calculation of least cost paths between selected end and starting points.

1.1 Technical Description *(Summary of standard technological characteristics)*

The technical characterisations are based on data reviews and expert interviews (see Trieb et al., 2006; Vailati et al., 2006; ABB, 2008; Siemens, 2008). Voltage of a corridor consisting of sea cable(s) and overhead line(s) was assumed to be ±600 kV for all corridor sectors technically possible until 2020. Maximal voltage of the complete line is limited by the sea cable (no DC-DC transformation possible) and also by the line capacity which is assumed to be not above 3200 MW per line for the reason of supply security in case of a line outage. It is not possible to include a DC-DC transformation in order to achieve a separate UHVDC voltage for overhead line sectors. On the other side higher investments in UHVDC are only recommended for bulk power transmission above 5000 MW which for safety reasons is not proposed for the electricity import to EU27+. Losses assumed: transformer/converter stations at start and end of corridor each 0.7%; sea cable 2.7%/1000 km; overhead line 600 kV 4.5%/1000 km. Investment costs assumed: stations 120 €/kW, sea cable 1.2 million €/km, overhead lines 270,000 €/km. Operating costs are assumed to be 1% of investment costs per year. A transmission capacity of 3200 MW requires two bipolar sea cables (i.e. 4 cables).

Corridor ELE_001

Source name & location: *Total available land for CSP in Morocco after exclusion of areas not usable. Representative starting point in suitable area with high insolation.*

Total resources: *174,700 km²* **Total max. production capacity:** *19,900 TWh/y*

Origin: *Zaouiet-ech-Cherradi (Region West of Marrakech), Morocco (AFR)*

Path: *land Morocco (591 km), sea (32 km), 2 corridor sectors*

Destinations: *Paloma Baja, Spain (EU border); defined internal paths to Brussels (BE), Sophia (BG), Prague (CZ), Paris (FR), Juelich (DE), Athens (GR), Budapest (HU), Milano (IT), Appledorn (NL), Warszaw (PL), Lissabon (PT), Bukarest (RO), Madrid (ES), London (UK)*

Other info: *Resources and capacities for solar thermal electricity generation assigned to this corridor are also linked to the alternative corridors ELE_002, _003 and _004.*

Corridor ELE_002
Source name & location: *Total available land for CSP in Morocco after exclusion of areas not usable. Representative starting point in suitable area with high insolation.* **Total resources:** *174,700 km²* **Total max. production capacity:** *19,900 TWh/y*
Origin: *Boulemane Province, Morocco (AFR)* **Path:** *land Morocco (394 km), sea (27 km), 2 corridor sectors* **Destinations:** *Casas de Porro, Spain (EU border); defined internal path to Lissabon (PT)*
Other info: *Resources and capacities for solar thermal electricity generation assigned to this corridor are also linked to the alternative corridors ELE_001, _003 and _004.*

Corridor ELE_003
Source name & location: *Total available land for CSP in Morocco after exclusion of areas not usable. Representative starting point in suitable area with high insolation.* **Total resources:** *174,700 km²* **Total max. production capacity:** *19,900 TWh/y*
Origin: *Boulemane Province, Morocco (AFR)* **Path:** *land Morocco (403 km), sea (16 km), 2 corridor sectors* **Destinations:** *Algeciras, Spain (EU border); defined internal path to Madrid (ES)*
Other info: *Resources and capacities for solar thermal electricity generation assigned to this corridor are also linked to the alternative corridors ELE_001, _002 and _004.*

Corridor ELE_004
Source name & location: *Total available land for CSP in Morocco after exclusion of areas not usable. Representative starting point in suitable area with high insolation.* **Total resources:** *174,700 km²* **Total max. production capacity:** *19,900 TWh/y*
Origin: *Boulemane Province, Morocco (AFR)* **Path:** *land Morocco (303 km), sea (149 km), 2 corridor sectors* **Destinations:** *San Agustin/El Ejido, Spain (EU border); defined internal paths to Brussels (BE), Sophia (BG), Prague (CZ), Paris (FR), Juelich (DE), Athens (GR), Budapest (HU), Milano (IT), Appledorn (NL), Warszaw (PL), Bukarest (RO), London (UK)*
Other info: *Resources and capacities for solar thermal electricity generation assigned to this corridor are also linked to the alternative corridors ELE_001, _002 and _003.*

Corridor ELE_005
Source name & location: *Total available land for CSP in Algeria after exclusion of areas not usable. Representative starting point in suitable area with high insolation.* **Total resources:** *1,422,300 km²* **Total max. production capacity:** *168,300 TWh/y*
Origin: *Benoud, Algeria (AFR)* **Path:** *land Algeria (296 km), land Morocco (558 km), sea (27 km), 3 corridor sectors* **Destinations:** *Casas de Porro, Spain (EU border); defined internal path to Lissabon (PT)*
Other info: *Resources and capacities for solar thermal electricity generation assigned to this corridor are also linked to the alternative corridors ELE_006 to ELE_009.*

Corridor ELE_006
Source name & location: *Total available land for CSP in Algeria after exclusion of areas not usable. Representative starting point in suitable area with high insolation.* **Total resources:** *1,422,300 km²* **Total max. production capacity:** *168,300 TWh/y*
Origin: *Benoud, Algeria (AFR)* **Path:** *land Algeria (431 km), sea (201 km), 2 corridor sectors* **Destinations:** *San José, Spain (EU border); defined internal paths to Brussels (BE), Sophia (BG), Prague (CZ), Paris (FR), Juelich (DE), Athens (GR), Budapest (HU), Milano (IT), Appledorn (NL), Warszaw (PL), Bukarest (RO), Madrid (ES), London (UK)*
Other info: *Resources and capacities for solar thermal electricity generation assigned to this corridor are also linked to the alternative corridors ELE_005, ELE_007 to ELE_009.*

Corridor ELE_007
Source name & location: *Total available land for CSP in Algeria after exclusion of areas not usable. Representative starting point in suitable area with high insolation.* **Total resources:** *1,422,300 km²* **Total max. production capacity:** *168,300 TWh/y*
Origin: *Dzioua, Algeria (AFR)* **Path:** *land Algeria (738 km), land Morocco (545 km), sea (27 km), 3 corridor sectors* **Destinations:** *Casas de Porro, Spain (EU border); defined internal path to Lissabon (PT)*
Other info: *Resources and capacities for solar thermal electricity generation assigned to this corridor are also linked to the alternative corridors ELE_005, ELE_006, ELE_008, ELE_009.*

Corridor ELE_008
Source name & location: *Total available land for CSP in Algeria after exclusion of areas not usable. Representative starting point in suitable area with high insolation.* **Total resources:** *1,422,300 km²* **Total max. production capacity:** *168,300 TWh/y*
Origin: *Dzioua, Algeria (AFR)* **Path:** *land Algeria (792 km), sea (201 km), 2 corridor sectors* **Destinations:** *San José, Spain (EU border); defined internal paths to Brussels (BE), Paris (FR), Juelich (DE), Appledorn (NL), Madrid (ES), London (UK)*
Other info: *Resources and capacities for solar thermal electricity generation assigned to this corridor are also linked to the alternative corridors ELE_005 to ELE_007, ELE_009.*

Corridor ELE_009
Source name & location: *Total available land for CSP in Algeria after exclusion of areas not usable. Representative starting point in suitable area with high insolation.* **Total resources:** *1,422,300 km²* **Total max. production capacity:** *168,300 TWh/y*
Origin: *Dzioua, Algeria (AFR)* **Path:** *land Algeria (511 km), sea (271 km), 2 corridor sectors* **Destinations:** *Setti Ballas (Sardegna), Italy (EU border); defined internal paths to Sophia (BG), Prague (CZ), Athens (GR), Budapest (HU), Milano (IT), Warszaw (PL), Bukarest (RO)*
Other info: *Resources and capacities for solar thermal electricity generation assigned to this corridor are also linked to the alternative corridors ELE_005 to ELE_008.*

Corridor ELE_010
Source name & location: *Total available land for CSP in Tunisia after exclusion of areas not usable. Representative starting point in suitable area with high insolation.* **Total resources:** *79,800 km²* **Total max. production capacity:** *8600 TWh/y*
Origin: *Bordj-Bouguiba, Tunisia (AFR)* **Path:** *land Tunisia (363 km), land Algeria (923 km), sea (199 km), 3 corridor sectors* **Destinations:** *Roquetas de Mar, Spain (EU border); defined internal path to Lissabon (PT)*
Other info: *Resources and capacities for solar thermal electricity generation assigned to this corridor are also linked to the alternative corridors ELE_011, ELE_012, ELE_013.*

Corridor ELE_011
Source name & location: *Total available land for CSP in Tunisia after exclusion of areas not usable. Representative starting point in suitable area with high insolation.* **Total resources:** *79,800 km²* **Total max. production capacity:** *8600 TWh/y*
Origin: *Bordj-Bouguiba, Tunisia (AFR)* **Path:** *land Tunisia (363 km), land Algeria (922 km), sea (201 km), 3 corridor sectors* **Destinations:** *San José, Spain (EU border); defined internal path to Madrid (ES)*
Other info: *Resources and capacities for solar thermal electricity generation assigned to this corridor are also linked to the alternative corridors ELE_010, ELE_012, ELE_013.*

Corridor ELE_012
Source name & location: *Total available land for CSP in Tunisia after exclusion of areas not usable. Representative starting point in suitable area with high insolation.* **Total resources:** *79,800 km²* **Total max. production capacity:** *8600 TWh/y*
Origin: *Bordj-Bouguiba, Tunisia (AFR)* **Path:** *land Tunisia (607 km), sea (196 km), 2 corridor sectors* **Destinations:** *Setti Ballas (Sardegna), Italy (EU border); defined internal paths to Brussels (BE), Prague (CZ), Paris (FR), Juelich (DE), Budapest (HU), Milano (IT), Appledorn (NL), Warszaw (PL), London (UK)*
Other info: *Resources and capacities for solar thermal electricity generation assigned to this corridor are also linked to the alternative corridors ELE_010, ELE_011, ELE_013.*

Corridor ELE_013
Source name & location: *Total available land for CSP in Tunisia after exclusion of areas not usable. Representative starting point in suitable area with high insolation.* **Total resources:** *79,800 km²* **Total max. production capacity:** *8600 TWh/y*
Origin: *Bordj-Bouguiba, Tunisia (AFR)* **Path:** *land Tunisia (430 km), sea (272 km), 2 corridor sectors* **Destinations:** *Mazara del Vallo (Sicilia), Italy (EU border); defined internal paths to Sophia (BG), Athens (GR), Bukarest (RO)*
Other info: *Resources and capacities for solar thermal electricity generation assigned to this corridor are also linked to the alternative corridors ELE_010, ELE_011, ELE_012.*

Corridor ELE_014
Source name & location: *Total available land for CSP in Libya after exclusion of areas not usable. Representative starting point in suitable area with high insolation.* **Total resources:** *1,184,900 km²* **Total max. production capacity:** *138,300 TWh/y*
Origin: *Sinawin, Libya (AFR)* **Path:** *land Libya (104 km), land Tunisia (438 km), land Algeria (923 km), sea (199 km), 4 corridor sectors* **Destinations:** *Roquetas de Mar, Spain (EU border); defined internal path to Lissabon (PT)*
Other info: *Resources and capacities for solar thermal electricity generation assigned to this corridor are also linked to alternative corridors ELE_015 to ELE_021.*

Corridor ELE_015
Source name & location: *Total available land for CSP in Libya after exclusion of areas not usable. Representative starting point in suitable area with high insolation.* **Total resources:** *1,184,900 km²* **Total max. production capacity:** *138,300 TWh/y*
Origin: *Sinawin, Libya (AFR)* **Path:** *land Libya (104 km), land Tunisia (438 km), land Algeria (922 km), sea (201 km), 4 corridor sectors* **Destinations:** *San José, Spain (EU border); defined internal path to Madrid (ES)*
Other info: *Resources and capacities for solar thermal electricity generation assigned to this corridor are also linked to alternative corridors ELE_014, ELE_016 to ELE_021.*

Corridor ELE_016
Source name & location: *Total available land for CSP in Libya after exclusion of areas not usable. Representative starting point in suitable area with high insolation.* **Total resources:** *1,184,900 km²* **Total max. production capacity:** *138,300 TWh/y*
Origin: *Sinawin, Libya (AFR)* **Path:** *land Libya (104 km), land Tunisia (669 km), sea (196 km), 3 corridor sectors* **Destinations:** *Setti Ballas (Sardegna), Italy (EU border); defined internal paths to Brussels (BE), Prague (CZ), Paris (FR), Juelich (DE), Milano (IT), Appledorn (NL), Warszaw (PL), London (UK)*
Other info: *Resources and capacities for solar thermal electricity generation assigned to this corridor are also linked to alternative corridors ELE_014, ELE_015, ELE_017 to ELE_021.*

Corridor ELE_017
Source name & location: *Total available land for CSP in Libya after exclusion of areas not usable. Representative starting point in suitable area with high insolation.* **Total resources:** *1,184,900 km²* **Total max. production capacity:** *138,300 TWh/y*
Origin: *Sinawin, Libya (AFR)* **Path:** *land Libya (104 km), land Tunisia (497 km), sea (272 km), 3 corridor sectors* **Destinations:** *Mazara del Vallo (Sicilia), Italy (EU border); defined internal paths to Sophia (BG), Athens (GR), Budapest (HU), Bukarest (RO)*
Other info: *Resources and capacities for solar thermal electricity generation assigned to this corridor are also linked to alternative corridors ELE_014 to ELE_016, ELE_018 to ELE_021.*

Corridor ELE_018
Source name & location: *Total available land for CSP in Libya after exclusion of areas not usable. Representative starting point in suitable area with high insolation.* **Total resources:** *1,184,900 km²* **Total max. production capacity:** *138,300 TWh/y*
Origin: *Jaghbub, Libya (AFR)* **Path:** *land Libya (550 + 773 km), sea Libya (164 km), land Tunisia (423 km), land Algeria (923 km), sea (199 km), 6 corridor sectors* **Destinations:** *Roquetas de Mar, Spain (EU border); defined internal path to Lissabon (PT)*
Other info: *Resources and capacities for solar thermal electricity generation assigned to this corridor are also linked to alternative corridors ELE_014 to ELE_017, ELE_019 to ELE_021.*

Corridor ELE_019
Source name & location: *Total available land for CSP in Libya after exclusion of areas not usable. Representative starting point in suitable area with high insolation.* **Total resources:** *1,184,900 km²* **Total max. production capacity:** *138,300 TWh/y*
Origin: *Jaghbub, Libya (AFR)* **Path:** *land Libya (550 + 773 km), sea Libya (164 km), land Tunisia (423 km), land Algeria (922 km), sea (201 km), 6 corridor sectors* **Destinations:** *San José, Spain (EU border); defined internal path to Madrid (ES)*
Other info: *Resources and capacities for solar thermal electricity generation assigned to this corridor are also linked to alternative corridors ELE_014 to ELE_018, ELE_020, ELE_021.*

Corridor ELE_020
Source name & location: *Total available land for CSP in Libya after exclusion of areas not usable. Representative starting point in suitable area with high insolation.* **Total resources:** *1,184,900 km²* **Total max. production capacity:** *138,300 TWh/y*
Origin: *Jaghbub, Libya (AFR)* **Path:** *land Libya (550 + 773 km), sea Libya (164 km), land Tunisia (654 km), sea (196 km), 5 corridor sectors* **Destinations:** *Setti Ballas (Sardegna), Italy (EU border); defined internal paths to Brussels (BE), Prague (CZ), Paris (FR), Juelich (DE), Milano (IT), Appledorn (NL), London (UK)*
Other info: *Resources and capacities for solar thermal electricity generation assigned to this corridor are also linked to alternative corridors ELE_014 to ELE_019, ELE_021.*

Corridor ELE_021
Source name & location: *Total available land for CSP in Libya after exclusion of areas not usable. Representative starting point in suitable area with high insolation.* **Total resources:** *1,184,900 km²* **Total max. production capacity:** *138,300 TWh/y*
Origin: *Jaghbub, Libya (AFR)* **Path:** *land Libya (550 + 375 km), sea Libya (164 km), sea (475 km), 4 corridor sectors* **Destinations:** *Maucini (Sicilia), Italy (EU border); defined internal paths to Sophia (BG), Athens (GR), Budapest (HU), Warszaw (PL)*
Other info: *Resources and capacities for solar thermal electricity generation assigned to this corridor are also linked to alternative corridors ELE_014 to ELE_020.*

Corridor ELE_022
Source name & location: *Total available land for CSP in Saudi Arabia after exclusion of areas not usable. Representative starting point in suitable area with high insolation.* **Total resources:** *1,149,900 km²* **Total max. production capacity:** *123,300 TWh/y*
Origin: *Halit Ammar, Saudi Arabia (MEA)* **Path:** *land Saudi Arabia (53 km), land Jordan (97 km), land Israel (12 km), land Egypt (1104 km), land Libya (571 + 770 km), sea Libya (222 km), land Tunisia (423 km), land Algeria (923 km), sea (202 km), 10 corridor sectors* **Destinations:** *San José (or Roquetas de Mar), Spain (EU border); defined internal paths to Lissabon (PT), Madrid (ES)*
Other info: *Resources and capacities for solar thermal electricity generation assigned to this corridor are also linked to the alternative corridors ELE_023, ELE_024, ELE_025.*

Corridor ELE_023
Source name & location: *Total available land for CSP in Saudi Arabia after exclusion of areas not usable. Representative starting point in suitable area with high insolation.* **Total resources:** *1,149,900 km²* **Total max. production capacity:** *123,300 TWh/y*
Origin: *Halit Ammar, Saudi Arabia (MEA)* **Path:** *land Saudi Arabia (53 km), land Jordan (97 km), land Israel (12 km), land Egypt (1104 km), land Libya (571 + 770 km), sea Libya (222 km), land Tunisia (654 km), sea (196 km),9 corridor sectors* **Destinations:** *Setti Ballas (Sardegna), Italy (EU border); defined internal paths to Paris (FR), Milano (IT), London (UK)*
Other info: *Resources and capacities for solar thermal electricity generation assigned to this corridor are also linked to the corridors ELE_022, ELE_024, ELE_025.*

Corridor ELE_024
Source name & location: *Total available land for CSP in Saudi Arabia after exclusion of areas not usable. Representative starting point in suitable area with high insolation.* **Total resources:** *1,149,900 km²* **Total max. production capacity:** *123,300 TWh/y*
Origin: *Halit Ammar, Saudi Arabia (MEA)* **Path:** *land Saudi Arabia (33 km), land Jordan (517 km), land Syria (473 km), land Turkey (1199 km), sea (227 km), 5 corridor sectors* **Destinations:** *Aghios Merkourios, Greece (EU border); defined internal path to Athens (GR)*
Other info: *Resources and capacities for solar thermal electricity generation assigned to this corridor are also linked to the alternative corridors ELE_022, ELE_023, ELE_025.*

Corridor ELE_025
Source name & location: *Total available land for CSP in Saudi Arabia after exclusion of areas not usable. Representative starting point in suitable area with high insolation.* **Total resources:** *1,149,900 km²* **Total max. production capacity:** *123,300 TWh/y*
Origin: *Halit Ammar, Saudi Arabia (MEA)* **Path:** *land Saudi Arabia (33 km), land Jordan (517 km), land Syria (473 km), land Turkey (996 + 165 km), sea Turkey (108 km), 6 corridor sectors* **Destinations:** *Strandzha, Bulgaria (EU border); defined internal paths to Brussels (BE), Sophia (BG), Prague (CZ), Juelich (DE), Budapest (HU), Appledorn (NL), Warszaw (PL), Bukarest (RO)*
Other info: *Resources and capacities for solar thermal electricity generation assigned to this corridor are also linked to the alternative corridors ELE_022, ELE_023, ELE_024.*

Corridor ELE_026
Source name & location: *Total available land for CSP in Jordan after exclusion of areas not usable. Representative starting point in suitable area with high insolation.* **Total resources:** *59,300 km²* **Total max. production capacity:** *6400 TWh/y*
Origin: *El Mudawwara, Jordan (MEA)* **Path:** *land Jordan (137 km), land Israel (12 km), land Egypt (1104 km), land Libya (571 + 770 km), sea Libya (222 km), land Tunisia (423 km), land Algeria (923 km), sea (202 km), 9 corridor sectors* **Destinations:** *San José (or Roquetas de Mar), Spain (EU border); defined internal paths to Lissabon (PT), Madrid (ES)*
Other info: *Resources and capacities for solar thermal electricity generation assigned to this corridor are also linked to the alternative corridors ELE_027, ELE_028, ELE_029.*

Corridor ELE_027
Source name & location: *Total available land for CSP in Jordan after exclusion of areas not usable. Representative starting point in suitable area with high insolation.* **Total resources:** *59,300 km²* **Total max. production capacity:** *6400 TWh/y*
Origin: *El Mudawwara, Jordan (MEA)* **Path:** *land Jordan (137 km), land Israel (12 km), land Egypt (1104 km), land Libya (571 + 770 km km), sea Libya (222 km), land Tunisia (654 km), sea (196 km), 8 corridor sectors* **Destinations:** *Setti Ballas (Sardegna), Italy (EU border); defined internal paths to Paris (FR), Milano (IT), London (UK)*
Other info: *Resources and capacities for solar thermal electricity generation assigned to this corridor are also linked to the alternative corridors ELE_026, ELE_028, ELE_029.*

Corridor ELE_028
Source name & location: *Total available land for CSP in Jordan after exclusion of areas not usable. Representative starting point in suitable area with high insolation.* **Total resources:** *59,300 km²* **Total max. production capacity:** *6400 TWh/y*
Origin: *El Mudawwara, Jordan (MEA)* **Path:** *land Jordan (465 km), land Syria (473 km), land Turkey (1199 km), sea (227 km), 4 corridor sectors* **Destinations:** *Aghios Merkourios, Greece (EU border); defined internal path to Athens (GR)*
Other info: *Resources and capacities for solar thermal electricity generation assigned to this corridor are also linked to the alternative corridors ELE_026, ELE_027, ELE_029.*

Corridor ELE_029
Source name & location: *Total available land for CSP in Jordan after exclusion of areas not usable. Representative starting point in suitable area with high insolation.* **Total resources:** *59,300 km²* **Total max. production capacity:** *6400 TWh/y*
Origin: *El Mudawwara, Jordan (MEA)* **Path:** *land Jordan (465 km), land Syria (473 km), land Turkey (996 + 165 km), sea Turkey (108 km), sea (227 km), 5 corridor sectors* **Destinations:** *Strandzha, Bulgaria (EU border); defined internal paths to Brussels (BE), Sophia (BG), Prague (CZ), Juelich (DE), Budapest (HU), Appledorn (NL), Warszaw (PL), Bukarest (RO)*
Other info: *Resources and capacities for solar thermal electricity generation assigned to this corridor are also linked to the alternative corridors ELE_026, ELE_027, ELE_028.*

Corridor ELE_030
Source name & location: *Total available land for CSP in Egypt after exclusion of areas not usable. Representative starting point in suitable area with high insolation.* **Total resources:** *598,400 km²* **Total max. production capacity:** *72,800 TWh/y*
Origin: *Al-Bahr al-ahmar, Egypt (AFR)* **Path:** *land Egypt (898 km), land Libya (564 + 770 km), sea Libya (222 km), land Tunisia (423 km), land Algeria (923 km), sea (202 km), 7 corridor sectors* **Destinations:** *San José (or Roquetas de Mar), Spain (EU border); defined internal paths to Lissabon (PT), Madrid (ES)*
Other info: *Resources and capacities for solar thermal electricity generation assigned to this corridor are also linked to alternative corridors ELE_031 to ELE_037.*

Corridor ELE_031
Source name & location: *Total available land for CSP in Egypt after exclusion of areas not usable. Representative starting point in suitable area with high insolation.* **Total resources:** *598,400 km²* **Total max. production capacity:** *72,800 TWh/y*
Origin: *Al-Bahr al-ahmar, Egypt (AFR)* **Path:** *land Egypt (898 km), land Libya (564 + 770 km), sea Libya (222 km), land Tunisia (654 km), sea (196 km), 6 corridor sectors* **Destinations:** *Setti Ballas (Sardegna), Italy (EU border); defined internal paths to Brussels (BE), Paris (FR), Juelich (DE), Milano (IT), Appledorn (NL), London (UK)*
Other info: *Resources and capacities for solar thermal electricity generation assigned to this corridor are also linked to alternative corridors ELE_030, ELE_032 to ELE_037.*

Corridor ELE_032
Source name & location: *Total available land for CSP in Egypt after exclusion of areas not usable. Representative starting point in suitable area with high insolation.* **Total resources:** *598,400 km²* **Total max. production capacity:** *72,800 TWh/y*
Origin: *Al-Bahr al-ahmar, Egypt (AFR)* **Path:** *land Egypt (200 + 279 km), sea Egypt (24 km), land Israel (148 km), sea to Cyprus (391 km), land Cyprus (13 km), sea to Turkey (95 km), land Turkey (841 km), sea (177 km), 9 corridor sectors* **Destinations:** *Potami, Greece (EU border); defined internal path to Athens (GR)*
Other info: *Resources and capacities for solar thermal electricity generation assigned to this corridor are also linked to alternative corridors ELE_030, ELE_031, ELE_033 to ELE_037.*

Corridor ELE_033
Source name & location: *Total available land for CSP in Egypt after exclusion of areas not usable. Representative starting point in suitable area with high insolation.* **Total resources:** *598,400 km²* **Total max. production capacity:** *72,800 TWh/y*
Origin: *Al-Bahr al-ahmar, Egypt (AFR)* **Path:** *land Egypt (200 + 279 km), sea Egypt (24 km), land Israel (148 km), sea to Cyprus (391 km), land Cyprus (13 km), sea to Turkey (95 km), land Turkey (804 + 165 km), sea Turkey (108 km), 10 corridor sectors* **Destinations:** *Strandzha, Bulgaria (EU border); defined internal paths to Sophia (BG), Prague (CZ), Budapest (HU), Warszaw (PL), Bukarest (RO)*
Other info: *Resources and capacities for solar thermal electricity generation assigned to this corridor are also linked to alternative corridors ELE_030 to ELE_032, ELE_034 to ELE_037.*

Corridor ELE_034
Source name & location: *Total available land for CSP in Egypt after exclusion of areas not usable. Representative starting point in suitable area with high insolation.* **Total resources:** *598,400 km²* **Total max. production capacity:** *72,800 TWh/y*
Origin: *Al-Wadi al-dschadid, Egypt (AFR)* **Path:** *land Egypt (976 km), land Libya (559 + 770 km), sea Libya (222 km), land Tunisia (423 km), land Algeria (923 km), sea (202 km), 7 corridor sectors* **Destinations:** *San José (or Roquetas de Mar), Spain (EU border); defined internal paths to Lissabon (PT), Madrid (ES)*
Other info: *Resources and capacities for solar thermal electricity generation assigned to this corridor are also linked to alternative corridors ELE_030 to ELE_033, ELE_035 to ELE_037.*

Corridor ELE_035
Source name & location: *Total available land for CSP in Egypt after exclusion of areas not usable. Representative starting point in suitable area with high insolation.* **Total resources:** *598,400 km²* **Total max. production capacity:** *72,800 TWh/y*
Origin: *Al-Wadi al-dschadid, Egypt (AFR)* **Path:** *land Egypt (976 km), land Libya (559 + 770 km), sea Libya (222 km), land Tunisia (654 km), sea (196 km), 6 corridor sectors* **Destinations:** *Setti Ballas (Sardegna), Italy (EU border); defined internal paths to Brussels (BE), Paris (FR), Juelich (DE), Milano (IT), Appledorn (NL), London (UK)*
Other info: *Resources and capacities for solar thermal electricity generation assigned to this corridor are also linked to alternative corridors ELE_030 to ELE_034, ELE_036, ELE_037.*

Corridor ELE_036
Source name & location: *Total available land for CSP in Egypt after exclusion of areas not usable. Representative starting point in suitable area with high insolation.* **Total resources:** *598,400 km²* **Total max. production capacity:** *72,800 TWh/y*
Origin: *Al-Wadi al-dschadid, Egypt (AFR)* **Path:** *land Egypt (816 km), land Israel (148 km), sea to Cyprus (391 km), land Cyprus (13 km), sea to Turkey (95 km), land Turkey (841 km), sea (177 km), 7 corridor sectors* **Destinations:** *Potami, Greece (EU border); defined internal path to Athens (GR)*
Other info: *Resources and capacities for solar thermal electricity generation assigned to this corridor are also linked to alternative corridors ELE_030 to ELE_035, ELE_037.*

Corridor ELE_037
Source name & location: *Total available land for CSP in Egypt after exclusion of areas not usable. Representative starting point in suitable area with high insolation.* **Total resources:** *598,400 km²* **Total max. production capacity:** *72,800 TWh/y*
Origin: *Al-Wadi al-dschadid, Egypt (AFR)* **Path:** *land Egypt (816 km), land Israel (148 km), sea to Cyprus (391 km), land Cyprus (13 km), sea to Turkey (95 km), land Turkey (804 + 165 km), sea Turkey (108 km), 8 corridor sectors* **Destinations:** *Strandzha, Bulgaria (EU border); defined internal paths to Sophia (BG), Prague (CZ), Budapest (HU), Warszaw (PL), Bukarest (RO)*
Other info: *Resources and capacities for solar thermal electricity generation assigned to this corridor are also linked to alternative corridors ELE_030 to ELE_036.*

DLR at a glance

DLR is Germany´s national research center for aeronautics and space. Its extensive research and development work in Aeronautics, Space, Transportation and Energy is integrated into national and international cooperative ventures. As Germany´s space agency, DLR has been given responsibility for the forward planning and the implementation of the German space program by the German federal government as well as for the international representation of German interests. Furthermore, Germany's largest project-management agency is also part of DLR.

Approximately 6000 people are employed at thirteen locations in Germany: Koeln (headquarters), Berlin, Bonn, Braunschweig, Bremen, Goettingen, Hamburg, Lampoldshausen, Neustrelitz, Oberpfaffenhofen, Stuttgart, Trauen and Weilheim. DLR also operates offices in Brussels, Paris, and Washington D.C.

DLR Deutsches Zentrum für Luft- und Raumfahrt e.V.
in der Helmholtz-Gemeinschaft